Universidade Federal do Rio Grande do Sul
Escola de Engenharia
Programa de Pós-Graduação em Engenharia Civil

Evaluation of the Behaviour of a Fibre-Reinforced Cemented Sand under Unconfined Cyclic Loading

Thaís Martins de Paula

Porto Alegre
2020

THAÍS MARTINS DE PAULA

EVALUATION OF THE BEHAVIOUR OF A FIBRE-REINFORCED CEMENTED SAND UNDER UNCONFINED CYCLIC LOADING

Thesis presented to the Civil Engineering Post-Graduation Program from the Universidade Federal do Rio Grande do Sul, as part of the requirements for the title of Doctor in Engineering

Porto Alegre
2020

THAÍS MARTINS DE PAULA

EVALUATION OF THE BEHAVIOUR OF A FIBRE-REINFORCED CEMENTED SAND UNDER UNCONFINED CYCLIC LOADING

This thesis dissertation was considered suitable for obtaining the title of DOCTOR IN ENGINEERING, in the field of Geotechnical Engineering, its final version was also approved by the supervisor and by the Civil Engineering Post-Graduation Program from the Federal University of Rio Grande do Sul.

Porto Alegre, December 18th 2020.

Prof. Nilo Cesar Consoli
Ph.D. Concordia University, Canada

Supervisor

Prof. Karla Salvagni Heineck
D.Sc. Universidade Federal do Rio Grande do Sul - BR

Co-supervisor

Prof. Nilo Cesar Consoli
PPGEC/UFRGS Coordinator

BOARD OF EXAMINERS

Prof. Luciano Pivoto Specht (UFSM)
D.Sc. Universidade Federal do Rio Grande do Sul - BR

Prof. Lucas Festugato (UFRGS)
D.Sc. Universidade Federal do Rio Grande do Sul - BR

Prof. Andrea Diambra (University of Bristol)
Ph.D. University of Bristol - UK

Prof. Erdin Ibraim (University of Bristol)
Ph.D. École Nationale des Travaux Publics de l'État (ENTPE) Ville de Lyon – FR

I dedicate this work to my family and friends
that supported me relentlessly throughout
this whole process. Thank you so much.

ACKNOWLEDGEMENTS

During the course of this doctorate there were many people that helped me in various ways and without them I certainly would not be able to accomplish this research. I am deeply grateful for everyone that shared the heavy load of experimental research, being by sharing knowledge, landing a helping hand or lending a sympathetic ear.

Firstly, I would like to thank Prof. Nilo Consoli, for being my advisor through my entire academic career. It was a great pleasure working with you. I cannot express how your dedication to your work and your work ethic inspire me every day. Thank you so much for helping and guiding my research in any way that was necessary, through all the ups and downs.

I would also like to thank Prof. Andrea Diambra, for being opened to receive me at the University of Bristol and for being always available to discuss about my work. The opportunity to work at the Geotechnical laboratory of the University of Bristol was immensurable for the development of this research.

Prof. Lucas Festugato, I would like to thank you for always being available to help and give insight in every issue brought to you.

From the laboratories, I would like to thank Garry for bringing to life all the pieces of the cyclic unconfined compression equipment and doing all my bender elements. Sérgio and Gustavo, thank you so much for helping fix the fatigue equipment, I would not have never able to do it by myself. Filipe, João and Júlia, thank you so much for helping me out during the experimental program and for always having questions and keeping me on my toes.

I would also like to thank the friends that the academic life gave me. Marina, we started it together and having you beside me every step of the way, having you to count on even overseas meant so much to me, thank you. Bruna, all the late nights at the lab and conversations during the last couple of years were so important to keep me going, thank you so much. Mozara, Marina, Guilherme and Eduardo thank you for all the help and advice during all these years.

At last, but certainly not least, I would like to thank my family and friends. Mom and dad, I am deeply thankful for all your support during all my life, you always will be my inspiration.

Gui, I cannot put into words how much I am thankful to have you in my life, always right beside me through thick and thin. I am so lucky. Hique and Sheila, thank you for all the support. Carol, Rodigo and Liah, thank you so much for the support and for making my life lighter during this last couple of years. Lu, having you in my life always ready to talk about anything no matter what is one of the most treasured things in my life. Muri, tamo junto. Thank you so much for always being there for me.

All things are difficult before they are easy.
Thomas Fuller

RESUMO

DE PAULA, T. M. Evaluation of the Behaviour of a Fibre-Reinforced Cemented Sand under Unconfined Cyclic Loading. 2020. Tese (Doutor em Engenharia) – Programa de Pós-Graduação em Engenharia Civil, UFRGS, Porto Alegre.

Os solos são o denominador comum entre todos os empreendimentos de Engenharia Civil. Entretanto, eles também são o material de construção mais variável, apresentando características heterogêneas e complexas únicas para cada local. Sendo assim, frequentemente as características do solo não atendem às necessidades do projeto de engenharia. A inserção do cimento na matriz do solo proporciona um aumento da resistência e rigidez do material, enquanto que a adição de fibras proporciona um aumento da ductilidade, reduzindo a perda de resistência pós-pico. O comportamento destes compósitos sob condições cíclicas não confinadas, para diferentes tensões, não é completamente conhecido em nível experimental e menos ainda é conhecido em nível de modelo teórico. Neste sentido, esta pesquisa visa analisar experimentalmente o comportamento mecânico da areia cimentada reforçada com fibras sob condições de carga cíclica não confinada, e propor um modelo constitutivo qualitativo para prever seu comportamento para compressão cíclica não confinada do mesmo compósito. Para isso, foi planejado um programa experimental para uma areia siltosa (solo residual de arenito de Botucatu), cimento Portland - CP - Tipo V (ARI), e fibras de polipropileno de 24 mm de comprimento e 0,023 mm de espessura. Foram definidos três pesos específicos aparentes secos (γ_d) (18, 19 e 19,7 kN/m^3), três teores de cimento (3, 5 e 7%) e 0 e 0,5% de fibras. Os testes planejados são divididos em: carregamento monotônico – 5 dosagens de ensaios de resistência à compressão simples e compressão diametral para validar o uso de dados apresentados por Festugato (2011) e testes de tração na flexão. Para ensaios cíclicos (compressão não confinada - CUC e fadiga - CF), foi escolhida uma mistura de referência (18 kN/m^3; 5% de cimento) para três cargas aplicadas diferentes (90, 80 e 70%) e duas porcentagens de fibras (0 e 0,5%). A fase monotônica do programa experimental forneceu os valores máximos de carga utilizados na porção cíclica da pesquisa em relação ao η/C_{iv} da mistura. Nos testes CUC, houve um aumento no número de ciclos (N) com a diminuição da carga aplicada. Entretanto, os valores de N diminuíram com a inserção de fibras quando comparados com as porcentagens aplicadas de amostras não reforçadas com fibras. Como a carga máxima para compósitos solo-cimento-fibra foi maior, as amostras reforçadas com fibras foram testadas com as mesmas cargas máximas que as não reforçadas com fibras. Houve uma grande melhoria no comportamento para todas as cargas aplicadas com inserção de fibras. Os dados do módulo de cisalhamento (G) mostraram uma diminuição nos valores totais para as amostras reforçadas com fibra. Houve um decréscimo significativo no G durante os ciclos iniciais. Compósitos que não foram levados a ruptura para os parâmetros indicados apresentaram um ligeiro aumento em G após a perda inicial. Os ensaios de fadiga também mostraram um aumento na N_f com diminuição da carga. Entretanto, as amostras reforçadas com fibras tiveram resultados drasticamente menores, o que poderia ser devido à anisotropia imposta pela inserção de fibras. Finalmente, foi desenvolvido um modelo qualitativo para descrever o comportamento da deformação axial devido à degradação cíclica de G de para testes cíclicos de compressão não confinada.

Palavras-chave: resistência à tração; carregamento cíclico; reforço com fibras; areia cimentada; modelos constitutivos.

ABSTRACT

DE PAULA, T. M. Evaluation of the Behaviour of a Fibre-Reinforced Cemented Sand under Unconfined Cyclic Loading. 2020. Thesis dissertation (Doctor in Engineering) – Civil Engineering Post-Graduation Program, UFRGS, Porto Alegre.

Soils are the common denominator between all civil engineering endeavours. However, they are also the most variable construction material, presenting heterogeneous and complex characteristics unique to each location. In being so, frequently soil characteristics do not attend to the necessities of the engineering design. The insertion of cement to the soil matrix provides an increase in strength and rigidity of the material, whereas, fibre addition provides an increase in ductility, reducing post-peak loss in strength. The behaviour of these composites under unconfined cyclic conditions, for different stresses, is not completely known in an experimental level and even less is known in a theoretical model level. In this sense, this research aims to experimentally analyse the mechanical behaviour of fibre-reinforced cemented sand under unconfined cyclic loading conditions, and to propose a qualitative constitutive model for predicting its behaviour for cyclic unconfined compression of the same composite. In order to do so, an experimental program was planned for a silty sand (Botucatu sandstone residual soil), early strength Portland cement – PC – Type III, and polypropylene fibres 24 mm long and 0.023 mm thick. Three different dry unit weights (γ_d) (18, 19 and 19.7 kN/m^3), three cement contents (3, 5 and 7%) and 0 and 0.5% of fibres were chosen. The planned tests are divided in: monotonic loading – flexural tensile tests and 5 dosages of unconfined compressive and split tensile tests. For cyclic testing (unconfined compression – CUC and fatigue – CF), a benchmark mixture (18 kN/m^3; 5% cement) was chosen for three different applied loads (90, 80 and 70%) and two fibre percentages (0 and 0.5%). The monotonic phase of the experimental program provided the maximum load values used in the cyclic portion of the research in respect to the η/C_{iv} of the mixture. From the CUC tests, there was an increase in the number of cycles (N) with the decrease of applied load. However, the values of N decreased with fibre insertion when compared to the applied percentages unreinforced specimens. Since the maximum load for soil-cement-fibre composites was higher, fibre-reinforced specimens were tested with the same maximum loads as the unreinforced ones. Then, there was a great improvement in behaviour for all applied loads with fibre insertion. The shear modulus (G) data showed a decrease in total values for the fibre-reinforced specimens. There was a significant decrease in G during the initial cycles. Combinations that did not reach failure for the given parameters presented a slight increase in G after the initial loss; this could be attributed to the decrease in void ratio during testing. Fatigue testing also showed an increase in N_f with decrease in loading. However, fibre-reinforced specimens had dramatically lower results, which could be due to anisotropy imposed by fibre insertion. Finally, a qualitative model was made to describe the behaviour of decrease in axial strain due to cyclic degradation of G of for CUC tests.

Key words: cyclic loading; cyclic unconfined compression tests; fatigue tests; fibre reinforcement; cemented sand; degradation of stiffness.

SUMMARY

FIGURES

TABLES

SYMBOLS

$\bar{\rho}$: average volumetric concentration of fibres (V_f/ V);

a = fibre aspect ratio (l/d);

b : average width (mm);

B : rate degradation of shear modulus;

c' : effective cohesion intersect (kN/m^2);

C_{iv} : volumetric cement content (%);

CUC : cyclic unconfined compression tests;

C : degradation of cementation parameter;

d : average depth (mm);

d : fibre diameter (mm);

D : specimen diameter (mm);

E : Young's modulus (MPa);

e : void ratio;

E_1 : Young's modulus at the 1st cycle (MPa);

E_N : Young's modulus at the Nth cycle (MPa);

f : inclination of the slope of E_N/E_1 (or G_N/G_1) versus N;

FL: flexural tensile tests;

FT: fatigue tests;

g : plastic potential.

G : shear modulus (MPa);

G : shear modulus (MPa);

G_0 : initial shear modulus (MPa);

G_1 : Shear modulus at the 1st cycle (MPa);

G_N : Shear modulus at the Nth cycle (MPa);

$I_{1,2,3}$: stress invariants;

K : bulk modulus (MPa);

l : fibre length (mm);

L : specimen length (mm);

l/d: aspect ratio (a);

l_c : critical length;

LEGG : Laboratório de Engenharia Geotécnica e Geoambiental;

M : constrained modulus (MPa);

M : slope inclination of the CSL in the *q-p'* plane;

M_c : slope inclination of the CSL in the *q-p'* plane for triaxial testes;

N : number of cycles;

N' : value of ν for p' = 1 kPa for NCL;

N_f : number of cycles in fatigue life;

P : maximum applied load (kN);

p' : mean effective stress (kN/m^2);

p'_y : maximum stress experienced by the soil (kN/m^2);

p_i' : initial mean effective stress (kN/m^2);

q : deviatoric stress (kN/m^2);

q_f : deviatoric stress at failure (kN/m^2);

q_f : flexural tensile strength (kPa);

q_t : split tensile strength (kPa);

q_u : unconfined compression strength (kN/m^2);

q_u : unconfined compression strength (kPa);

r = fibre radius (mm);

s : slip;

s = fibre slip length (mm);

ST : split tensile tests;

UC : unconfined compression tests;

UFRGS : Universidade Federal do Rio Grande do Sul;

V : total specimens volume (m^3);

V_{ci} : volume of cement (m^3);

V_f : total volume of fibres (m^3);

V_P : velocity of p-waves (m/s);

V_S : velocity of s-waves (m/s);

V_v : volume of voids (m^3);

H : porosity;

η/C_{iv}: porosity/volumetric cement content ratio;

σ_c : unconfined compression strength (kN/m^2);

σ_t : splitting tensile strength (kN/m^2);

τ : shear stresses (kPa);

ψ: dilatancy angle (^{o});

Γ : value of ν for p' = 1 kPa for CSL;

T_C : displacement of the cemented NCL;

T_U : displacement of the uncemented NCL;

δ_D : stiffness degradation;

$\delta\varepsilon_{a,N}$: increment in axial strain at the N^{th} cycle;

$\delta\varepsilon_{a,N}^{E}$ = elastic portion on the increment in axial strain at the N^{th} cycle;

$\delta\varepsilon_{a,N}^{P}$ = plastic portion on the increment in axial strain at the N^{th} cycle;

ε_1 : shear strain (%);

ε_a : axial strain (%);

ε^e_p : incremental elastic volumetric strain (%);

ε^p_{ij} : incremental plastic strain rate (%);

ε_q : distortional strain (%);

ε_r : radial displacement (%);

ε_v : volumetric strain (%);

ϕ' : internal friction angle of the uncemented soil (^{o});

ϕ_w : sand/fibre interface friction angle (^{o});

γ_d : dry unit weight (kg/m^3);

κ : elastic parameter of Cam Clay;

κ : gradient value for expansion curve.

λ : gradient value for NCL;

λ : inclination of the NCL;

μ = Poisson ratio;

ν : Poisson's ratio;

ν_k : value of ν for p' = 1 kPa ;

ρ : density (kg/m^3);

$\rho(\theta)$: volumetric concentration of fibres per infinitesimal volume;

σ_{ij} : stress tensor; (kN/m^2)

σ_n : stress normal to the fibre surface (kN/m^2);

σ_o : fibre yield stress (kN/m^2);

υ : specific volume (m^3/kg).

1 INTRODUCTION

The following introductory chapter presents the relevance and justification for this research, main and specific objectives of the thesis, as well as the structure developed to present the study.

1.1 RESEARCH RELEVANCE AND JUSTIFICATION

Soils are the common denominator between all civil engineering endeavours. It can range from foundation of buildings, embankments and road subgrades, to dams and offshore structures. However, soil is an extremely variable construction material, presenting heterogenic and complex characteristics unique to each location. In being so, frequently, soil characteristics do not attend to the necessities of the engineering design.

A solution for the aforementioned issue is to improve the mechanical properties of the soil through the insertion of cementing agents, pozzolans, fibres, etc. This research will evaluate the use of Portland cement and polypropylene fibres as soil improvements.

The addition of Portland cement to the soil increases the resistance and stiffness of the mixture. However, it also increases its brittleness, consequently, the enhanced soil usually presents a fragile rupture. This is especially important when the cemented soil is subjected to flexural loading; the more fragile behaviour leads to tensile cracking that reduces the load bearing capacity of the cemented material. As for fibre addition, which are essentially tension resisting intrusions, it increases the ductility and tenacity of the reinforced material usually without disrupting the strength of the composite.

This way, the inclusion of randomly oriented fibres to cemented soils generates a composite that has the necessary mechanical strength, ductility and post-crack load bearing strength (MAHER; HO, 1993; CONSOLI *et* al., 1997). The combination of both inclusions provides a relatively low-cost solution when compared to traditional geotechnical designs. For example, pavement construction, when there are no granular bases available near the site; or foundation construction on low bearing capacity soils, when the deep foundation costs would be incoherent with the design cost (CONSOLI *et* al., 2010a). Many of these engineering designs

are subjected to repeated successive compressive and tensile stresses – i.e. cyclic loading. Cyclic loading can be induced by different sources: traffic, industrial sources, repeated filling and emptying operations and environmental sources (e.g. waves, wind and earthquakes) (CORTI, 2016).

Most of the researches done so far through experimental analysis of these composites concentrated in its mechanical behaviour under unconfined and confined monotonic loading and confined cyclic tests. Notably at the Postgraduate Program in Civil Engineering (PPGEC) at the Federal University of Rio Grande do Sul (UFRGS): Ulbrich (1997), Feuerharmel (2000), Specht (2000), Casagrande (2001), Heineck (2002), Casagrande (2005), Festugato (2008), Festugato (2011), Venson (2015), Miguel (2020). Most of the research in cycling compression loading is carried out under triaxial confined conditions (LI; DING, 2002; SHARMA; FAHEY, 2003; DA FONSECA *et* al., 2013; GÁLVEZ, 2017). As for split tensile fatigue testing, literature mainly concentrates on the elastic behaviour the studied materials (MOHAMMAD *et* al., 2000; GASPARD, MOHAMMAD; WU, 2003; KHATTAK; ALRASHIDI, 2006; TAKAIKAEW *et* al., 2018).

When studying cemented composites, the structure imposed by the cementation process guarantees the integrity of the cemented sand without the aid of triaxial confinement. Also, the use of the relatively low confining pressures used to simulate cyclic behaviour in pavement design or shallow foundations on cyclic triaxial tests should not interfere greatly on the mechanical behaviour of the cemented material. Given these factors, the use of unconfined cyclic proves to be a simpler testing procedure that provides the necessary data to evaluate the behaviour of the studied materials. Thus, there are still aspects to be evaluated regarding the mechanical behaviour of fibre-reinforced cemented sands under cyclic unconfined compression and split tensile fatigue loading conditions, concentrating on its behaviour leading to failure.

Besides the experiments aforementioned, many authors have proposed modelling approaches for predicting the contribution of the fibres to shear strength (e.g. GRAY; AL-REFEAI, 1986; MICHALOWSKI; ZHAO, 1996). Diambra *et* al. (2017) proposed a constitutive model to predict the behaviour of artificially cemented granular soils, whereas Festugato *et* al. (2018) proposed a model to predict the behaviour of fibre-reinforced cemented granular soils.

However, a qualitative model for fibre-reinforced cemented granular soils under uniaxial unconfined cyclic compression conditions is a relevant theme to be researched.

In being so, this research has two main goals: to experimentally analyse the mechanical behaviour leading to failure of fibre-reinforced cemented sands under two different unconfined cyclic loading conditions – compression and split tensile; and to propose a qualitative model for depicting the influence of the degradation of shear modulus of unconfined uniaxial compression cyclic loading conditions of fibre-reinforced cemented granular soils.

1.2 OBJECTIVES

The objectives of this research are divided in main and secondary, and are presented below.

1.2.1 Main objective

The main objective of this thesis is to evaluate, through experimental analysis, the behaviour of a cemented fibre-reinforced sand under unconfined cyclic loading and provide a qualitative model to represent its behaviour under uniaxial cyclic unconfined compression tests.

1.2.2 Specific objectives

The specific objectives are the following.

(a) evaluate the mechanical behaviour of the studied composites under monotonic split tensile and flexural tensile loading conditions;

(b) evaluate the mechanical behaviour of the studied composites diametric compression fatigue loading conditions;

(c) evaluate the mechanical behaviour of the studied composites under cyclic unconfined compression loading;

(d) evaluate the stiffness degradation of the studied composites under very-small strains during cyclic unconfined compression loading through the use of bender elements;

(e) propose a qualitative model to describe the influence of the degradation of shear modulus under very-small strains on the number of cycles until rupture

on the ν *vs* log p' plane for the studied soil composites under uniaxial cyclic unconfined compression loading.

1.3 THESIS STRUCTURE

This thesis is organized in eight chapters. The first presents the motivation for the research, alongside its objectives. The second chapter presents a literary review of the relevant published works on important subjects for this research, such as mechanical behaviour of fibre-reinforced soil-cement composites, and constitutive models for reinforced and unreinforced granular soils. In the third chapter, it is presented the studied materials and methods adopted in this research. In the fourth chapter, the results and analysis of monotonic tests are shown. In chapter five, the test data and analysis for the cyclic unconfined tests are presented. Next, the results and analysis for the split tensile fatigue tests are presented in chapter six. The seventh chapter entails the presentation of the proposed qualitative model. Lastly, the conclusions drawn from the tests and model presented is shown in chapter eight.

2 BACKGROUND

In order to have a better understanding of the engineering community knowledge on the behaviour of artificially cemented sands with fibre insertion under static and cyclic loading, as well as the pertinent constitutive models to represent this composite, this literary review aims to present previous studies on these topics. Firstly, it is presented a review of soil improvement, giving emphasis to soil stabilization. Next, the mechanical, physical and chemical properties of fibre composites are shown. Then, it is explored the published works on literature regarding the behaviour of fibre composites under cyclic loading. After that, a brief literary review is presented on plasticity and critical state theories. Following, it is presented the published work concerning granular soils constitutive models. Finally, is presented a literary review of constitutive models for granular composites.

2.1 SOIL IMPROVEMENT – ADDITION OF FIBRE AND CEMENT

Soil improvement is defined as the use of a physical and/or chemical process aiming to improve mechanical properties of soils. Usually the objective of the improvement is to enhance strength of soils and to mitigate its compressibility and permeability (CASAGRANDE, 2005). On the present research two different materials were added to the soil in order to enhance its mechanical characteristics – Portland cement and polypropylene fibres. Due to the nature of these materials, the first will be treated by the term soil stabilization, the second, soil reinforcement. Both soil improvement techniques are described on the following topics.

2.1.1 Soil stabilization

Burroughs (2001) states on his Ph. D. Thesis that, even though the soil-cement technique was only vastly applied and studied during the Second World War, the concept of permanent soil stabilization with cement is accredited to Brook-Bradley. In 1917 this company added cement to the existing soil during the construction of a road in Salisbury Plain in England. Still, the urgent War infrastructure needs during the 1930s financed large-scale studies conducted in South Carolina/USA, that provided the ground support – in form of published works – that all soil improvement researches to arise.

According to Sparkes and Smith[1] (1945 apud BURRIUGHS, 2001):

> "The purpose of stabilisation is to maintain the moisture content and the mechanical properties of the soil at a satisfactory level so that it will retain its originally compacted state indefinitely under traffic and weather conditions. This is achieved to an appreciable extent by compacting the soil to an adequate density. The same object can also be secured by adjusting the grading of the soil, by adding certain cementitious binders or resin."

Soil stabilization by cement addition is the most used soil improvement technique, being largely employed on road construction, mainly as base or subbase course layers of pavements, or as base layer underneath foundations. Regarding the its process, Van Impe (1989) classifies them into:

a) temporary: only necessary for a limited amount of time, usually during the execution of a construction phase – e.g. freezing soils and lowering the water table;

b) permanent: consists on changing permanently soils properties – e.g. compaction of soils and thermic treatment;

c) permanent with new materials addition: combines changing permanently soils properties such as compaction with the addition of inorganic material – e.g. lime, cement, sand and gravel columns, metallic strips or geosynthetics.

2.1.1.1 Cement

The Building Research Establishment (2002) states that there are two types of binders: hydraulic and non-hydraulic. The first only needs water in order to set, whereas the second requisite the aid of a latent hydraulic material (i.e. pozzolans) and water to react. A hydraulic binder can stabilize any soil, given that the appropriate mixing of the materials is made, non-hydraulic binders usually react with the clay minerals of the soil resulting in the improvement of its geotechnical properties.

Cement is a hydraulic binder; therefore, its activation depends only on water contact to bind the soil as glue would. This binder does not alter the soil structure to the same extent as a non-

[1] SPARKES, M. M.; SMITH, R. G. Adobe Brick Construction, Office of Technical Services, **US Department of Commerce**, n. TAS98, 1945.

hydraulic binder. However, the soil might present dryness due to the water absorption during the hydration reaction (BUILDING RESEARCH ESTABLISHMENT, 2002).

Hall *et* al. (2012) highlight on their book chapter on soil stabilization and earth construction that the addition of cement on soil can reach amounts of 20% of the weight of dry soil. However, usually soil stabilizations do not surpass 10% of the dry weight. This kind of stabilization is more effective on low cohesion soils since the larger granular particles can be coated by the cement paste more easily than on cohesive clays.

Given that cement is the higher costing component on soil stabilization, usually many laboratory tests are conducted in order to decide the minimum necessary amount of this binding agent so it meets the design specification. In some cases, it is also necessary to establish the maximum cement content required to prevent retraction cracking (INGLES; METCALF, 1972). When cement hydration occurs, the stabilized soil will be more weather resistant. They also highlight that small amounts (from 2%) are already enough to permanently alter the soil properties, whereas, greater amounts of the binding agent change dramatically its properties.

According to the NBR 12553 (ABNT, 1992), for the use of soil-cement as a pavement layer, the ideal cement content for soil-cement mixtures is the one that reaches at least 2,1 MPa at a seven days curing period on unconfined compression tests.

2.1.1.2 Mechanical behaviour of cemented soils

The most common measurements of effectiveness for soil stabilization with cement are unconfined compression and durability tests (wetting and drying/freezing and thawing) (EL-RAWI *et* al., 1967; INGLES; METCALF, 1972; PORBAHA *et* al., 2000; CONSOLI *et* al., 2017 a, 2017 b). According Ingles and Metcalf (1972), the unconfined compression strength increases linearly with the percentage of cement added, however, at different rates for each given soil (figure 2.1). Regarding the durability of soil-cement materials, Consoli and Tomasi (2017) state that an increase in cement content provides a durability gain under wet/dry conditions.

Unconfined compression tests on cemented sands show that the strength gain has a direct relationship to the increase of cement content (PRIETTO, 1996; FOPPA, 2005; CONSOLI *et* al., 2007 a). However, Prietto (1996) also emphasises that other factors such as density, shape

and surface nature of the particle can influence the resistance of the soil-cement blend. A given cement amount can lead to different strengths for the same soil under different densities, or for same density and different nature soils.

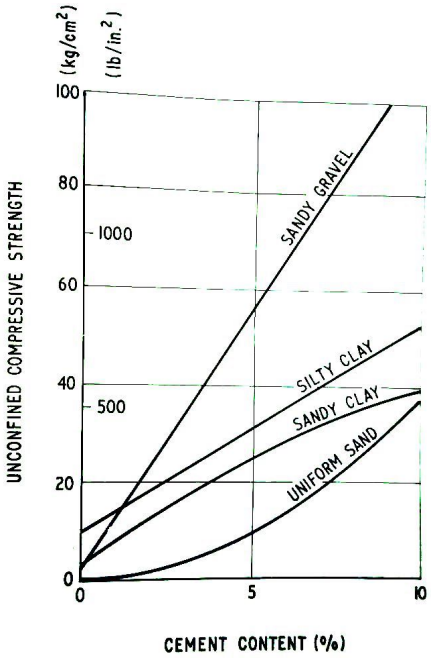

Figure 2.1: Relationship between unconfined compressive strength and cement content (INGLES; METCALF, 1972)

Studying the key-parameters controlling mechanical strength on cemented soils Foppa (2005) also concluded that small amounts of cement (1% to 7%) induce a considerable strength gain under unconfined compression tests. Moreover, the researcher affirmed that rate of strength gain increased with the increase in dry-unit weight of the compacted soil-cement, which indicates a greater efficacy of cementation in more compacted mixtures. This can be explained by the greater number of contacts between particles on more densely packed structures, which can lead to a greater probability of cementation on the particle bond.

The tensile strength of soil-cemented materials is of great interest for various cases in engineering designs and has been studied buy many researchers (Dass et. al., 1994; Specht, 2000; Consoli *et* al., 2011b; Viana da Fonseca *et* al., 2013). Usually the tensile strength of soil-cement mixtures reaches about 10% of the unconfined compression strength, given that both are moulded on optimum moisture content and maximum dry-unit weight (INGLES; METCALF, 1972; CLOUGH *et* al., 1981; DASS *et* al., 1994).

Regarding split tensile tests, Consoli *et* al. (2011b) evaluated the effect of the increase of cement content on three different soils – Osorio sand, Botucatu sand and Porto Sand. These researches also found a power function relationship between the amount of cement inserted in the mixture and the tensile strength increase observed.

Analysing stress-strain curves of artificially cemented sands with 4%, 6% and 8% of cement content under split tensile, unconfined compression and direct tension tests Dass *et* al. (1994) concluded that:

(a) for cement contents higher than 4% the direct tension test reached higher strength values than split tensile tests, and as the cement amount increased so did the difference between the tests. However, the tensile strain was the same for both tests under all studied cement ratios;

(b) the tensile and compressive strengths increase while the tensile and compressive strains decrease with the rise of cement content for all tests carried out;

(c) the relationship between tensile and compressive strength for both split tensile and direct tension tests were between 11 and 14%.

On studying the mechanical behaviour of cemented sands. Coop and Atkinson (1993) studied the effect of cementation on stress-strain behaviour of the mixture. The authors defined a framework of the behaviour of the cemented material, regarding its confining pressure and cement bond strength (figure 2.2). The researchers defined three classes:

(1) the mixture reaches its yield stress during isotropic compression: shearing produces similar behaviour to that observed on an equivalent non-structured soil;

(2) occurs when the mixture is subjected to intermediate stress states: bonds brake during shear, the curve for stress-strain shows a well-defined yield point after an apparent linear behaviour. The strength of the cemented material is controlled by the frictional component of the non-structured soil;

(3) the cemented soil mixture is sheared at low confining stresses, when compared to the bond strength. There is a peak in strength at low strains on the stress-

strain curves that is higher than the limit state surface of an equivalent non-structured soil.

The unconfined compression strength for cemented soil has a direct correlation to the degree of cementation of the material. In being so, the shear strength for the triaxial tests can be expressed as a function of the internal friction angle of the material on its non-structured state and its unconfined compression strength (PRIETTO, 1996).

Studying the stress-strain-strength behaviour of Botucatu silty sand with Portland Cement Schnaid *et* al. (2001) assessed that, for a given range of stresses, the shear strength can be represented by the Mohr-Coulomb envelope, defined by the cohesive intercept – function of the cementation – and a friction angle that does not seem to be affected by the cementation. The researches also suggest the existence of an ultimate state envelope that is not affected by the cementation, where the deviatory stress meets a constant value with the axial strain increase.

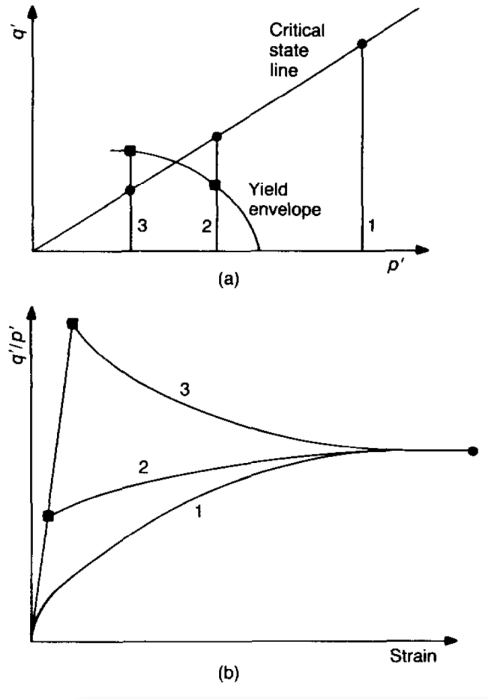

Figure 2.2: Idealized behaviour of cemented soils: (a) stress paths; (b) stress-strain behaviour (COOP; ATKINSON, 1993)

By analysing the effect of cementation on carbonated sands Huang and Airey (1998) concluded that the cementation is only effective for stresses below the pre-consolidation

stress. They evaluated that the cement addition causes a translation to the right of the normal compression line, which leads to an increase in the apparent pre-consolidation stress, resulting on a strength and stiffness of the material.

After conducting an experimental program on cemented soils Prietto (1996) states that the deviatoric stress at failure attained through conventional triaxial tests, for artificially cemented soils can be expressed by equation 2.1. Given that the following hypothesis are true:

(a) the failure envelope is linear;

(b) the friction angle of the cemented material is in the same order of magnitude of the non-cemented soil;

(c) the non-cemented soil is not cohesive.

The author applied this equation on various cemented soils available on the literature, and despite great range of densities, mineralogy and nature of cementing agents, there was achieved a great conformity between the empirical data and the predicted values (PRIETTO, 1996).

$$q_f = \frac{2 \cdot \sin \phi'}{1 - \sin \phi'} \cdot p_i' + q_u \qquad (2.1)$$

Where:
q_f = deviatoric stress at failure (kN/m^2);
ϕ' = internal friction angle of the uncemented soil (^{o});
p_i' = initial mean effective stress (kN/m^2);
q_u = unconfined compression strength (kN/m^2).

In soil-cement mixtures the air cannot be completely expelled, even after compaction. Thus, the use of the water/cement ratio applied for concrete dosage is not valid for soil stabilization. Larnach[2] (1960 apud LOPES JUNIOR, 2007) proposed a ratio between the volume of voids (V_v) and the volume of cement (V_{ci}), as presented on equation 2.2, while studying the relationship between dry density, void/cement ratio and strength of soil-cement mixtures,

[2] LARNACH, W. J. Relationship between dry density, voids/cement ratio and strength of soil-cement mixtures. **Civil Engineering and Public Works Reviews**, London, v. 55, n. 648, p. 903-905, 1960.

through the conduction of unconfined compressive strength (σ_c) and flexural strength tests at 7 curing days. Figure 2.3 illustrates the result attained by the author. The author also observed a direct relationship between σ_c and flexural strength tests.

This parameter has been largely studied for several soils, pozzolans and binding agents by the PPGEC of UFRGS (CONSOLI *et* al., 2010 a, 2011 b, 2013 a, 2013 b; FOPPA, 2005; LOPES JUNIOR, 2007; DALLA ROSA, 2009; SILVANI, 2013; SALDANHA, 2014; DE PAULA, 2016). This extensive research on the subject led authors to conclude that the rate in which the volume of voids – represented by the porosity (η) of the mixture – and the volume of cement – represented by the volumetric content of cement (C_{iv}) – do not progress at the same rate. Thus, the use of an exponent on the binding ratio is sufficient to adjust the relationship. Foppa (2005) researching a dosage method for the Brazilian silty sand, known as Arenito Botucatu, and early strength Portland cement concluded that for these materials the value of 0.28 is the ideal exponent.

$$\frac{V_V}{V_{ci}} = \frac{\text{Absolute void volume (water + air)}}{\text{Absolute cement volume}} \tag{2.2}$$

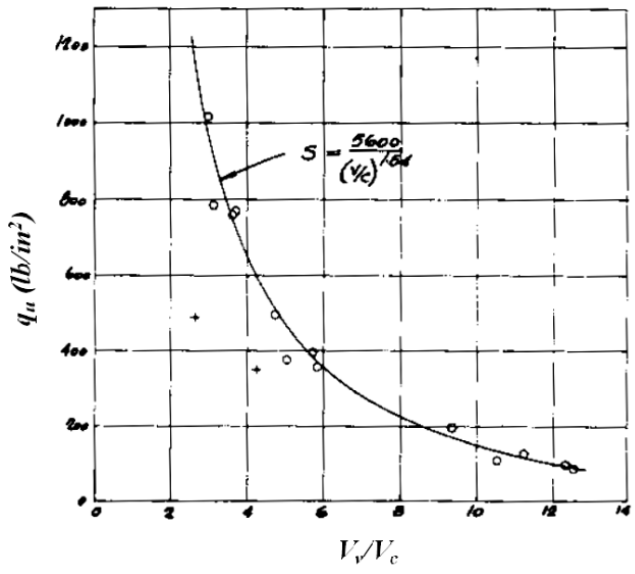

Figure 2.3: Volume of voids/cement *versus* simple compression strength (LARNACH[3], 1960 apud LOPES JUNIOR, 2007)

[3] LARNACH, W. J. Relationship between dry density, voids/cement ratio and strength of soil-cement mixtures. **Civil Engineering and Public Works Reviews**, London, v. 55, n. 648, p. 903-905, 1960.

Consoli *et* al. (2010 a), researching Osorio sand–cement mixture under a varied range of cement content and dry unit weights, demonstrated that the porosity/cement ratio (η/C_{iv}) is an appropriate parameter to evaluate the σ_c and the splitting tensile strength (σ_t) of soil-cement mixtures. The authors also call attention to the σ_t/σ_c ratio, that is a scalar independent from the η/C_{iv} ratio. Therefore, the dosage methodology can be used for either compression or tensile stresses, since they are interdependent. This independent ratio has also been found for different soils and cementing agents by Consoli *et* al. (2011a, 2013b).

Based on de aforementioned dosage method and σ_t/σ_c ratio, Consoli *et* al. (2013a) proposed a method for the assessment of the failure envelopes for cemented sandy soils. By assuming that σ'_{1c} equals to σ_c; σ'_{3c} equals to zero; σ'_{1t} equals to $-3\sigma_t$ and σ'_{3t} equals to σ_t for the Mohr-Coulomb failure theory, it is possible to conclude that ϕ' and c' for the failure envelope of the cement treated soil can be represented by the equations 2.3 and 2.4, respectively. The parameter Σ is presented in equation 2.5. The authors concluded that the proposed methodology was effective in determining the failure envelope for artificially and naturally cemented soils through simpler laboratory tests.

$$\phi' = \arcsin\left(\frac{1-\Sigma}{1-2\Sigma}\right) \tag{2.3}$$

$$c' = \frac{\sigma_c\left[1-\left(\frac{1-4\Sigma}{1-2\Sigma}\right)\right]}{2\cos\left[\arcsin\left(\frac{1-4\Sigma}{1-2\Sigma}\right)\right]} \tag{2.4}$$

$$\Sigma = \frac{\sigma_t}{\sigma_c} \tag{2.5}$$

Where:

ϕ' = internal friction angle of the uncemented soil (^{o});

c' = effective cohesion intersect (kN/m^2);

σ_c = unconfined compression strength (kN/m^2)

σ_t = splitting tensile strength (kN/m^2).

2.1.2 Soil reinforcement

The term soil reinforcement is used when an inclusion is inserted on the soil (e.g. fibres, rectangular strips, round bars, continuous sheets, etc.). However, the overall load deformation

performance of the system is dependent on the inclusion type – relatively inextensible or extensible (MCGOWN *et* al., 1978). For relatively inextensible inclusions (e.g. round bars) the term "reinforced earth" is proposed by Vidal (1969), whereas, for relatively extensible inclusions (e.g. fibres) the proposed term is "ply-soil" (MCGOWN; ANDRAWES, 1977).

The use of soil reinforcement is an ancient technique. On the old testament of the Bible (Exodus) the fundamentals of the system are mentioned, in which the mixture of straw and reeds with clay for the constructions of residencies is cited. These constructions have been known to exist since the 5^{th} and 4^{th} millennia B.C. The oldest remaining structures where soil reinforcement was used are the ziggurat in Agar-Quf (1000 B.C.) and the Great Wall of China (200 B.C.) (JONES, 1996). Despite the long utilization of soil improvement, Van Impe (1989) observes that from a technical point of view, this practise is still the most intriguing of the common executive methods used in civil engineering.

However, technical research as seen in the modern standards of the use of fibres as soil reinforcement begun a little over forty years ago. Said solution can be considered a relatively new research line, when compared to the more traditional composites used in civil construction such as concrete, for example. Gray and Ohashi (1983) highlight that research on the subject begun through the analysis of the influence of plant roots on the mechanical behaviour of natural slopes regarding its improvement in shear strength. They also state that fibre reinforcement is used nowadays for many purposes, such as retaining structures, embankments, base layer on footings and pavements sub-base.

As the mechanical behaviour of mixtures with fibre insertion is one of the main focuses of this research, a more detailed analysis of its behaviour will be carried out on topics to come.

2.2 FIBRE-SOIL COMPOSITES

In order to better understand fibre-soil composites and its possible applications in geotechnical engineering, it is necessary to understand its mechanical, physical and chemical properties and its interaction with the soil/soil-cement matrix. Thus, the aforementioned properties are discussed in this topic.

2.2.1 Fibres in reinforced soils

The major contribution of fibre reinforcement is on the post-cracking stage of the composite. In this stage, the fibres have a more effective roll on the resistance of the composite by increasing its capacity to absorb energy. This phenomenon is attributed to fact that the strain necessary to cause cracking of the cemented matrix is much inferior to the rupture strength of fibres, so it expected little to none increase in cracking strength (HANNANT, 1994; ILLSTON, 1994).

Fibre inclusion maintains the interface of cracks together, enhancing post-cracking mechanic properties (i.e. increasing ductility). That being said, the performance response of fibre composites depends mainly on: fibre content and length; the physical properties of fibre and matrix; and the fibre-matrix bond (HANNANT, 1994). Various authors also highlight the importance of fibre orientation on the matrix (GRAY; OHASHI, 1983; GRAY; AL-REFEAI, 1986; JOHNSTON, 1994).

Fibre insertion on a cemented matrix can lead to two important mechanical effects. The first is the strength reinforcement of the composite under different tensile stress loadings (e.g. indirect tension, flexural and shearing tests). The second is the improvement of the toughness of a matrix with fragile behaviour (JOHNSTON, 1994).

There are various types of fibres used in soil reinforcement. Its behaviour characteristics (physical, chemical and mechanical) affect the behaviour of the composite. These characteristics are intimately related to the fibre components and its manufacturing process (FEURHARMEL, 2000).

Fibres are classified in four main groups: natural (e.g. palm and coconut); polymeric (e.g. polypropylene, polyethylene and polyester); mineral (e.g. glass and carbon); and metallic (e.g. steel) (FESTUGATO, 2011). According to Hollaway (1994), the main parameters related to the performance of fibre on composite materials are: fibre content, fibre elastic modulus, fibre resistance, fibre length, fibre orientation, and fibre-soil interaction. Thus, it is presented in this section the experience accumulated over the years on the subject.

2.2.1.1 Fibre content

Gray and Al-Refeai (1986) state that the increase in fibre content can lead to an increase in the compaction effort (energy) of the mixture for a given porosity, which can cause greater

fibre entanglement and distortion that can disturb the mechanical response of the composite. However, after their experimental program, the authors concluded that the strength increased linearly for fibre amounts up to 2% of the weight, after which the fibre-reinforced soil reaches an asymptotic upper limit. Other authors also observed a linear increase of strength in fibre-reinforced soils with the increase of fibre content (MCGROWN *et* al., 1978; MAHER; HO, 1994; ULBRICH, 1997; SPECHT, 2000; VENDRUSCOLO, 2003; FESTUGATO, 2011). An increase in peak shear strength is also observed by the increase in fibre content, alongside with an increase of strain at failure and a considerable decrease in stiffness of the material (MICHALOWSKI; ZHAO, 1996).

2.2.1.2 Elasticity modulus of the fibre

Fibres with low elastic modulus behave as ideally extensible insertions, which means that the maximum rupture strain of the fibre is greater than the maximum tensile strain of the unreinforced soil. The addition of fibres with higher elastic modulus result in greater shear strengths, however, the strength gain is not proportional to the increase of the modulus of the fibre (GRAY; OHASHI, 1983). Nevertheless, greater roughness of the fibre is considered more important on strength gain then a higher modulus. The increase in roughness of the material provides an increase in friction between the matrix and the insertions (GRAY; AL-REFEAI, 1986).

Higher modulus fibres reduce the critical confining stress, which means that the fibres can be more easily pulled out from the matrix. Thus, low elastic modulus fibres have a higher resistance to pull out, but have smaller resistance to shear strength (MAHER; GRAY, 1990).

2.2.1.3 Critical confining stress

In fibre-reinforced soils there is a critical confining strength below which the insertions are pulled out (GRAY; OHASHI, 1983; TEODORO, 1999; MOREL; GOURC, 1997; HEINECK, 2002). This critical confining strength is sensible to some properties of composite materials: aspect ratio, uniformity coefficient, and shape of soil particles (MAHER; GRAY, 1990).

2.2.1.4 Fibre length/aspect ratio

The fibre length (l) and its relation to the fibre diameter (d), known as aspect ratio (l/d), have an important role on fibre-reinforced soils as was assessed by Gray and Ohashi (1983). The authors concluded that larger fibres increase the shear strength of the mixtures up to a threshold, above

which any further increase in fibre length has no effect. Later, Gray and Al-Refeai (1986) observed that fibre length is not as important as the aspect ratio on the behaviour of the composite material. The increase in aspect ratio provides a proportional increase in resistance. Moreover, Michalowski and Zhao (1996) concluded that a higher aspect ratio leads to higher peak in strength.

Festugato (2008) studying the mechanical behaviour of a fibre-reinforced Brazilian soil regarding different aspect ratios concluded the aspect ratio exerts a strong influence on composites behaviour. The following points are the main topics highlighted by the author.

(a) the greater the aspect ratio, the greater the strength gain ratio is;

(b) a higher aspect ratio leads to a decrease on the expansive tendency of the material;

(c) the aspect ratio do not alter the internal fiction angle of the composite;

(d) an increase in aspect ratio leads to an increase in the cohesive intercept;

(e) the critical confining stress value increases with the reduction of the aspect ratio.

2.2.1.5 Fibre orientation

Given that reinforced earth is a system that works only under tensile strength, the orientation of the inclusions is vital for the system to work (MICHALOWSKI AND ZAHO, 1996). Thus, the understanding of the stress/strain distribution of the engineering design on the soil is vital in order to properly use the reinforcement, especially if it is not randomly distributed on the matrix.

Gray and Ohashi (1983) proposed a theoretical model to predict the behaviour of a fibre-reinforced sand, through a series of direct shear tests with natural, synthetic and metallic fibres. In order to better understand the proposed model, figure 2.4 illustrates the model of long elastic fibres placed in the middle of the shear zone. The authors assume that the fibres are thin enough so they do not impose any resistance to bending during the shear process.

During the study the researchers considered different fibre orientations regarding the shear surface. As a result of the research the authors observed that a 60^{o} inclination with respect of the shear plane presented the greatest contribution to the strength gain. Also, the inclination of 120^{o}

generated a reduction of shearing strength. These results can be observed of figure 2.5 (GRAY; OHASHI, 1983).

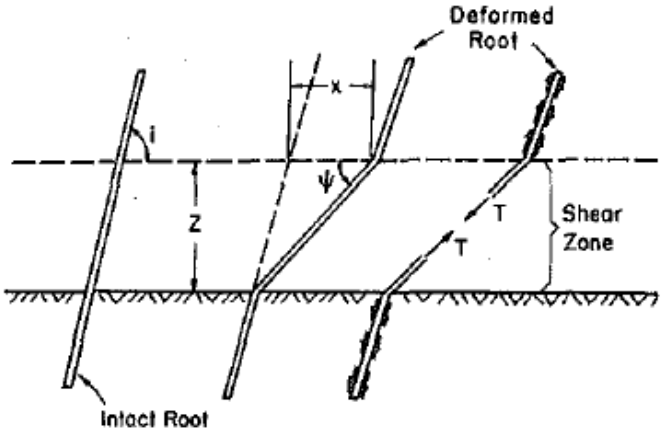

Figure 2.4: Fibre-reinforced model with fibres oriented at an angle regarding the shear plane (GRAY; OHASHI, 1983)

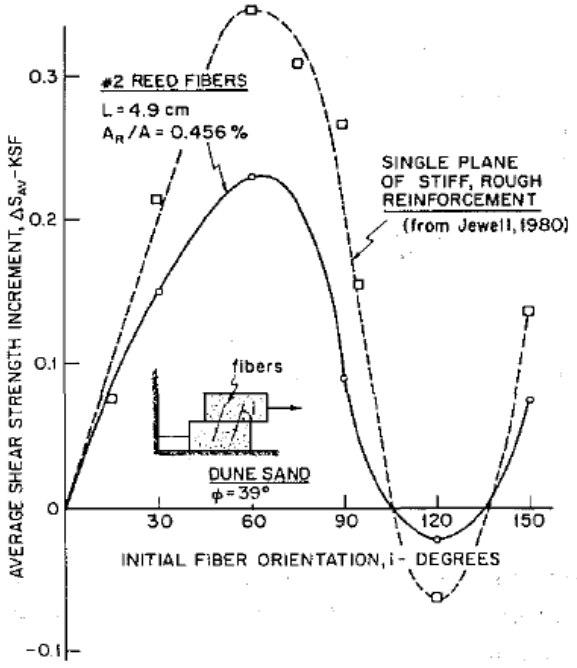

Figure 2.5: Shear strength gain regarding fibre inclination (GRAY; OHASHI, 1983)

Randomly distributed fibres, such as discrete short inclusions, are randomly oriented throughout the soil matrix. This way, avoiding a preferential failure plane. Such form of fibre distribution gives an isotropy to strength to the composite (GRAY; AL-REFEAI, 1986). However, this idealistic perspective of the problem is not true. Following the proposed distribution presented by

Michalowski and Cérmak (2002) – where it was proposed that the fibres are distributed anisotropically due to the compaction layers of the reinforced composite – Diambra *et* al. (2007), used an axisymmetric distribution with respect to the normal axis to the normal plane to assess the orientation of fibres distribution in reinforced sands (which usually coincides with the compaction process). Using the moist tamping technique (usual on reinforced earth), the authors concluded that 97% of the fibres are oriented between -45° to 45° regarding the horizontal plane. Which confirms Michalowski and Cérmak (2002) distribution theory and proves that the reinforced material studied is anisotropic having a near-horizontal distribution. In order to evaluate said distributions, the researchers employed the spherical coordinates presented in figure 2.6.

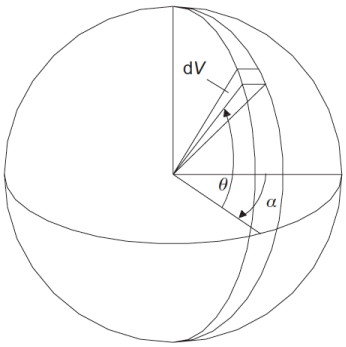

Figure 2.6: Sphere and coordinates used to define orientation distribution (DIAMBRA *et* al., 2007)

Michalowski and Cérmak (2002) propose that the fibre concentration can be represented by the equation 2.6. The authors state that any function can be used for ρ(θ), given that equation 2.7 is respected. A, B and n are constant, however only two of them are independent, and can be linked by equation 2.8.

$$\rho(\theta) = \bar{\rho}\ (A + B|\cos^n\theta|) \tag{2.6}$$

$$\bar{\rho} = \frac{1}{V}\int_V \rho(\theta)\ \mathrm{d}V \tag{2.7}$$

$$B = \frac{1 - A}{\int_0^{\pi/2}\cos^{n+1}\theta\ \mathrm{d}\theta} \tag{2.8}$$

Where:

ρ(θ) = volumetric concentration of fibres per infinitesimal volume;

V = total specimens' volume;

V_f = total volume of fibres;

$\bar{\rho}$ = average volumetric concentration of fibres (V_f/ V);

A = coefficient that represents the quantity of vertical fibres;

B = coefficient that represents isotropic behaviour.

2.2.1.6 Fibre-soil interaction

As mentioned on the previous topics, the interaction between fibre and soil matrix is influenced by various different properties of the fibre and the soil. So, it is of vital importance to the way in which the stress is transferred between the different phases. Hollaway (1994) states that when the reinforcement is under loading the fibres have two failure mechanisms: slip (pull out), or rupture due to tensile strength (fracture). The author also indicates the existence of a critical length (l_c) above that the fibre rupture will occur due to fibre rupture. Figure 2.7 presents said failure mechanisms.

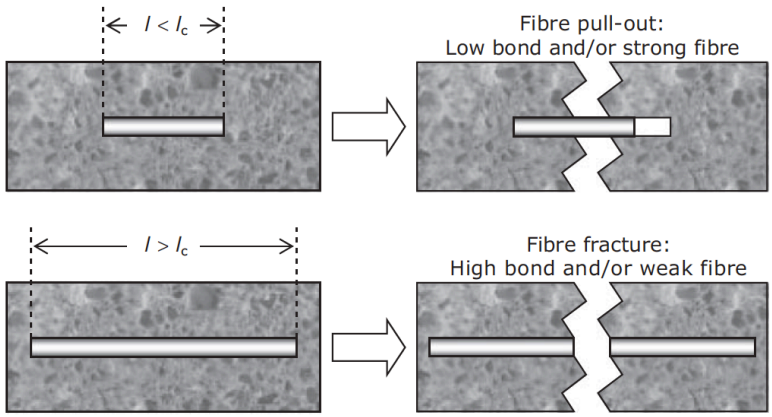

Figure 2.7: Fibre failure mechanisms (HOLLAWAY, 1994)

Michalowski and Zhao (1996) suggest that the aforementioned failure mechanisms may happen at the same time. This occurs due to the fact that not all the length of the fibre is mobilized by the tensile stress. Thus, the middle section of the fibre may break while the ends might slip. This phenomenon is illustrated on figure 2.8, where the stress distribution for a rigid-perfectly plastic fibre submitted to shear and axial stress distributions, respectively.

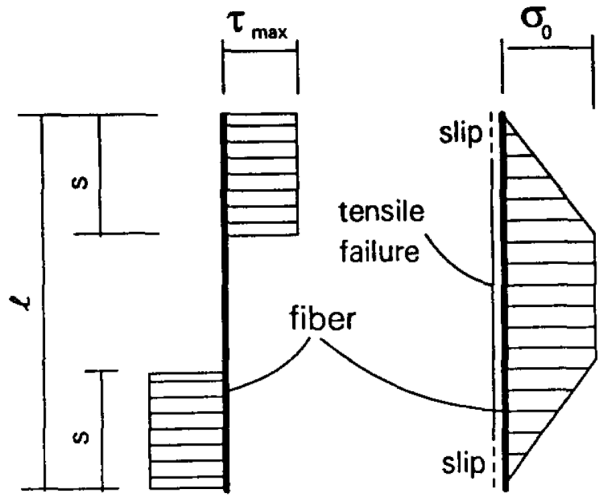

Figure 2.8: Stress distribution for fibre composites submitted to shear and axial stress distributions (MICHALOWSKI; ZHAO, 1996)

As can be observed in figure 2.8, when a fibre rupture occurs, a slip at both ends of the fibre happen. The length of said slip (s) is given by the equation 2.9. Pure slip only occurs when the length of the fibre (l) is smaller the two times the slip length (s) or, if the aspect ratio complies with equation 2.10 (MICHALOWSKI; ZHAO, 1996).

$$s = \frac{r}{2}\frac{\sigma_0}{\sigma_n \tan(\emptyset_w)} \tag{2.9}$$

$$a < \frac{1}{2}\frac{\sigma_0}{\sigma_n \tan(\emptyset_w)} \tag{2.10}$$

Where:

σ_o = fibre yield stress;

σ_n = stress normal to the fibre surface;

ϕ_w = sand/fibre interface friction angle;

s = fibre slip length;

r = fibre radius;

a = fibre aspect ratio.

Machado *et* al. (2002) studying constitutive models for landfills, proposed a simpler way of representing the fibre slip length (f_b). By introducing a dimensionless sliding factor that accounts for the imperfections of the interfacial bonds. The factor f_b is a relation between the

fibre strain and the composite strain. For $f_b = 1$ the factor represents perfect fibre-matrix bond and for $f_b = 0$ there is full sliding between the matrix and the insertions.

2.2.2 Mechanical properties of fibre-reinforced soils

There are many changes in the mechanical behaviour of the material due to fibre insertion. On the following topics are presented the main changes in the soil behaviour: compaction, strength, deformability, failure mode, volumetric variation, and initial stiffness.

2.2.2.1 Compaction

Studying the influence of polypropylene fibres insertion on a sandy gravel, Hoare[4] (1979) apud Festugato (2011) observed that the addition of fibres provides a resistance to compaction. For the same compaction energy, porosity increased linearly with the increase in fibre content used. Results from two different reinforcements pointed that compaction is influenced by soil-fibre interaction – aspect ratio, grain size distribution of the soil, shape and texture of particles and superficial area of the reinforcement.

Gray and Al-Refeai (1986) reported that the addition of fibre to a granular soil increased the compaction effort in order to achieve the same porosity. However, the authors highlight that a greater compaction effort leads to a higher entanglement and distortion of fibres, thus, modifying the reinforced soil response.

Maher and Ho (1994) observed that the inclusion of fibres on kaolinite, ranging from 0.5% to 4% by weight of dry soil, did not cause any significant variation in the maximum dry density or the optimum water content. The authors also did not observe any significant changes in these parameters when the fibre length was altered from 6.4 to 25.4 mm.

While studying the hydraulic and mechanical behaviour of geotechnical materials as impermeable barriers, Heineck (2002) carried out compaction tests with Botucatu sand with and without 24 mm polypropylene fibres. The author also did not observe a significant difference due to fibre inclusion on maximum dry unit weight and optimum water content.

[4] HOARE, D. J. Laboratory study of granular soils reinforced with randomly oriented discrete fibres. In: INTERNATIONAL CONFERENCE ON SOIL REINFORCEMENT, 1979, Paris. **Proceedings**. v. 1, p. 47-52, 1979.

2.2.2.2 Peak shear strength

Festugato (2011) stresses that fibres inhibit rupture associated cracks on fibre composites, which leads to an increase in the area bellow stress-strain curves. This property is called tenacity and represents the capacity of the composite in absorbing energy.

The fibre length influences the peak strength of reinforced soils. Teodoro (1999) observed that for a granular soil the increase in fibre length (up to 30 mm) provided an increase in strength. However, using the same fibres, but for a cohesive soil, the maximum strength gain observed was for 15 mm fibres.

Regarding the amount of fibre added to the mixture, Nataraj and McManis (1997) observed an increase in peak shear strength and the compressive strength of a reinforced sand and clay (figure 2.9). The same behaviour was noticed by Stauffer and Holtz (1995) when researching the difference in mechanical behaviour between continuous and staple fibres on fibre-reinforced sands.

Maher and Gray (1990) studied the effect of different fibre insertion (glass, rubber and natural) on soils with uniform grain size distribution but different average particle grain size (D_{50}). The researches concluded that an increase D_{50} from 0.25 to 0.6 mm did not affect the critical confining stress, however, the fibre contribution diminished regarding the peak strength of the composite.

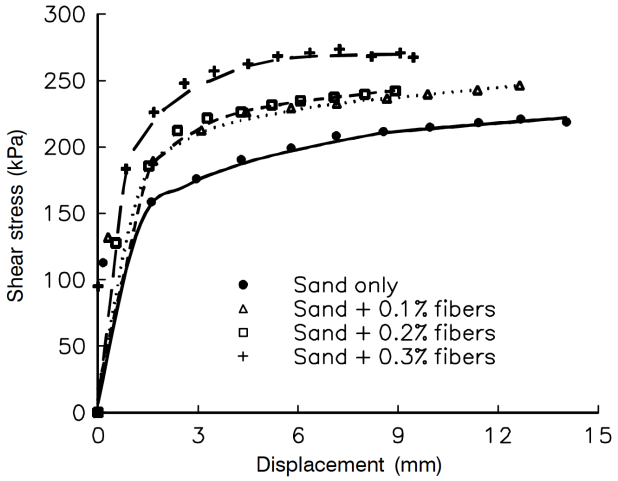

Figure 2.9: Shear stress-strain for fibre-reinforced and unreinforced sand (NATARAJ; MCMANIS, 1997)

Various scientists described an increase in the internal frictional angle and cohesive intercept of sands with an increase in fibre content (GRAY; OHASHI, 1983; NATARAJ; MCMANIS, 1997; STAUFFER; HOLTZ, 1995). Nevertheless, Casagrande (2001) studying the impact of fibre reinforcement of a silty sand observed only an increase in the cohesive intercept and no significant increase in the internal friction angle.

Vendruscolo (2003) affirmed that fibres could bestow a cohesive intercept as well as increase the internal frictional angle of sands. Nevertheless, for artificially cemented sands, the author concluded that fibres have a greater influence on residual cohesion and frictional angle. Consoli *et* al. (1998) found that the higher the cement content is, the smaller the effect of the fibre in strength gain is.

Heineck (2002) observed a bi-linearity of the failure envelope whilst studying a fibre-reinforced silty sand. The first part has a frictional angle over twice of the unreinforced soil and an almost null cohesive intercept. On the second, above the critical confining stress, the internal friction angle is almost the same as the unreinforced soil, and the cohesive intercept presents a considerable increase. A similar behaviour was observed by various other researchers through the years (GRAY; OHASHI, 1983; GRAY; AL-RAFAEI, 1986; MAHER; GRAY, 1990; SATUFFER; HOLTZ, 1995; KANIRAJ; HAVANGI, 2001) while studying the behaviour of fibre-reinforced sands, as can be observed in figure 2.10 by Maher and Gray (1990). Moreover, Gray and Al-Refeai (1986) observed that lower fibre roughness or lower interface friction, lead to higher critical confining stress. Rougher fibres result in a more effective increase in resistance.

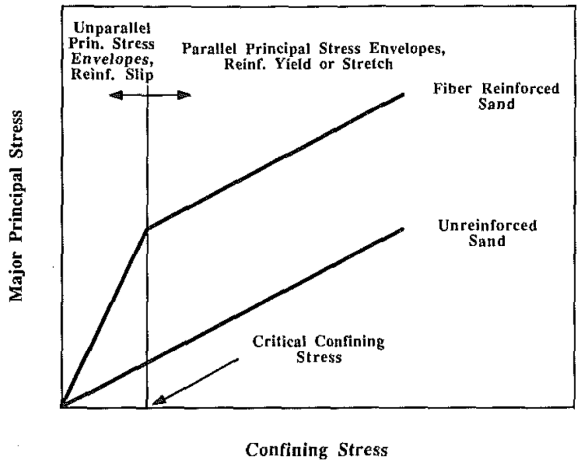

Figure 2.10: Effect of fibre inclusion on failure envelope of sand (MAHER; GRAY, 1990)

Consoli *et* al. (2007 b) studied different stress paths for drained triaxial tests for reinforced sands with randomly oriented polypropylene fibres. The authors demonstrated that the failure envelope, and consequently the strength parameters of the reinforced material are independent of the stress path applied during the triaxial tests. The adjusted failure envelope of the composite was bi-linear and it was not observed any fibre rupture, only fibre elongation.

2.2.2.3 Post-peak shear strength

Practically all studies that evaluated the behaviour of fibre-reinforced soils regarding strength of the composite concluded that the fibre addition mitigates the post-peak strength reduction (GRAY; OHASHI, 1983; GRAY; AL-RAFAEI, 1986; CONSOLI *et* al., 1997, 1998, 2003, 2007 a; DONATO *et* al., 2004; CASAGRANDE *et* al., 2006).

2.2.2.4 Deformability

Maher and Ho (1994) and Nataraj *et* al. (1996) observed an increase in the deformation modulus of fibre-reinforced clays with the increase in fibre content. On the other hand, Ulbrich (1997) noticed a decrease in the modulus with fibre insertion for fibre-reinforced sands.

The compression volumetric deformation during rupture is increased by fibre insertion. Said increase is more pronounced for poorly graded sands than for well graded ones, given that both sands have the same D_{50} particle grain size (STAUFFER; HOLTZ, 1995).

Regarding the deformation rate, Heineck (2002) and Heineck *et* al. (2003) concluded that the rate where the fibres begin to have an effective contribution to the shear strength gain is directly dependent on the matrix type.

Through reduced dimensions plate tests for reinforced sands, McGown *et* al. (1985) observed that a great portion of strain due to loading is recovered during unloading, being recovered almost 20% of the total imposed vertical settlement. The authors observed an increase in the elastic response of the material due to fibre insertion, especially where loading was repeated, highlighting the relevance of studying the deformation properties of these materials under cyclic loading.

Fibre inclusion has a great influence in the resilient modulus of reinforced materials. The studies carried out by Donato (2003) showed that fibres insertions have a significant impact

on the resilient deformability, reducing the resilient modulus in 65%. Researching the influence of polypropylene fibres on sand under cyclic triaxial loading, Florez *et* al. (2016) concluded that the addition of fibres controls the magnitude of the permanent deformations and the increase in pore pressure.

2.2.2.5 Failure mode

There was an increase in ductility for the fibre-reinforced soils was unanimously observed by various authors that studied the parameter (e.g. MCGOWN *et* al., 1978; MAHER; HO, 1994; CONSOLI *et* al., 1998; TANG at al., 2007). The observed increase in ductility was more pronounced for higher fibre contents.

Specht (2000) studying the influence of different fibres insertion (filaments and mesh) on an artificially cemented soil found that with the addition of more malleable fibres (filaments), the fragile behaviour of the cemented material became ductile. For the more rigid insertion it was not noticed a modification of the rupture mode.

According to Feuerharmel (2000), soil failure is altered by the insertion of polypropylene fibres, since it reduces the fragility of the cemented composite. The level of impact of the insertion is controlled by the adhesion between fibre and matrix. This adhesion can be achieved by the reaction of cementing agent, that provides a strong cemented structure, or by the combination of fibre length and the acting mean normal effective stress.

The same increase in ductility was observed by Donato (2003) where all cemented mixtures presented a fragile failure. However, through the addition of 0.5% of polypropylene fibres respect the dry weight of materials, the specimens presented a change in the failure mode, displaying a ductile failure mode.

Donkor and Obonyo (2016) using of polypropylene fibres additions to a cement stabilized sand under flexure tests noticed two failure modes: single crack that exhibited deflection-softening; and multiple cracks that presented deflection-hardening behaviour. On the first, there is a decrease in resistance after the cracking of the specimen. On the latter, an increase in tensile strength (hardening) is observed even after rupture.

2.2.2.6 Volumetric variation

Fibre insertion increases the compression volumetric strains at failure. The aforementioned increase is more pronounced for uniform then for well-graded sands, given that both present the same average particle diameter (STAUFFER; HOLTZ, 1995).

Through a series of isotropic compression tests, Consoli *et* al. (2005) verified that fibre inclusion significantly affects the compressive behaviour of an uniform sand. The insertion of fibres changed the placement of the Isotropic Compression Line. The authors stated that when a reinforced material is subjected to isotropic compression, the relative movements of the grains under high stresses leads the fibres to have plastic tensile deformations that can induce its rupture.

2.2.2.7 Initial Stiffness

Some researchers found that the deformation modulus increased with the amount of fibre added for sands (MCGOWN *et* al., 1985) and for clays (MAHER; HO, 1994). On the other hand, other scientists attained a reduction on the modulus due to fibre inclusion (CONSOLI *et* al., 1998; CASAGRANDE, 2001).

Michalowski and Cérmak (2002) observed an increase in initial stiffness due to steel fibre insertion, however, for a synthetic fibre the content increase led to a decrease in initial stiffness. Feuerharmel (2000) observed that the insertion of fibres in the soil matrix also could alter the elasticity modulus. Studying a clay, a silty sand, a sand the author found that soil characteristics also influences in the initial modulus of the composite, decreasing for clay and silty sand, and not presenting alteration for sands. However, through the addition of cement, all three soil mixtures presented an important decrease in the initial modulus after fibre addition. Thus, it can be concluded that the effect of fibre addition on the initial stiffness of fibre-reinforced soils depends on its characteristics.

Dynamic tests using bender elements carried out by Heineck (2002) did not account any variation in G_0 (initial shear modulus at very small strains) in a sand reinforced with fibres. Festugato (2011) also did not observe any significant changes in G_0 for a polypropylene fibre-reinforced tailing.

2.2.2.8 Unconfined compressive strength

Analysing the unconfined compression strength of a sandy clay reinforced with three different synthetic fibres, Freitag (1986) concluded that the insertion of fibres provided an increase in

strength if the mixture had a moisture content higher then the optimum. However, higher strengths were observed for moisture content slightly lower then the optimum. In this case, it was not noticed a great difference between soil and fibre-reinforced soil.

Tang *et* al. (2007) evaluated the inclusion of polypropylene fibres for a cemented and uncemented fine soil. Through a series of unconfined compression tests (q_u) the authors stated that fibre addition provides an increase in peak strength, decreases stiffness and the loss of post-peak strength observed on cemented and uncemented soils. Just as observed for tests with confining stresses. It is also highlighted that the "bridge effect" due to fibre insertion impedes further development of tension cracks and soil deformation. However, the cementation process confers to the composite a stronger bonding between the fibre/matrix interfaces.

The unconfined compressive behaviour of fibre-reinforced cemented material has been studied by the geotechnology laboratory (LEGG) of UFRGS aiming to evaluate the validity of fibre insertion on the η/C_{iv} parameter. Consoli *et* al. (2010b) conducted an experimental program studying the behaviour of polypropylene fibre insertion on a Portland cement stabilized silty sand. The authors stated that the fibre insertion provided an increase in the unconfined compressive strength of the cemented soil. Also, they concluded that the η/C_{iv} is a suitable parameter for the dosage of this composite and that the fibre inclusion did not alter the volumetric cement ratio exponent of 0.28. It was observed that the strength increased with the reduction of the porosity as can be seen in figure 2.11.

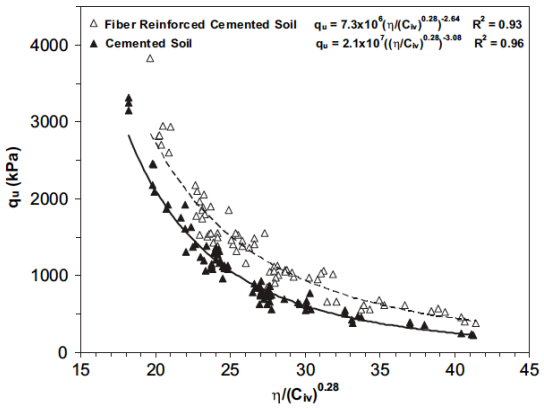

Figure 2.11: Unconfined compression strength versus porosity/volumetric cement ratio of unreinforced and fibre-reinforced Botucatu sand (CONSOLI *et* al., 2010b)

2.2.2.9 Unconfined tensile strength

Maher and Ho (1994) carried out an extensive research on the mechanical behaviour of fibre-reinforced clay. Regarding splitting tensile strength (q_t), the insertion of fibres increased significantly the tensile strength. An increase in moisture content and also in fibre length reduced the fibre contribution to strength gain. As for flexural strength, using the third-point loading method, the addition of fibres act as crack inhibitor, increasing the composites toughness.

Tensile strength under split tensile tests for 24 mm polypropylene fibre-reinforced, cemented Botucatu sand, increased with fibre insertion. Also, η/C_{iv} is a suitable parameter for the dosage of this composite under this loading. As for unconfined compressive strength, fibre inclusion did not alter the volumetric cement ratio exponent of 0.28. Strength increased with the reduction of the porosity as can be demonstrated in figure 2.12 (CONSOLI *et* al., 2011a).

Comparing unconfined compressive strength to split tensile strength for the same aforementioned soil an addition, Consoli *et* al. (2013b) observed that the relationship between q_t and q_u constant, and for this composite is 0.14. This relationship is true for all studied cementation range and fibre content studied, as can be seen in figure 2.13.

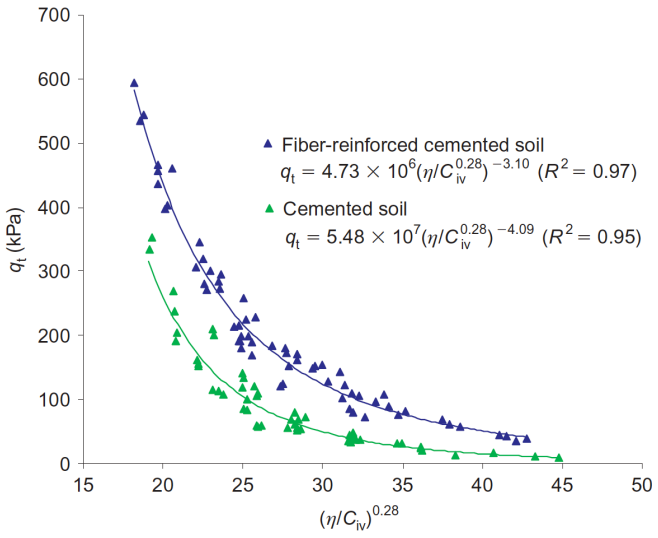

Figure 2.12: Split tensile strength versus porosity/volumetric cement ratio of unreinforced and fibre-reinforced Botucatu sand (CONSOLI *et* al., 2011a)

Using steel and polypropylene fibres to improve the mechanical behaviour of an artificially cemented soft clay, Sukontasukkul and Jamsawang (2012) studied the flexural performance of the composite. It was noticed an increase in the flexural strength after first crack due to fibre insertion and a great energy absorption of the fibres, meaning that the post-peak behaviour of the material was a lot more ductile then of non-reinforced specimens. The energy absorption is dependent in fibre length and type, being more efficient in polypropylene fibres, given its highly deformable characteristics.

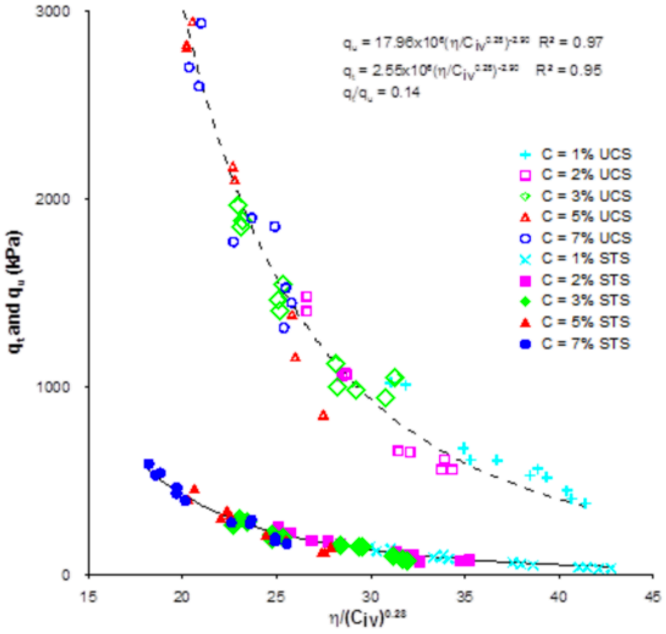

Figure 2.13: Comparison of q_u and q_t versus porosity/volumetric cement ratio of unreinforced and fibre-reinforced Botucatu sand (CONSOLI *et* al., 2013b)

Donkor and Obonyo (2016) investigated the applicability of polypropylene fibres addition in Portland cement stabilized sand as compressed soil blocks. The addition of randomly distributed fibres into the matrix improved the flexural performance of the composite by preventing catastrophic failure, significantly deforming after the peak strength but not collapsing. Being the impact more important for fibre content between 0.6 and 0.8% and declining thereafter.

2.3 FIBRE COMPOSITES UNDER CYCLIC LOADING

Cyclic loading generally refers to loads that present a clear pattern of repetition. It is characterized by regularity in amplitude and return period. The nature of this loading pattern can have an environmental or anthropogenic origin. The first consists primarily of seasons, waves, tide, current, wind, earthquakes; the latter of traffic, blasting operations and rotating machinery (ANDERSEN *et* al., 2013). The characteristics of loading type can be as diverse as its magnitude as can be observed on figure 2.14.

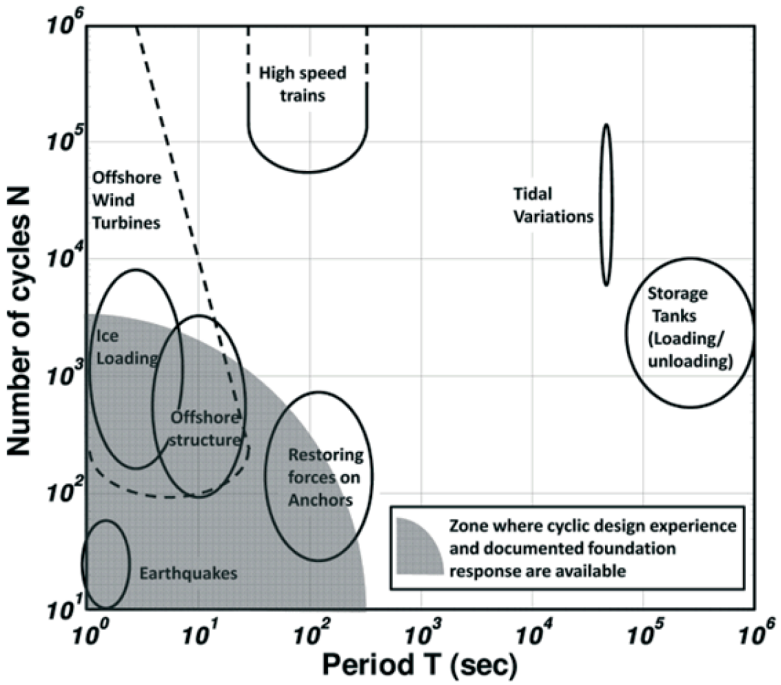

Figure 2.14: Periods and number of cycles characterising typical cyclic loading events (ANDERSEN *et* al., 2013)

The usual practice is to conduct a series of uniform cyclic load or displacement, applying a fixed frequency and amplitude. Said regular cycle testing are defined by number of cycles, period, average load and amplitude or displacement (ANDERSEN at al., 2013). Regarding load pulse form, in practice it is used three forms: haversine, triangular and square. For cyclic triaxial tests the required pulse form is haversine (ASTM D3999, 2011 a; ASTM D5311, 2011 b).

Monotonic loading creates continuously larger cracks (damage). Cyclic loading, however, generates intermittent damage. This means that during the loading period damage increases, and during unloading the damage remains constant (MEDINA; MOTTA, 2005). Being so, the

cyclic loading produces material failure by periodically repeated stresses that are lower than the attained under static loading.

According to ASTM E 1823 (ASTM, 2013) fatigue is defined as:

> "the process of progressive localized permanent structural change occurring in a material subjected to conditions that produce fluctuating stresses and strains at some point or points and which may culminate in cracks or complete fracture after sufficient number of fluctuations."

Stinchomb and Reifsnider (ASTM, 1979) emphasize the complexity of understanding and difficulty of describing the mechanisms of fatigue damage. The damage state of a composite is influenced by matrix, fibre, interfacial damage, and interaction and combination between phases. Investigations show that the state of damage is also extremely reliant on geometry, stress state, load history and environment.

Medina and Motta (1997) proposes three stages which materials subjected to cyclic loading conventionally present (figure 2.15). The first stage (I) is where the first micro cracks form, the strain grows, and irreversible damage begin; The second (II) is characterized by macro cracks, originated by the merger of micro cracks; The third (III), presents the development of macro cracks leading rapidly to total collapse.

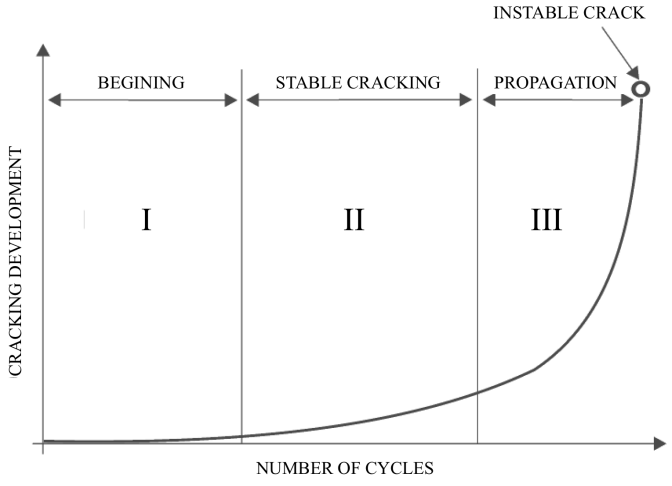

Figure 2.15: Fatigue failure stages (adapted from MEDINA; MOTTA, 1997)

Maher and Woods (1990) carried out laboratory resonant-column and torsional tests on fibre-reinforced sand aiming to determine its dynamic response, through shear modulus (G) and

damping (D). It was concluded that fibres have a significant influence on the dynamic response of sands. The increase in confining stress decreased the fibres influence on the shearing modulus, but did not significantly increase its contribution on damping. Both parameters increased linearly with the increase of fibre content up to 4% of dry weight, after which an asymptotic plateau is reached. The aspect ratio and elasticity modulus of fibres increase lead to an increase in shear modulus of the composite. However, only the aspect ratio provided an increase in damping.

Regarding cyclic behaviour of fibre-reinforced cemented sand, Maher and Ho (1993) evaluated cyclic compression behaviour of the composite. It was observed a resistance gain compared to non-reinforced sand, both number of cycles and magnitude of strain increased due to fibre insertion. For 0.5% fibre addition the authors observed a 4 times increase in the number of cycles and an increase in strain of 1.1 times.

Specht (2000) carried out a series of laboratory tests – unconfined compression, split tensile, flexural, fatigue, resilient modulus, and triaxial tests – in order to evaluate the behaviour of an artificially cemented silty sand reinforced with two different synthetic fibres, aiming to employ the composite as pavement base-course layer. The author concluded that the fibre addition leads to a reduction in resilient modulus and an increase in fatigue number of cycles.

Li and Ding (2002) studied fibre-reinforced silt under cyclic triaxial loading at small strains. The authors highlighted that fibre insertion provides a higher linear elastic modulus, however, loading repetition deteriorates the modulus.

The use of artificially cemented soil reinforced with cellulose fibres for road construction was evaluated by Khattak and Alrashidi (2005). Through cyclic indirect tensile tests at 1 Hz using 10% of dry soil weight of cement, 0.15% of fibres regarding the cement weight with aspect ratio of 200 and tensile strength of 500 MPa. The authors reported an increase or stagnation of the resilient modulus.

Festugato (2011) studied the behaviour of a polypropylene fibre insertion on a Portland cement stabilized sand observed under cyclic simple shear tests. The author observed an increase in shear modulus and a reduction of cycles to the beginning of the more pronounced exponential strain tendency.

2.4 PLASTICITY AND CRITICAL STATE THEORIES

The base for the model proposed in this research to predict the behaviour of the composites studied is based on critical state theory, thus making it important that its concepts are understood. Critical state theory is based on the application of plasticity theory to soil mechanics. Therefore, a basic overview of plasticity theory and critical state theory are presented next.

2.4.1 Plasticity theory

The concept of plasticity theory was first developed to describe the permanent strain observed on metals. In being so, the concept is easier understood when a metal is analysed. However, the understanding of such concept for soil mechanics is very important (BRITTO; GUNN, 1987).

Reversibility, rather than the linearity, is what determines if a material presents an elastic or plastic behaviour. In order to exemplify this, figure 2.16 presents the idealized concept as a stress-strain curve developed for metals. From the graph is possible to observe the following:

(a) when a metal is loaded between OA: the unloading process of the metal follows the same path, which is known as elastic behaviour;

(b) when the material is stressed until point B: the material still presents an elastic behaviour but non-linear. After point B the material enters the plastic realm, thus, point B is known as the yield point;

(c) when the material is subjected to further loading (point C): permanent deformation ensues constituting plastic behaviour;

(d) when the material is unloaded after point C is reached: a different unloading path will be followed (CD). A plastic strain is observed (OD) and cannot be recovered;

(e) when reloaded (DC): an elastic strain (DE) is presented, thus, point C becomes the new yielding point of the material. This phenomenon of increasing the yielding point of a material is known as hardening.

Even though the behaviour observed for soils is more complex than the ones presented for metals, an analogue plastic behaviour has been proven to be adequate to represent the plastic behaviour of soils. In order to do so it is necessary to take into consideration the following three statements (BRITTO; GUNN, 1987).

(a) yield function: generalizes the concept of the yield stress previously described for two-and three-dimensional stress states;

(b) flow rule: relative magnitudes of the incremental plastic strains during the yielding process;

(c) hardening law: relationship between material hardening and the plastic strain undergone, or the work exerted on the material during yielding.

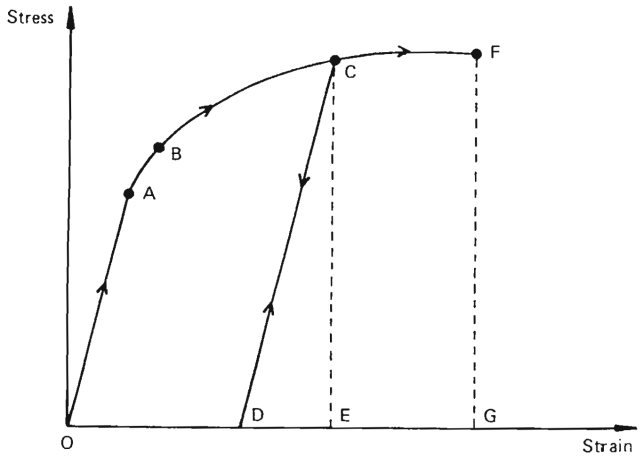

Figure 2.16: Stress-strain curve typical for many metals
(BRITTO; GUNN, 1987)

2.4.2 Critical state theory

A brief literary review is presented on the following topic regarding critical state theory based on the work published by Schofield and Wroth (1968), Atkinson and Bransby (1978) and Atkinson (1993).

Critical State is defined by the state where a stable limit – where the strength and void ratio reach a plateau and do not vary – is reached. In being so, the soil behaves as a fluid and the effective mean stress values are also constant. The critical state can be expressed mathematically by equation 2.11.

$$\frac{\partial q}{\partial \varepsilon_1} = \frac{\partial p'}{\partial \varepsilon_1} = \frac{\partial e}{\partial \varepsilon_1} = 0 \tag{2.11}$$

where:
q = deviatoric stress;
p' = mean effective stress;
e = void ratio;
ε_1 = shear strain.

The basic compressive mechanism following this theory happens in soils occurs through grain rearrangement. For granular soils this mechanism can be accompanied by particle breakage, as for cohesive soils the phenomena can be accompanied by contraction or expansion of the particles.

When considering isotropic loading, it is common to represent the behaviour on the ν - ln p' plane. Usually, compression and expansion are represented in an idealized form as linear tendency for sands and clays. These tendencies are represented by q and p', that are stress invariants used to describe the current state of specimens as well as the specific volume ν. The aforementioned parameters are represented in equations 2.12, 2.13 ad 2.14.

$$q = (\sigma'_a - \sigma'_r) \tag{2.12}$$

$$p' = \tfrac{1}{3}(\sigma'_a + 2\sigma'_r) \tag{2.13}$$

$$\nu = 1 + e \tag{2.14}$$

where:
q = deviatoric stress;
p' = mean effective stress;
e = void ratio;
ν = specific volume.

On figure 2.17 it is presented the behaviour of the isotropic loading of materials. It can be observed that during the unloading the soil presents a more rigid behaviour than the seen during the first loading, given that the material already suffered a great plastic deformation.

Line AO presents the first loading and is known as Normal Compression Line (NCL), shown in equation 2.15. The BC line is known as the expansion curve and is expressed by equation 2.16. The parameters λ, κ and N are constant for each soil, thus, there is a unique NCL defined by them. From equations 2.15 and 2.16 it is possible to calculate the state of the specimens at any given moment during isotropic loading.

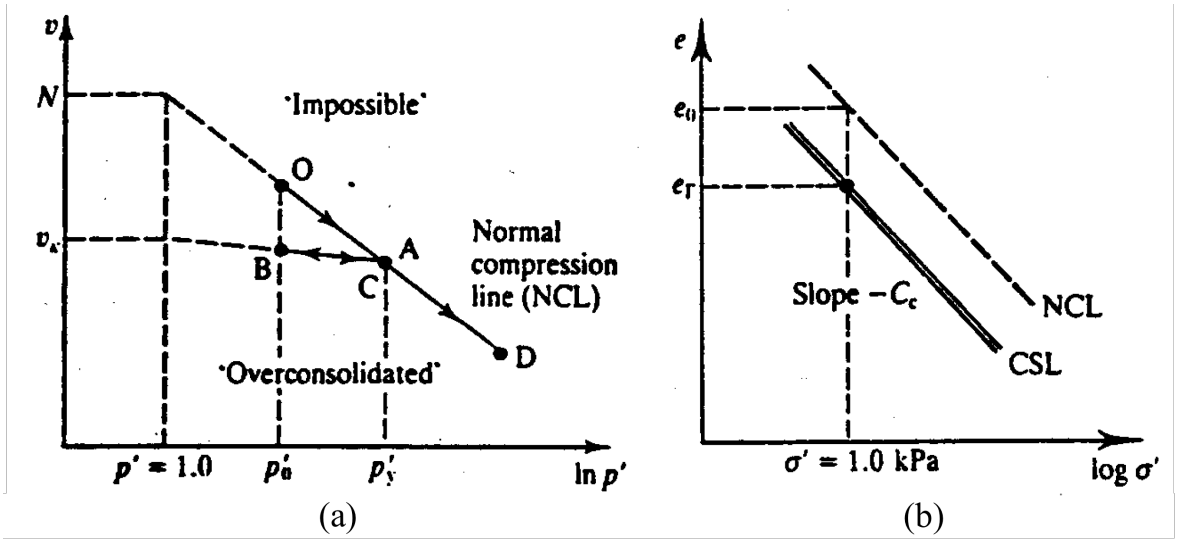

Figure 2.17: Critical state theory (a) Normal compression line (b) critical state line (adapted form ATKINSON, 1993)

$$\nu = N - \lambda . \ln p' \tag{2.15}$$

$$\nu = \nu_{\kappa} - \kappa . \ln p' \tag{2.16}$$

Where:

ν = specific volume;

N' = value of ν for p' = 1 kPa for NCL;

p' = mean effective stress;

λ = gradient value for NCL;

ν_k = value of ν for p' = 1 kPa ;

κ = gradient value for expansion curve.

Considering figure 2.17 (a), a soil isotropically loaded follows the OD line. When unloaded, the soil follows the AB line, known as expansion line. It is important to note that a soil will never be on a state at the right side of the NCL, thus, this line represents the limit between possible and impossible states. After loading, if a material is on the NCL, it is considered normally consolidated (NC). If the soil is on a state on the left of the NCL, the soil is considered overconsoliated (OC). Following this train of thought, point C represents the maximum stress experienced by the soil (p'_y).

The critical state line (CSL) can also be represented in the ν-ln p' space. It is a parallel line to the NCL and can be expressed by equation 2.17.

$$\nu = \Gamma - \lambda \ln p' \tag{2.17}$$

where:
ν = specific volume;
Γ = value of ν for p' = 1 kPa for CSL;
λ = gradient value for NCL;
p' = mean effective stress.

Considering equation 2.17, Γ defines the localization of the CSL similarly to N that defines the NCL localization. The projection of the CSL on the q - p' plane is described by the line represented in equation 2.18. For triaxial compression, M is defined by equation 2.19.

$$q = \mathrm{M} p' \tag{2.18}$$

$$\mathrm{M}_c = \frac{6 \operatorname{sen} \phi'}{3 - \operatorname{sen} \phi'} \tag{2.19}$$

where:
q = deviatoric stress;
M = slope inclination of the CSL in the *q-p'* plane;
p' = mean effective stress;
M_c = slope inclination of the CSL in the *q-p'* plane for triaxial testes;
ϕ' = effective friction angle.

The CSL represents a limit for all possible states during isotropic compression. Specimens on the right of the CSL, also known as the humid side, will compress during shearing and will not present strength peaks (normally consolidated, or lightly overconsolidated clays and loose sands). However, if a soil is initially on the left of the CSL (known as the dry side), it will expand after a small contraction during shearing (heavily overconsolidated clays and dense sands). The peak envelope represents a limit to all possible states, since it represents the maximum strength points by definition (figure 2.18 (a)). It is important to note that for each specific volume there is a peak envelope and that together, all possible points form a surface on the three-dimensional space q - p'- ν. This surface can be observed on figure 2.18 (b).

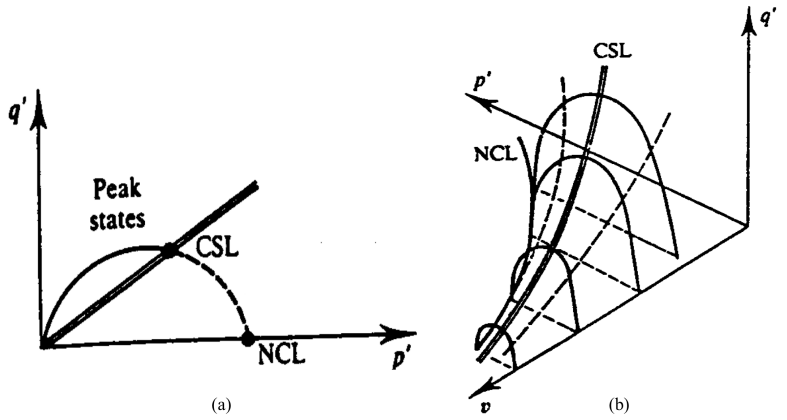

Figure 2.18: Critical state theory (a) peak states envelope (b) state limit surface (adapted form ATKINSON, 1993)

In conclusion, this method states that if during shearing the soil is within the limit state surface, all deformations are considered as purely elastic. When the soil is on the limit surface, elastic and plastic deformations happen simultaneously. It is important to highlight that this model portraits an idealized behaviour and in reality inelastic strains occur inside the limit state surface.

2.4.3 State parameter

Analysing the behaviour of various sands with different amounts of fines, it was observed that if the sands were in similar state regarding the critical state the soil behaved similarly. With this information, Been and Jefferies (1985) proposed a state parameter that represents the behaviour of granular soils by considering the void ratio and stress level of the soil.

This state parameter is defined as the difference between the void ratio of the granular material and its void ratio at critical state for the same mean effective stress. This relationship remains valid when using specific volume. From this parameter it is possible to infer that soils with positive values of state parameters are loose sands; sands with negative values are dense. The state parameter is related to various properties of sands (friction angle, dilatation, etc.). Thus, this parameter has a wide range of applicability for practical engineering designs (BEEN; JEFFERIES, 1985). Yu (2006) reinforces this notion by emphasizing that simplifications can be made by the application of this parameter in constitutive models such as Cam clay.

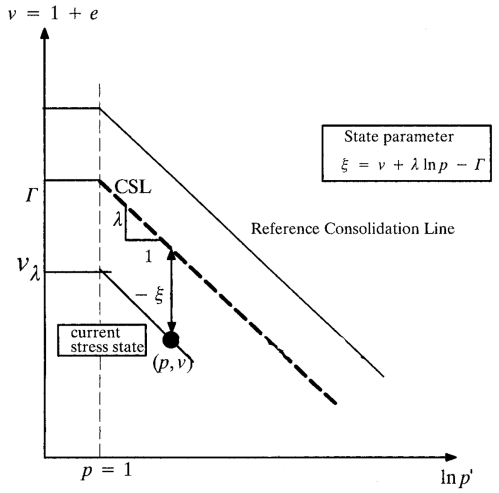

Figure 2.19: Representation of state parameter
(adapted form Yu, 2006)

2.4.4 Cam clay model

The Cam Clay model is the base of many constitutive models for soils. It was developed for clays, being considered the first hardening plastic model. This is an elastic-plastic model, thus presenting elastic properties, yield surface, plastic potential and hardening rule (MUIR WOOD, 2004; MUIR WOOD, 1990).

Figure 2.20 presents a typical oedometric test response. From this test, it is possible to observe two trend lines that meet at a point (“knee”). This point where the lines meet is known as the preconsolidation pressure. This pressure identifies the vertical effective stress history of the soil. The trend line of the left of the preconsolidation stress represents the reloading line of the soil, meaning that the soil has already experienced these stresses and,

therefore, present lower deformations. The behaviour presented after the preconsolidation stress is for stresses never experienced before by the tested soil, also known as virgin compression line. If the soil is unloaded after being on the virgin compression line, the response of the material will be parallel to the line on the left of the preconsolidation stress. Also, the stress where the soil was unloaded becomes the new preconsolidation stress of the material. From this graph, it is possible to obtain the necessary parameters for the Cam Clay elastic properties, as shown in equation 2.20 (DAVIS; SELVADURAI, 2002).

Based on the soil response to this test behaviour, the Cam Clay model considers a linear relationship specific volume and the effective mean stress. Equation 2.20 has a close relationship with the bulk modulud (K) as shown in equation 2.21. The second elastic constant can be obtained with equations 2.22 and 2.23 (MUIR WOOD, 2004; YU, 2006).

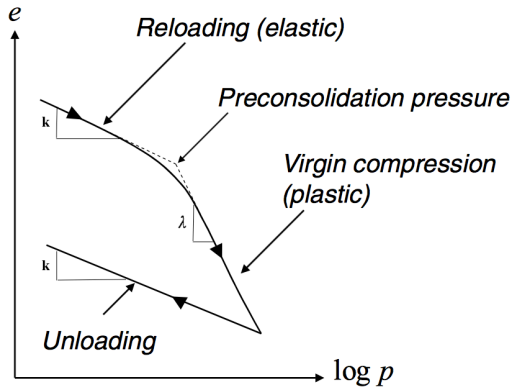

Figure 2.20: Typical soil response to an oedometric test
(DAVIS; SELVADURAI, 2002)

$$\dot{\varepsilon}_p^e = \kappa \frac{\dot{p}'}{\nu p'} \tag{2.20}$$

$$K = \frac{\dot{p}'}{\dot{\varepsilon}_p^e} \tag{2.21}$$

$$G = \frac{3\,(1-2\mu)}{2\,(1+\mu)} K \tag{2.22}$$

$$\mu = \frac{3K - 2G}{2G + 6K} \tag{2.23}$$

where:

ε^e_p = incremental elastic volumetric strain;

κ = elastic parameter of Cam Clay;

ν = specific volume;

p' = incremental mean effective stress;

K = bulk modulus;

G = shear modulus;

μ = Poisson ratio.

The elastic properties attained through the aforementioned equations of the Cam Clay model can be used to express the yield surface (f). This model considers that the soil has an associated flow rule, which means that the plastic potential (g) is identical to the yield surface. The Cam Clay yield surface is presented in equation 2.24 and graphically on figure 2.21 (YU, 2006; DAVIS; SELVADURAI, 2002).

$$f = g = \frac{q}{Mp} + ln\left(\frac{p}{p_0}\right) = 0 \tag{2.24}$$

where:

q = deviatoric stress;

M = slope inclination of the CSL in the *q-p'* plane;

p_o = preconsolidation stress;

p = mean stress.

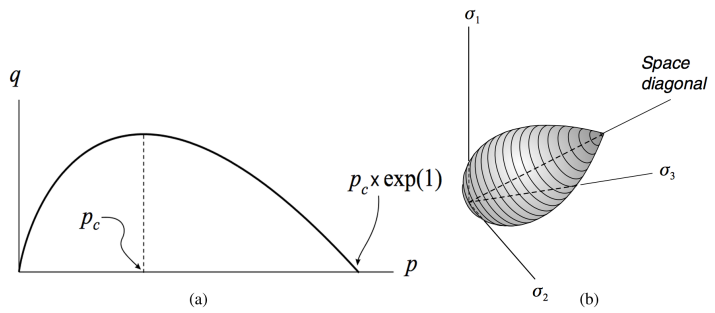

Figure 2.21: Yield surface of Cam Clay model (a) q:p' plane
(b) principal stress plane
(adapted form DAVIS; SELVADURAI, 2002)

Observing figure 2.21, it can be inferred that the preconsolidation stress controls the size of the yield surface, thus, p_0 changes with the plastic volumetric strain following the hardening rule (equation 2.25). Besides this, it is important to notice that variations in mean pressure do not lead to plastic strains, as shown in equation 2.26 (MUIR WOOD, 1990).

$$dp_0 = \frac{\nu p_0}{\lambda - \kappa} d\varepsilon_p^p \tag{2.25}$$

$$\frac{dp_0}{d\varepsilon_q^p} = 0 \tag{2.26}$$

where:

p_o = mean effective stress;

ε^p_p = plastic volumetric strain;

ε^p_q = plastic shear strain;

ν = specific volume;

κ = elastic parameter of Cam Clay;

λ = gradient value for NCL.

Historically, the Cam Clay model represented a big advance for geotechnical models. However, this model still presents some shortcomings. Other models, such as the modified Cam Clay models, address a few of this lacking topics (ROSCOE; BURLAND, 1968).

2.5 GRANULAR SOILS COSTITUTIVE MODELS

Having the knowledge of the basic concepts of constitutive modelling is a very important to understand the more complex recent models. A pair of elastic constants can describe elastic properties of a soil. The first constitutive models were based on Hooke's law and expressed the elastic properties of a material through the Young's Modulus (E) and Poisson ratio (μ), however, the use of bulk modulus (K) and shear modulus (G) can be convenient given that they describe volumetric and distortional elastic response of the material, respectively (MUIR WOOD, 2004; LEIVA, 2004). Given this, the elastic properties of the material can be associated to q and p' through equation 2.27.

$$\begin{bmatrix} \dot{p'} \\ \dot{q} \end{bmatrix} = \begin{bmatrix} K & 0 \\ 0 & 3G \end{bmatrix} \begin{bmatrix} \dot{\varepsilon_v} \\ \dot{\varepsilon_q} \end{bmatrix} \quad (2.27)$$

where:

p' = mean effective stress;

q = deviatoric stress;

K = bulk modulus;

G = shear modulus;

ε_v = volumetric strain;

ε_q = distortional strain.

As for the plastic portion of the elastic-perfectly plastic models for soils, it can be described by the Mohr-Coulomb failure criterion. This theory defines a linear failure envelope on the normal (σ) and shear (τ) stresses. This envelope is described by two properties of the soil: friction angle (ϕ') and cohesive intercept (c'). Equation 2.28 describes the relationship described by the Mohr-Coulomb model (MUIR WOOD, 2004).

$$\tau = c' + \sigma \, tan(\phi') \quad (2.28)$$

For the aforementioned model, there is a linear behaviour for stress states of a soil within the yield surface. When the yield surface is reached, there is a perfectly plastic failure defined by equation 2.24. On the q – p' plane, this surface is purely frictional soil defined by a straight line that is represented by the slope M (equation 2.19). Given this, the yield function can be rewritten as equation 2.29. Also, M can be expressed in terms of friction angle for compression (equation 2.30) and extension (equation 2.31). When the soil reaches the yield surface, the relationship between incremental plastic strains can be presented by equation 2.32 (MUIR WOOD, 2004).

$$f(p', q) = q - Mp' \quad (2.29)$$

$$M_c = \frac{6 \, sin(\phi')}{3 - sin(\phi')} \quad (2.30)$$

$$M_e = -\frac{6\,sin(\phi')}{3 + sin(\phi')} \tag{2.31}$$

$$\frac{\dot{\varepsilon}_v^p}{\dot{\varepsilon}_q^p} = -M^* \tag{2.32}$$

where:

p' = mean effective stress;

q = deviatoric stress;

M = slope inclination of the CSL in the *q-p'* plane;

ϕ' = internal friction angle;

ε_v = volumetric strain;

ε_q = distortional strain.

2.6 GRANULAR COMPOSITES COSTITUTIVE MODELS

This item presents some important studies on modelling of fibre-reinforced granular soils. The first constitutive models only predicted the shear strength of the soil. As the geotechnical community developed more researches increasingly more complete modelling frameworks were proposed.

Gray and Ohashi (1983) and Gray and Al-Refeai (1986) proposed a model predicting the shear strength of fibre-reinforced soils based on the force-equilibrium analysis. The model considered that fibres contributed as an individual component oriented perpendicularly or inclined to the shear surface of sands. Moreover, it assumed that as the sand sheared, it mobilized tensile resistance of the fibres through friction on the fibre-sand interface. Maher and Gray (1990) added on the proposed model accounting for randomly oriented fibres,

Michalowski and Zhao (1996) considered an energy-based homogenization approach to arrive at a macroscopic failure stress of the composite. The authors considered that the fibres were distributed randomly and isotropically in the matrix and considered that the fibres would deform at the same rate as the matrix or slip between the grains. This model was the first to account for these features, as well as a flow rule and a Mohr Coulomb failure envelope for the composite.

However, the previous models did not account for anisotropic distribution of fibres through the matrix. Michalowski and Cérmak (2002) developed a model, also based on energy dissipation, that accounts for this distribution by using the well-known function previously presented in equation 2.6. This model considered that the specimen initially had an isotropic distribution and showed a kinematic hardening effect. This behaviour was due to the evolution of fibre orientation during the deformation process. The model accounts for the energy work dissipation happens during the sliding or plastic deformation after yielding of the fibres in relation to the sand matrix.

When considering cyclic loading modelling, Li and Ding (2002) evaluated the influence of fibre content, confining pressure and loading repetition on the shear modulus on cyclic shear by caring out tests using conventional triaxial apparatus. The authors proposed a hyperbolic function to describe the non-linear stress-strain curve under cyclic loading. This model expressed the elastic modulus as a function of shear modulus and two other parameters related to initial tangential modulus and ultimate cyclic loading stress. Nonetheless, this model could only express the response of the composite under small strains.

Villard and Jouve (1989) proposed a constitutive model for assessing the behaviour of granular soils reinforced by continuous threads. By assuming that the composite is a continuum material that is formed by the superposition of the granular phase and the network of continuous threads. The threads were considered as an elastic multidirectional network and the sand phase was modelled taking into account dilatancy and hardening. The model describes the behaviour of the composites under loading, unloading and reloading conditions through the use of five parameters. The authors applied a power law to describe the elastic behaviour and the plastic response by using a yield function and a non-associate potential function. This model was able to predict the plastic strains due to isotropic compression as well as simulating the soil response under axisymmetric stresses, thus a allowing a comparison to triaxial test results.

In recent years many contributions were made on both the drained and undrained behaviour of randomly distributed fibre-reinforced sand (DIAMBRA *et* al., 2007; 2010; 2011; 2013; IBRAIM *et* al., 2010). It was shown the a study carried out by Diambra *et* al., 2007 that fibre orientation in specimens prepared using moist tamping technique typically occurs within $\pm$ 45° of the horizontal plane (DIAMBRA *et* al., 2007). The rule of mixtures was applied in the models,

which means that the contribution of the sand matrix and fibre are done according to their volumetric contribution and each phase is governed by its own constitutive law (DIAMBRA *et* al., 2010).

Diambra *et* al. (2013) made further contributions to the model by addressing the volume of voids. The authors considered that the volume of voids of the matrix is distributed between the sand and fibre phases. Thus, part of the voids is taken by the fibres leading to a densification of the sand matrix.

2.6.1 Cemented sands

Diambra *et* al. (2017) presented a theoretical derivation for the unconfined compression strength of artificially cemented granular soils. The authors proposed that the changes in the composite mass are based on the superposition of failure strength for the soil and for the cement phases. The model considers that the granular matrix obeys the critical state theory concepts, and the strength of the cemented phase is described through the Drucker-Prager failure criterion.

The model proposed by Diambra *et* al. (2017) adjusted the proposed parameter porosity/cement ratio by Consoli *et* al. (2007a) where the equation 2.33 was proposed. However, the authors emphasise that although the proposed analytical response fits the experimental data for different granular soils and cement curing time well, further parametric analysis is necessary so that the effect of different material parameters on the unconfined compression strength of artificially cemented granular soils can be further explored.

$$q_u = \frac{6M\sigma_c^c(-0.6+0.45K_c)\eta_{cs}^a}{100[K_c(1-\beta)+3(\beta+1)]}\left(\frac{\eta}{C_{iv}^{1/a}}\right)^{-a} = B\left(\frac{\eta}{C_{iv}^{1/a}}\right)^{-a} \tag{2.33}$$

Festugato *et* al. (2018) proposed a theoretical model for predicting splitting tensile strength/ unconfined compressive strength (q_t/q_u) ratio for fibre-reinforced cemented sand. The authors based their model on the presented by Diambra *et* al. (2017), following the same premises the previous work did, and that the fibres contribution to strength is related to the composite deformation. The authors consider that the composite material is made of three separate constituents: the soil matrix, the cementing phase and the fibres. Also, the following four assumptions are made on the model.

(a) the behaviour of the composite at failure point is determined by superposing the strength contributions of the three constituent phases;

(b) there is a strain compatibility between the composite and its three constituent phases (soil, cement and fibres);

(c) at failure, the soil matrix phase is at peak condition, the cement phase is at failure conditions, and the fibre phase is stretched following the deformation state of the composite material;

(d) fibres are one-dimensional elastic elements that resist only to tension. Also, the filaments orientation is considered all horizontal due to the compaction process.

After the testing the model for fibre-reinforced cemented Botucatu residual soil, for 7 days of cure, the proposed analytical relation has a good fit to the experimental data for this composite. The proposed modelling confirms the existence of a rather constant q_t/qu ratio with moulding density, cement and fibre contents (FESTUGATO *et* al., 2018).

3 METHODOLOGY AND EXPERIMENTAL PROGRAM

The established experimental program aimed to investigate and identify the effect of polypropylene fibre inclusion on the monotonic and cyclic behaviour of an artificially cemented silty sand when subjected to cyclic loading. In order to do so, this chapter presents a description of the steps that were carried out in order to meet the objectives.

Firstly, it is presented the characterization of the materials used on the experimental program. Then, the variables to conduct the experimental program for each proposed test is shown. Lastly, it is presented the methods that the program follows.

3.1 MATERIALS

This item presents the properties of the materials that comprise the composites studied on this research. They are: soil (Botucatu sandstone residual soil); Portland cement; polypropylene fibres; and water.

3.1.1 Soil

The soil used in this research was a residual sandstone soil of the Botucatu formation. This soil has been used in research carried out in the soil mechanics laboratories, especially on the LEGG, of UFRGS which contributed to the understanding of their physical, chemical and mechanical properties (NÚÑEZ 1991; PRIETTO 1996; HEINECK, 1998; SPECHT, 2000; FOPPA, 2005; FESTUGATO, 2011).

Besides the existence the aforementioned studies, the selection of this soil was based on three basic factors: it is a soil that covers an extensive area of the territory of Rio Grande do Sul (area greater than 1,300,000 km^2) in regions of relevant economic importance; has characteristics like erodibility and low capacity of support, making this a material that needs some type of adaptation or improvement in order to be used in more severe conditions from an engineering point of view; and for its uniformity of physical characteristics and good laboratory workability.

The reservoir, from which the specimen was collected, is located alongside the RS-240 state highway, in Vila Scharlau, São Leopoldo city, Rio Grande do Sul (figure 3.1).

(a) (b)

Figure 3.1: Botucatu sandstone residual soil reservoir (a) natural slope (b) collected material

The grain size distribution is presented on figure 3.2 The granulometric fraction and other results attained through the characterization tests are presented of table 3.1 alongside the values observed by different authors.

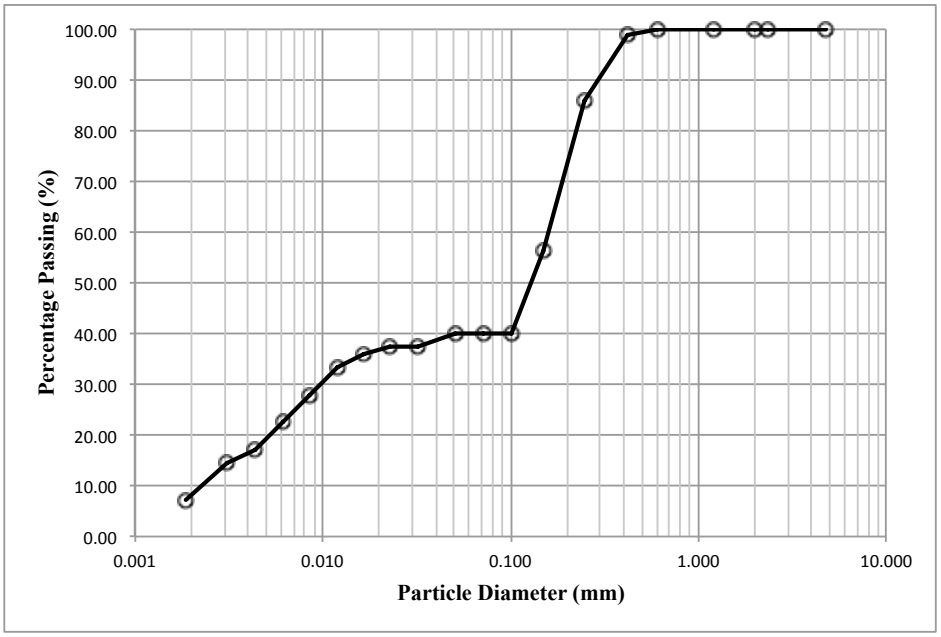

Figure 3.2: Grain size distribution of Botucatu sandstone residual soil

This soil is classified as silty sand (SC) according to the Unified Soil Classification System (SUCS), with a uniformity coefficient of 60 and curvature coefficient 0.22. It can be observed that the material presents a plasticity index (IP) closer to the one observed by Núñez (1991), however, the grain size distribution is closer to the values observed by Foppa (2005) and Consoli *et* al. (2011 a). It is worth noting that the data presented in Consoli *et* al. (2011 a) is the same used on Festugato (2011).

The results of the compression tests with normal energy of compaction are presented on the figure 3.3. Figure 3.4 show the results obtained by Foppa (2005) for normal, intermediate and modified energies for the same material.

Figure 3.5 shows typical behaviour of the studied soil under CD conditions for three confining stresses (20, 60 and 100 kPa) realized by Specht (2000). Its respective strength and deformability parameters are presented in table 3.2

Table 3.1: Physical characterization of Botucatu sandstone residual soil

PROPRIEDADES	Values	Values Nuñez (1991)	Values Foppa (2005)	Values Consoli et al. (2011 a)	Standard for classification or test	Observations
Liquid Limit (LL)	21%	21%	23%	23%	NBR 6459/16	-
Plasticity Limit (PL)	17%	17%	13%	13%	NBR 7180/16	-
Plasticity Index (PI)	4%	4%	10%	10%	-	-
Specific gravity	2.67	2.67	2.64	2.64	NBR 6458/16	Average of 2 samples
% Medium sand ($0.2 < \phi < 0.6$ mm)	14.15%	4.30%	16.20%	6.40%	NBR 7181/16	With deflocculant
% Fine sand ($0.06 < \phi < 0.2$ mm)	48.82%	50.30%	45.40%	52.20%		
% Silt ($0.002 < \phi < 0.06$ mm)	29.68%	32.42%	33,4%	41.40%		
% Clay ($\phi < 0.002$ mm)	7.35%	13.00%	5,0%			
Mean particle diameter (D_{50})	0.13 mm	-	-	0.12 mm		
Effective diameter (D_{10})	0.0027 mm	0.003 mm	0.0032 mm	-	NBR 6502/95	-
Coefficient of uniformity (C_u)	60	43	50	50	NBR 6502/95	-

3.1.2 Cement

The cementitious material used was Portland cement of initial high strength CP Type III (CP V-ARI). This material was chosen because of its accelerated resistance gain, reaching 7 days

of age about 80% of the resistance obtained at 28 days. In addition, the advanced hydration stage reached at this age tends to generate a lower dispersion of test results. The specific gravity tests of the cement followed the recommendations of NBR 16605 (ABNT, 2017), from three determinations the mean value of 3.15.

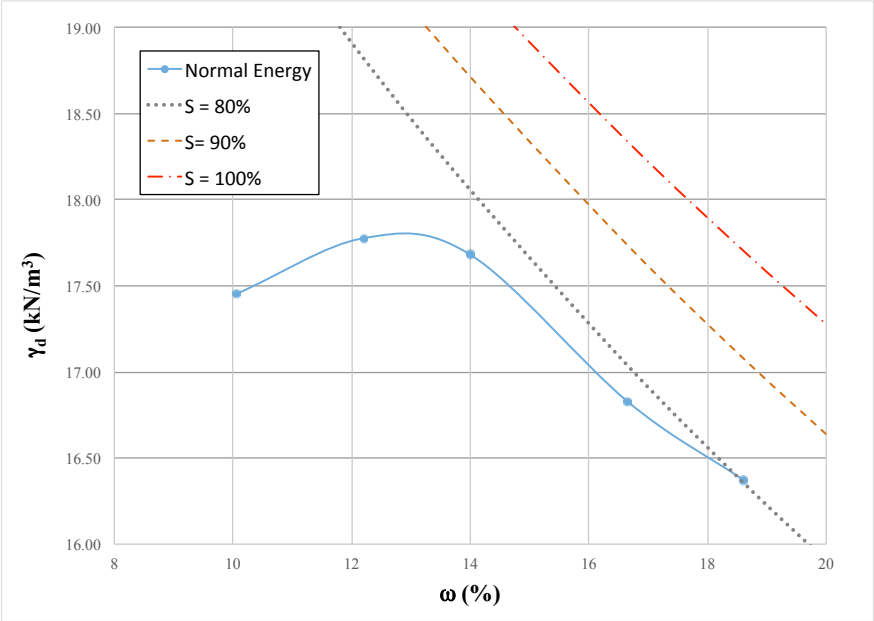

Figure 3.3: Compaction curve for normal compaction energy of Botucatu sandstone residual soil

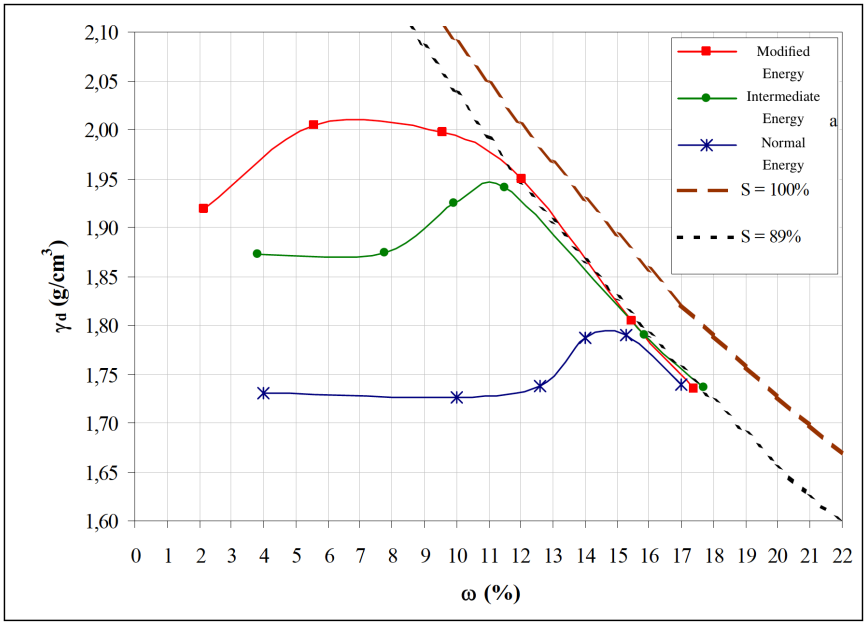

Figure 3.4: Compaction curve for various compaction energies of Botucatu sandstone residual soil (FOPPA, 2005)

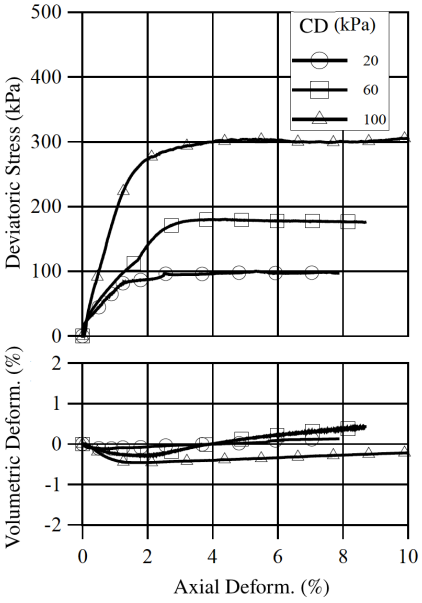

Figure 3.5: Typical stress-strain behaviour of Botucatu sandstone residual soil (adapted from SPECHT, 2000)

Table 3.2: Mechanical properties of compacted soil (adapted from SPECHT, 2000)

Confining Stress (kPa)	$q_{failure}$ (kPa)	$\varepsilon_{a(failure)}$ (%)	$E_{s(0.001\%)}$ (MPa)	$E_{s(0.1\%)}$ (MPa)	$E_{s(failure)}$ (MPa)	$E_{s(10\%)}$ (MPa)	ϕ' (°)	c' (kPa)	$\phi'_{failure}$ (°)
20	100	5.30	164	23	4	10			
60	179	3.51	40	23	4	17	35	5	35
100	303	4.53	98	12	11	27			

3.1.3 Fibre

The fibres used were polypropylene and are commercially available in the form of small filaments and are widely used in LEGG. They were chosen due to its uniform and well-defined characteristics and also for being inert chemically.

Polypropylene fibres are produced by Fitesa Fibras e Filamentos S/A and are used mainly in the textile industry. They present 0.023 mm in diameter and 24 mm in length. The elasticity modulus of fibres is 3 GPa and the ultimate tensile strength is 120 MPa and a specific gravity of 0.91. (FESTUGATO, 2008).

3.1.4 Water

Distilled water was used for characterization tests and specimen moulding.

3.2 INVESTIGATED VARIABLES

Many authors emphasise that the stress-strain behaviour of fibre-reinforced cemented composites is influenced by factors related to the soil matrix (e.g. grain size distribution, void ratio, moisture content), cementation (e.g. type and amount of cementing agent, curing period), and fibre properties (e.g. modulus, aspect ratio, thickness, roughness, orientation, amount and shape).

Even though the aforementioned factors are important, the present research was restricted to one soil type (Botucatu sandstone residual soil), with one fibre type (polypropylene) at different cementation levels using early strength Portland cement (Type III), under different loading conditions. The choice of said variables and its variations was made due to the necessity of a delimitation of the research and was based on previous studies (CASAGRANDE, 2001; 2005; HEINECK, 2002; VENDRUSCOLO, 2003; DONATO, 2007; FESTUGATO, 2008; SPECHT, 2000; FOPPA, 2005 CONSOLI *et* AL., 2010b, 2011a, 2011b; FESTUGATO, 2011; VENSON, 2015; DA SILVA, 2017).

Once identified the most important variables, it was evaluated its influence through the controlled variation of each one, whilst maintaining the others fixed. The fixed variables were:

(a) soil type: Botucatu sandstone residual soil;

(b) cement type: Portland cement with high initial strength CP Type-III (CP V – ARI);

(c) curing period: 7 days;

(d) water content: 10%;

(e) deformation rate for automatic press in unconfined monotonic tests: 1.14 mm/minute.

The nomenclature adopted in this research to identify the specimens is presented below.

18-5-0-90-I

Where:
18 = specific dry unit weight (kN/m^3);
5 = cement content (%);
0 = no fibre inclusion/ F = with fibre inclusion;
90 = loading percentage (%)
I = repetition number.

The possible variation rate for the controlled variables investigated was based on tests that were carried out, and are presented next.

3.2.1 Unconfined compression tests

The results used in this research were form a previous research published by Festugato (2011). In order to validate these data, this experimental program selected 5 mixtures with the same variable contents as the ones carried out for flexural tests to be tested under unconfined compression (UC). These results were compared to the results showed by the previous research, thus validating it. The chosen mixtures are presented on table 3.3, for each combination three specimens were moulded. The response variable of the unconfined compression test is unconfined compressive strength (q_u), expressed in [kPa]. The values of q_u used are presented in the form of a fitted equation for the experimental data and is shown in chapter four.

Table 3.3: Unconfined compression experimental program

Dry unit weight (γ_d) (kN/m^3)	Cement Content (%)	Fibre Content (%)	Test	Total of samples
18	5	0 and 0.5	UC	6
19	3	0 and 0.5	UC	6
19.7	7	0	UC	3
			Total	15

3.2.2 Split tensile tests

The initial plan of the research was to also use the split tensile (ST) data from Festugato (2011) for the diametric compression tests, only testing a few combinations of the 5 x 10 cm (diameter x height) specimens in order to validate the data, presented in table 3.4. This data is presented in chapter 4. However, for reasons that are also explained in chapter four, it was necessary to test specimens with the actual dimensions used in the fatigue testing – 10 x 5 cm (diameter x height). Table 3.5 presents the combinations made for this specimen size. For each combination three repetions were made.

The response variable of the split tensile test is split tensile strength (q_t), expressed in [kPa]. The values of q_t used are presented in the form of a fitted equation for the experimental data and is shown in chapter four.

Table 3.4: Split tensile experimental program for 5 x 10 cm specimens

Dry unit weight (γ_d) (kN/m^3)	Cement Content (%)	Fibre Content (%)	Test	Total of samples
18	5	0 and 0.5	ST (5x10)	6
19	3	0 and 0.5	ST (5x10)	6
19.7	7	0	ST (5x10)	3
			Total	15

Table 3.5: Split tensile experimental program for 10 x 5 cm specimens

Dry unit weight (γ_d) (kN/m^3)	Cement Content (%)	Fibre Content (%)	Test	Total of samples
18	1	0.5	ST (10x5)	3
18	3, 5	0 and 0.5	ST (10x5)	12
19	5	0 and 0.5	ST (10x5)	6
19	7	0	ST (10x5)	3
19.7	7	0 and 0.5	ST (10x5)	6
			Total	30

3.2.3 Flexural tensile tests

The variables used for the experimental program for flexural tensile tests (FL) are presented on table 3.6. The response variable of this test was flexural tensile strength (q_f) expressed in [kPa]. The results of these tests are presented in chapter 4.

Table 3.6: Flexural tensile tests investigated variables

Dry unit weight (γ_d) (kN/m^3)	Cement Content (%)	Fibre Content (%)	Number of repetitions	Total of samples
18, 19 and 19.7	3, 5 and 7	0 and 0.5	3	54

3.2.4 Ultrasonic pulse velocity test

The ultrasonic pulse velocity (UPV) tests were made to assess the development of the shear modulus through the duration of the cyclic tests. This study was relevant since the cyclic tests could last up to 36 h, so, to measure the progress of increase in stiffness due to the cementation process became an important data to evaluate. Six specimens were made for the benchmark mixture – 18 kN/m^3; 5% cement – with and without fibres. They were tested at 1, 2, 5, 6, 7, 8 and 9 days.

3.2.5 Cyclic unconfined compression tests

The cyclic unconfined compression tests (CUC) were carried out for a benchmark mixture (18 kN/m^3 - 5% cement) with and without fibre insertion for three different percentages of the estimated maximum load (90, 80 and 70%). Another mixture combination, with the same $\eta/C_{iv}^{0.28}$ as the benchmark mixtures, was tested for 80% of the estimated maximum load. Bender elements were used to assess shear modulus at small strains at established cycles.

The controlled variables for this test are presented on table 3.7. This test had as response variables number of cycles (N); cyclic unconfined compression strength (q_u) [kPa]; Young's modulus at N cycles (E) [MPa]; axial strain (ε_a) and shear modulus (G) [MPa].

Table 3.7: Cyclic unconfined compression tests investigated variables

Dry unit weight (γ_d) (kN/m^3)	Rupture load percentage (%)	Cement Content (%)	Fibre Content (%)	Test	Total of samples
18	90, 80, 70	5	0 and 0.5	CUC	18
18	90 ML, 80 ML, 70ML	5	0.5	CUC	6
19	80	3	0 and 0.5	CUC	6
				Total	30

3.2.6 Fatigue tests

The cyclic unconfined diametric compression fatigue tests (DCF) were carried out for a benchmark mixture with and without the addition of fibres for three different load percentages, 90, 80 and 70% of the estimated maximum value for monotonic testing. For one load percentage (80%) two other combinations were tested. These combinations are presented on table 3.8. There were three repetitions for each defined combination. The response variable of this test is number of cycles in fatigue life (N_f) and radial displacement (ε_r) [%].

Table 3.8: Fatigue tests investigated variables

Dry unit weight (γ_d) (kN/m^3)	Rupture load percentage (%)	Cement Content (%)	Fibre Content (%)	Test	Total of samples
18	90, 80, 70	5	0 and 0.5	FT	18
18	80	3	0 and 0.5	FT	6
19	80	5	0 and 0.5	FT	6
				Total	30

3.3 METHODS

As part of the experimental program, this item describes the methods used for material collection, specimen preparation, and characterization tests for the materials. Also it is described the equipment and test procedures used on this experimental program.

3.3.1 Material collection

The soil specimen was collected on its deformed state through manual tool excavation. Was gathered a sufficient amount so all foreseen tests could be done. The soil was stored in plastic barrels and properly sealed. Specimen collection was cautiously dug in order to avoid specimen contamination.

The cement utilized was bought in a 40 kg pack. The material was stored in sealed containers in order to prevent premature hydration due to air humidity.

3.3.2 Specimen preparation

The soil specimen preparation for characterization and specimen moulding followed the procedures established by the standard NBR 6457 (ABNT, 2016a). The soil was air-dried, the lumps were broken, sieved to remove organic materials and eventual gravel, and its hygroscopic moisture content was measured. After the soil was prepared, it was stored in sealed containers

3.3.3 Characterization tests

For soil characterization the following tests were carried out: grain size distribution, specific gravity, liquid limit, plastic limit, hygroscopic moisture content, and compaction. The grain size distribution test followed the method described in the standard NBR 7181 (ABNT, 2016e). The determination of the specific gravity of the soil followed the procedures described on NBR 6458 (ABNT, 2016b). As for the Atterberg limits, the liquid limit value attained obeyed the NBR 6459 (ABNT, 2016c) and the plastic limit by NBR 7180 (ABNT, 2016d). The value of hygroscopic moisture content followed NBR 6457 (ABNT, 2016a). Finally, the compaction test was done for the normal energy of compaction as described on NBR 7182 (ABNT, 2016f) with material reuse.

3.3.4 Specimen moulding and curing

All specimen mixtures were made following the same steps: weighing, mixing, compacting, packing, storing and curing the materials. These procedures are presented in this item. After the explanation of the steps that are common to all tests it is presented the compaction process for the different tests.

The calculated amount of each material used on the specimen was weighed with a 0.01g resolution. The amount of cement added was calculated regarding the mass of dry soil used; the fibre quantities were calculated regarding the mass of dry soil and cement used. As for the water weight, it was assessed by the mass of all dry materials.

After all materials were weighed, the soil and cement were mixed with the aid of a spatula until a uniform mixture is achieved. Then, water was added and the mixture process continued until the mass was uniform. For specimens with fibre addition, the fibres were frayed with the aid of compressed air and manual fraying prior to the beginning of the moulding process. When the mixture was homogeneous, they were added in layers, being folded in small amounts at a time in order to prevent entanglement.

The total amount of mixture was enough to prepare the specimen and two capsules to determine its moisture content. The weight for each layer of the specimen was weighed and the material stored in separate sealed containers until compaction. Of the remaining mixture, a small amount was placed into two capsules. The capsules were then placed on a laboratory stove set at 100^{o}C for 2 days in order to determine its moisture content. The average value of humidity of the two capsules was considered the moisture content of the specimen.

After the static compaction, the specimen carefully unmoulded and its measurements and weight assessed with 0.01 mm and 0.01 g resolution, respectively. Then, the specimens were adequately identified and conditioned in plastic bags in order to prevent significant changes in moisture content. The specimens were then placed in a temperature-controlled room (23 ± 2 ^{o}C) for the curing period.

The cylindrical specimens of 50 mm diameter and 100 mm high were made for unconfined compression tests (cyclic and monotonic). The compaction process happens in three equal layers that are statically compressed on a tripartite mould until each layer reaches the targeted dry unit weight, always scarifying between layers. For the CUC tests small acrylic pieces were used to make grooves on the top and bottom faces of the specimen in order to facilitate the insertion of the bender elements later.

In diametric compression, used for split tensile and fatigue tests, specimens are 10 mm in diameter and 50 mm high. The compaction process happens in one statically compressed layer on a tripartite mould until the targeted dry unit weight is reached.

The flexural specimens are prismatic shaped with 4 cm x 4 cm x 17 cm (depth x width x length). The compression was made in a single layer statically compressed on a partible mould, reaching the specified moisture content and dry unit weight. Figure 3.6 presents typical specimens.

In order to assess worst possible scenario, after being cured for 6 days, all specimens were submerged during the remainder 24 h. This aims to minimize the effects of suction and thus the lower resistance possible is measured under the stipulated circumstances. On the seventh day the specimen is tested. The water temperature is kept at 23 ± 2 ^{o}C. Immediately before testing the specimen was carefully superficially dried with the aid of a soft fabric.

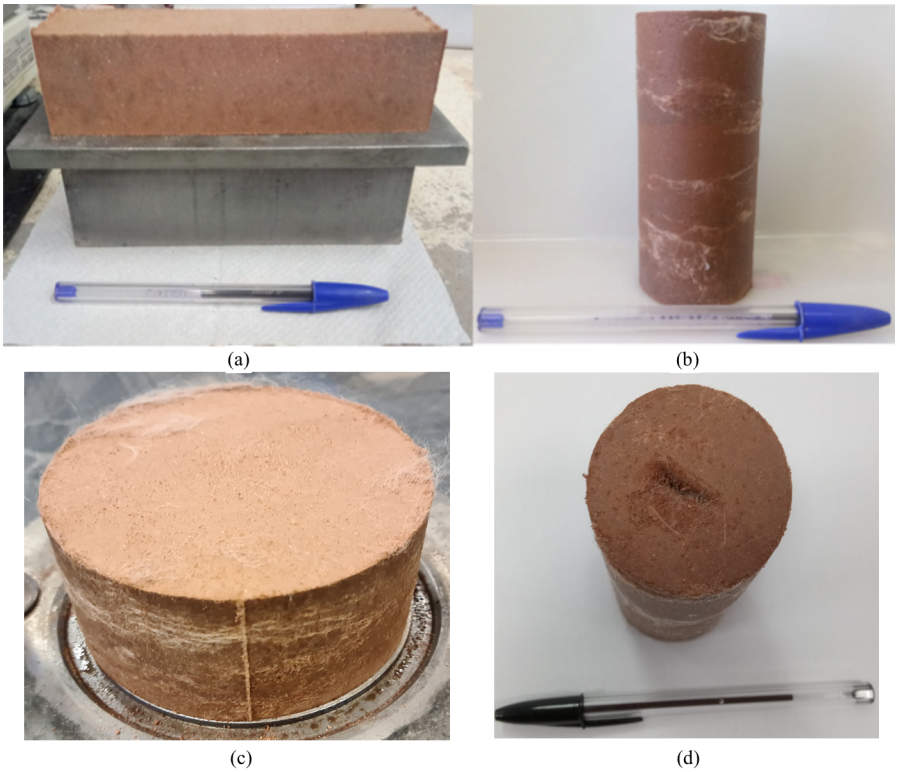

Figure 3.6: Specimen specimens (a) prismatic (b) cylindrical 5 x 10 cm (c) cylindrical 10 x 5 cm (d) bender grooves

3.3.5 Unconfined compression test

Unconfined compression tests are largely used on artificially cemented materials (e.g. concrete and cemented soil). Also, has been extensively used in researches conducted by the LEGG/UFRGS research group. It is simple, rapidly executed, low coast, reliable and largely disseminated in the technical community.

For this test it was used an automatic press with maximum capacity of 100 kN, equipped with calibrated dynamometer ring with load capacity of 10 kN and resolution of 0.005 kN (0.5 kgf). The strain velocity was fixed at 1.14 mm per minute. Then, the test was carried out with the maximum load registered. The test apparatus and specimen rupture are shown in figure 3.7. Equation 3.1 was used to calculate the unconfined compression strength.

The test was validated if the individual resistances of three individual specimens do not deviate more than 10% from the average resistance of the group. This criterion is used for all researches carried out for this test in the PPGEC, so it is also employed on this research.

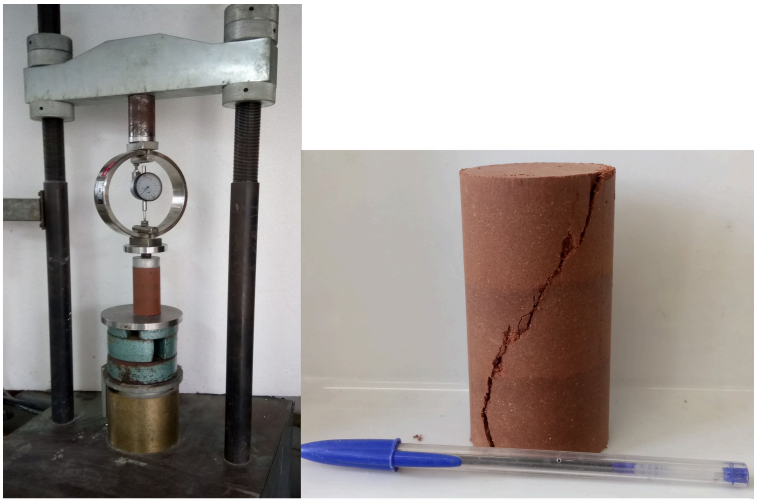

(a) (b)

Figure 3.7: Unconfined compression test (a) apparatus (b) rupture mode

$$q_u = \frac{P}{\left(\pi \cdot \frac{D^2}{4}\right)} \tag{3.1}$$

Where:

q_u = unconfined compression strength (kPa);

P = maximum load from the test (kN);

D = specimen diameter (mm).

3.3.6 Split tensile test

Professor Fernando Luiz Lobo Carneiro, aiming to assess the tensile strength of concrete specimens through static loading, developed the split tensile test, or Brazilian test, in 1943. The NBR 7222 (ABNT, 2011) describes test procedures. It was used an automatic press with maximum capacity of 100 kN, equipped with calibrated dynamometer ring with load capacity of 10 kN and resolution of 0.005 kN (0.5 kgf). The strain velocity was fixed at 1.14 mm per minute.

The same specimen preparation procedures described for unconfined compression tests apply for this test. The test for the 5 x 10 cm and the 10 x 5 cm specimens are shown in figure 3.8. The failure mechanisms are presented in figure 3.9. The NBR 7222 (ABNT, 2011) relates the attained test load with the geometric properties of the specimen to calculate the split tensile strength of the material as expressed in equation 3.2.

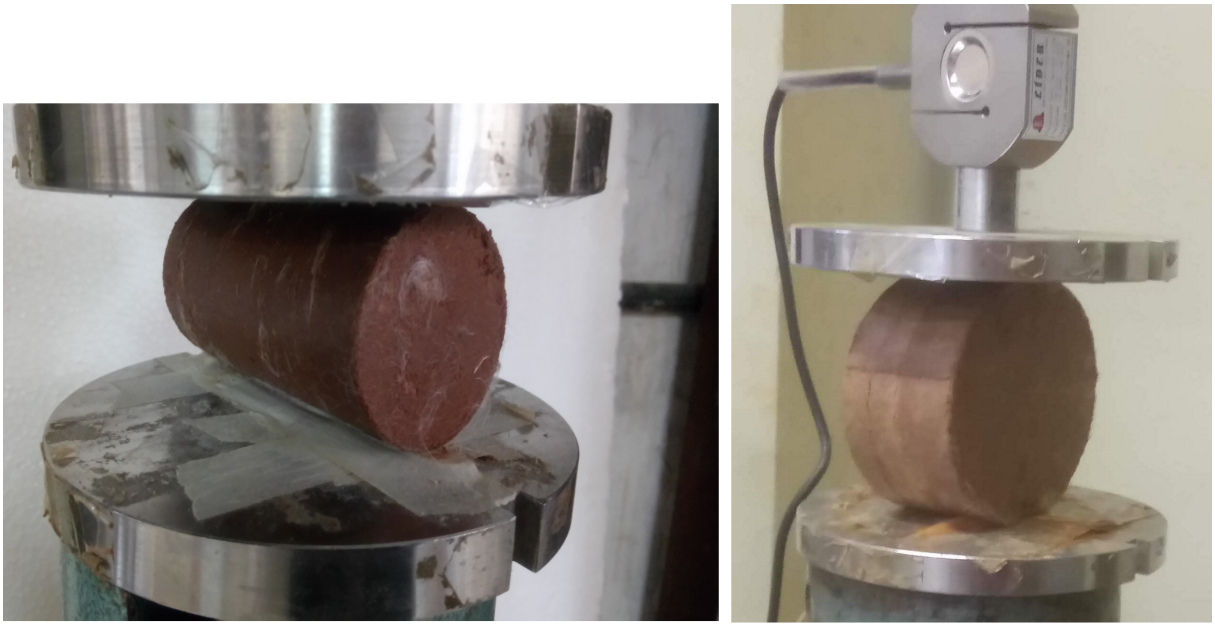

(a) (b)

Figure 3.8: Split tensile test (a) 5 x 10 cm specimens
(b) 10 x 5 cm specimens

$$q_t = \frac{2 \cdot P}{\pi \cdot D \cdot L} \tag{3.2}$$

Where:

q_t = split tensile strength (MPa);

P = maximum load from the test (kN);

D = specimen diameter (mm);

L = specimen length (mm).

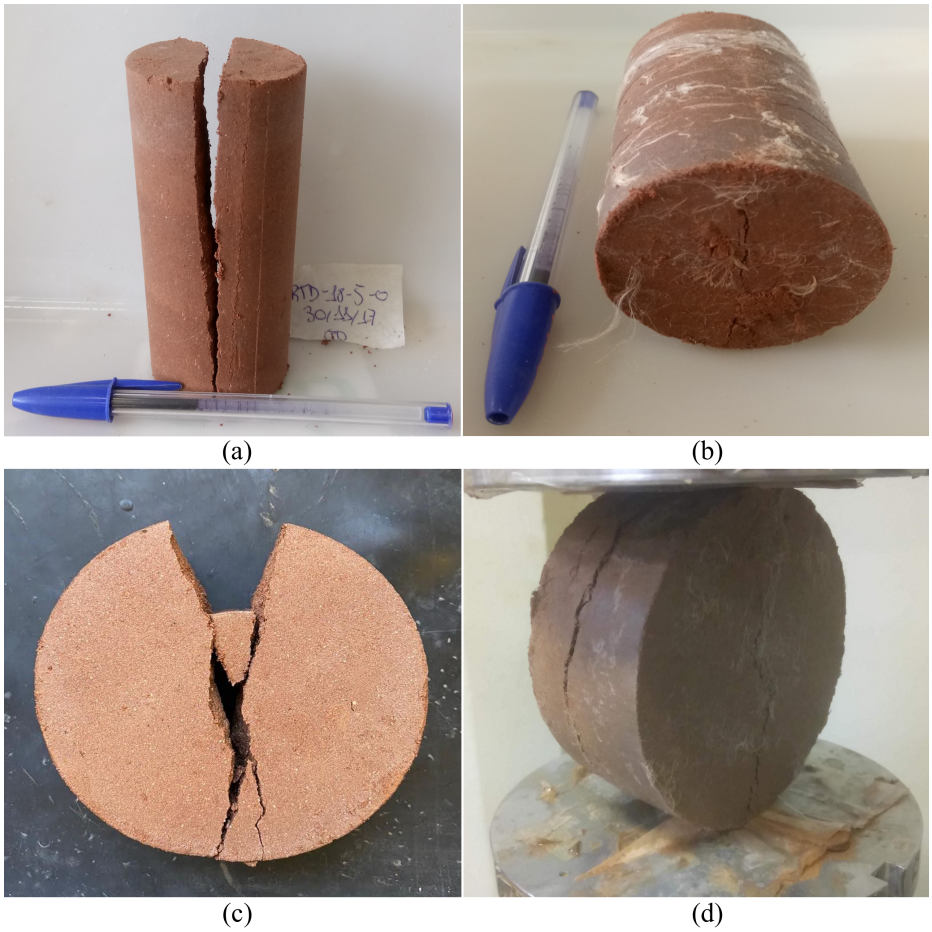

(a) (b) (c) (d)

Figure 3.9: Failure mechanism for split tensile test (a) 5 x 10 cm specimens without fibres (b) 5 x 10 cm specimens with fibres (c) 10 x 5 cm specimens without fibres (d) 10 x 5 cm specimens with fibres

3.3.7 Flexural tensile test

The flexural tensile test follows the procedures presented on ASTM D1635 (ASTM, 2012). It was used an automatic press with maximum capacity of 100 kN, equipped with calibrated dynamometer ring with load capacity of 10 kN and resolution of 0.005 kN (0.5 kgf). The strain velocity was fixed at 1.14 mm per minute.

The same specimen preparation procedures described for unconfined compression tests apply for this test. The test apparatus and specimen rupture are shown in figure 3.10. The ASTM D1635 (ASTM, 2012) relates the attained test load with the geometric properties of the specimen to calculate the flexural strength of the material as expressed in equation 3.3.

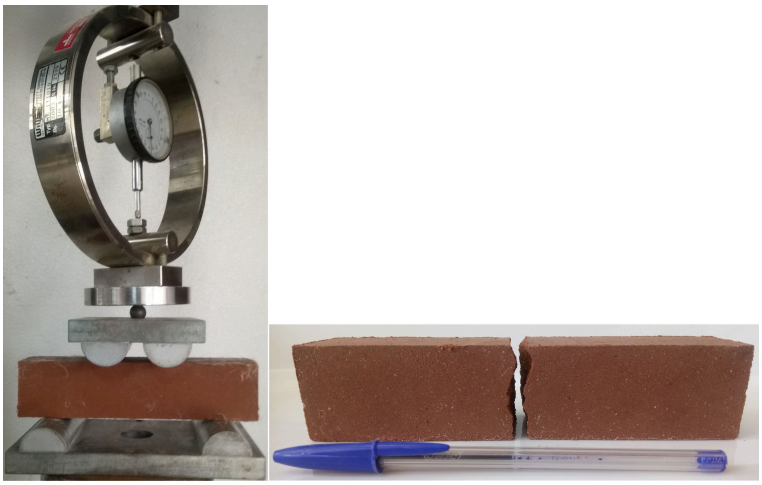

(a) (b)

Figure 3.10: Split tensile test (a) apparatus
(b) rupture mode

$$q_f = \frac{PL}{bd^2} \tag{3.3}$$

Where:

q_f = flexural tensile strength (MPa);

P = maximum load from the test (N);

L = span length (mm);

b = average width (mm);

d = average depth (mm).

3.3.8 Ultrasonic pulse velocity test

The ultrasonic pulse velocity tests (UPV) were made using the equipment Pundit from Proceq applying the first arrival wave method. Firstly, the p-waves were calibrated using a calibration rod, where the time for the wave travel from the transmitter to the receiver is used to calculate the velocity of the wave. For p-waves, the specimens are on the horizontal position. P-waves present roughly half the travelling time then the s-waves, being a good control assessment of

the s-waves. After calibration, the p-waves were measured using the software of the equipment. Then, s-waves were calibrated on the vertical position, using the same calibration rod. Finally, s-waves were measured for the specimens.

Considering the specimen are a continuous, elastic, isotropic and homogeneous media, the values of G and M are calculated following equations 3.4 and 3.5 (SANTAMARINA; KLIEN; FAM, 2001; MITCHELL; SOGA, 2005; CLAYTON, 2011). The value of Poisson's ratio (v) can be estimated through equation 3.6 (LEE; SANTAMARINA, 2005).

$$M = \rho \cdot {V_P}^2 \tag{3.4}$$

$$G = \rho \cdot {V_S}^2 \tag{3.5}$$

$$\frac{V_P}{V_S} = \sqrt{\frac{2 \cdot (1 - \nu)}{1 - 2 \cdot \nu}} \tag{3.6}$$

Where:
M = constrained modulus (MPa);
G = shear modulus (MPa);
ρ = density of the specimen at time of testing (kg/m^3);
V_P = velocity of p-waves (m/s);
V_S = velocity of s-waves (m/s);
ν = Poisson's ratio.

3.3.9 Cyclic unconfined compression tests

3.3.9.1 Adapted equipment

The apparatus at the University of Bristol Geomechanics laboratory consisted of a hydraulic stress path triaxial cell with the stresses controlled by stepper motor driven air-pressure regulators. This equipment was adapted to conduct cyclic unconfined compression tests. The

software used to perform the tests – *TRIAX* – was previously altered at the university to be used in Windows™. It was used the PROCcylic procedure to perform low frequency cyclic tests. The apparatus is capable of executing and automatically log the data of the predetermined tests.

The original triaxial equipment was set up for 38 and 75 mm specimens. For this research special top and bottom caps were made to accommodate 50 mm specimens with built in space for the introduction of bender elements on the top and bottom faces of the specimen. Internal displacement measurement devices (LVDTs without springs) were secured with the aid of metallic claws. The ram was attached a moving pedestal, and the axial stress as assessed by a 10 kN load cell and the movement was controlled through the ram pressure in the bottom chamber. The external movement of the ram was measured by an external LVDT attached to the bottom chamber. The calibrations of the three LVDTs and the load cell are presented in figure 3.11. The applied loads were supplied through air-water interfaces divided by bladders by using a stepper motor to regulate the necessary air pressure from the compressed air supplied to the laboratory that was maintained at 800 kPa. Then, the water pressure applied load to the ram through a water-oil interface. The stepper motors was controlled by digital output from an 8255 input/output (16 channel I/O card by Flytech) card in the PC used for control. When a stipulated air pressure is required the control system sends a series of pulses to the stepper motor. The pressure controllers provide a resolution of approximately 0.07 kPa and a maximum air pressure of 800 kPa.

Figure 3.12 illustrates the schematic described. In order to use the apparatus without a confining pressure weights had to be added to the bottom chamber. As for the measurement of the internal data, plastic extensions were 3D printed and glued to the specimen in the middle third. Water was dripped from the top cap during testing in order to maintain specimen saturation. These adaptations can be observed in figure 3.13.

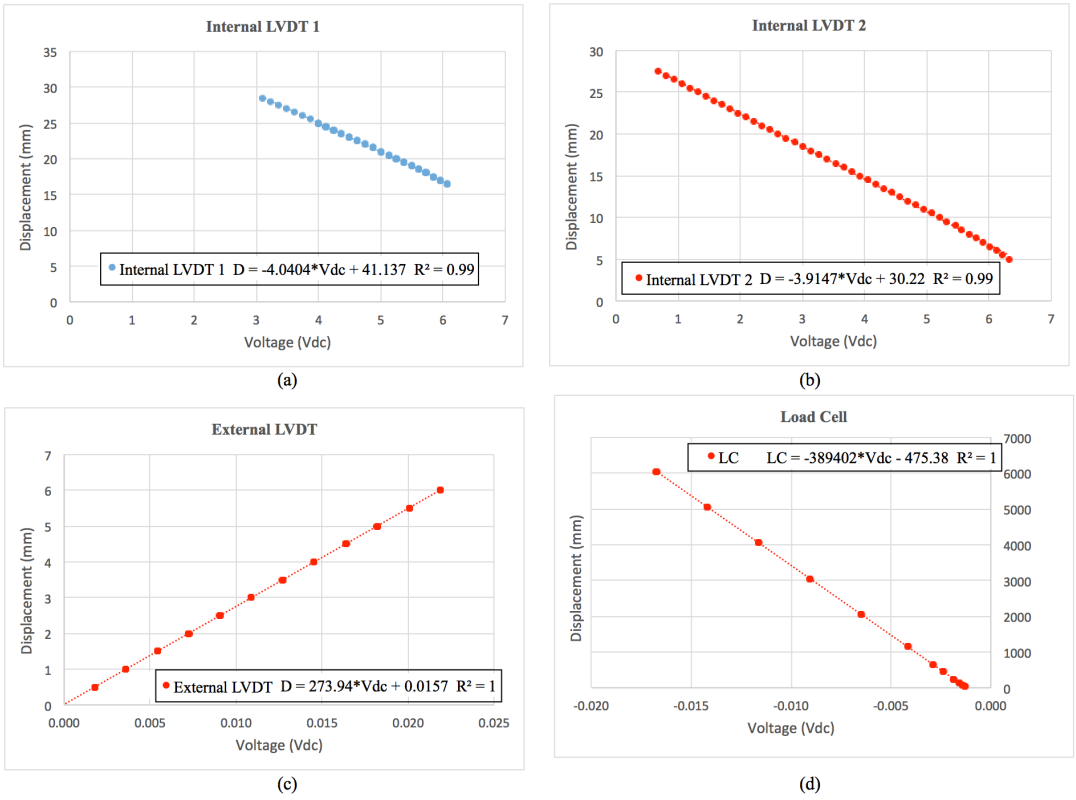

Figure 3.11: Calibration for cyclic unconfined tests (a) Internal LVDT 1 (b) Internal LVDT 2 (c) External LVDT (d) Load Cell

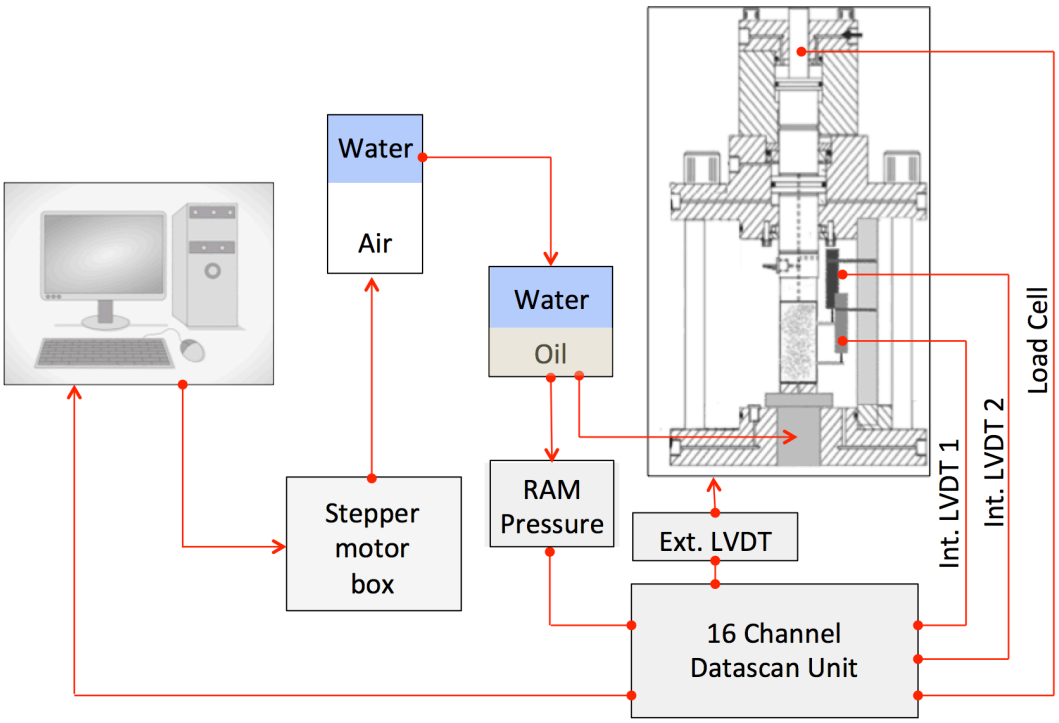

Figure 3.12: Schematic of the unconfined cyclic test apparatus at the University of Bristol

3.3.9.2 Bender elements

A pair of transmitter and receiver benders was connected to a switching box that allowed changing from one pair of benders to another by using digital output from a 8255 I/O card in the PC that was also connected to a wave for generator. The switching box also worked as a signal amplifier. Cables from the switching box carrying the transmitted and received signals were connected to a two-channel PICO ADC-216 A/D converter that was used to obtain and store the data before it is downloaded to the PC. The Picoscope software was also used to plot and save data. The apparatus used is presented in figure 3.14.

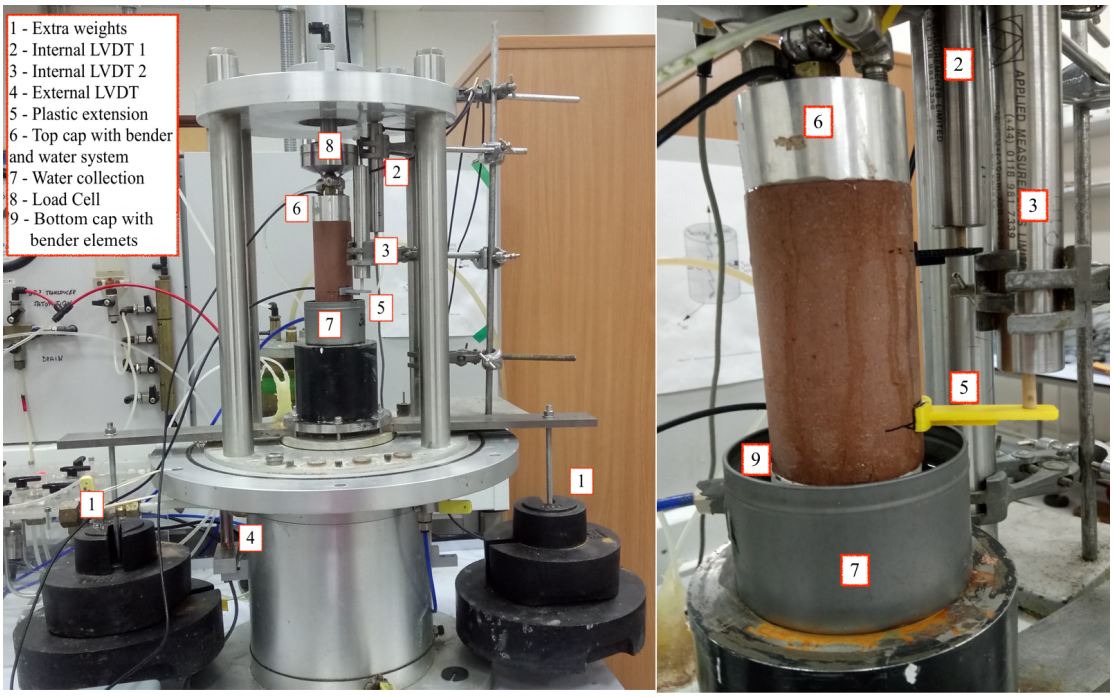

Figure 3.13: Alterations made to the cyclic unconfined compression apparatus of the University of Bristol (a) overview (b) specimen

The bender element readings were made at constant intervals during cycling. After the specified cycle number, the cycling was suspended briefly for the reading of the bender elements without loading. For fibre reinforced specimens a small load had to be applied in order to be possible to make the reading. It was stipulated that 10% of the cyclic load would be the used load for bender readings for fibre-reinforced specimens.

For the initial reading four different frequencies were tested in order to assess which provided the more reliable results. After which, only the chosen frequency was used to determine the

time of propagation. The bender elements were calibrated by measuring the initial time of wave propagation when transmitted bender is directly touching the receiving bender. The values measured used the peak-to-peak method. The equation used to attain the value of G is the same used for the UPV tests, equation 3.4.

Figure 3.14: Bender element test apparatus at the University of Bristol

3.3.10 Fatigue test

The 10 x 5 cm (diameter x height) specimen were employed in the fatigue testing using the same loading apparatus developed by Venson (2015) according to British standard BS EN 12697-24 (BSMT, 2004). It uses a pneumatic piston and an electronic haversine generator that is computer controlled by a solid-state relay. The pulse load applied during cyclic loading was calibrated by varying the amount of air let through the system using the flux control valve until it was consistent with the AASTHO T-307-99 (AASTHO, 2007) specifications, presented in figure 3.15.

The tests are conducted at a frequency of 2 Hz until specimen rupture being measured the number of cycles until rupture (N_f) and radial displacement (ε_r) [%]. Figure 3.16 (d) shows the pulse calibration for the fatigue tests carried out. Given equipment limitations, each pulse lasts 0.2 s followed by a resisting period of 0.3 s. The LVDTs have a range of 50 mm and 100 mm, respectively, and the load cell has a capacity of 10 kN. Their calibration is shown in figure 3.16 (a), (b) and (c).

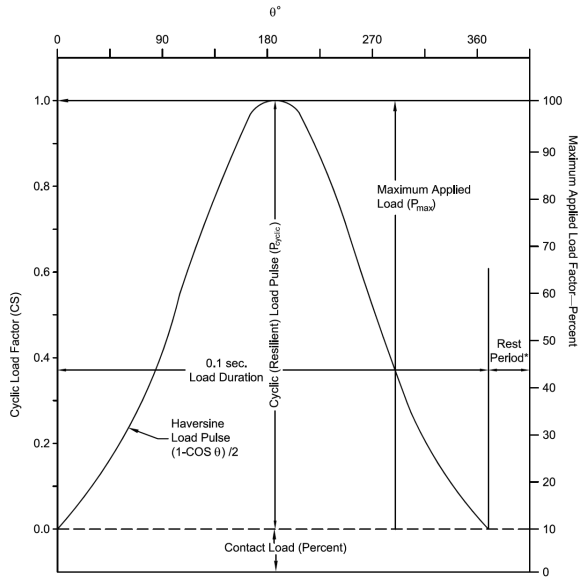

Figure 3.15: Load curve for fatigue tests (AASTHO, 2007)

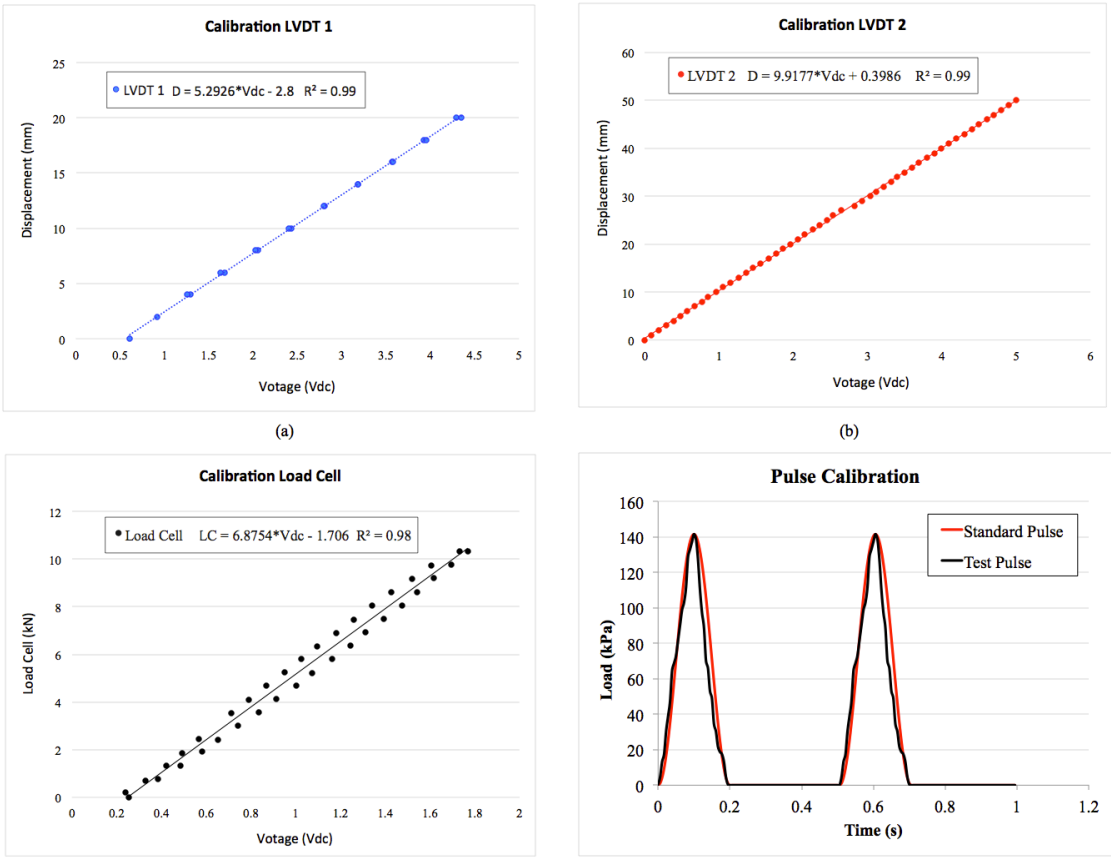

Figure 3.16: Calibration for fatigue tests (a) LVDT 1 (b) LVDT 2 (c) Load Cell (d) Load Pulse

The apparatus also has an electronic pressure regulator, a gas canister as the air system capacitance, a data acquisition box, and a water reservoir. The fatigue test was controlled by the program developed at the laboratory by previous students using the LabVIEW software developed by National Instruments. Before each test, a calibration specimen was used to ascertain the appropriate air pressure necessary to induce the desired load. Also, after the tested specimen was set up 10 cycles at 30 kPa (minimum pressure that the system operates) were performed to eliminate deformations from the accommodation of the system. The test is presented in figures 3.17 and 3.18.

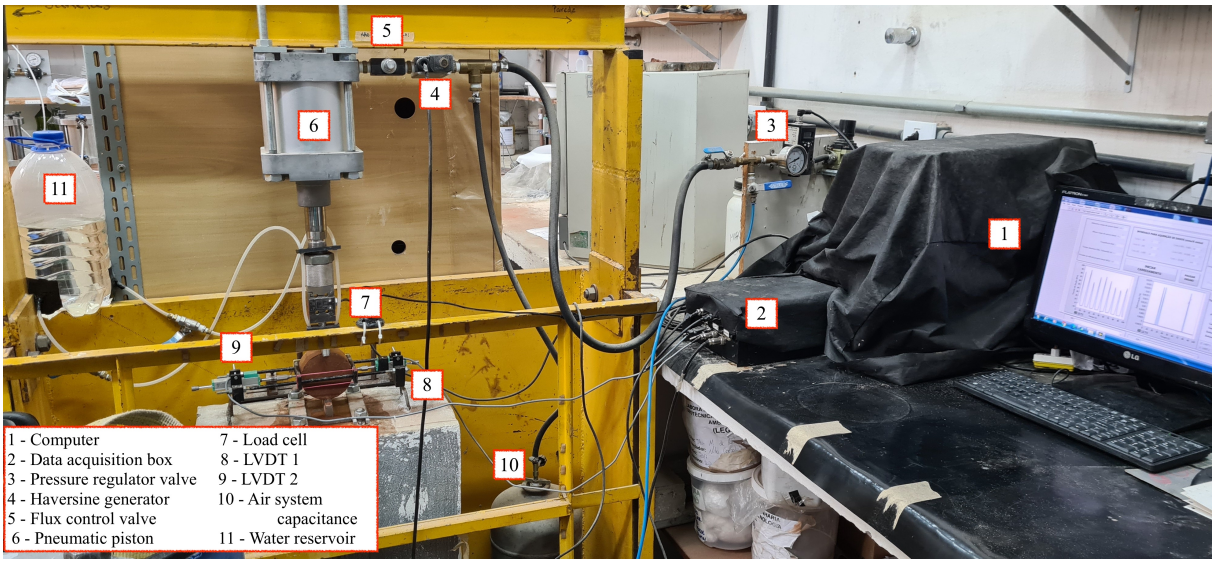

Figure 3.17: Fatigue apparatus

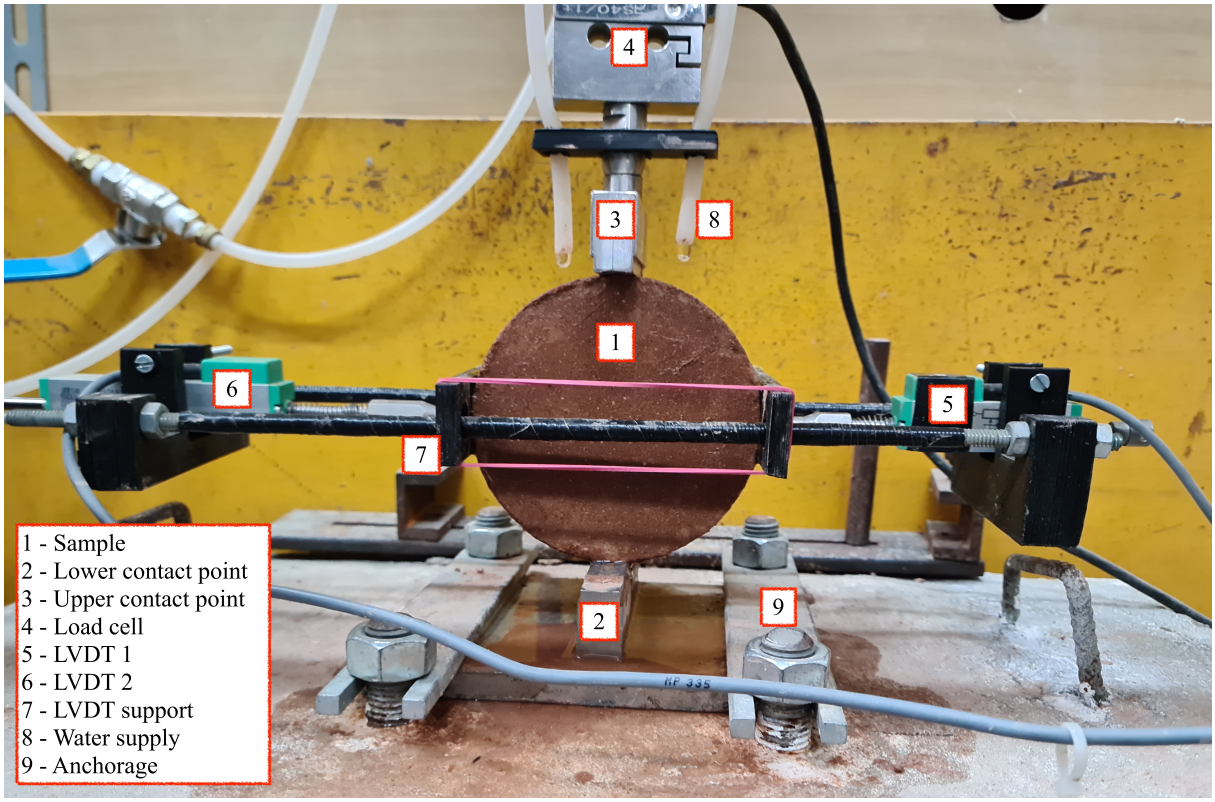

Figure 3.18: Fatigue apparatus: specimen set up

4 PRELIMINARY TESTS

This chapter presents the preliminary test results carried out to assess the maximum expected values of strength used as reference for cyclic testing – cyclic unconfined compression (CUC) and fatigue testing (FT) – followed by a brief analysis of the data. The monotonic phase of the experimental program entailed a small number of unconfined compression (UC) and split tensile (ST) tests for 5 x 10 cm specimens, aiming to validate the use of the results presented by Festugato (2011). Also, it is presented a more comprehensive evaluation of the studied composites under split tensile strength of 10 x 5 cm specimen and of flexural tensile strength. Besides the monotonic tests, this chapter presents the evaluation of the shear modulus at very-small strains for the chosen mixture through the use of ultrasonic pulse velocity wave test.

4.1 MONOTONIC TESTS

In this topic it is presented the results for the monotonic tests carried out in this research aiding the completion of the cyclic tests. Firstly, it is presented the results for the unconfined compression tests (UC), followed by the data from the split tensile tests (ST). Lastly, there is a brief analysis of the data from the flexural tensile tests (FL). Even though this research did not conduct flexural tensile fatigue tests due to equipment limitations, the monotonic study was made, and is presented.

4.1.1 Unconfined compression tests

The values for the estimated unconfined compression strength (UC) used in this research were the ones attained by Festugato (2011). However, in order to use this data, it was necessary to evaluate if the materials used in the present research and their interaction would result on similar strengths as the ones observed by the previous research.

As presented in section 3.1.1, the residual soil studied presented similar characteristics to the ones studied by the previous authors. The binder was of the same standardized type and the fibres were the same, from the same manufacturer. From this, it was plausible to assume that the values of strength attained would be similar. In order to confirm this hypothesis, five combinations of dry unit weight, binder content and fibre content were chosen to make the comparison to the previous data. Three specimens for each chosen combination were

moulded. Said combinations and results for UC are presented on table 4.1 alongside the results presented by Festugato (2011).

It can be inferred from table 4.1 that the strength values were at the same level of magnitude since the mean average strength between experimental programs was within an acceptable limit of variation. It was observed a greater variability for specimen combinations with fibres, but still within reasonable variation (less then 5%). However, this could be explained by a difficulty of precisely determining the strength at rupture given the effect of fibre insertion in the increase in ductility of the composites.

In conclusion, these tests validated the use of the values presented by Festugato (2011) for all other mixture combinations. Therefore, the data used as reference for the cyclic unconfined compression tests (CUC) on the present research will be the presented by the previous research. The q_u versus $\eta/C_{iv}^{0.28}$ relationship used for the CUC tests is presented in figure 4.1. The fitted equations for specimens without fibres and with fibres are presented in equations 4.1 and 4.2, respectively.

Table 4.1: Comparison between unconfined compression test results

Combiantions	q_u (kN/m^2)	Average q_u (kN/m^2)	q_u Festugato (2011) (kN/m^2)	Average q_u (kN/m^2)	Variantion (%)
γ_d = 18	1319.44	1198.30	1116.00	1196.67	-0.14
%C = 5	1154.87		1159.00		
%F = 0	1120.58		1315.00		
γ_d = 19	1132.01	1116.78	1126.00	1136.33	1.72
%C = 3	1111.44		1086.00		
%F = 0	1106.87		1197.00		
γ_d = 19.7	3145.73	3191.45	3317.00	3238.67	1.46
%C = 7	3086.30		3249.00		
%F = 0	3342.30		3150.00		
γ_d = 18	1408.59	1379.63	1262.77	1325.41	-4.09
%C = 5	1335.44		1388.06		
%F = 0.5	1394.87		-		
γ_d = 19	1497.73	1511.44	1408.35	1474.38	-2.51
%C = 3	1509.16		1467.87		
%F = 0.5	1527.44		1546.93		

$$q_u = 2.1\times10^7[\eta/(C_{iv})^{0.28}]^{-3.08} \quad (4.18)$$

$$q_u = 7.3\times10^7[\eta/(C_{iv})^{0.28}]^{-2.64} \quad (4.2)$$

Where:

q_u = unconfined compression strength (kPa);

η = porosity (%);

C_{iv} = volumetric cement content (%).

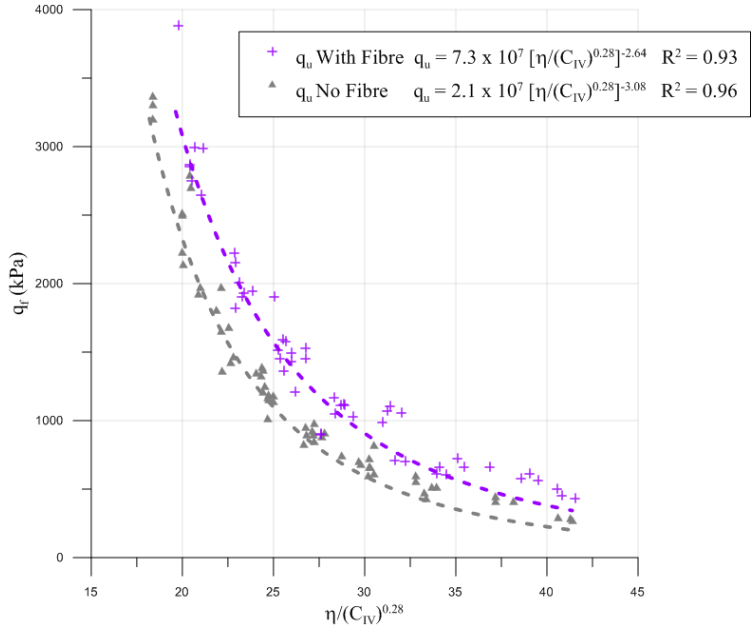

Figure 4.1: Unconfined compression strength *versus* porosity/volumetric cement content index (adapted from FESTUGATO, 2011)

4.1.2 Split tensile tests

Table 4.2 presents the preliminary results from the comparison of the data presented by Festugato (2011) and the one attained by this research for cylindrical specimens of 5 x 10 cm (diameter x height). It can be observed in table 4.2 that the mean average strength between experimental programs was within an acceptable limit of variation. Even though the values of variation were higher than the observed for UC tests, the strength values were at the same level of magnitude (around 6%). As observed with the unconfined compression, there was a greater variability for mixtures with fibres (around 12%). This could be explained also by the effect of fibre insertion in the increase in ductility of the composites that leads to a difficulty of precisely determining the strength at rupture.

At first, it was assumed that the maximum split tensile strength (q_t) used for the cylindrical fatigue tests (10 x 5 cm – diameter x height) would be able to be assessed through the data for split tensile

tests for 5 x 10 cm (diameter x height) specimens presented by Festugato (2011). This assumption was based on the fact that in equation that determines q_t (equation 3.2) the diameter (D) and height (H) of the specimen are both dividing the load (P). Thus, having the values of D and H interchanged should not affect the split tensile strength of the mixture. However, during the experimental stage, it was observed that the maximum values of q_t attained for the 5 x 10 cm (D x H) were different than the q_t values obtained for the 10 x 5 cm (D x H), especially for the fibre reinforced specimens.

Table 4.2: Comparison between split tensile test results for 5 x 10 cm specimens

Combiantions	q_t (kN/m^2)	Average q_t (kN/m^2)	q_t Festugato (2011) (kN/m^2)	Average q_t (kN/m^2)	Variantion (%)
γ_d = 18	169.83	146.89	168.93	158.08	7.08
%C = 5	119.68		141.33		
%F = 0	151.17		163.98		
γ_d = 19	97.06	101.73	93.55	96.00	-5.97
%C = 3	111.63		94.49		
%F = 0	96.50		99.95		
γ_d = 19.7	381.95	364.46	-	343.41	-6.13
%C = 7	350.26		334.72		
%F = 0	361.17		352.09		
γ_d = 18	270.70	282.95	307.17	324.43	12.79
%C = 5	268.95		346.00		
%F = 0.5	309.19		320.12		
γ_d = 19	321.45	311.33	300.68	352.07	11.57
%C = 3	300.62		384.59		
%F = 0.5	311.93		370.93		

Figure 4.2 presents the relationship between the split tensile strength (q_t) and the porosity/ volumetric cement void ratio ($\eta/C_{iv}^{0.28}$) for the 10 x 5 cm specimens. It can be observed that, differently to what was found for the 5 x 10 cm specimens, the trends are extremely similar for mixtures with and without fibres. The specimens without fibres show slightly higher strength values (on average 2%) than the specimens with fibres. The difference in values of q_t between unreinforced and fibre-reinforced specimens increased with the decrease of $\eta/C_{iv}^{0.28}$. Indicating that fibre addition leads to further disruption of the formation of cementitious

bonds with the increase of cementation and/or decrease in porosity as observed by Consoli *et* al., 2009.

This same data is presented in figure 4.3 alongside the data from Festugato (2011) for the 5 x 10 cm specimens. This graph indicates that the q_t values for the larger diameter specimens without fibres are higher than the specimens with smaller diameter, especially for specimens with higher $\eta/C_{iv}^{0.28}$.

As for the mixtures with fibres, there is a clear decrease in resistance (about 29% decrease) for the specimens with higher diameter. This phenomenon could be attributed to the difference in the diameter/height ratio, for the 5 x 10 specimens the height (or depth alongside the z axis where the loading is applied) of the specimen is twice the diameter, having a ratio of 0.5. Thus, it could be assumed that there is continuous plain strain loading condition across the loaded axis. However, when the diameter and height of the specimen are interchanged (10 x 5 cm), the diameter/height ratio is 2 and plain strain across the loaded axis can no longer be assumed (FESTUGATO *et* al., 2018). This would be especially important in fibre-reinforced specimens where strains are higher due to the increase in ductility of the composite.

Besides this, the anisotropy imposed during the moulding process should be taken into account. For the 10 x 5 cm fibre-reinforced specimens, the orientation of the fibres is preferentially horizontal, alongside de diameter, having few fibres alongside the loaded (height) axis. Not having aid of the fibres alongside the loaded could lead to the stagnation and even decrease in resistance (DIAMBRA *et* al., 2018). Figure 3.12 illustrates the difference in the failure mode presented buy the 5 x 10 and 10 x 5 cm for unreinforced and fibre-reinforced specimens.

Even though there was an acceptable fit for the q_t *versus* $\eta/C_{iv}^{0.28}$ relationships, it was decided to use the average value of three split tensile tests for each chosen mixture as the benchmark maximum values for the fatigue tests instead of the fitted curve. This choice was made as an effort to diminish variability of data. The values of split tensile strength are quite low when compared to unconfined compression (q_t are around 15% of q_u values), and the error correspondent to the use of the approximation of the q_t values when using the $q_t - \eta/C_{iv}^{0.28}$ equations proved important when associated with the intrinsic limitations of the fatigue equipment when loading precision is concerned. The use of the fitted equations caused a great variability in results leading to the aforementioned decision.

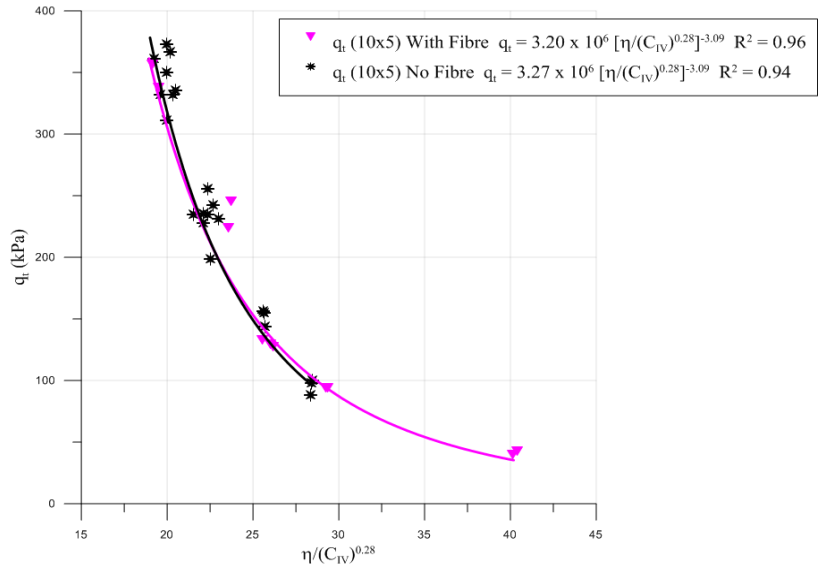

Figure 4.2: Split tensile strength *versus* porosity/volumetric cement content index for 10 x 5 cm specimens

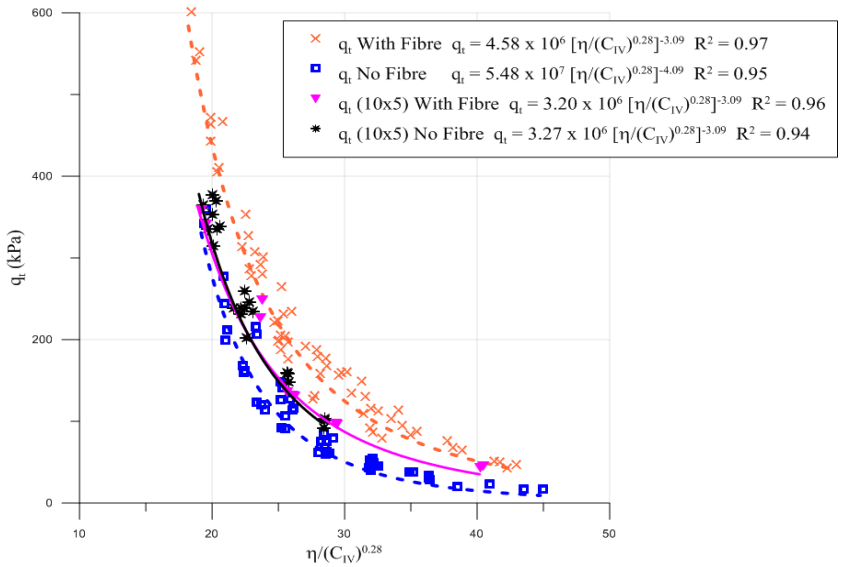

Figure 4.3: Split tensile strength *versus* porosity/volumetric cement content index for 10 x 5 cm specimens and 5 x 10 specimens by Festugato (2011)

4.1.3 Flexural tensile tests

The results of the flexural tensile testing program were presented regarding the effect of cement content (C), dry unit weight (γ_d), fibre insertion (F), and lastly, porosity/volumetric cement ratio ($\eta/C_{iv}^{0.28}$). The mentioned data is shown in the next topics.

4.1.3.1 Effect of cement content

Results considering the amount of cement added to the mixture are presented in figures 4.4 and 4.5. As expected from previous researches with Botucatu sandstone and cement from Specht (2000), Foppa (2005) and Festugato (2011), it can be observed an increase in strength with the increase in cement content.

It is also observed an increase in strength due to fibre insertion, especially for the specimens with lower dry unit weight. This increase for lower γ_d (18 kN/m^3) can be due to a greater fibre mobilization on the shear band on specimens with lower porosity. The average increase in strength due to cement addition from 3 to 7% for unreinforced specimens was of 87, 70 and 119% for 18, 19 and 19.7 kN/m^3, respectively. As for fibre-reinforced composites, the average increase in strength was of 90, 68 and 90% for the same dry unit weights.

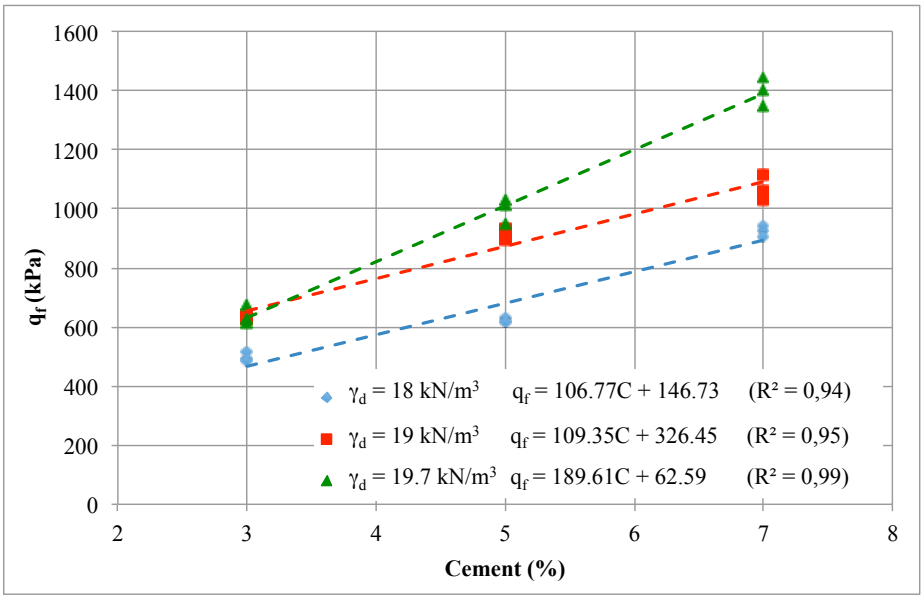

Figure 4.4: Effect of cement content on flexural strength for soil cement composites

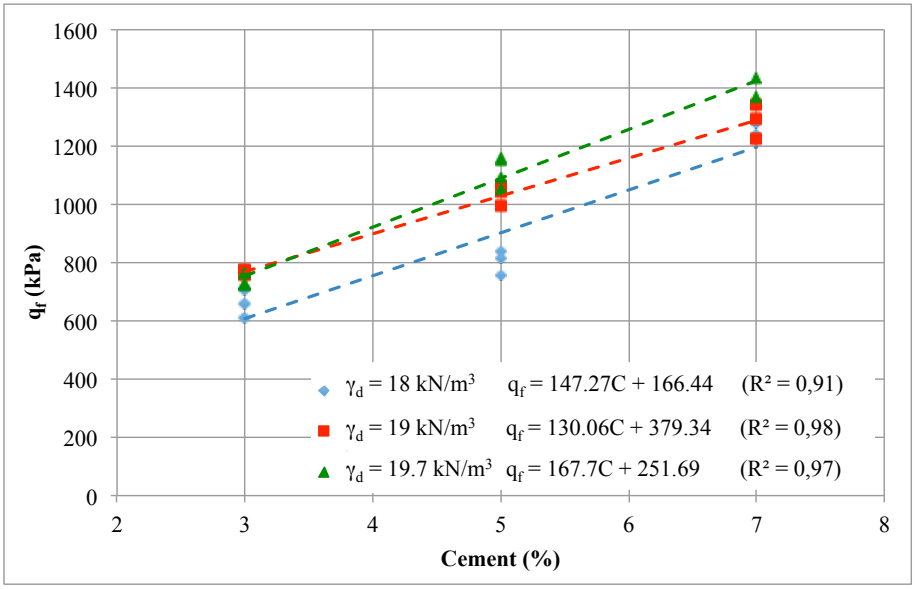

Figure 4.5: Effect of cement content on flexural strength for fibre-reinforced soil cement composites

4.1.3.2 Effect of dry unit weight

The influence of dry unit weight on the strength of the studied composites is presented in figures 4.6 and 4.7. It can be observed from the presented graphs that an increase of γ_d from 18 to 19.7 kN/m^3 did not generate as great an impact in strength gain as the increase in cement content did. This can especially be observed for the lowest cementation content (3%), where the increase in strength was of 29 and 12% for unreinforced and reinforced composites, respectively. As for the higher cement percentages, the average increase in resistance observed was of 60 and 51% for unreinforced specimens at 19 and 19.7 kN/m^3, respectively. And of 38 and 13% for 19 and 19.7 kN/m^3, respectively for reinforced specimens.

Also, it can be inferred by the data presented that the rate of strength gain for fibre-reinforced composites was smaller than for the unreinforced specimens when reduction of porosity was concerned. This suggests that the addition of fibres physically disrupts bond formation due to increased compaction. Gray and Al-Rafeai (1986) pointed out that a greater compaction effort leads to a higher entanglement and distortion of fibres, thus, modifying the reinforced soil response.

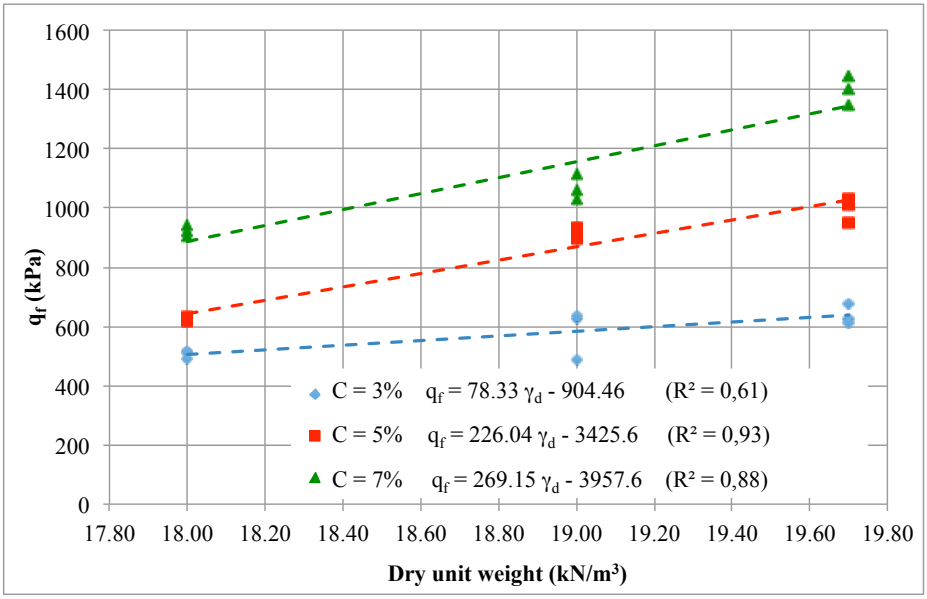

Figure 4.6: Effect of dry unit weight on flexural strength for soil cement composites

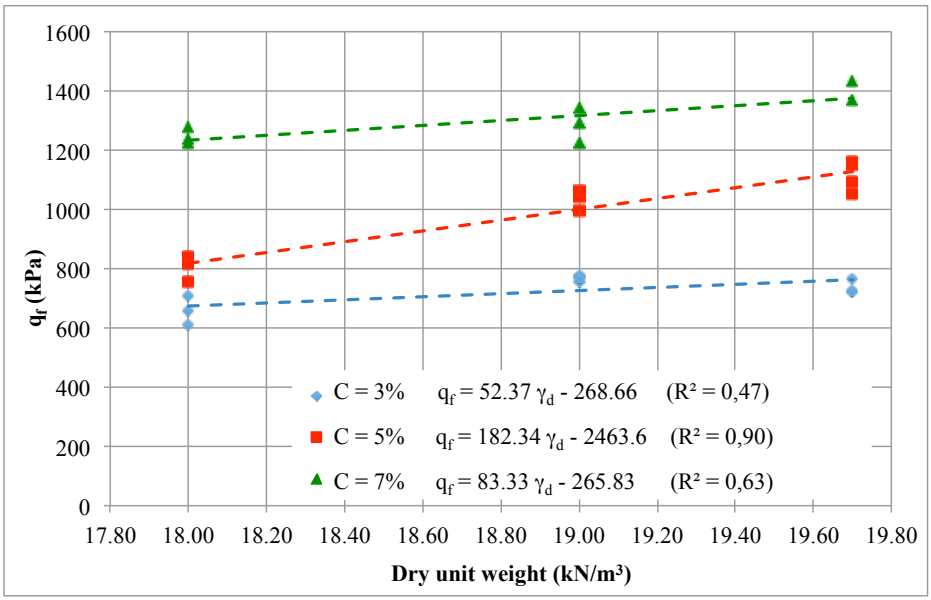

Figure 4.7: Effect of dry unit weight on flexural strength for fibre-reinforced soil cement composites

4.1.3.3 Effect of fibre content

Figure 4.8 shows the effect of fibre insertion on flexural tensile strength. It can be observed a strength improvement on the specimens with lower dry unit weight, however, as the compaction effort increases the influence of fibre addition on strength gain decreases. This behaviour can be better seen in figure 4.9, where the effect of fibre insertion was evaluated with respect to cement content variation for the three studied dry unit weights.

On average, the difference between unreinforced and reinforced composites was of 33, 18 and 7% for 18, 19 and 19.7 kN/m^3, respectively. This corroborates with the observation made on the previous paragraph that the addition of fibres improves strength for lower compaction efforts.

The great advantage of fibre addition to the improved composites was on the failure mechanism. Fibre-reinforced composites presented a dramatic reduction in the brittle behaviour presented by cemented soil. The fibre-reinforced specimens did not present a significant post-peak strength loss, resisting the tensile strength at great deformations. Thus, the rupture mode could be considered as deflexion-hardening, as suggested by Donkor and Obonyo (2016). This failure mode improvement can be qualitatively observed in figure 4.10, and corroborates the data presented by other authors such as Festugato (2011) for split tensile strength and Sukontasukkul and Jamsawang (2012) for flexural tensile strength. The authors stressed that fibres inhibit rupture associated cracks on fibre composites. This leads to an increase in the area below stress-strain curves, representing a greater capacity of the composite in absorbing energy.

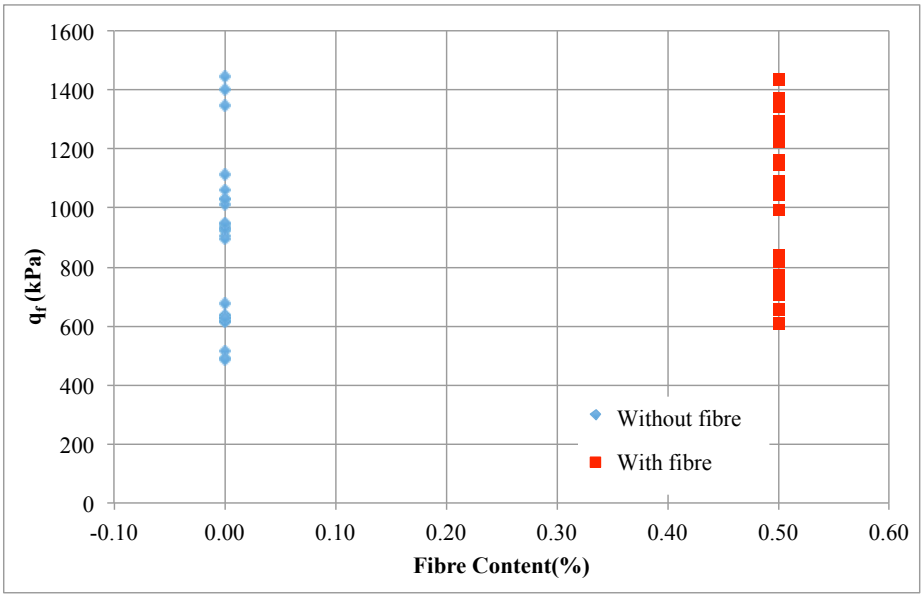

Figure 4.8: Effect of fibre insertion on flexural strength for soil cement composites

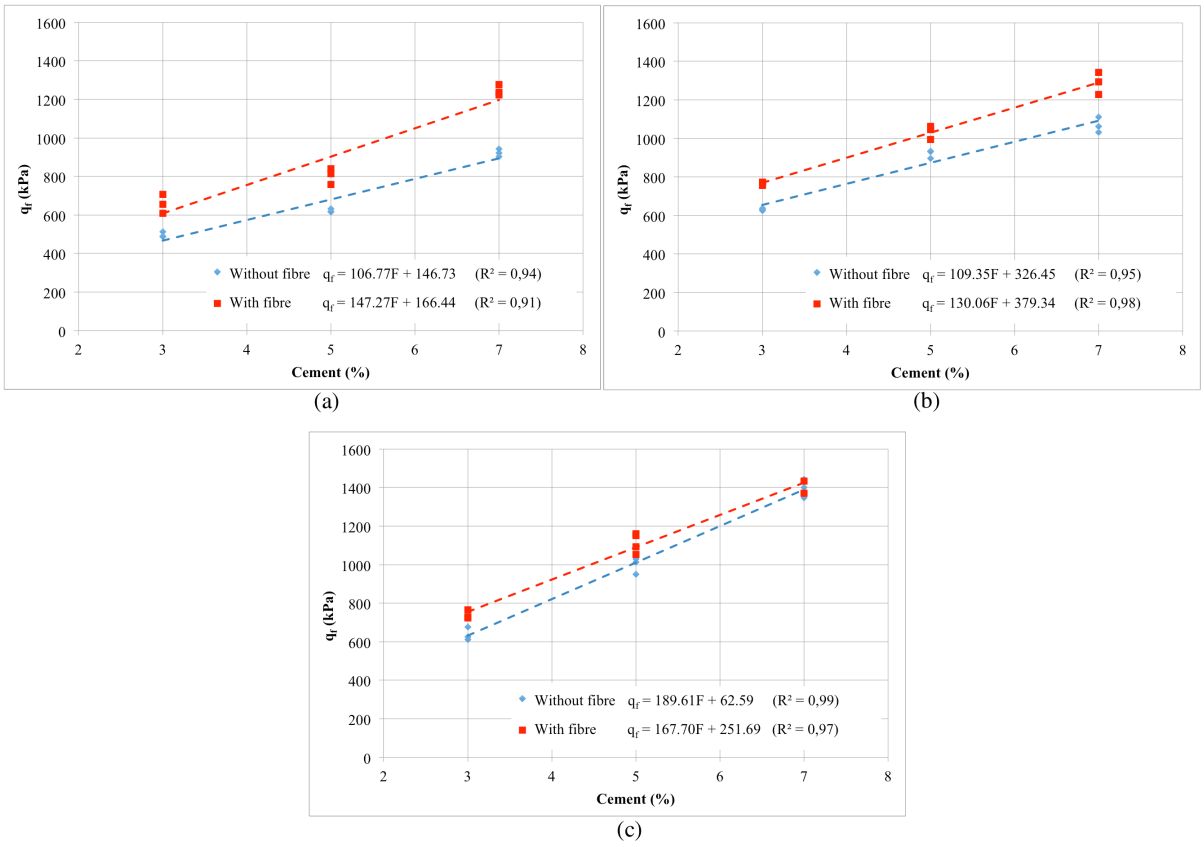

Figure 4.9: Effect of fibre insertion on flexural strength for soil cement composites with respect to cement content variation for (a) γ_d = 18kN/m^3 (b) γ_d = 19kN/m^3 (c) γ_d = 19.7kN/m^3

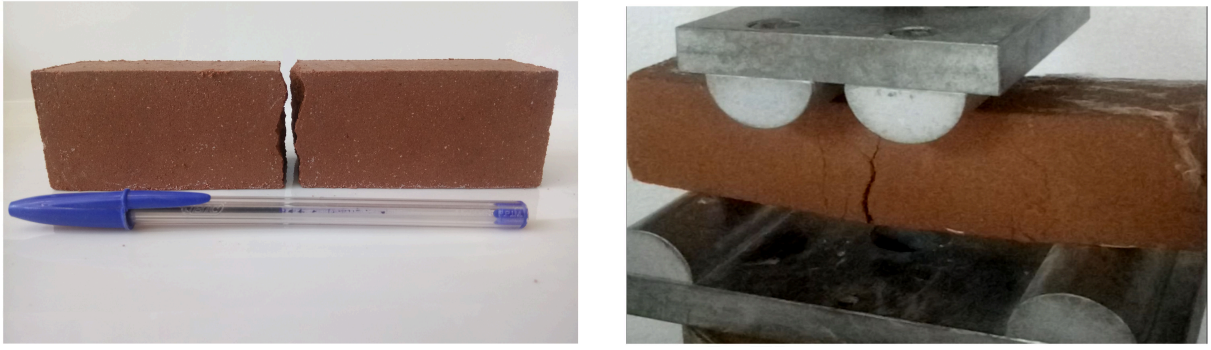

(a) (b)

Figure 4.10: Rupture mode (a) soil cement – brittle (b) fibre-reinforced soil cement – ductile

4.1.3.4 Effect of porosity/volumetric cement ratio

The results previously shown are presented using the porosity/volumetric cement ratio (η/C_{iv}) that has been largely used on the LEGG research group. In figure 4.11 is presented the results for the unreinforced cemented soil, and in figure 4.12 the results for fibre-reinforced cemented soil are presented.

The use of an exponent of 0.28 on the volumetric cement content was considered suitable to equate the variation ratio between the porosity and the volumetric cement content, with high coefficients of determination, as observed by Foppa (2005), Consoli *et* al. (2010 b), Festugato (2011), Consoli *et* al. (2011 a).

It can be observed for all studied mixtures that there was an increase in flexural strength with the reduction of the $\eta/(C_{iv})^{0.28}$, which implicates that the reduction in the porosity and/or an increase in binder content leads to an increase in flexural tensile strength.

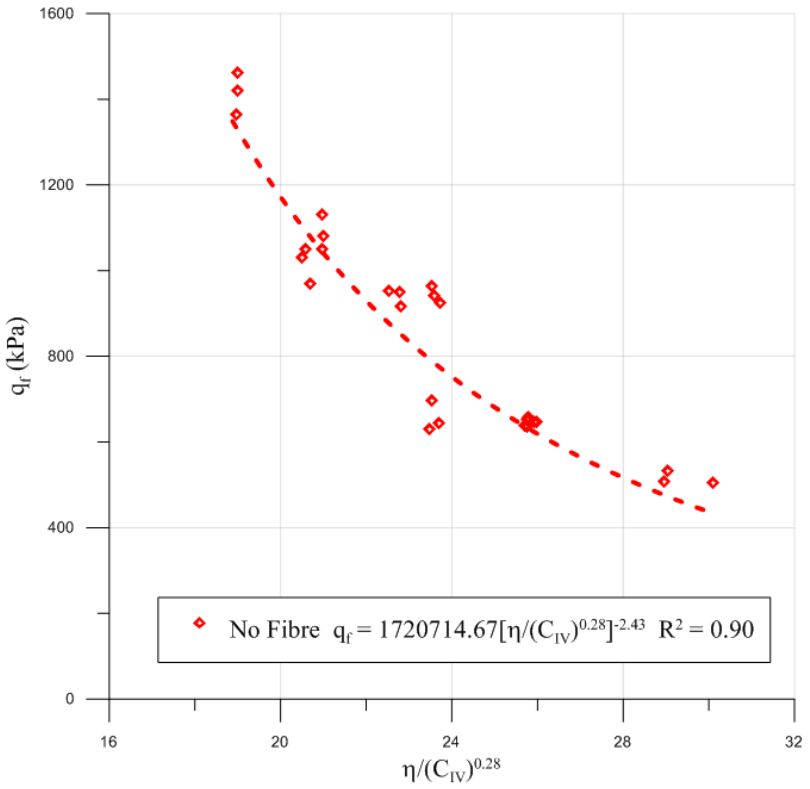

Figure 4.11: Adjusted porosity/volumetric cement ratio for unreinforced cemented soil

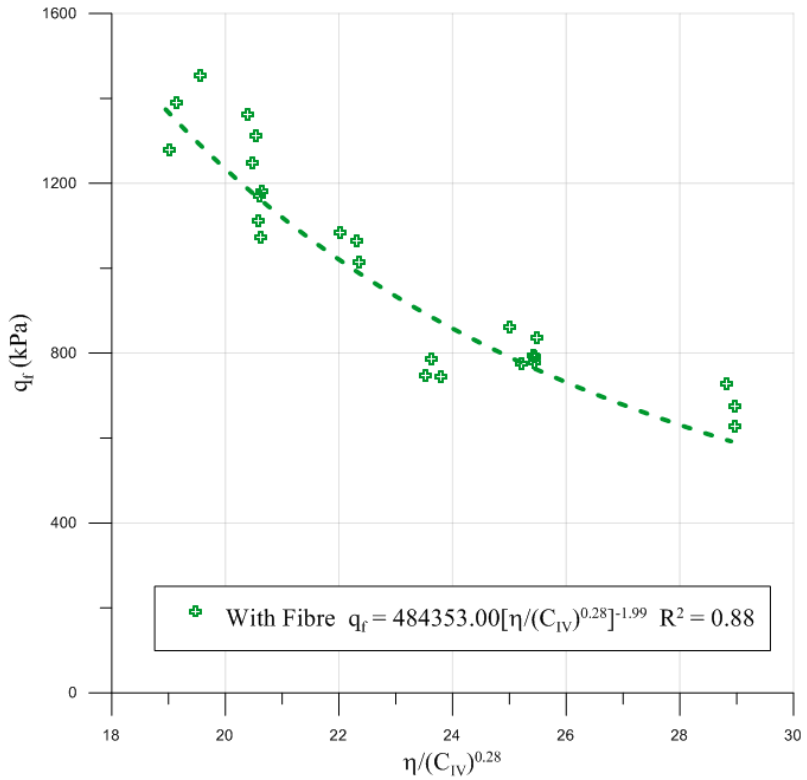

Figure 4.12: Adjusted porosity/volumetric cement ratio for fibre-reinforced cemented soil

Through the analysis of the figure 4.13 the following observations can be made: fibre insertion leads to an increase in flexural tensile strength for lower $\eta/(C_{iv})^{0.28}$, however, as the η/C_{iv} increases, the effect of fibre addition diminishes; there was an increase in data dispersion for fibre-reinforced composites, which can be explained by the shift in rupture mode (brittle rupture became ductile), making it more difficult to determine where peak-strength occurs.

Figure 4.14 shows a comparison between the results presented on this research for flexural tensile strength and the data presented by Festugato (2011) for unconfined compressive strength and split tensile strength. The power function increase in strength with the reduction of η/C_{iv} was observed for all test types. For all dosages the fibre-reinforced mixes presented higher strength values for the same η/C_{iv}.

It can be observed that the strength a specimen subjected to flexural stress endures was higher than the ones subjected to split tensile stress, and lower than the strength achieved for unconfined compressive stress. The same trend was observed on the experimental data presented by Specht (2000).

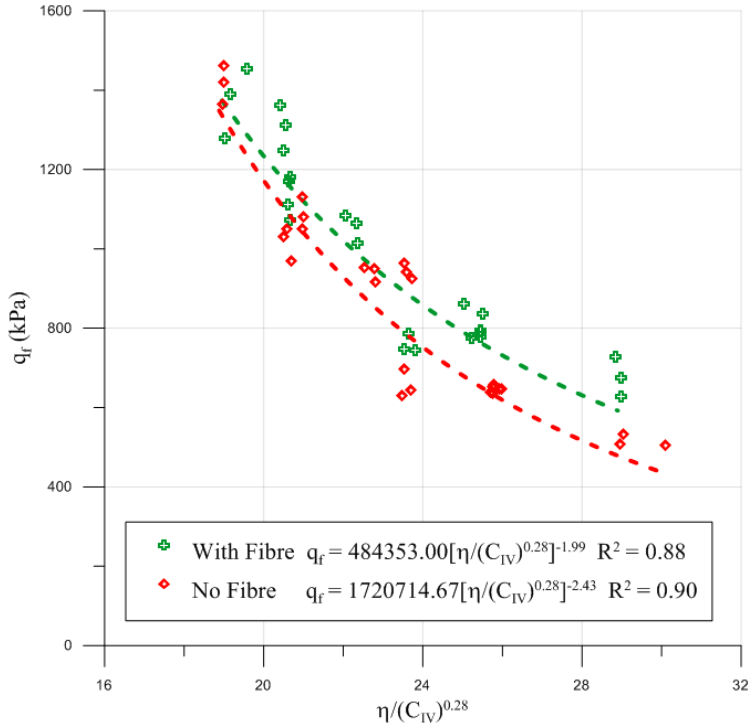

Figure 4.13: Adjusted porosity/volumetric cement ratio for unreinforced and fibre-reinforced cemented soil

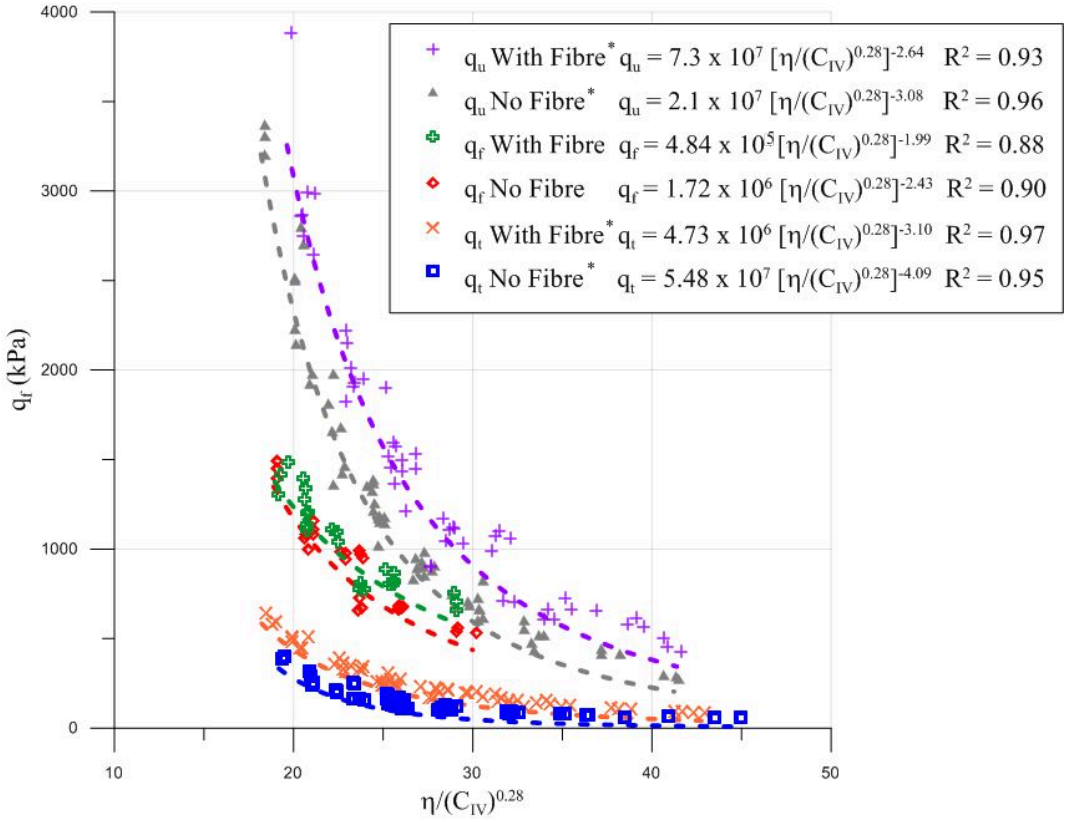

Figure 4.14: Adjusted porosity/volumetric cement ratio for unreinforced and fibre-reinforced cemented soil under different test conditions (* adapted from FESTUGATO (2011))

4.2 ULTASSONIC PULSE VELOCITY TESTS

This research used the Pundit equipment in order to assess the development of the shear modulus of the studied specimens over 9 days after moulding. This time frame was chosen because the maximum established limit of cycling time for CUC and FT was of 36 h after 7 days of curing. Even though the majority of the cementation process should occur within the first 7 days when using early strength Portland cement, it was important to verify what was the impact of the development of the cementation process during testing on the initial shear strength (G_0). Three specimens were made for the benchmark mixture without fibres and three with fibre addition. However, it was not possible to read the results with fibres. The fibre insertion probably caused the wave pulse to disperse, making the reading inaccurate. Thus, it was assumed that the development of cementation bonds was not affected by fibres insertion.

The results from the ultrasonic pulse velocity tests are shown in table 4.3 and figure 4.15. The values of V_P/V_S were between 1.65 and 1.86, which are consistent with the values attained by Bortolotto (2017). Using equation 3.4, 3.5 and 3.6 and considering the specimen a continuous, elastic, isotropic and homogeneous medium, the values of G_0, M and ν were estimated.

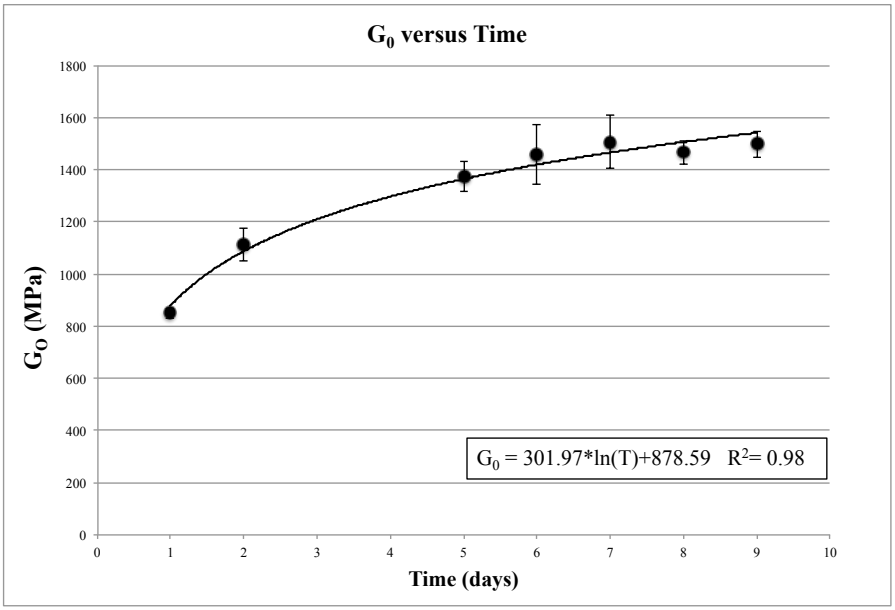

Figure 4.15: Shear modulus development with curing time for benchmark specimens without fibre addition

Table 4.3: Ultrasonic pulse wave test results

Sample	Day	P-wave time (μs)	S-wave time (μs)	W (g)	H (cm)	ρ (kg/m^3)	V_P (m/s)	V_S (m/s)	V_P/V_S	ν	M (MPa)	G (MPa)
	1	83.37	153.00	393.52	10.11	1932.48	1212.32	660.57	1.84	0.29	2840.18	843.23
	2	74.51	128.90	391.83	10.11	1924.18	1357.25	784.59	1.73	0.25	3544.60	1184.48
	5	68.87	117.00	390.98	10.11	1920.01	1468.05	864.10	1.70	0.23	4137.97	1433.62
CP1	6	69.50	114.80	390.74	10.13	1918.83	1458.03	882.69	1.65	0.21	4079.17	1495.06
	7	66.23	114.00	390.09	10.12	1915.64	1527.43	887.43	1.72	0.25	4469.26	1508.62
	8	66.37	117.50	390.02	10.10	1915.29	1522.35	859.86	1.77	0.27	4438.79	1416.08
	9	66.33	115.20	390.05	10.11	1915.44	1524.12	877.60	1.74	0.25	4449.46	1475.25
	1	83.37	152.20	391.23	10.03	1921.24	1202.72	658.78	1.83	0.29	2779.13	833.81
	2	71.23	132.70	390.45	9.99	1917.41	1402.90	753.08	1.86	0.30	3773.71	1087.41
	5	65.13	118.30	390.32	10.01	1916.77	1536.85	846.15	1.82	0.28	4527.22	1372.36
CP2	6	65.70	111.30	390.24	10.02	1916.38	1525.11	900.27	1.69	0.23	4457.44	1553.19
	7	66.03	109.30	389.89	10.01	1914.66	1515.90	915.83	1.66	0.21	4399.80	1605.90
	8	64.53	112.00	383.87	10.02	1885.09	1552.17	894.35	1.74	0.25	4541.62	1507.80
	9	64.00	114.40	389.06	10.01	1910.58	1563.54	874.71	1.79	0.27	4670.72	1461.81
	1	82.53	149.40	390.23	10.07	1916.33	1220.52	674.25	1.81	0.28	2854.68	871.19
	2	75.40	134.60	388.20	10.06	1906.36	1334.66	747.65	1.79	0.27	3395.83	1065.61
	5	66.93	121.10	388.24	10.06	1906.55	1503.49	830.99	1.81	0.28	4309.71	1316.57
CP3	6	65.57	120.30	388.12	10.05	1905.96	1533.30	835.69	1.83	0.29	4480.94	1331.08
	7	65.87	117.10	388.15	10.05	1906.11	1525.30	857.96	1.78	0.27	4434.67	1403.07
	8	65.90	114.40	388.02	10.06	1905.47	1527.06	879.66	1.74	0.25	4443.40	1474.47
	9	65.57	111.40	388.02	10.07	1905.47	1535.33	903.65	1.70	0.23	4491.67	1555.98

It was possible to infer from the data presented data that after 7 days of curing the initial shear modulus is mostly stabilized. There was an increase of 3% in G_0 from day 7 to day 8 and a further 2% from day 8 to day 9. If the average values are taken into consideration instead of the fitted logarithmic relationship, there is 2% in G_0 variability between the 7th and the 9th day. Given this, for the present research it was assumed that was not a significant change in G values during cycling due to increase in stiffness by the cementation process. The average Poisson's ratio for the material was of 0.26, which is consistent with data presented by Felt and Abrams (1957) and Diambra *et* al. (2018) for cemented sand.

5 CYCLIC UNCONFINED COMPRESSION TESTS

This chapter presents the results and analysis of the cyclic unconfined compression testes carried out at the Geomechanics laboratory of Bristol University. Firstly, it is presented the data for the soil-cement tests, analysing the influence of percentage of applied load on the number of cycles, axial strain, and shear modulus. Then, the data for soil-cement-fibre admixtures is presented, where the same variables are analysed for the stipulated load and a modified loading condition – soil-cement composites load. Finally, the results and analysis are discussed as a whole. Water was provided for the specimen during the cyclic test, however, given that the studied composite was sufficiently porous that and the frequency of the cyclic loading was sufficiently slow, the experiment could be considered a drained test. Thus, the presented data are in terms of effective stresses. The moulding data of the following tests are presented in Appendices A.

At first, this research intended to vary the $\eta/C_{iv}^{0.28}$ and study the influence of its variation regarding cyclic loading. However, after preliminary tests were made with Huston sand and cement Type-II, that was readily available at the English university, it was concluded that the variability of results was too broad. Which led to a fear that the results for the studied materials would not be very consistent. There was another important factor on the decision-making process, the amount of material available to carry out the research abroad. There was a limitation due to the quantities that were possible to ship overseas. Based on these factors and on research on cyclic triaxial tests that showed that the variation of loading, rather than of mixture led to more consistent data (SHARMA; FAHEY, 2003), this research reassessed its objectives, presenting the following.

It was determined a benchmark mixture: γ_d of 18 kN/m^3; 5% of cement content; and 0 or 0.5% of fibre content. This mixture was chosen because the values from the unconfined compression tests carried out during preliminary testing showed the lowest variation from the data from Festugato (2011) and the fitted trending line q_u *versus* $\eta/C_{iv}^{0.28}$ for specimens with and without fibres. Thus, suggesting that there should be a lower dispersion of testing results.

For each test, data was acquired from one external LVDT, two internal LVDTs without springs, a load cell and two bender elements. The response variables were: axial strain – ε_a [%]; axial strain at peak loading – ε_a max [%]; and Young's modulus – E [MPa], for external

and internal measurements; also: number of cycles – N; initial shear strain – G_0 [MPa]; and shear strain – G [MPa] for a range of cycles (1, 2, 10, 30, 50, 100, 200, 300, 500, 1000, 1500 and 2000). It was stipulated that the maximum N would be of 2000 cycles, which represents around 36 h of testing.

The elasticity modulus was assessed from the strain measurements during the loading and unloading process. Given that the applied loads were beyond the yielding point of the composite, the most adequate nomenclature for this measurement would be Young's modulus rather than the term elastic modulus, which would imply that there were no permanent strains due to the loading/unloading process. Figure 5.1 presents an example schematic of how the values of the Young's modulus (E) were calculated for each cycle.

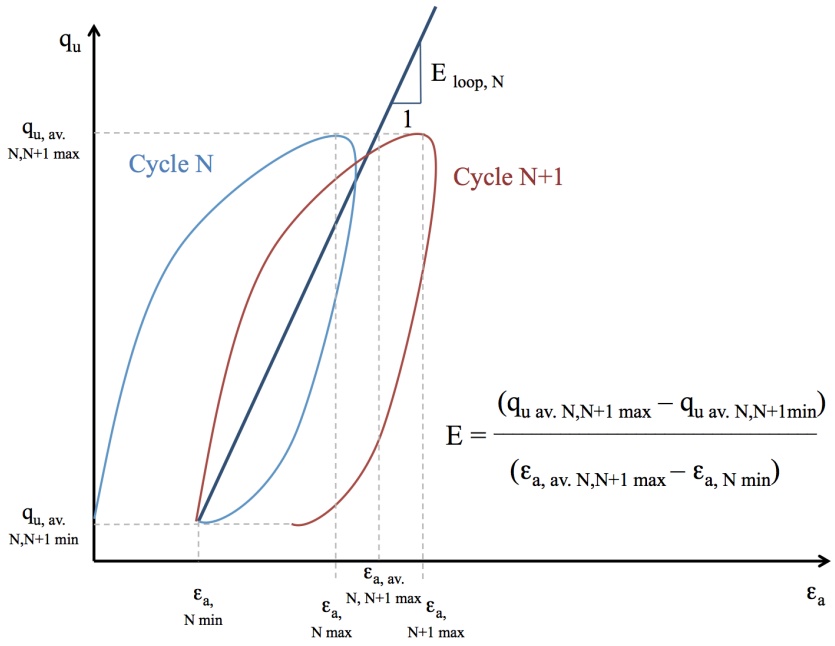

Figure 5.1: Schematic of Young's modulus calculation for an idealized cycle

5.1 SOIL-CEMENT

In this topic is presented the results of the tests carried out for the benchmark mixture (18 kN/m^3; 5% cement) for the stipulated load percentages (90, 80 and 70%). Also, for 80% of the maximum load, it was tested a different mixture combination with the same $\eta/C_{iv}^{0.28}$ (19 kN/m^3; 3% cement), aiming to assess the influence of $\eta/C_{iv}^{0.28}$ in cyclic loading. Because it is an unconfined

test, three repetitions of each point were done. During testing, bender elements were used to assess the shear modulus under very-small strains; this data is also presented in this section.

The value of the maximum load for each specimen studied was derived from the equation of q_u *versus* $\eta/C_{iv}^{0.28}$ presented by Festugato (2011) (Figure 4.1), as mentioned previously. The $\eta/C_{iv}^{0.28}$ of each specimen was calculated after moulding of the specimen and through the fitted formula (equation 4.1), its corresponding q_u value assessed. Table 5.1 presents the values attained for the moulded specimens.

Table 5.1: Soil-cement mixtures: loading determination for cyclic unconfined compression tests

Mixture	Ideal Load %	Repetition	$\eta/C_{IV}^{0.28}$	Theoretical Load (kPa)	Theoretical Load (N)	% Load (kPa)	% Load (N)	Applied Load (N)	Actual %
18 kN/m^3 - 5% cement	90	I	24.58	1094.70	2152.99	985.23	1937.69	2009.63	93.34
	90	II	24.30	1133.15	2216.45	1019.84	1994.81	2058.68	92.88
	90	III	24.61	1090.95	2153.19	981.86	1937.87	1956.69	90.87
	80	I	24.49	1107.08	2195.13	885.66	1756.11	1854.76	84.49
	80	II	24.40	1119.48	2211.74	895.58	1769.40	1810.85	81.87
	80	III	25.02	1036.83	2026.87	829.47	1621.49	1618.34	79.84
	70	I	24.30	1133.56	2231.39	793.49	1561.97	1605.94	71.97
	70	II	24.77	1069.50	2111.32	748.65	1477.92	1557.74	73.78
	70	III	24.76	1070.39	2109.70	749.27	1476.79	1525.64	72.32
19 kN/m^3 - 3% cement	80	I	24.70	1077.65	2126.12	862.12	1700.90	1756.49	82.61
	80	II	24.47	1109.52	2189.14	887.61	1751.31	1804.44	82.43
	80	III	24.97	1042.27	2058.24	833.81	1646.59	1685.46	81.89

The acquired data is presented in the form of graphs. Each test is presented in the form of two figures, one for the external data and another for the internal. Each figure has three graphs: q_u *versus* ε_a; $\varepsilon_{a\ max}$ *versus* N; and E *versus* N. There is also the data for the shear modulus (G) that is presented on its own item, where the relationship between G and N is presented for the different load percentages.

5.1.1 Applied load percentage: 90%

The specimens tested at 90% of its maximum estimated load are presented in figures 5.2 through 5.7. Figures 5.2 and 5.3 show the results for the external and internal data of the first

specimen, respectively. Then, figures 5.4 and 5.5 present the values for the external and internal data, respectively, of the second specimen. Lastly, figures 5.6 and 5.7 show the data for the external and internal LVDTs of the third specimen, respectively.

Table 5.2 presents a summary of the tests, including number of cycles until rupture (N), initial shear modulus (G_0), and the estimated value of the initial Young's modulus at very-small strains (E from G_0). The values of E presented derived from equation 5.1 and was used for all the other mixture combinations in this research. Even though it is an estimate of the initial value of the Young's modulus, it is attained through a relation from a very-small strain test, thus its direct comparison with the values of Young's modulus from cyclic testing is more qualitative than quantitative. From the data presented in this table, it is possible to assess that the $\eta/C_{iv}^{0.28}$ of the replicas have low dispersion results – less than 1%. As for the G_0, the dispersion of data is less than 10%. This indicates that the initial condition of all specimens is very similar.

$$E = 2 \cdot G(1 + \nu) \tag{5.1}$$

where:

E = Young's modulus (MPa);

G = Shear modulus (MPa);

ν = Poison's ratio (adopted 0.26).

Table 5.2: Summary of Cyclic UC tests for 90% of estimated maximum loading for specimens without fibres

Mixture	Ideal Load %	Repetition	$\eta/C_{IV}^{0.28}$	Applied Load (N)	Actual %	Number of Cycles	Numeber of Cycles Rupture	Initial Bender (μs)	G_0 (MPa)	E from G_0 (MPa)
18 kN/m³ 5% cement	90	I	24.58	2009.63	93.34	3	3	111.40	1539.16	3878.67
	90	II	24.30	2058.68	92.88	25	25	127.20	1410.86	3555.37
	90	III	24.61	1956.69	90.87	23	23	120.20	1617.95	4077.23

Even though the addition of cement to the specimens should improve the variability of results intrinsic to the natural soil (SHARMA; FAHEY, 2003), the number of cycles until rupture (N) of the studied material presents some variability for this loading condition. Which is to be expected when dealing with cyclic testing.

The first specimen (18-5-0-90-I) (figures 5.2 and 5.3) lasted only three cycles. The only difference between this to the other specimens was the percentage of load actually applied in respect to its estimated load, which was slightly higher than the other two. However, this discrepancy can likely be attributed to the intrinsic variability of testing. The other repetitions (figures 5.4 through 5.7) show similar trends and values of number of cycles, deformation and Young's modulus.

From the external data (figure 5.2) for the first specimen it is observed a high strain during the first cycle of around 1.253%, after which there is a steady increase in strain until rupture around 1.751% (figure 5.2 (b)). This initial strain, which is over half the total, is partly due to equipment accommodation. The Young's modulus (figure 5.2 (c)) presented an increase during the first and second cycles, followed by rupture.

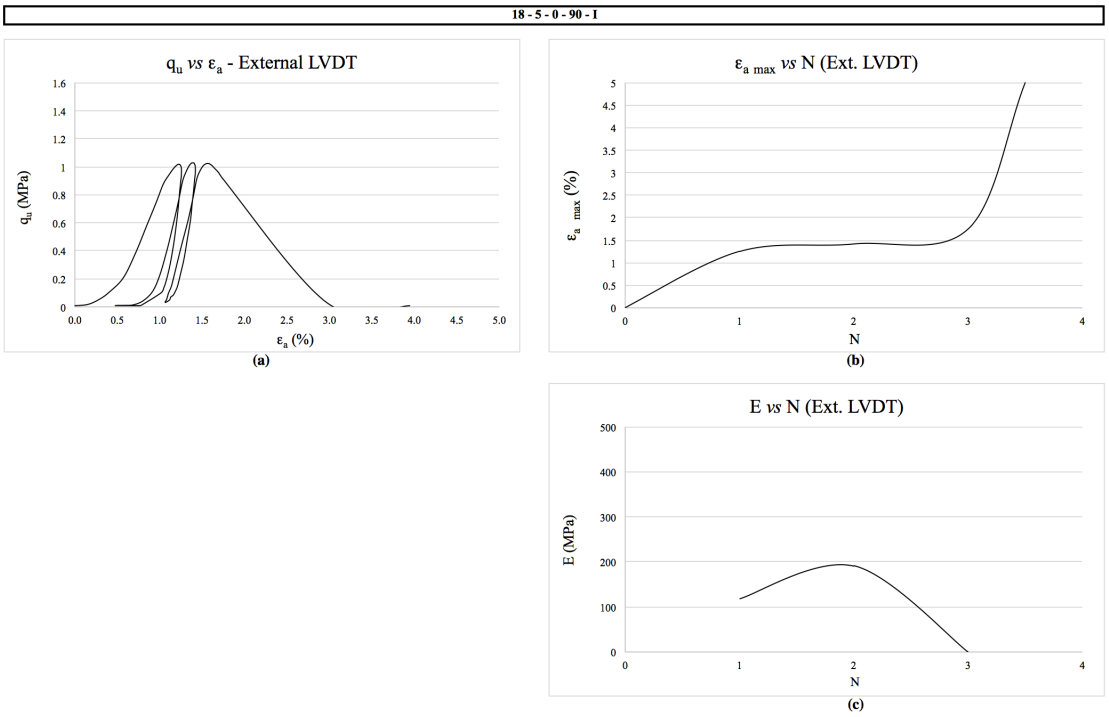

Figure 5.2: External data from specimen 18-5-0-90-I (a) q_u *versus* ε_a (b) $\varepsilon_{a\ max}$ *versus* N (c) E *versus* N

When focusing on the internal data for the same specimen, a lower overall strain is observed and the overall stiffness of the specimen was higher. Thus, inferring that the external data only provides a broad estimative of the data. Figure 5.3 (b) shows that there is an initial strain of 0.378% followed by an increase in strain until rupture at 1.216%, over four times the initial strain. As for the Young's modus (figure 5.3 (c)), the initial values were around 339.66 MPa.

The specimen presented a decrease in E with cycling until rupture. This indicates a rapid degradation of stiffness that led to rupture.

The second specimen lasted 24 cycles. From the external data (figure 5.4) it is observed an initial strain during the first cycle of around 0.759%, after which there is a steady increase in strain until rupture around 1.313% (figure 5.4 (b)). This initial strain, which is over half the total, is partly due to equipment accommodation. The Young's modulus (figure 5.4 (c)) presented an increase during the first and second cycles, followed by a steady decrease in E values until rupture at the 24th cycle.

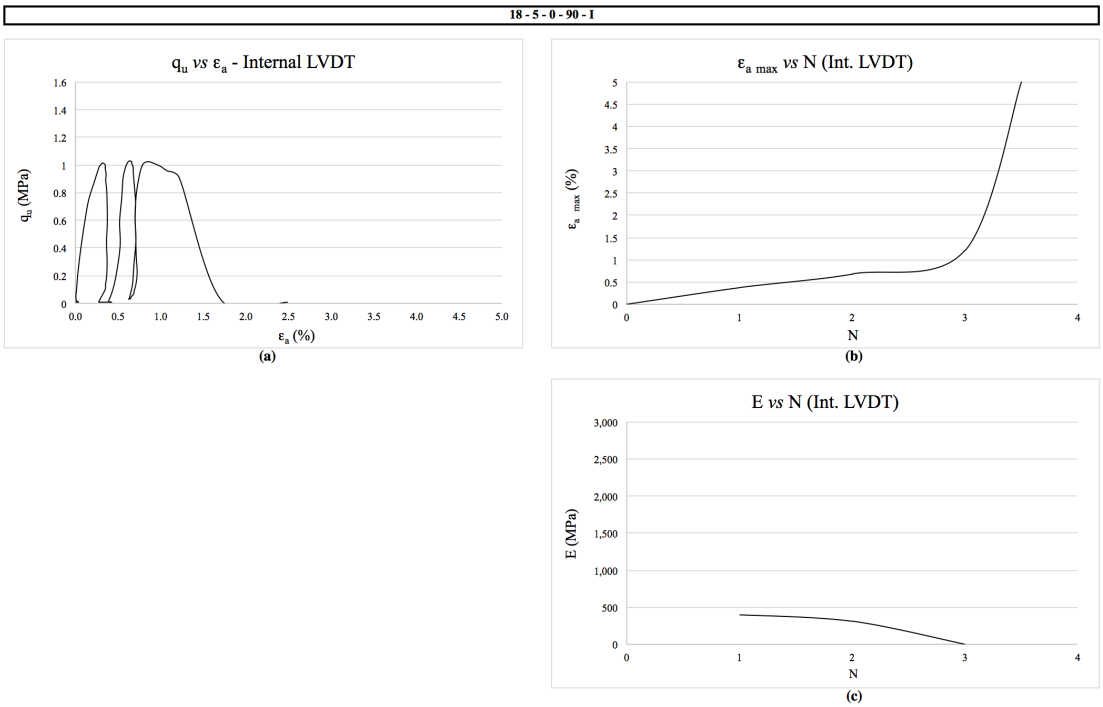

Figure 5.3: Internal data from specimen 18-5-0-90-I (a) q_u *versus* ε_a (b) $\varepsilon_{a\ max}$ *versus* N (c) E *versus* N

When focusing on the internal data for the same specimen, a lower overall strain is observed and the overall stiffness of the specimen was higher. Figure 5.5 (b) shows that there is an initial strain of 0.172% followed by an increase in strain until rupture at 0.459%, over two and a half times the initial strain. As for the Young's modulus (figure 5.5 (c)), the initial values were around 1430.61 MPa. The specimen presented an increase of 57.2% in E due to cycling over the first 3 cycles, reaching 2248.7 MPa. After, the Young's modulus decreased at a somewhat constant rate until the last 3 cycles. Then, there was a rapid increase (around 27%) in stiffness until rupture occurred. This indicates an initial accommodation of the specimen,

followed by a degradation of the modulus that can be attributed to a progressive failure of the weaker cemented bonds resulting in increase in plastic deformation of the matrix. Finally, there was an increase in E likely due to a critical number of cement bonds failing. This led to a significant decrease in the void ratio of the matrix, presenting increasingly larger plastic deformations (meaning an increase in the rate of $\varepsilon_{a\ min}$ in respect to the increase in $\varepsilon_{a\ max}$), ultimately leading to an abrupt failure.

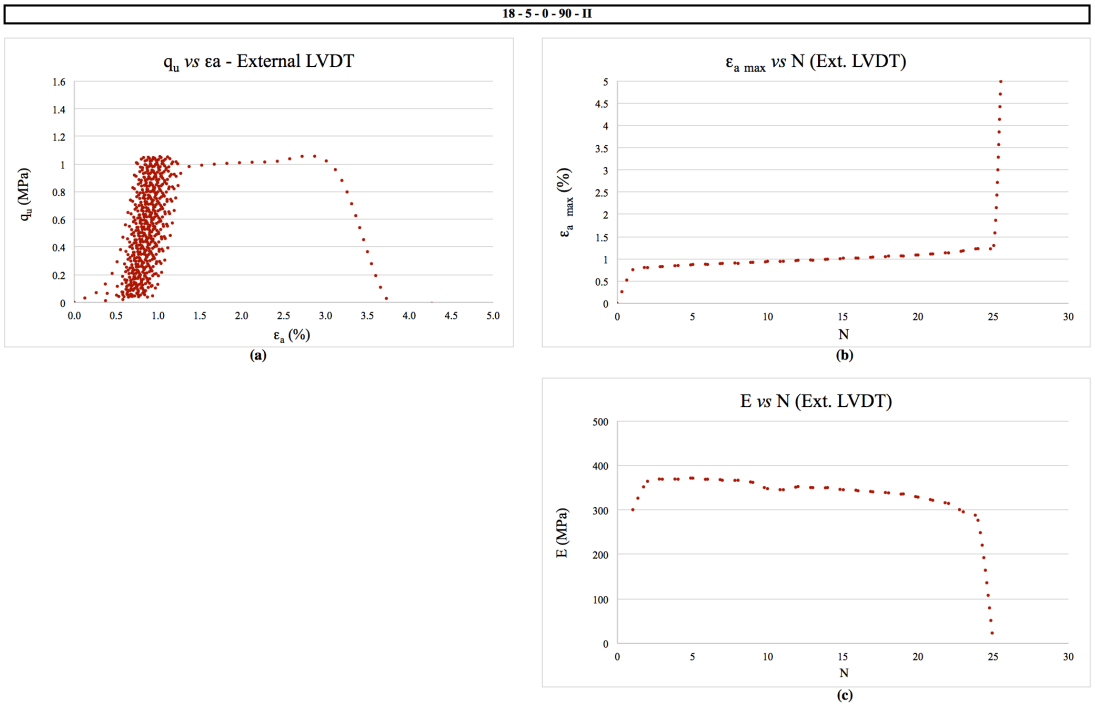

Figure 5.4: External data from specimen 18-5-0-90-II (a) q_u *versus* ε_a (b) $\varepsilon_{a\ max}$ *versus* N (c) E *versus* N

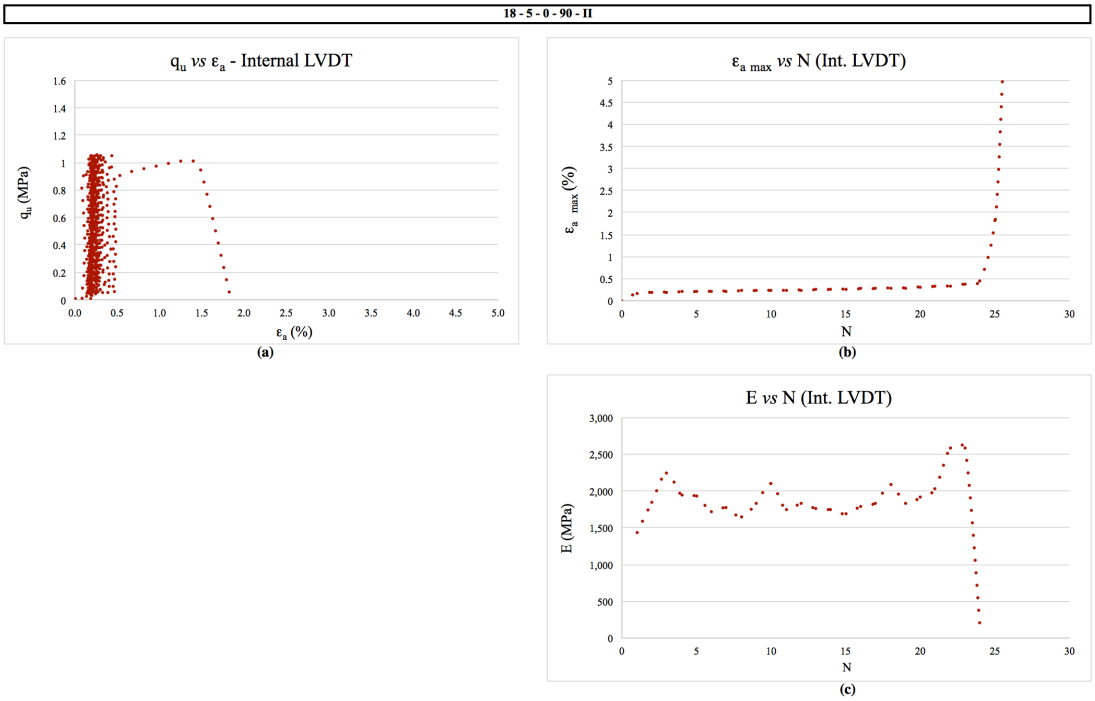

Figure 5.5: Internal data from specimen 18-5-0-90-II (a) q_u *versus* ε_a (b) $\varepsilon_{a\ max}$ *versus* N (c) E *versus* N

As for the last repetition for this combination, the third specimen lasted 23 cycles. From the external data (figure 5.6) it is observed an initial strain during the first cycle of around 0.973%, after which there is a steady increase in strain until rupture around 1.416% (figure 5.6 (b)). This initial strain, which is over half the total, is partly due to equipment accommodation. The Young's modulus (figure 5.6 (c)) presented an increase during the first and second cycles, followed by a steady decrease in E values until rupture at the 24th cycle.

When focusing on the internal data for the same specimen, a lower overall strain is observed and the overall stiffness of the specimen was higher. Figure 5.7 (b) shows that there is an initial strain of 0.319% followed by an increase in strain until rupture at 0.657% over two times the initial strain. As for the Young's modus (figure 5.7 (c)), the initial values were around 1467.2 MPa. The specimen presented an increase of 78.5% in E due to cycling over the next 15 cycles, reaching 2619.6 MPa. After, the Young's modulus decreased rapidly (around 99%) until rupture occurred. This indicates a gradual decrease in porosity during cycling and that the stiffness of the specimen while cementation bonds degraded until a critical cementation break occurred and the structure matrix began to collapse causing the degradation of stiffness and ultimately rupture.

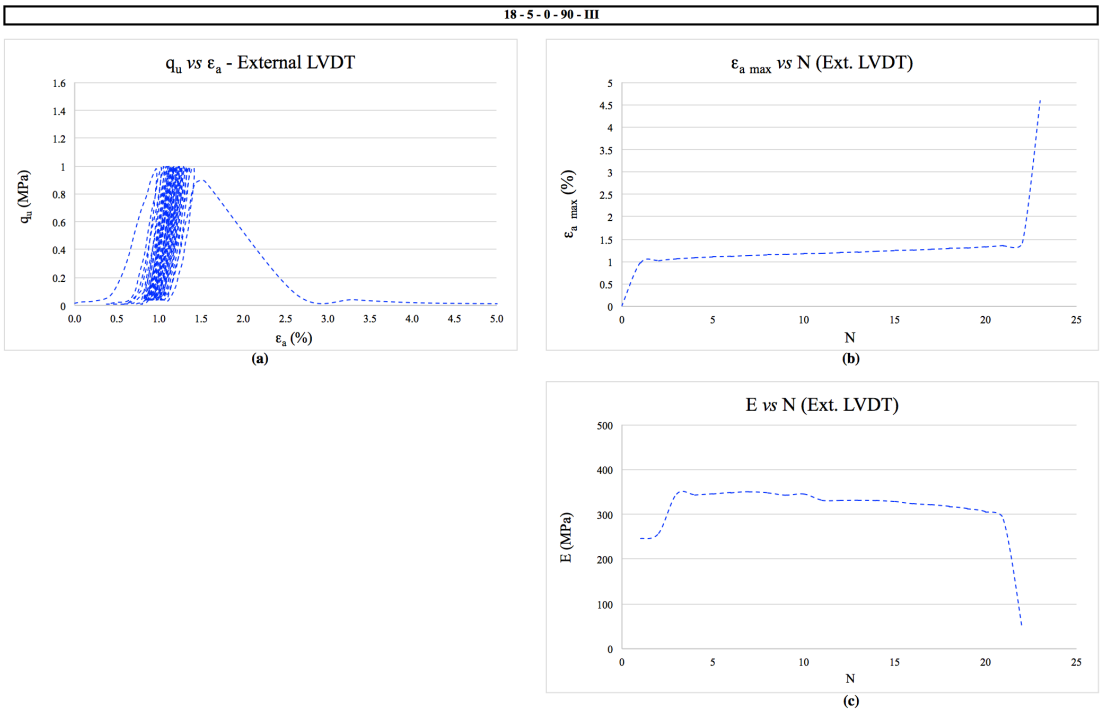

Figure 5.6: External data from specimen 18-5-0-90-III (a) q_u *versus* ε_a (b) $\varepsilon_{a\ max}$ *versus* N (c) E *versus* N

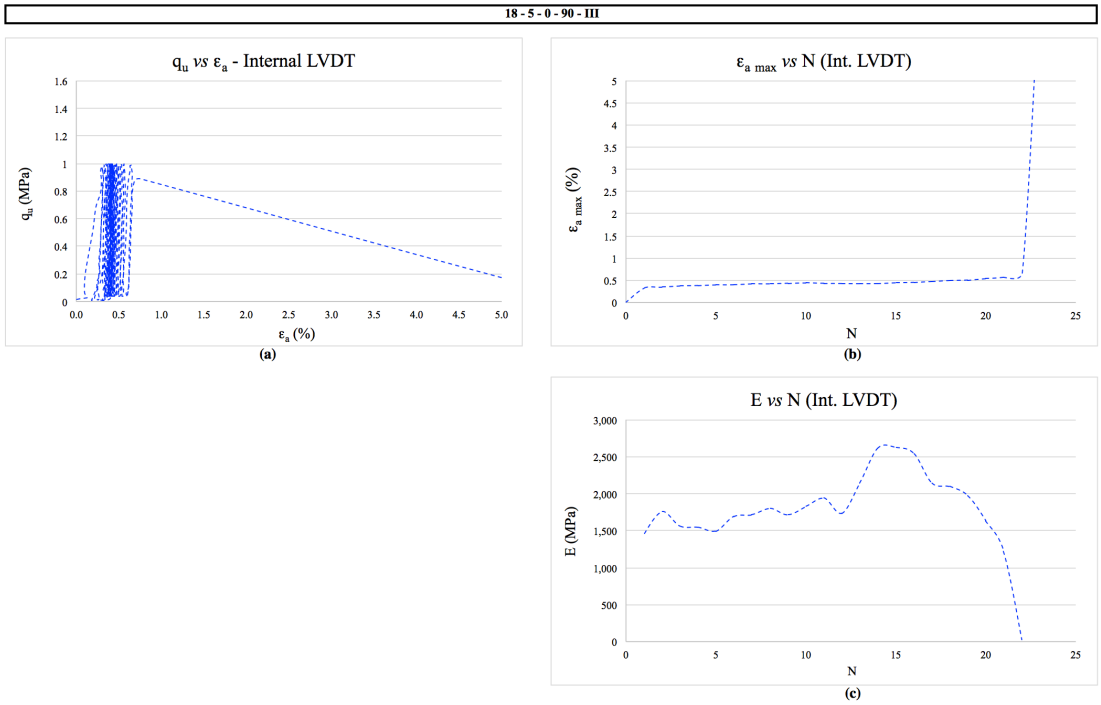

Figure 5.7: Internal data from specimen 18-5-0-90-III (a) q_u *versus* ε_a (b) $\varepsilon_{a\ max}$ *versus* N (c) E *versus* N

Figures 5.8 and 5.9 present the combined external and internal data for the three repetitions, respectively. When comparing the data from the external LVDT and the two internal ones, it can be observed that there is a greater accuracy from the internal data, as it should be expected. The location of the external LVDT outside the apparatus leads to many losses in accuracy, giving only a broad estimative of the overall comportment.

When focusing in figure 5.8 (b), there is an initial deformation, which especially for the external data, can be attributed in part to the accommodation of the equipment. The other portion of the deformation is due to the initial deformation of the specimen. However, it is impossible to differentiate the two values. Afterwards, for specimens II and III, there is a steady increase in deformation until the strain at rupture is reached. On average, the axial strain increased 0.4% until specimen failure. The Young's modulus (Figure 5.8 (c)) reaches a maximum around 350 MPa after a couple of cycles. Then, there is a steady decrease in the modulus until rupture, around 300 MPa.

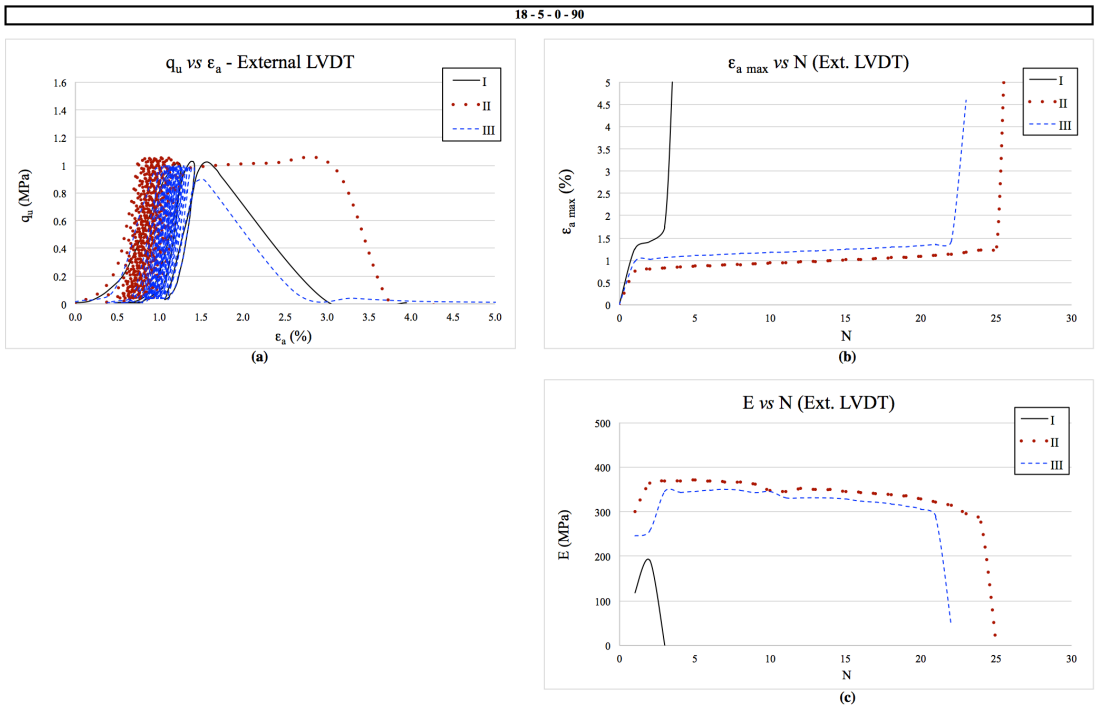

Figure 5.8: External data from specimen 18-5-0-90-I, II and III (a) q_u *versus* ε_a (b) $\varepsilon_{a\ max}$ *versus* N (c) E *versus* N

From figure 5.9 (b), it is possible to observe that after the initial deformation, which is also partly due to accommodation of the equipment but to a smaller extent, had the same trend of

increase in axial strain. On average, for specimens II and III, there was an increase of 0.3% in strain after the first cycle.

As for the Young's modulus (figure 5.9 (c)), it was observed a different trend than the one seen for the external LVDT. There is an initial increase in E after the first couple of cycles where accommodation is taking place and the weaker cementation bonds are mobilized. Da Fonseca *et* al. (2013) observed an initial increase in the modulus during the first cycles on cyclic triaxial tests and attributed the phenomenon to accommodation of the point of anchorage of the LVDTs and also stressed that this behaviour was more pronounced for lower confining stresses. After which, the values of E stabilized (1800 MPa) while cementation was gradually braking, but the structure of the matrix was still stable, accumulating plastic deformation. Then, there was a spike the modulus value (around 2700 MPa), indicating that the structure was failing and there is an important reduction in porosity after a significant break in cementation bonds due to cycling.

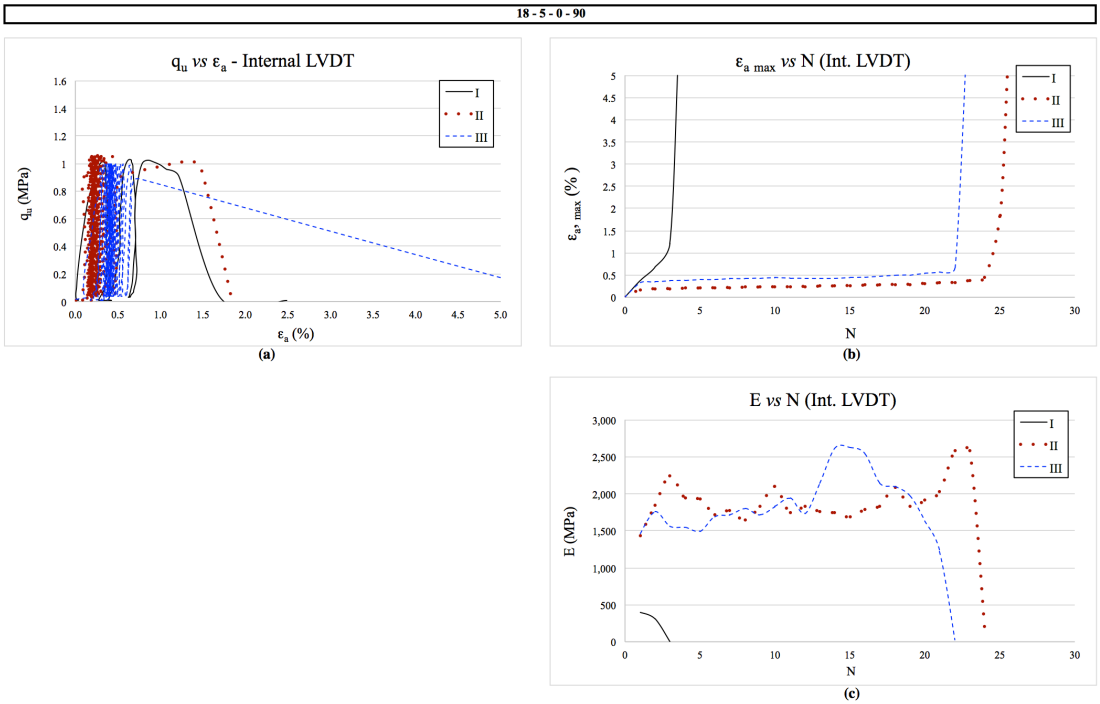

Figure 5.9: Internal data from specimen 18-5-0-90- I, II and III (a) q_u *versus* ε_a (b) $\varepsilon_{a\ max}$ *versus* N (c) E *versus* N

5.1.2 Applied load percentage: 80%

For this load percentage there were two different mixtures made, as mentioned previously. The first was the benchmark combination – figures 5.10 through 5.17, and the second was the 18

kN/m^3, 3 % cement content specimens – figures 5.18 through 5.25. Both mixtures have the same $\eta/C_{iv}^{0.28}$ and the data from their tests is presented in the following two topics.

5.1.2.1 Benchmark mixture

Figures 5.10 and 5.11 show the results for the external and internal data of the first specimen, respectively. Followed by figures 5.12 and 5.13 that present the values for the external and internal data, respectively, of the second specimen. Lastly, figures 5.14 and 5.15 show the data for the external and internal LVDTs of the third specimen, respectively.

The summary of the tests is shown in Table 5.3. It presents number of cycles until rupture (N), initial shear modulus (G_0), and the estimated value of the initial Young's modulus at small strains (E from G_0), again, the E values are just an estimative. From the presented data, it is possible to infer that the dispersion of $\eta/C_{iv}^{0.28}$ for the replicas is less than 2%. The dispersion of data for the G_0 is less than 6%, indicating a similar initial condition for the studied specimens.

Table 5.3: Summary of Cyclic UC tests for 80% of estimated maximum loading for benchmark mixtures without fibres

Mixture	Ideal Load %	Repetition	$\eta/C_{IV}^{0.28}$	Applied Load (N)	Actual %	Number of Cycles	Numeber of Cycles Rupture	Initial Bender (μs)	G_0 (MPa)	E from G_0 (MPa)
18 kN/m^3 5% cement	80	I	24.49	1854.76	84.49	78	77	105.30	1736.83	4376.80
	80	II	24.40	1810.85	81.87	245	245	108.30	1640.04	4132.91
	80	III	25.02	1618.34	79.84	79	79	114.40	1844.60	4648.39

As observed for the 90% loading specimens, there was variability in the number of cycles until rupture. However, the results are in the same order of magnitude, and all the moulding indicators – $\eta/C_{iv}^{0.28}$; actual loading percentage in respect to its estimated maximum load; and G_0 – suggest that the specimens have similar initial conditions.

The first specimen lasted 77 cycles. From the external data (figure 5.10) it is observed a high strain during the first cycle of around 0.78%, after which there is a steady increase in strain until rupture around 1.421% (figure 5.10 (b)). This initial strain, which is over half the total, is partly due to equipment accommodation. The Young's modulus (figure 5.10 (c)) presented a steady decline until rupture where the final value was 18% lower than the initial (disregarding the first cycle), suggesting constant stiffness degradation.

When focusing on the internal data for the same specimen, a lower overall strain is observed and the overall stiffness of the specimen was higher. Thus, reinforcing the idea that the external data only provides a broad estimative of the data. Figure 5.11 (b) shows that there is an initial strain of 0.165% followed by an increase in strain until rupture at 0.508% over three times the initial strain. As for the Young's modus (figure 5.11 (c)), the initial values were around 780 MPa, the specimen presented an increase in E with cyclic until around 50 cycles (1797 MPa and strain of 0.317% – double the initial strain), after there was a decline in stiffness until rupture (around 1100 MPa). This indicates a gradual decrease in porosity during cycling and that the stiffness of the specimen while cementation bonds degraded until a critical cementation break occurred and the structure matrix began to collapse causing the degradation of stiffness and ultimately rupture.

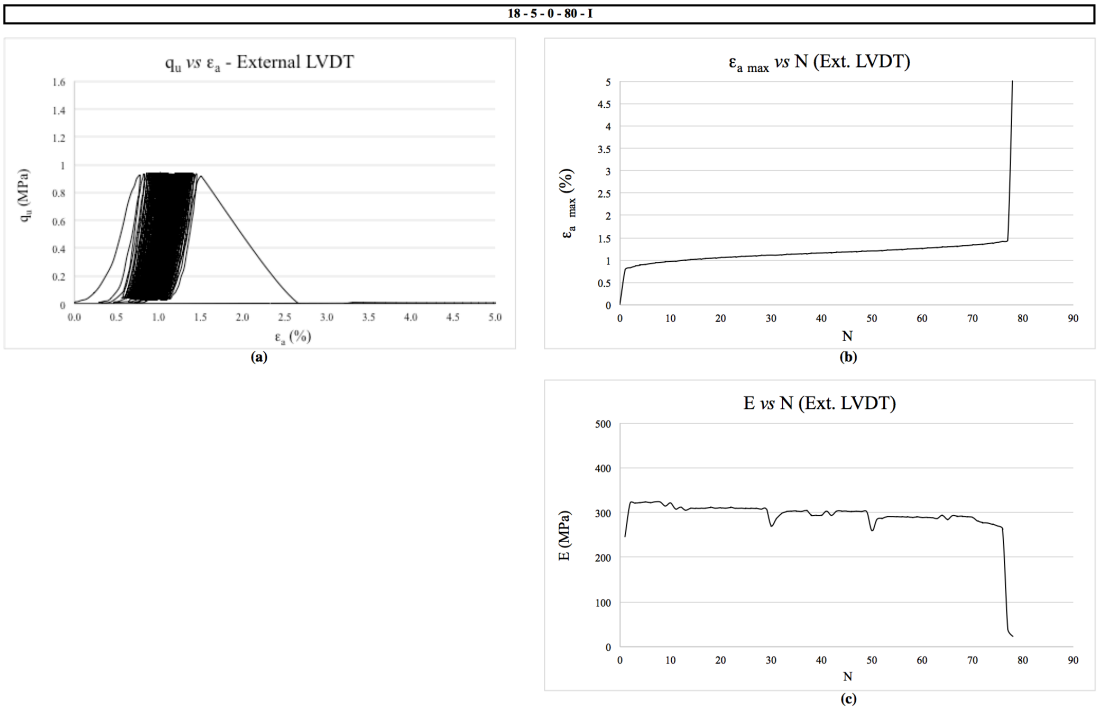

Figure 5.10: External data from specimen 18-5-0-80-I (a) q_u *versus* ε_a (b) $\varepsilon_{a\ max}$ *versus* N (c) E *versus* N

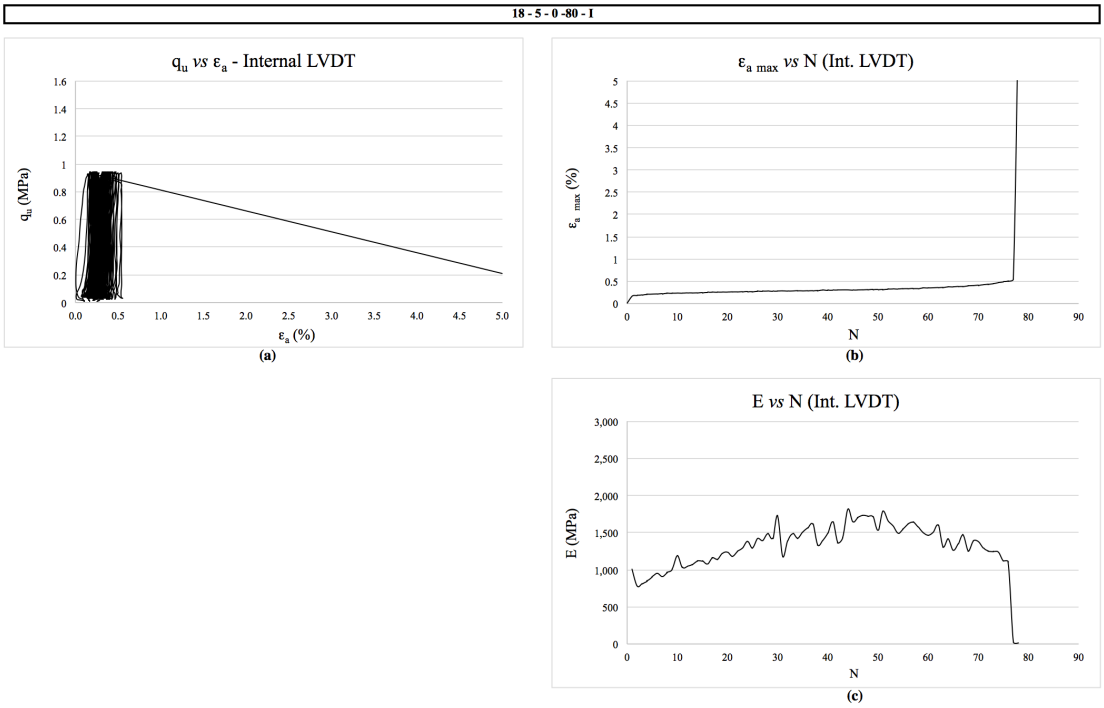

Figure 5.11: Internal data from specimen 18-5-0-80-I (a) q_u *versus* ε_a (b) $\varepsilon_{a\ max}$ *versus* N (c) E *versus* N

The second repetition for this combination withstood 245 cycles. Which is three times the average number of cycles the other two repetitions. From the external data (figure 5.12) it is observed a high strain during the first cycle of around 1.123%, after which there is an increase in strain until rupture around 1.688% (figure 5.12 (b)). The initial strain is over half the total being partly due to equipment accommodation. The Young's modulus (figure 5.12 (c)) presented a decrease of 16% until rupture (disregarding the first two cycles), suggesting a constant stiffness degradation that was not observed when analysing the internal data.

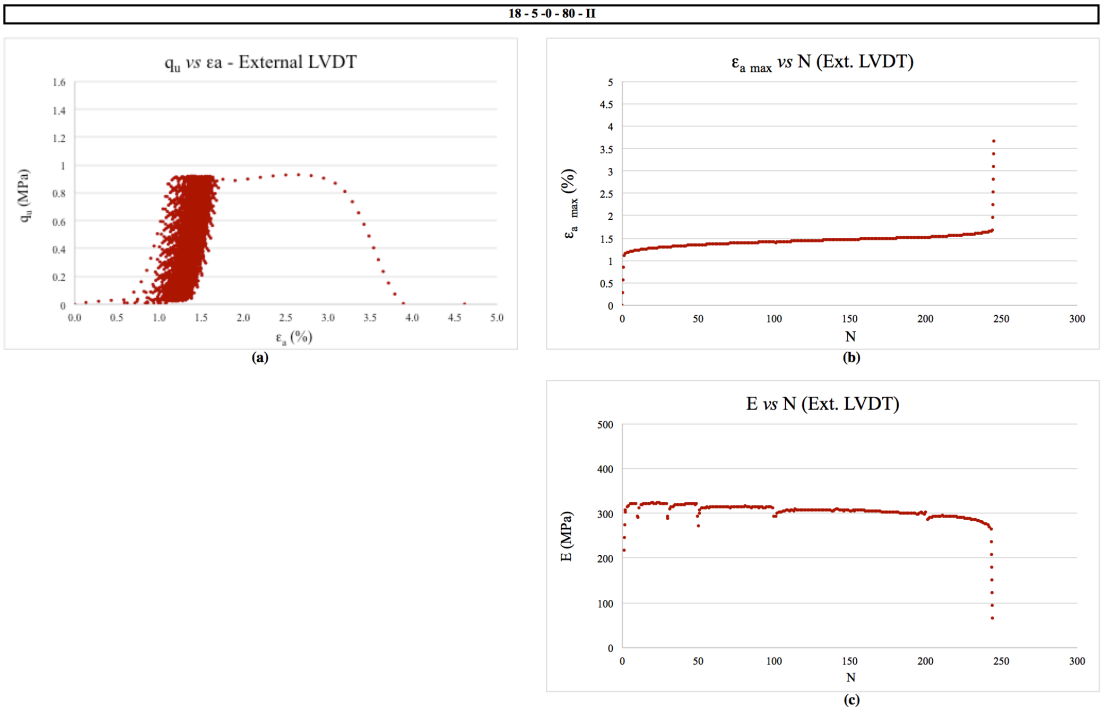

Figure 5.12: External data from specimen 18-5-0-80-II (a) q_u *versus* ε_a (b) $\varepsilon_{a\ max}$ *versus* N (c) E *versus* N

The internal data (figure 5.13) indicated a lower overall strain and higher overall stiffness than the observed by the external. When analysing figure 5.13 (b), it is observed an increase in the maximum strain after the first cycle from 0.109% to 0.664% in the last – an increase of 6.1 times the initial value. At around the 50 first cycles there was an increase of 146% in the maximum axial strain. Over the next 175 cycles the increase in $\varepsilon_{a\ max}$ was of 96% in respect to the 50th cycle. Then, during the last 20 cycles the $\varepsilon_{a\ max}$ augmented in 22%. This indicates a rapid increase in $\varepsilon_{a\ max}$ over the first 50 cycles – on average 2.97% per cycle, followed by a steady increase over the next 175 cycles – 0.64% per cycle. Then, again during the final portion of the test, there was a higher rate in strain gain – 1.39% per cycle – leading to failure.

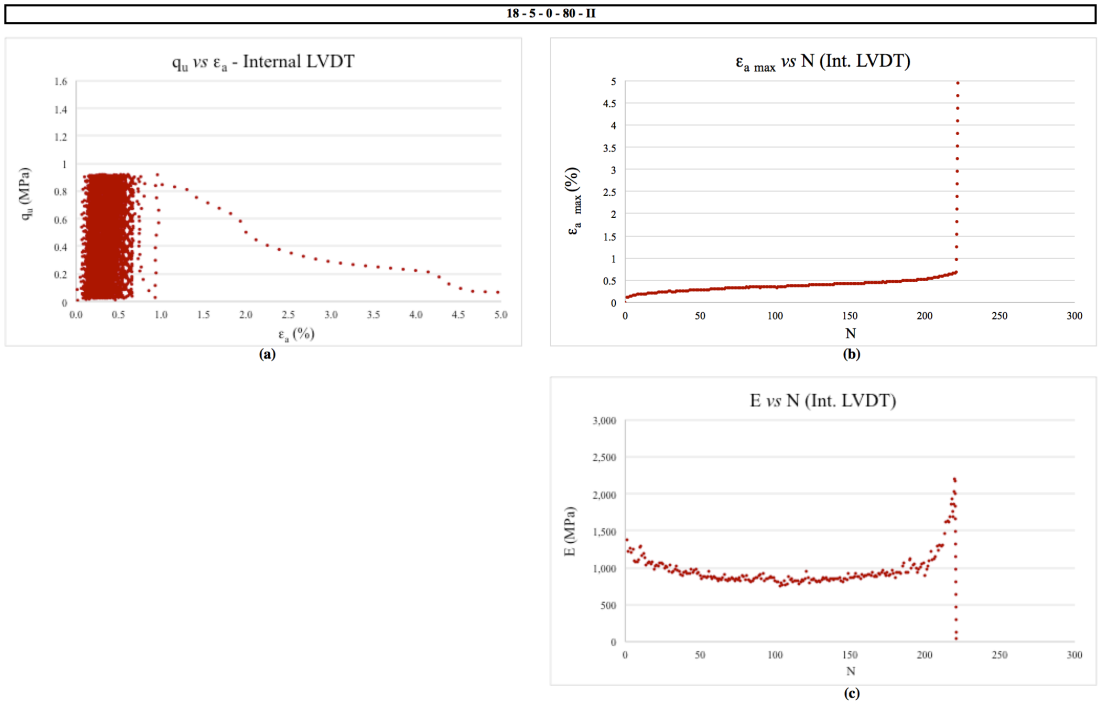

Figure 5.13: Internal data from specimen 18-5-0-80-II (a) q_u *versus* ε_a (b) $\varepsilon_{a\ max}$ *versus* N (c) E *versus* N

When analysing the Young's modus (figure 5.13 (c)), the initial values were around 1376 MPa, the specimen presented a decrease of 32% in E due to cycling through the first 50 cycles (936 MPa). After, the modulus remained somewhat constant until the last 30 cycles. Then, there was a rapid increase (around 131%) in stiffness until rupture occurred. This indicates an initial degradation of the Young's modulus that can be attributed to a progressive failure of the weaker cemented bonds resulting in increase in plastic deformation of the matrix. This phenomenon is followed by a stabilization of E with cycling, where the degradation of the stronger cementitious bonds of the matrix occurs slowly over the loading-unloading process, accumulating plastic deformation at a constant rate. Finally, there was an increase in E likely due to a critical number of cement bonds failing. This led to a significant decrease in the void ratio of the matrix, presenting increasingly larger plastic deformations (meaning an increase in the rate of $\varepsilon_{a\ min}$ in respect to the increase in $\varepsilon_{a\ max}$), ultimately leading to an abrupt failure.

The last specimen repetition of this combination failed at 79 cycles. From the external data (figure 5.14) it was observed a high strain during the first cycle of around 0.826%, after which there was a steady increase in strain until rupture around 1.339% (figure 5.14 (b)). This initial strain, which was over 60% of the total, was partly due to equipment accommodation. The Young's modulus (figure 5.14 (c)) presented a steady average value (300 MPa) until rupture.

The internal data (figure 5.15) indicated a lower overall strain and higher overall stiffness than the observed by the external. When analysing figure 5.15 (b), it was observed an increase in the maximum strain after the first cycle from 0.277% to 0.418% in the last – an increase of 5 times the initial value. At around the 13th cycle there was an increase of 26% in the maximum axial strain. Over the next 62 cycles the increase in $\varepsilon_{a\ max}$ was of 7.3% in respect to the 13th cycle. Then, during the last 4 cycles the $\varepsilon_{a\ max}$ augmented in 16.7%. From this data it is possible to infer that there is a rapid increase in $\varepsilon_{a\ max}$ over the first 13 cycles – on average 2.2% per cycle, followed by a almost stable value of $\varepsilon_{a\ max}$ over the next 62 cycles – 0.037% per cycle. Then, again during the final portion of the test, there was an increase in the strain gain rate – 4.19% per cycle – leading to failure.

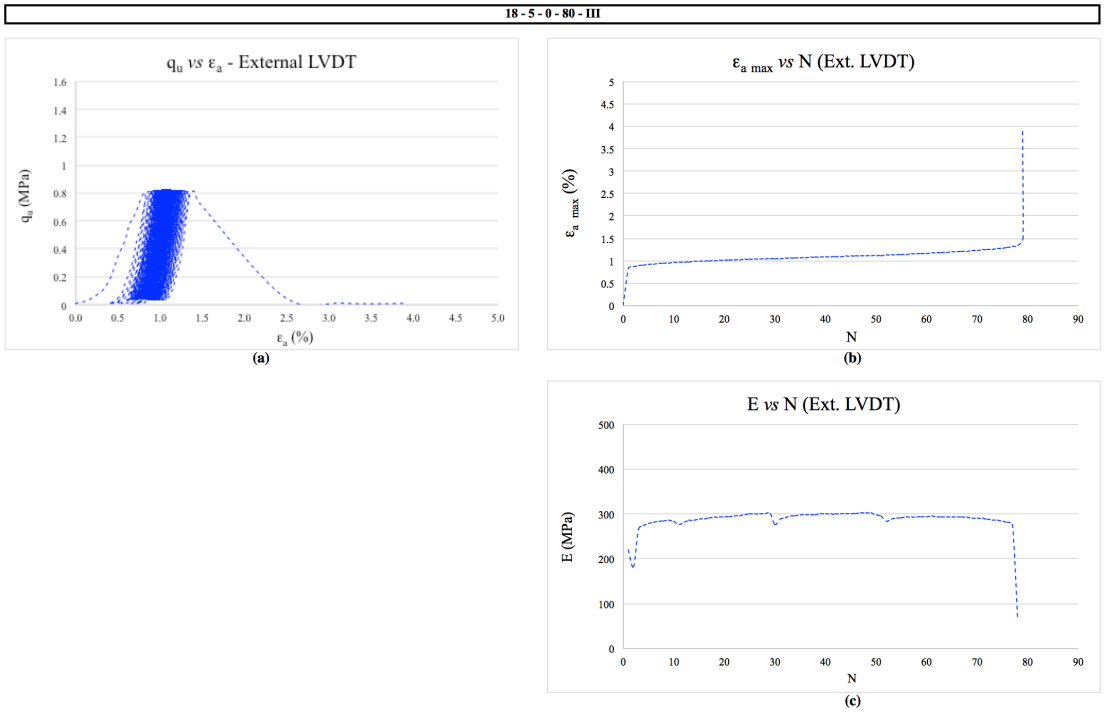

Figure 5.14: External data from specimen 18-5-0-80-III (a) q_u *versus* ε_a (b) $\varepsilon_{a\ max}$ *versus* N (c) E *versus* N

Examining the Young's modus (figure 5.15 (c)), the initial values were around 385 MPa, the specimen presented an increase of 36% in E due to cycling through the first 62 cycles (525 MPa). Then, there was a decrease (around 24%) in stiffness until rupture occurred (398 MPa). During this test there was a gradual decrease in porosity during cycling increasing the stiffness of the specimen while cementation bonds degrade, until a critical cementation break occurred and the structure matrix began to collapse causing the degradation of stiffness and

ultimately rupture. This specimen presented a more elastic response to cycling. The overall values in E were considerably lower and the than the values attained for specimens I and II. This the fact that the applied load was lower than the other two specimens due to its lower initial $\eta/C_{iv}^{0.28}$, as presented in table 5.3.

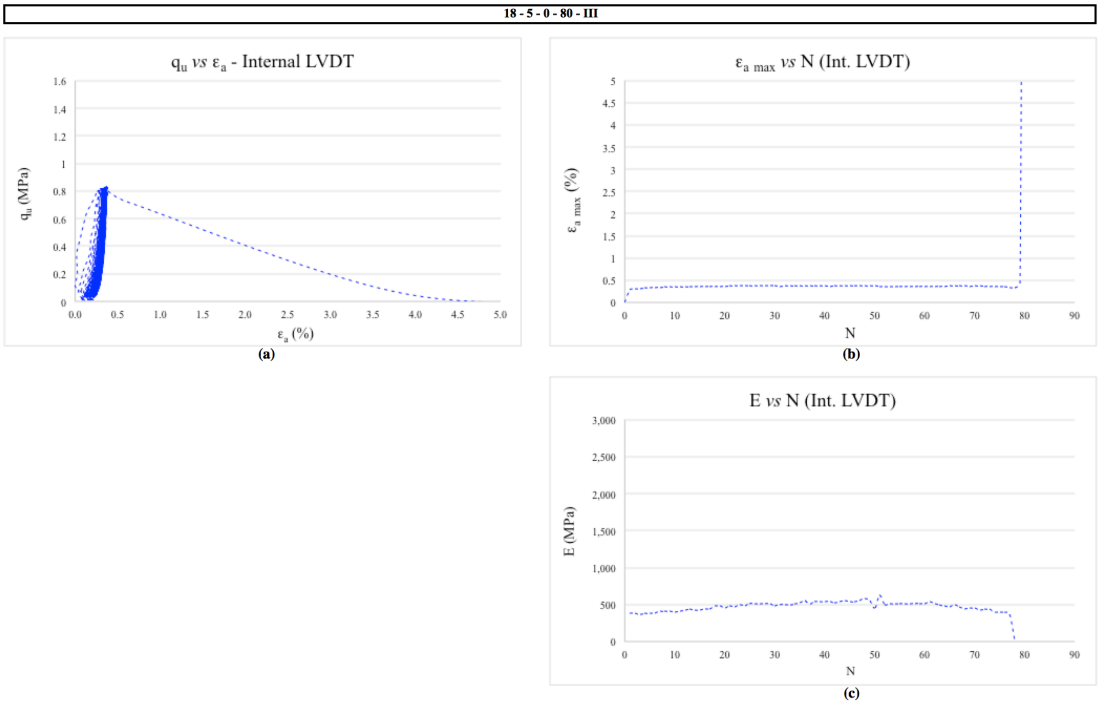

Figure 5.15: Internal data from specimen 18-5-0-80-III (a) q_u *versus* ε_a (b) $\varepsilon_{a\ max}$ *versus* N (c) E *versus* N

Figure 5.16 and 5.17 present the combined external and internal data for the three repetitions, respectively. When comparing the data from the external LVDT and the two internal ones, as expected there is a greater accuracy from the internal data.

Similarly to what was observed for the previous combination, in figure 5.16 (b) there is an initial deformation, which can be attributed in part to the accommodation of the equipment. The other portion of the deformation is due to the initial deformation of the specimen. However, it is impossible to differentiate the two values. All specimens presented very similar trends for $\varepsilon_{a\ max}$ and E during cycling, even though the number of cycles was greater for the second specimen. There was a steady increase in deformation until the strain at rupture is reached. On average, the axial strain increased 0.57% until specimen failure. As for the Young's modulus (Figure 5.16 (c)) specimens I and II reached a maximum around 350 MPa after a couple of cycles followed by a steady decrease in the modulus until rupture, around

263 MPa. As for the third specimen, as mentioned for figure 5.14 (c) there is an increase in E until 300 MPa followed by a steady decrease in value until rupture at 281 MPa.

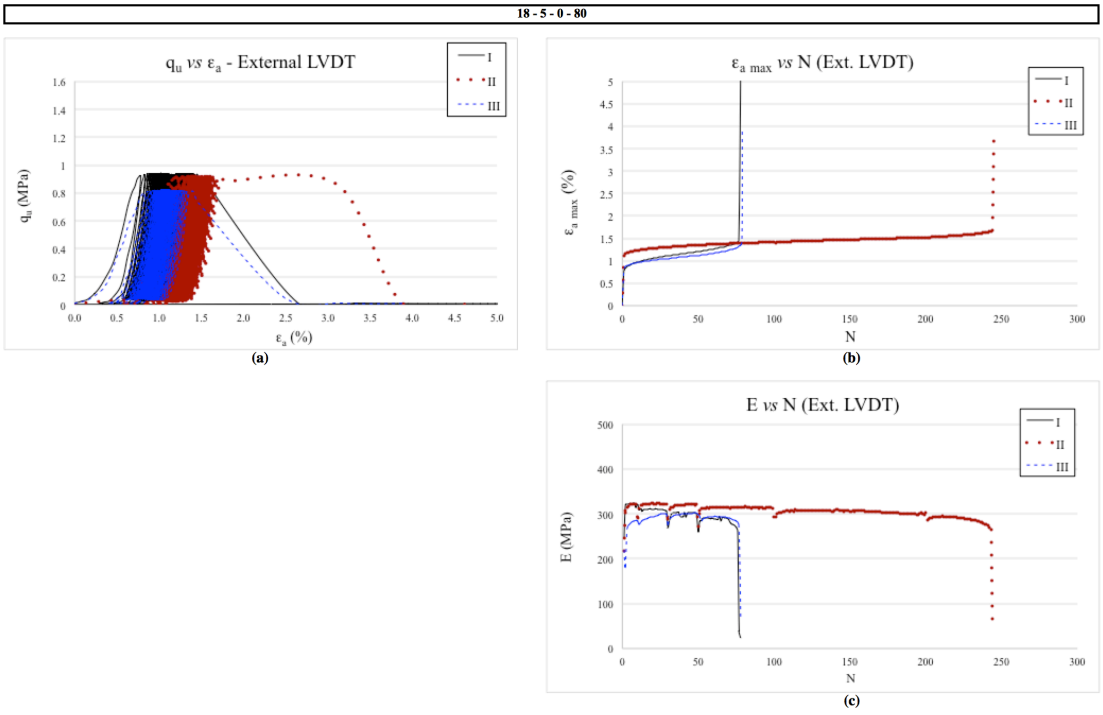

Figure 5.16: External data from specimen 18-5-0-80-I, II and III (a) q_u *versus* ε_a (b) $\varepsilon_{a\ max}$ *versus* N (c) E *versus* N

From figure 5.17 (b), it is possible to observe that after the initial deformation, which is to a smaller extent also partly due to accommodation of the equipment, had the similar trends of increasing in maximum axial strain for all specimens, even though the rates were different for all specimens. The first had a 0.343% increase in respect to the first cycle until rupture. The second specimen endured over three times the number of cycles the other two did and also had the highest strain in respect to the first cycle of all repetitions, 0.532%. The third specimen presented only a 0.141% increase in $\varepsilon_{a\ max}$, which is considerably lower than the other two specimens, especially the second, indicating a stiffer specimen that is corroborated by the measured G_0.

As for the Young's modulus (figure 5.17 (c)), again there was a difference in the trend observed when compared than the one seen for the external LVDT. Specimens I and III presented a similar behaviour, reaching a peak in E at around two-thirds of the cycles followed by a decrease leading to failure. This behaviour might be caused by the higher initial G_0 values. The second specimen presented an initial degradation rate of E, followed by a

plateau until an increase in E at the last third portion of the test leading to failure. This increase in E could be due to an increase in plastic deformation due to the brake in the cementitious bonds.

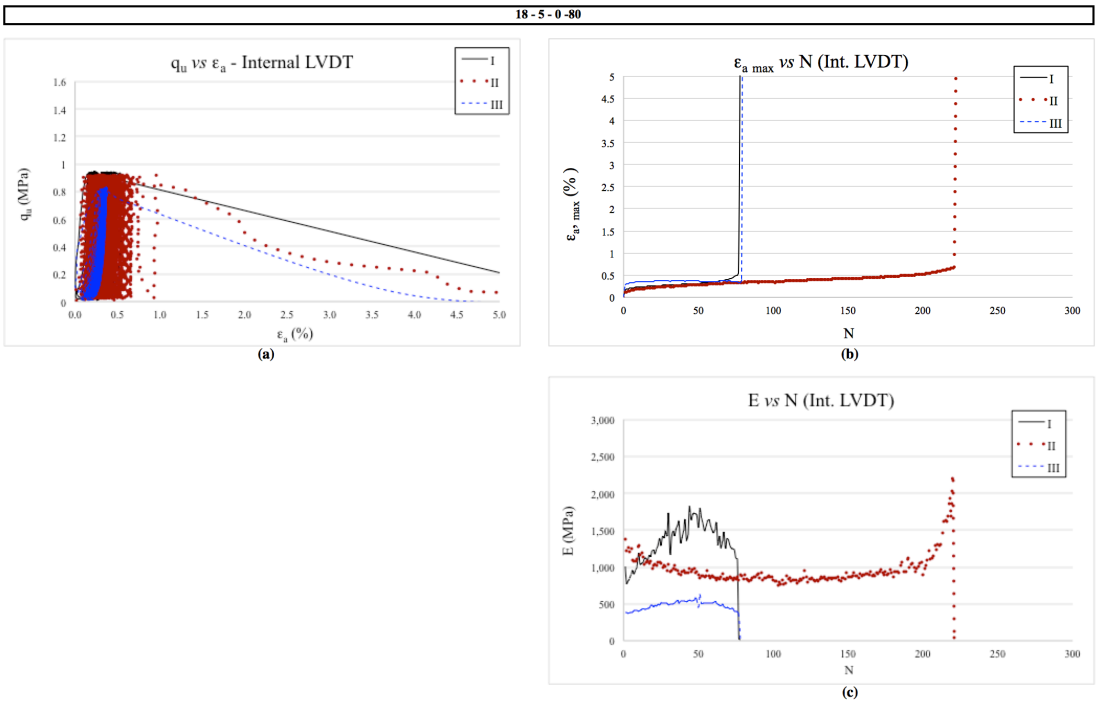

Figure 5.17: Internal data from specimen 18-5-0-80- I, II and III (a) q_u *versus* ε_a (b) $\varepsilon_{a\ max}$ *versus* N (c) E *versus* N

5.1.2.2 Alternative mixture

Figures 5.18 and 5.19, present the data results for the external and internal data of the first specimen, respectively. Followed by figures 5.20 and 5.21 that show respectively the values for the external and internal data for second specimen. Finally, figures 5.22 and 5.23 illustrate the results attained for the external and internal LVDTs of the third specimen, respectively.

The summary of the tests is shown in Table 5.4. It presents of cycles until rupture (N), initial shear modulus (G_0), and the estimated value of the initial Young's modulus at small strains (E from G_0), again, the E values are just a estimative. From the presented data, it is possible to infer that the dispersion of $\eta/C_{iv}^{0.28}$ for the replicas is less than 1.1%. The dispersion of data for the G_0 is less than 7%. This indicates a similar initial condition for the studied specimens.

Table 5.4: Summary of Cyclic UC tests for 80% of estimated maximum loading for 19 kN/m^3 - 3% mixtures without fibres

Mixture	Ideal Load %	Repetition	$\eta/C_{IV}^{0.28}$	Applied Load (N)	Actual %	Number of Cycles	Numeber of Cycles Rupture	Initial Bender (μs)	G_0 (MPa)	E from G_0 (MPa)
19 kN/m^3 3% cement	80	I	24.70	1756.49	82.61	3	3	125.70	1487.73	3749.08
	80	II	24.47	1804.44	82.43	4	4	116.40	1325.57	3340.43
	80	III	24.97	1685.46	81.89	20	20	111.00	1487.24	3747.85

There was variability in the number of cycles until rupture. However, the results are in the same order of magnitude, and all the moulding indicators – $\eta/C_{iv}^{0.28}$; actual loading percentage in respect to its estimated maximum load; G_0 – suggest that the specimens have similar initial conditions.

The first specimen withstood 3 cycles. From the external data (figure 5.18) it was observed a high strain during the first cycle of around 1.117%, after which there was a steady increase in strain until rupture around 1.589% (figure 5.18 (b)). This initial strain, which was over 70% of the total strain, was partly due to equipment accommodation. The Young's modulus (figure 5.18 (c)) presented a 13.4% decline between the second and first cycles, being null at the third.

Observing the internal data for the same specimen, a much lower overall strain is observed and the overall stiffness of the specimen was higher. Figure 5.19 (b) shows that there was an initial strain of 0.238% followed by a 20% decrease in strain over the next cycle, reaching rupture in the third. As for the Young's modus (figure 5.19 (c)), the initial value was 757 MPa. The specimen presented an increase in E with the second cyclic (1679 MPa), after, the specimen abruptly failed. This indicates that even though the observed strains and E were within the same order of magnitude of the benchmark specimens, when this combination was subjected to 80% of the estimated maximum load, there was a rapid break in the cementation bonds, reaching failure on the 3rd cycle.

The second specimen withstood 4 cycles. From the external data (figure 5.20) it was observed a high strain during the first cycle of around 1.255%, after which there is an increase in strain until rupture at 1.535% (figure 5.20 (b)). This initial strain, which was over 80% of the total strain, was partly due to equipment accommodation. The Young's modulus (figure 5.20 (c)) presented an 18% increase between the first and second cycles, followed by a 64% decline between the second and third cycles, reaching failure.

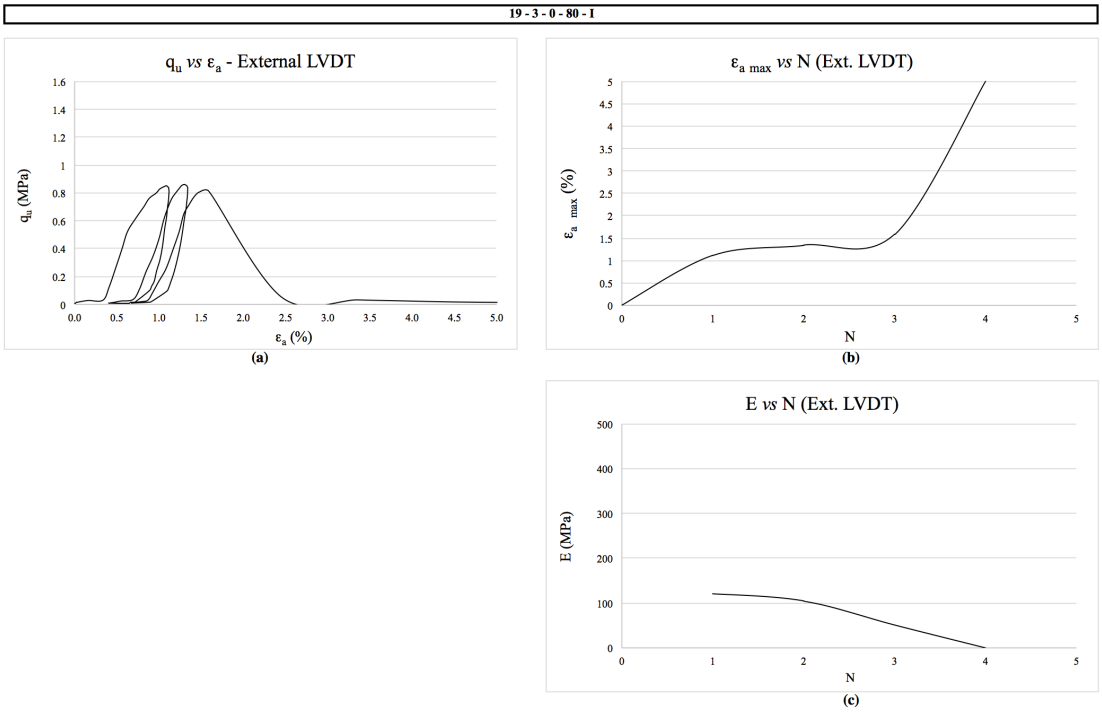

Figure 5.18: External data from specimen 19-3-0-80-I (a) q_u *versus* ε_a (b) $\varepsilon_{a\ max}$ *versus* N (c) E *versus* N

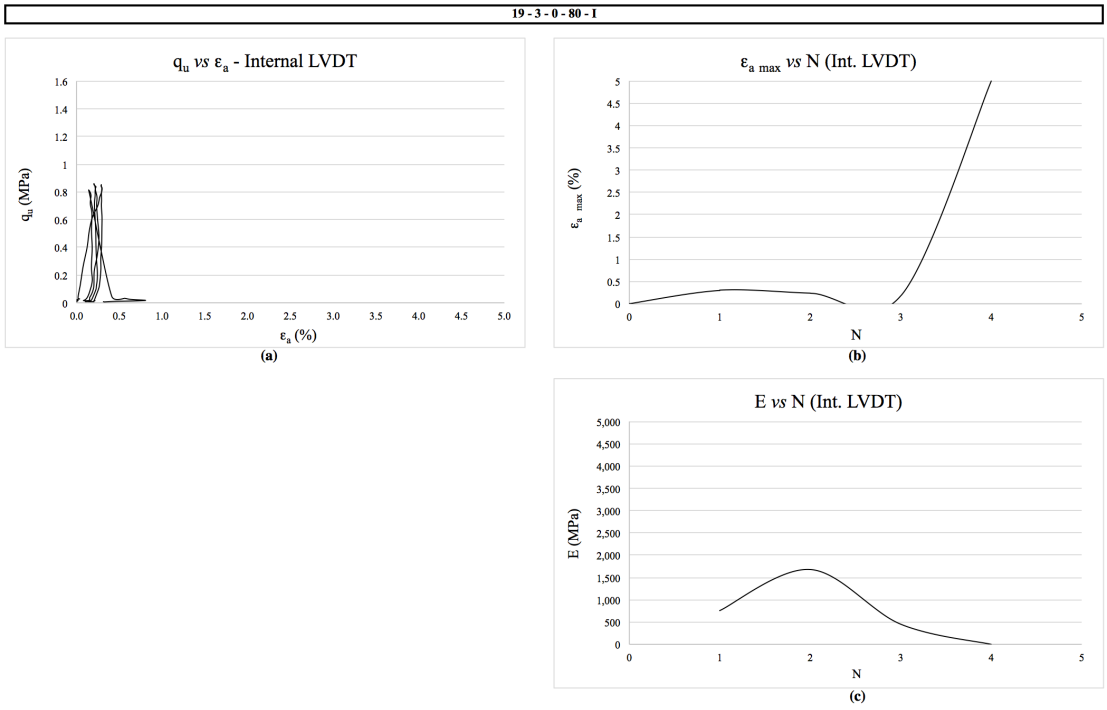

Figure 5.19: Internal data from specimen 19-3-0-80-I (a) q_u *versus* ε_a (b) $\varepsilon_{a\ max}$ *versus* N (c) E *versus* N

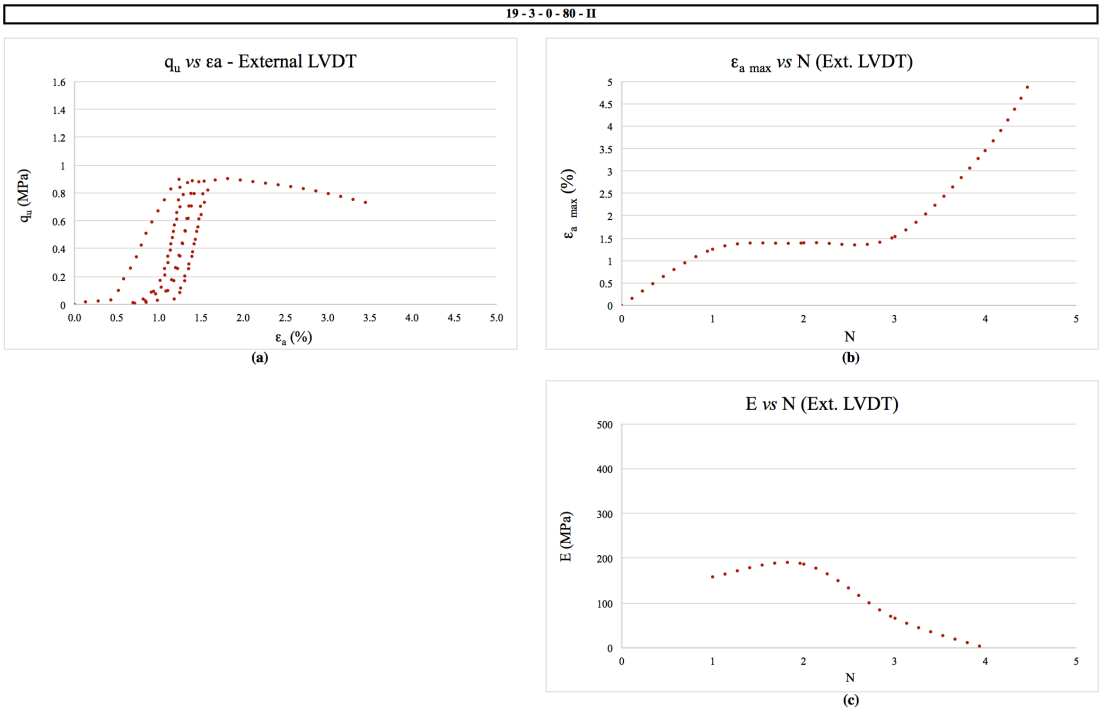

Figure 5.20: External data from specimen 19-3-0-80-II (a) q_u *versus* ε_a (b) $\varepsilon_{a\ max}$ *versus* N (c) E *versus* N

Form the internal data for the same specimen, a much lower overall strain was observed and the overall stiffness of the specimen was higher. Figure 5.21 (b) shows that there was an initial strain of 0.077% followed by a 16% increase in strain over the next couple of cycles, reaching rupture in the fourth cycle at 0.37%. As for the Young's modus (figure 5.21 (c)), the initial value was 1332 MPa. The specimen presented a 20% decrease in E with the second cycle (1069 MPa), over the next cycle there was a 63% decrease in the Young's modulus, leading to failure during the fourth. This indicates that even though the observed strains and E were within the same order of magnitude of the benchmark specimens, when this combination was subjected to 80% of the estimated maximum load, there was a rapid break in the cementation bonds, reaching failure on the 4th cycle.

The last repetition failed after the 20th cycle. From the external data (figure 5.22) it was observed a high strain during the first cycle of around 0.781%, after which there was a continuous increase in strain of 66% over the next 18 cycles. The last cycle had e 169% increase in strain in reference to the 19th cycle, reaching rupture at 3.501% (figure 5.22 (b)). Again, the initial strain is partly due to equipment accommodation. The Young's modulus (figure 5.22 (c)) presented an 18% decrease between the first and 18th cycles, followed by a 90 % decline over the last two cycles, reaching failure.

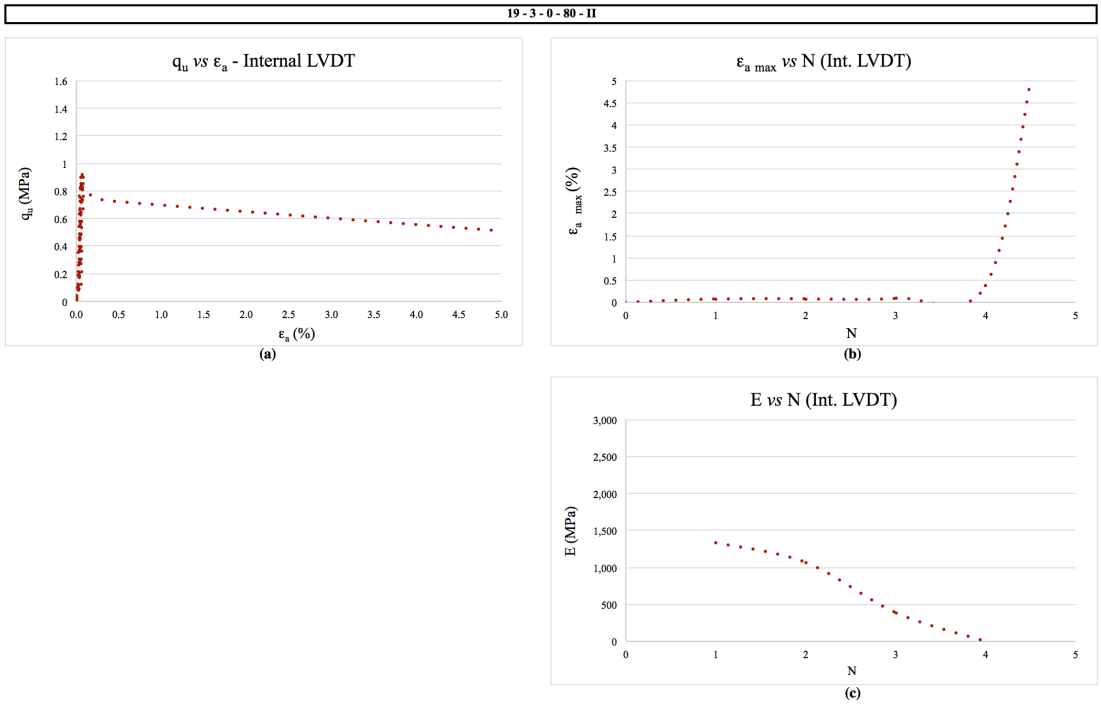

Figure 5.21: Internal data from specimen 19-3-0-80-II (a) q_u *versus* ε_a (b) $\varepsilon_{a\ max}$ *versus* N (c) E *versus* N

Form the internal data for the same specimen, a much lower overall strain was observed and the overall stiffness of the specimen was higher. Figure 5.23 (b) shows that there was an initial strain of 0.035% followed by a 254% increase in strain over the next two cycles. Then, over the following seventeen cycles there was a 50% increase in the maximum axial strain, reaching rupture in the 20th cycle after a 45% increase in strain in the last cycle. As for the Young's modus (figure 5.23 (c)), the initial value was 1514 MPa. The specimen presented a 19% decrease in E over the next couple of cycles (9.5% per cycle). For the next seventeen cycles there was a total of 25% decrease in the Young's modulus (on average 1.47% per cycle). The last two cycles had a 99% decrease in E leading to failure during the twentieth cycle. This specimen lasted over 5 times the number of cycles as the other two repetitions, even though, when observing the initial data of table 5.4 there was not a large variation in values between the specimens. Only the applied load was a 5% lower than the average of the other two repetitions, which might be the cause of the variation.

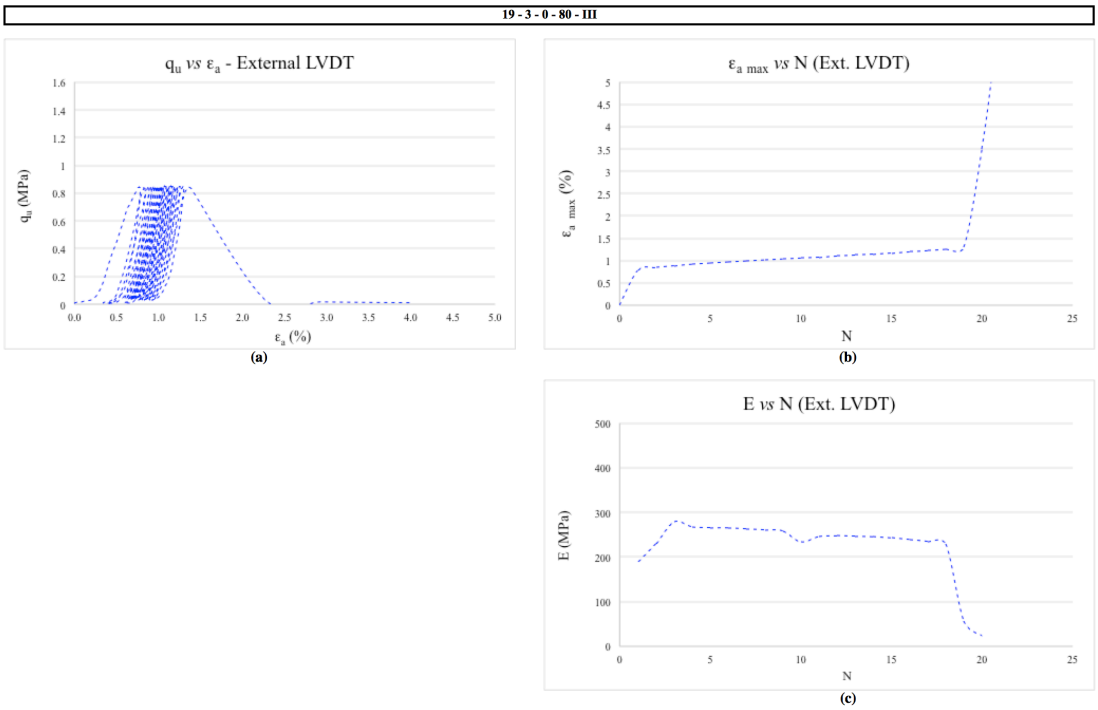

Figure 5.22: External data from specimen 19-3-0-80-III (a) q_u *versus* ε_a (b) $\varepsilon_{a\ max}$ *versus* N (c) E *versus* N

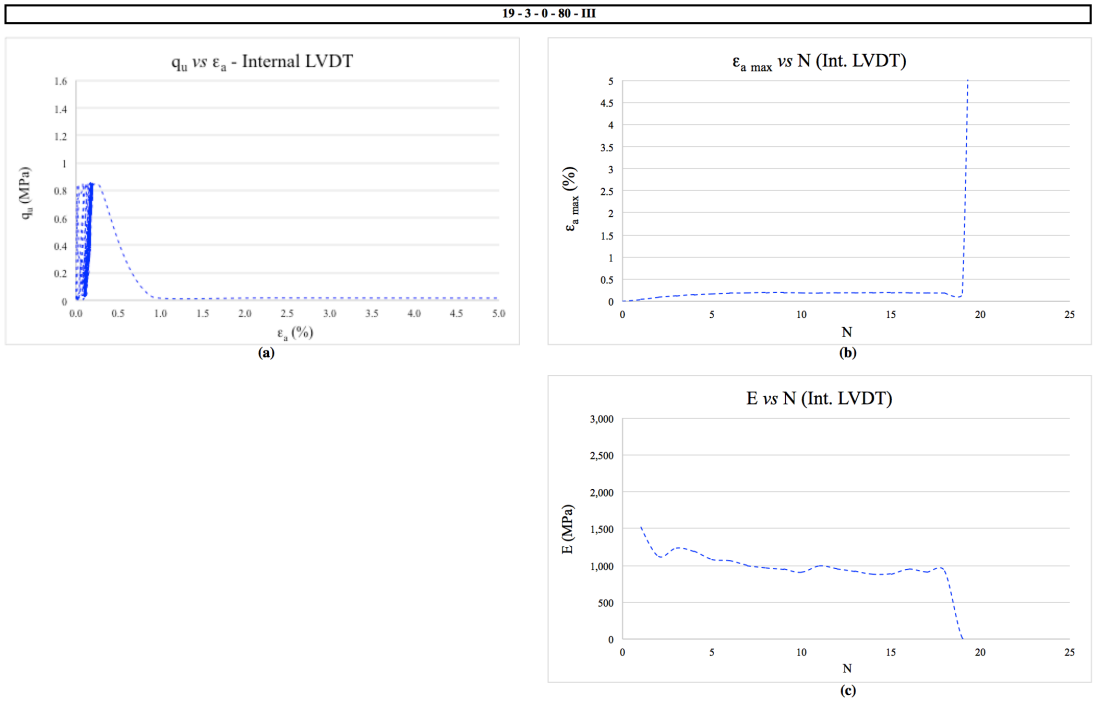

Figure 5.23: Internal data from specimen 19-3-0-80-III (a) q_u *versus* ε_a (b) $\varepsilon_{a\ max}$ *versus* N (c) E *versus* N

Figures 5.24 and 5.25 show the combined external and internal data for the three repetitions, respectively. Focusing in the external data, figure 5.24 (b), showed an initial deformation,

which can be attributed in part to the accommodation of the equipment. Specimen III had a higher N and presented a lower initial $\varepsilon_{a\ max}$ compared to the other two repetitions. Afterwards, there was a steady increase in strain until rupture was reached for all repetitions. The $\varepsilon_{a\ max}$ increased in 0.47% until specimen failure for the first specimen, 0.28% for the second, and 0.52% for the third. The Young's modulus (Figure 5.24 (c)) reached a maximum around of 121 MPa for the first repetition, 187 MPa for the second and 278 MPa for the last over the first couple of cycles. After cycling the first two specimens presented an abrupt fall in E leading to failure. For the third specimen there was a steady decrease in the modulus where plastic deformations accumulate over cycling, reaching failure around 228 MPa.

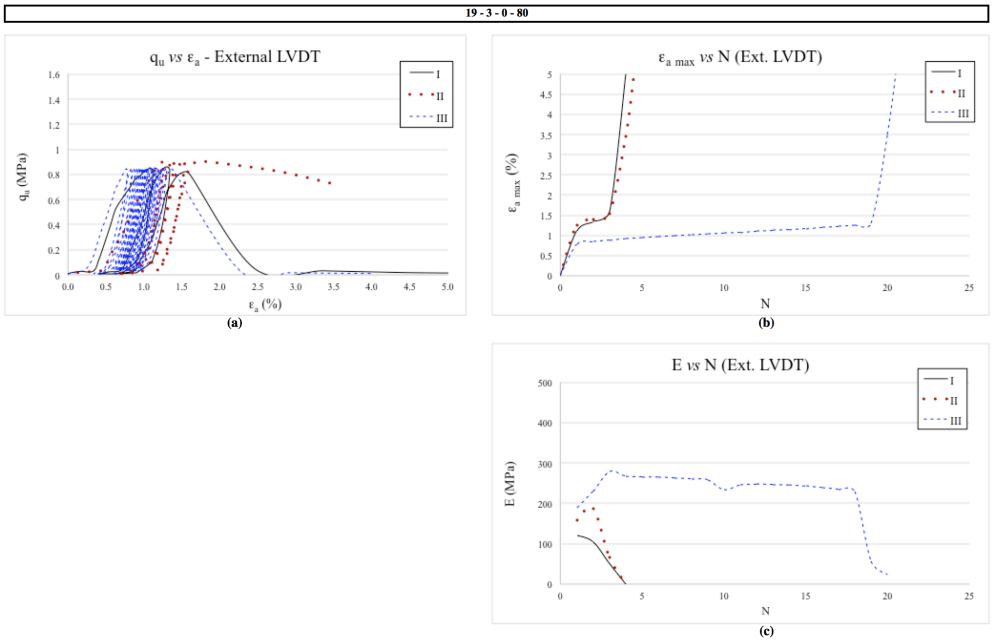

Figure 5.24: External data from specimen 19-3-0-80-I, II and III (a) q_u *versus* ε_a (b) $\varepsilon_{a\ max}$ *versus* N (c) E *versus* N

From figure 5.25 (b), it is possible to observe that after the initial deformation the same trend of increase in axial strain. On average, for specimens II and III, there was an increase of 0.3% in strain after the first cycle. As for the Young's modulus (figure 5.25 (c)), it was observed a different trend than the one seen for the external LVDT. There was an initial increase that is likely because during the first couple of cycles accommodation was taking place and the weak cement bonds mobilized. Then, the values of E are stabilized and align with E from G_0 values. After, a slight decrease in value was observed, indicating degradation of stiffness of the specimen, brought by cementation breakage. However, before rupture, a spike in the Young's

modulus occurs. This could be attributed to a reduction in porosity after a significant brake in cementation due to cycling.

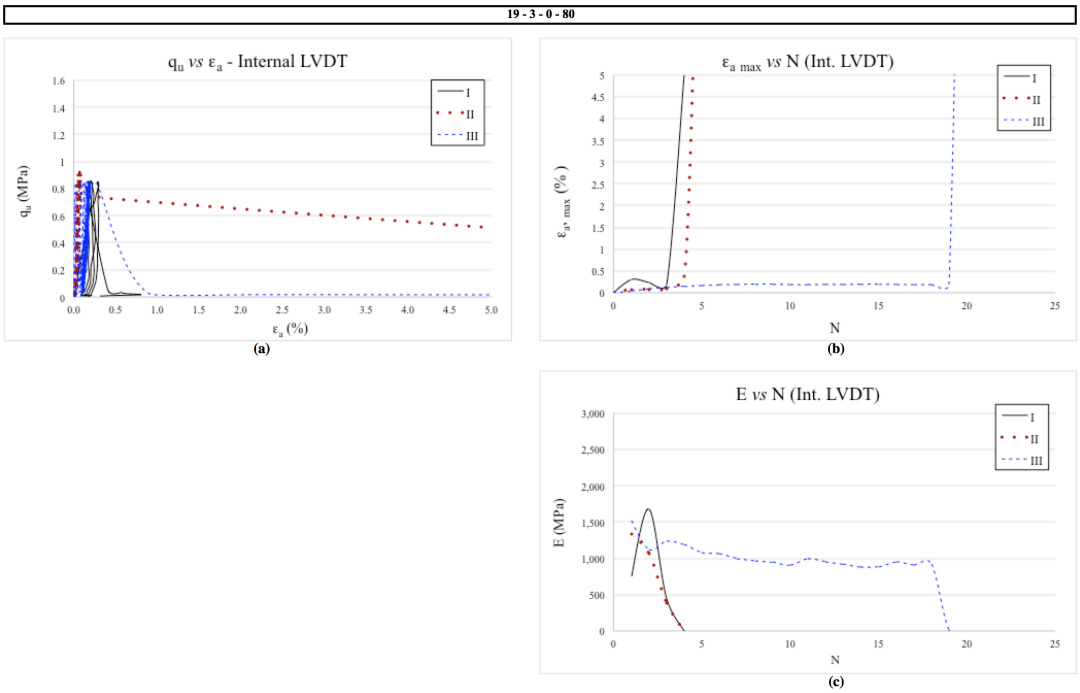

Figure 5.25: Internal data from specimen 19-3-0-80- I, II and III (a) q_u *versus* ε_a (b) $\varepsilon_{a\ max}$ *versus* N (c) E *versus* N

5.1.3 Applied load percentage: 70%

Figures 5.26 and 5.27 show the results for the external and internal data of the first specimen, respectively. Then, figure 5.28, present the values for the internal data of the second specimen, there was a problem with the external measurements for this specimen. Lastly, figures 5.29 and 5.30 show the data for the external and internal LVDTs of the third specimen, respectively.

The summary of the tests is shown in Table 5.5. It presents number of cycles until rupture (N), initial shear modulus (G_0), and the estimated value of the initial Young's modulus at small strains (E from G_0), again, the E values are just a estimative. From the presented data, it is possible to infer that the dispersion of $\eta/C_{iv}^{0.28}$ for the replicas is less than 1.5%. The dispersion of data for the G_0 is less than 10%. Indicating a similar initial condition for the studied specimens. However, it is relevant to note that even though the initial G_0 value for third repetition is within a 10% dispersion of the average values, when considering only the average values of the first two specimens, this specimen has a 16% higher value of G_0,

indicating a higher initial stiffness, which might be the reason why the specimen failed after 1231 cycles.

Table 5.5: Summary of Cyclic UC tests for 70% of estimated maximum loading for benchmark mixtures without fibres

Mixture	Ideal Load %	Repetition	$\eta/C_{IV}^{0.28}$	Applied Load (N)	Actual %	Number of Cycles	Numeber of Cycles Rupture	Initial Bender (μs)	G_0 (MPa)	E from G_0 (MPa)
18 kN/m³ 5% cement	70	I	24.30	1605.94	71.97	2000	-	112.30	1514.66	3816.94
	70	II	24.77	1557.74	73.78	2000	-	121.60	1566.16	3946.73
	70	III	24.76	1525.64	72.32	1231	1231	116.00	1785.51	4499.49

The first repetition for this combination did not fail for the stipulated maximum number of cycles. From the external data (figure 5.26) it is observed a high strain during the first cycle of around 0.989%, after which there is an increase in strain until around 1.322% when testing was stopped (figure 5.26 (b)). Over the first 100 cycles there was an increase rate of $\varepsilon_{a\ max}$ of 0.19% per cycle. The following 1900 cycles had an average rate of $\varepsilon_{a\ max}$ of 0.006% per cycle, thus, it is possible to conclude that the cyclic test was stopped while the specimen still was on its plateau where plastic deformation slowly accumulates over cycling. Regarding the Young's modulus, figure 5.26 (c)) presented an average increase rate of 0.06% per cycle over the first 100 cycles, followed by a 0.012% increase rate over the next 1900 cycles.

The internal data (figure 5.27) also indicated a lower overall strain and higher overall stiffness than the observed by the external. When analysing figure 5.27 (b), it was observed an initial decrease in the maximum strain over the first 50 cycles from 0.110% to 0.051% (a decreasing rate of 1.07% per cycle), this might due to accommodation of the specimen and the mobilization of the weaker cement bonds. During the next 50 cycles there was an increase in the maximum axial strain reaching a $\varepsilon_{a\ max}$ of 0.51% (ratio of 1.33% per cycle). Over the next 400 cycles, the increase rate was of 0.24% per cycle. After the 500th cycle, it was observed a steady increase rate of 0.02% per cycle until the test end, with a $\varepsilon_{a\ max}$ of 0.213%.

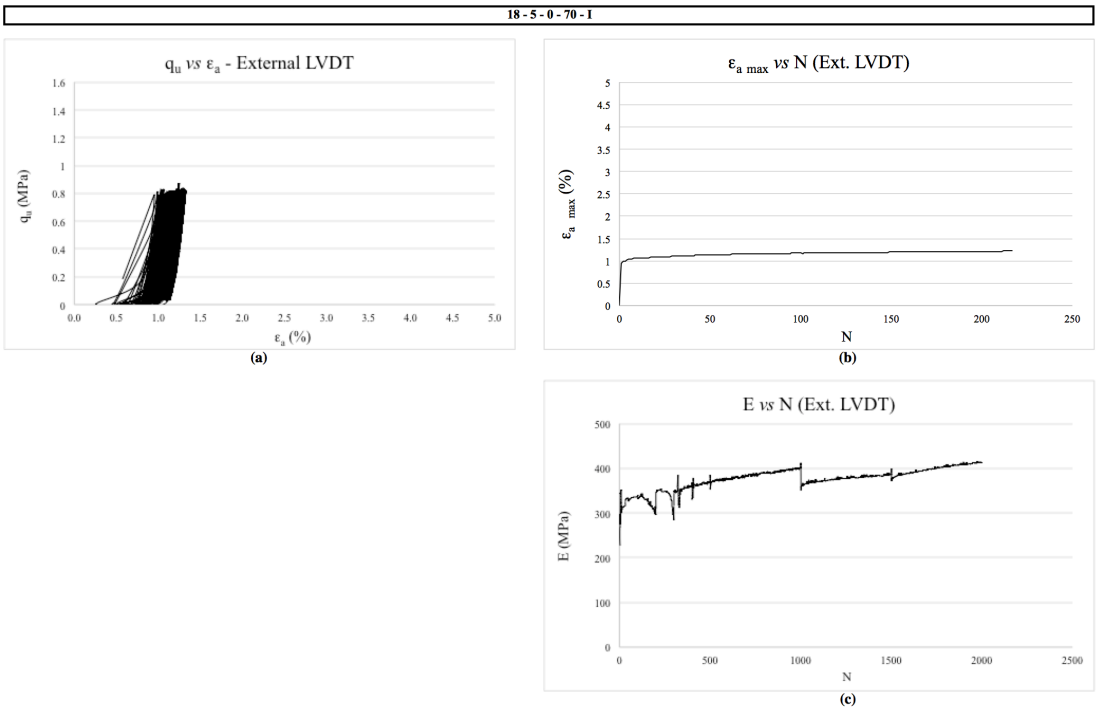

Figure 5.26: External data from specimen 18-5-0-70-I (a) q_u *versus* ε_a (b) $\varepsilon_{a\ max}$ *versus* N (c) E *versus* N

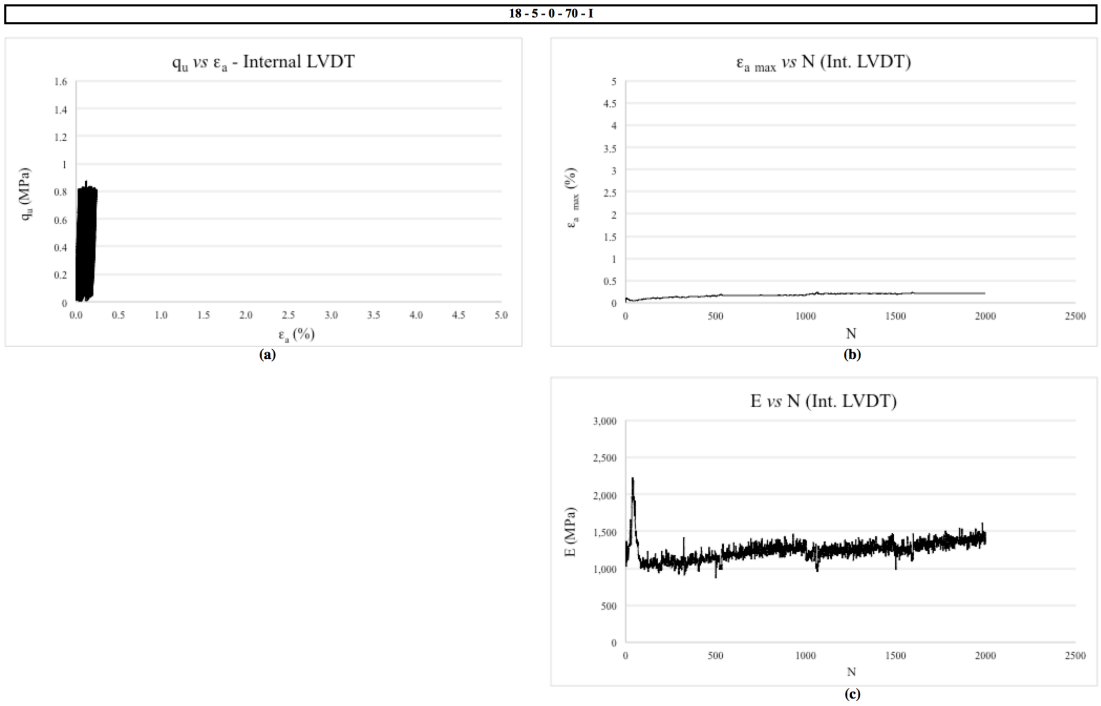

Figure 5.27: Internal data from specimen 18-5-0-70-I (a) q_u *versus* ε_a (b) $\varepsilon_{a\ max}$ *versus* N (c) E *versus* N

When analysing the Young's modus (figure 5.27 (c)), the initial values were around 1022 MPa, the specimen presented an increase of 118% (2.36% per cycle) in E through the first 50 cycles (2229 MPa), probably to due to the mobilization of the weaker cementation bonds of the structure. Over the next 50 cycles there was a decrease in E reaching almost the same values as the initial E (1053 MPa). This indicates a degradation of the modulus that can be attributed to a progressive failure of the weaker cemented bonds resulting in increase in plastic deformation of the matrix. Then, the Young's modulus presented a stable trend with a much lower increase rate (0.022% per cycle) until the test was stopped. This phenomenon suggests a slow degradation of the stronger cementitious bonds of the matrix occurs over the loading-unloading process, accumulating plastic deformation at an almost constant rate, but not reaching the critical value of cementation bond failure.

The second repetition had a technical issue that made it impossible to analyse the external data. But as it has been observed for all specimens so far, the external data provides a more qualitative idea of the behavioural trends of the specimen, thus this issue will not exclude the use of this repetition. The internal data is presented in figure 5.28. When analysing figure 5.28 (b), it was observed an initial increase in the maximum strain over the first 25 cycles from 0.108% to 0.121% (an increasing rate of 0.481% per cycle). During the next 275 cycles there was a decrease in $\varepsilon_{a\ max}$ at a ratio of 0.042% per cycle. Over the next 700 cycles, there was again an increase in the values of $\varepsilon_{a\ max}$ reaching 0.159% (0.069% increase per cycle). After the 1000^{th} cycle, it was observed a steady increase at the rate of 0.031% per cycle of the strain until the test end, with a $\varepsilon_{a\ max}$ of 0.209%.

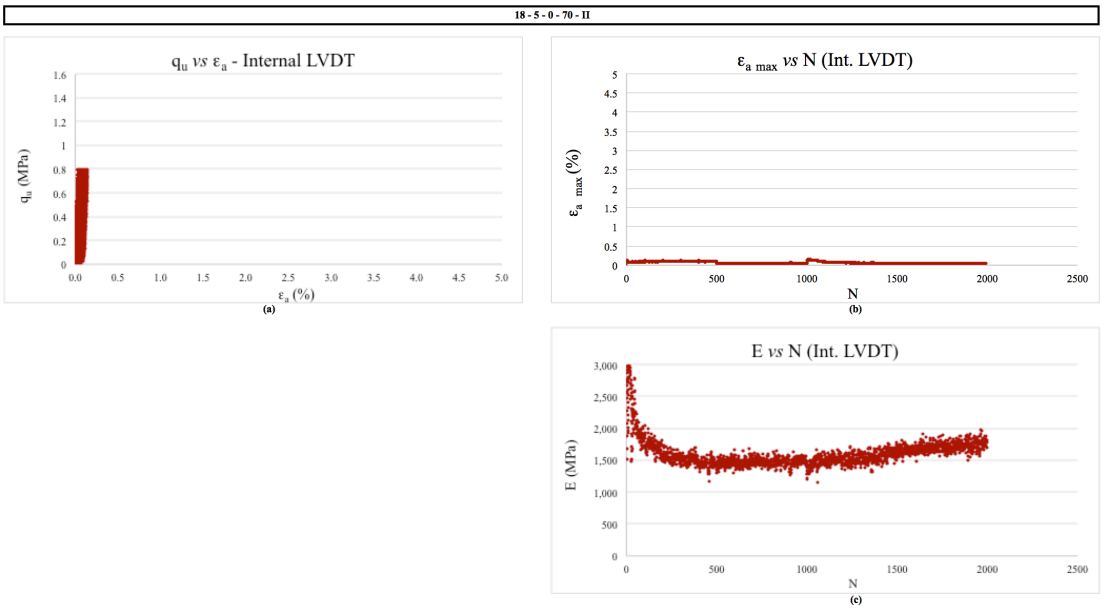

Figure 5.28: Internal data from specimen 18-5-0-70-II (a) q_u *versus* ε_a (b) $\varepsilon_{a\ max}$ *versus* N (c) E *versus* N

When analysing the Young's modus (figure 5.28 (c)), the initial values were around 1921 MPa, the specimen presented an increase of 49.4% (16.5% increase per cycle) in E through the first 3 cycles (2870 MPa), probably to due to the mobilization of the weaker cementation bonds of the structure. Over the next 297 cycles there was a decrease in E reaching 1053 MPa (0.181% decrease per cycle). This indicates a degradation of the Young's modulus that can be attributed to a progressive failure of the weaker cemented bonds resulting in increase in plastic deformation of the matrix. Then, the modulus presented a stable trend with a much lower increase rate (0.015% per cycle) until the test was stopped. This phenomenon suggests a slow degradation of the stronger cementitious bonds of the matrix occurs over the loading-unloading process, accumulating plastic deformation at an almost constant rate. However, the critical value of cementation bond failure was not reached.

The last repetition made for this combination failed at 1231 cycles. From the external data (figure 5.29) it was observed a high strain during the first cycle of around 0.841%. After, there was an increase in strain until around 1.034% at 100 cycles. Then, the same trend continued until cycle 1190, but at a slower pace reaching a strain of 1.209%. The last 40 cycles showed a decrease in the maximum axial deformation until rupture at $\varepsilon_{a\ max}$ equal to 1.242% (figure 5.29 (b)). Over the first 100 cycles there was an increase rate of $\varepsilon_{a\ max}$ of 0.229% per cycle. The following 1090 cycles had an average increase rate of $\varepsilon_{a\ max}$ of 0.016%

per cycle, indicating a slower pace in the progression of plastic deformation accumulation. The last 40 cycles showed a decrease rate of $\varepsilon_{a\ max}$ of 0.068% per cycle, until rupture occurred. Thus, it is possible to conclude that the last part of the cyclic test represents the collapse of the cemented matrix leading to high plastic deformation reaching failure. Regarding the Young's modulus, figure 5.26 (c)) presented the data where an average increase rate of 0.030% per cycle was observed over the first 100 cycles, followed by a 0.010% increase rate over the next 1090 cycles. Finally, at the third stage of cycling, there was a decrease rate of 0.565% per cycle, reaching failure at 1231 cycles.

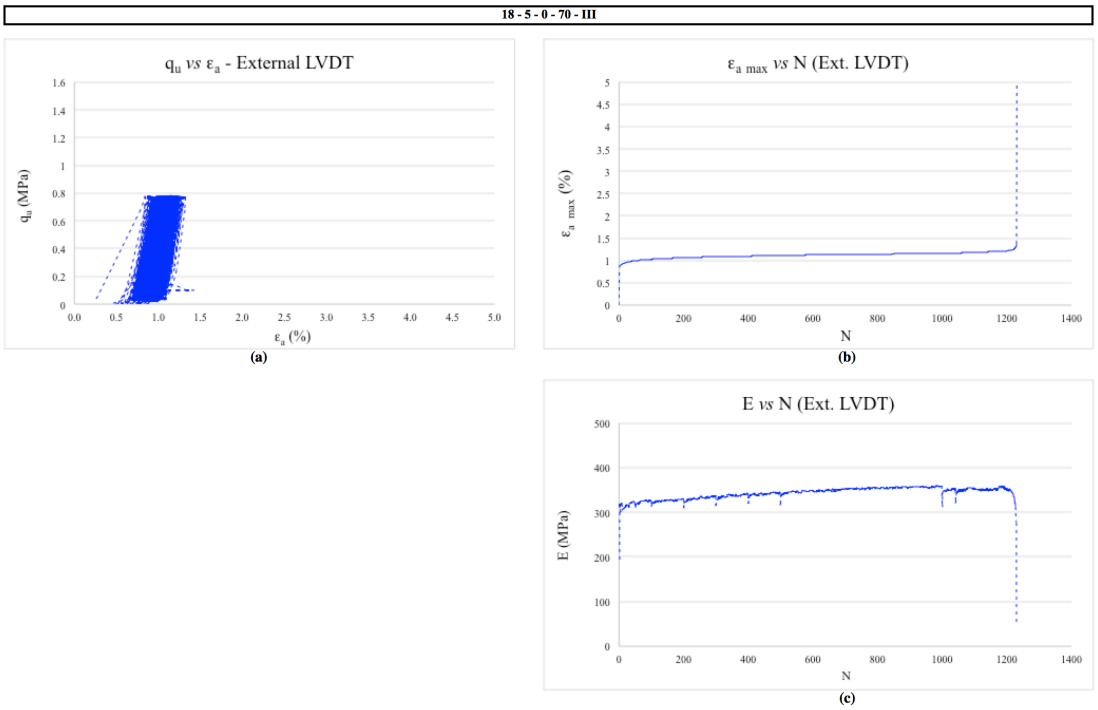

Figure 5.29: External data from specimen 18-5-0-70-III (a) q_u *versus* ε_a (b) $\varepsilon_{a\ max}$ *versus* N (c) E *versus* N

From the internal data (figure 5.30) it was observed higher overall stiffness than the observed by the external. However, overall strain values were quite similar. When analysing figure 5.30 (b), it was observed an increase in the maximum strain after the first cycle from 0.139% to 1.074% in the last – an increase of 7.72 times the initial value. At around the 300 first cycles there was an increase of 439% in the maximum axial strain. Over the next 890 cycles the increase in $\varepsilon_{a\ max}$ was of 74% in respect to the 300th cycle. Then, during the last 40 cycles the $\varepsilon_{a\ max}$ diminished in 28%. This indicates a rapid increase in $\varepsilon_{a\ max}$ over the first 50 cycles – on average 1.46 % per cycle, followed by a steady increase over the next 890 cycles – 0.084 %

per cycle. Then, during the final portion of the test, there was a high rate in strain loss – 0.45% per cycle – leading to failure.

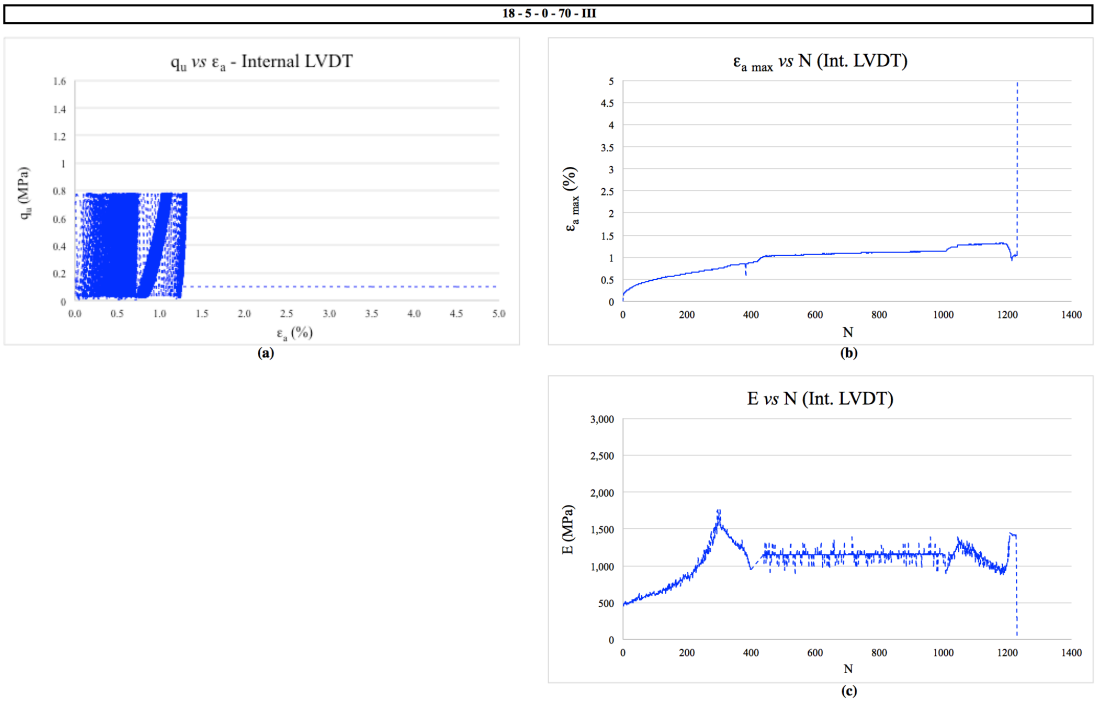

Figure 5.30: Internal data from specimen 18-5-0-70-III (a) q_u *versus* ε_a (b) $\varepsilon_{a\ max}$ *versus* N (c) E *versus* N

When analysing the Young's modulus (figure 5.30 (c)), the initial values were around 451 MPa, the specimen presented a decrease of 289% in E due to cycling through the first 300 cycles (1758 MPa). After, the modulus fell 41% over the next 100 cycles (rate ratio of 0.41% loss per cycle). Then, E values remained somewhat constant until the last 231 cycles, when, there was a rapid decrease (around 73%) in stiffness until cycle 1191 (rate ratio of 0.317% loss per cycle) leading to rupture. This indicates an initial mobilization of the weaker cementation bonds of the structure combined with a decrease in void ratio, corroborated by the high increase ratio of $\varepsilon_{a\ max}$ during this first phase. This was followed by degradation of the Young's modulus that can be attributed to a progressive failure of the weaker cemented bonds resulting in increase in plastic deformation of the matrix. This phenomenon was followed by a stabilization of E with cycling, where the degradation of the stronger cementitious bonds of the matrix occurs slowly over the loading-unloading process, accumulating plastic deformation at a constant rate. Finally, there was a decrease in E likely due to a critical number of cement bonds failing. The somewhat different behaviour presented by this specimen when compared to the other two might be due to the higher initial shear

stiffness of the specimen. Also, it could be associated to a distortion of the plastic extenders that allows the measurement of the internal data. However, for specimens without fibres that are a lot more rigid then the reinforced ones, and therefore present lower overall deformations before an abrupt rupture (brittle behaviour) this distortion is uncommon.

Figure 5.31 and 5.32 present the combined external and internal data for the three repetitions, respectively. Figure 5.31 does not have the data for the second specimen due to a technical issue during testing, however, as previously stated the internal data presented a more accurate description of the specimen behaviour. Figure 5.31 (b) show that there was an initial deformation that can partly attributed to the accommodation of the equipment. The other portion of the deformation is due to the initial deformation of the specimen. However, it is impossible to differentiate the two values. Afterwards, specimens I and III display a steady increase in deformation. Then, for the third specimen rupture occurred after an increase in the rate of $\varepsilon_{a\ max}$ gain, the Young's modulus presented in figure 5.31 (c)) show a steady increase. Specimen III presented a decrease in E followed by rupture, around 350 MPa.

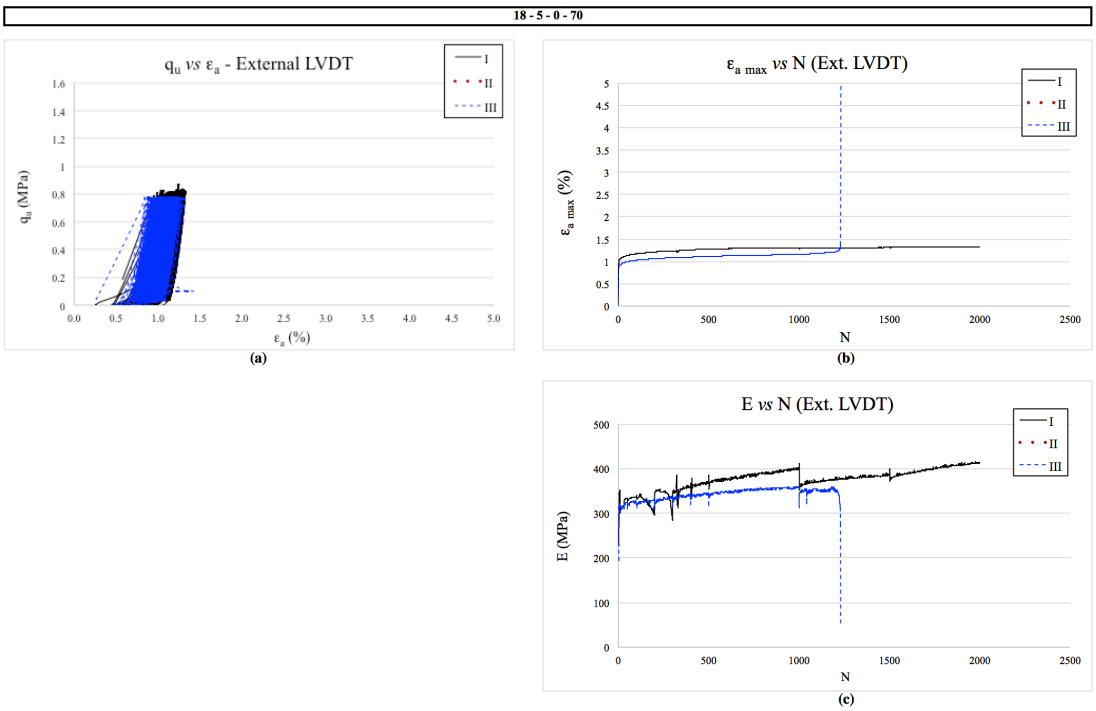

Figure 5.31: External data from specimen 18-5-0-70-I, II and III (a) q_u *versus* ε_a (b) $\varepsilon_{a\ max}$ *versus* N (c) E *versus* N

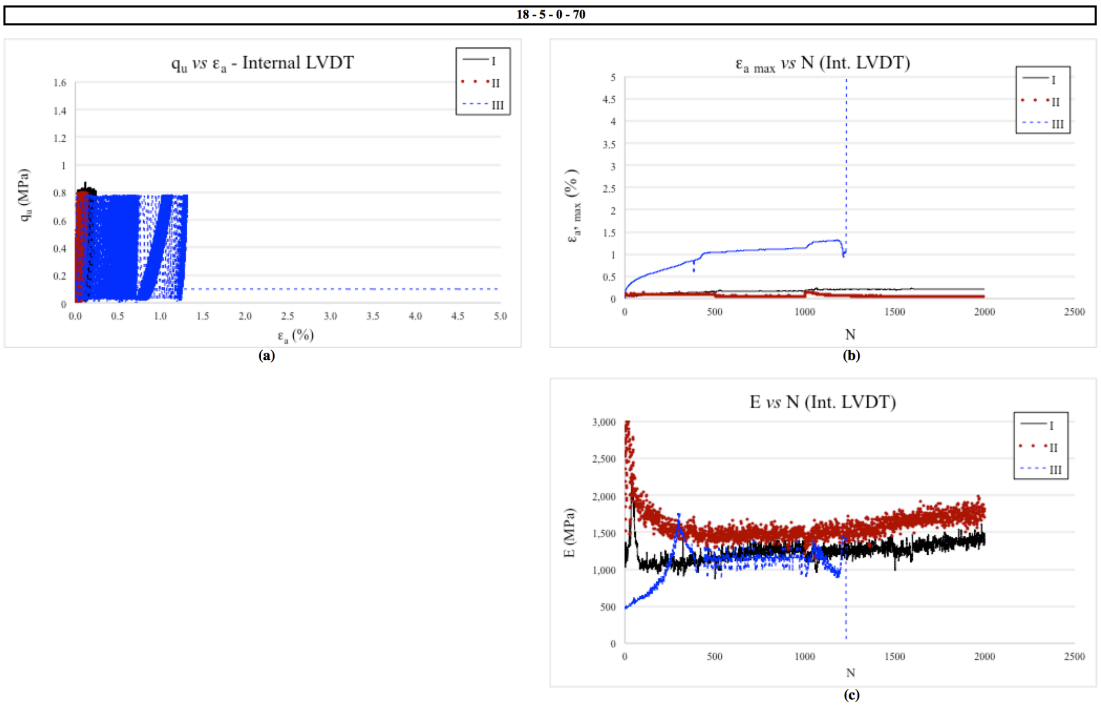

Figure 5.32: Internal data from specimen 18-5-0-70- I, II and III (a) q_u *versus* ε_a (b) $\varepsilon_{a\ max}$ *versus* N (c) E *versus* N

From figure 5.32 (b), it is possible to observe that after the initial deformation, which is also partly due to accommodation of the equipment, but to a smaller extent, showed the same trend of increase in axial strain. On average, for specimens I and II there was an increase of 0.07% in strain after the first cycle. As for the second repetition, the increase in maximum axial strain was much higher, being at around 0.55%. As mentioned previously, this difference in trends might not be only due to degradation of the cementation bonds, but also because of its higher G_0 and a possible distortion of the plastic extensor of the specimen.

As for the Young's modulus (figure 5.32 (c)), There was an initial increase that is likely because during the first couple of cycles accommodation is taking place and the mobilization of the weaker cementitious bonds pointing to a deification of the structure. After which, the values of E were aligned with the values of E from G_0. Then, a decrease in value was observed, indicating degradation of stiffness of the specimen, brought by cementation brake of the weaker bonds. Then, a gradual increase in E occurs. For the third specimen, before rupture, there was a decrease in the Young's modulus.

5.1.4 Shear Modulus

During testing bender element tests were carried out at pre-established intervals – 0, 1, 2, 10, 30, 50, 100, 200, 300, 400, 500, 1000, 1500, and 2000 cycles. For every reading the cyclic test was stopped so that the specimen was tested unloaded. The values attained are presented in appendices B. As stated in item 3.2.10.2, at the beginning of every test a frequency screening was made in order to assess the best one to conduct the tests. Figure 5.33 presents as an example of this screening the results attained for specimen 18-5-0-80-II, where frequency 25 Hz was chosen because it provided the sharper curves, making it easier to pinpoint the first arrival peak.

In figure 5.34 it is possible to observe how the progression of the bender readings with cycling, also for specimen 18-5-0-80-II. From this image it is possible to clearly see the gradual advance of the peaks to the right, increasing the arrival time reading and therefore the values of G.

Figure 5.35 presents the values of shear modulus *versus* number of cycles for all the repetitions for the 19-5-0 combinations. It is possible to conclude that the values of G obtained for all repetitions are within the same order of magnitude and have similar tendencies. Figure 5.35 (a) presents the values of shear modulus *versus* the number of cycles for the benchmark mixtures at 90% of the estimated maximum load. A decreasing in G trend can be observed for all repetitions. The same trend can be observed in figure 5.35 (b) where the benchmark mixtures were tested for 80% of the estimated maximum load, For the third repetition a more pronounced rate of stiffness degradation can be observed over the last two readings (100 and 200 cycles). Figure 5.35 (c) presents the benchmark mixtures tested for 70% of the estimated maximum load, in these graphs it is possible to note a slight increase in the G_N values for the specimens that did not fail after 500 cycles. This could indicate a rearrangement of the soil structure after the first quarter of testing, leading to a denser specimen. Accumulating plastic deformation until an eventual collapse of the structure. As for the specimen that failed (18-5-0-70-III) the same reduction in G_N with cycling trend as observed for the other load percentages occurred.

Plotting the average values of the repetitions, figure 5.36 displays the relationships between G and N for the three percentages of applied loads studied and their respective fitted equations. It is possible to infer form the presented data that the G_N values withstood a lower decrease rate as the applied load decreased, as it should be expected, lower applied load should result in less damage to the structure for a given number of cycles. For the 70% load percentage, the trend observed in

figure 5.35 (c) was put into perspective regarding the other to load percentages. It can be observed a clear stabilization followed by an increase in G_N values after 100 cycles. For the applied load of 90 and 80% there was a consistent degradation of stiffness with cycling, leading to rupture.

The G_N values were normalised by the G_0 values of the mixtures, as shown in figure 5.37. From these graphs it is easier to differentiate the aforementioned trends. The G_N values withstood a higher decrease rate for the 90% applied load decreased. For the other two load percentages there was not initially a pronounced difference, however, with the progression of the number of cycles the difference was considerable. For the 70% load percentage, the clear stabilization of values followed by an increase in G_N values after 100 cycles is even clearer. For the applied load of 80% there was a significant degradation of stiffness over the last 150 cycles before rupture. From this data it is possible to conclude that the measurement of G values during cyclic loading is a good indicator for the prediction of failure for the tested specimens. If the shear modulus degradation consistently decreases with cycling, failure is eminent. However, if the degradation of stiffness reaches a plateau or increases after 100 cycles, the specimen will withstand higher N values.

Figure 5.38 presents the values of shear modulus *versus* number of cycles for all the repetitions for the 19-3-0-80 combination. It is possible to conclude that the values of G obtained for all repetitions are within the same order of magnitude and have similar tendencies. When observing figure 5.39, that compares it data to the one from the benchmark mixture at the same applied load percentage, it is possible to conclude that there is a much more pronounced degradation of shear stiffness for the specimen with lower cementation, even though the present similar $\eta/C_{iv}^{0.28}$. When comparing the fitted equation of the 19-3-0-80 from figure 5.39 (a) to the equation for 19-5-0-90 specimens (figure 5. 36) it was observed a higher degradation rate for the material with lower cementation. Suggesting that the amount of cementation bonds (cement content) might play a larger role in cyclic loading than its porosity for the studied materials.

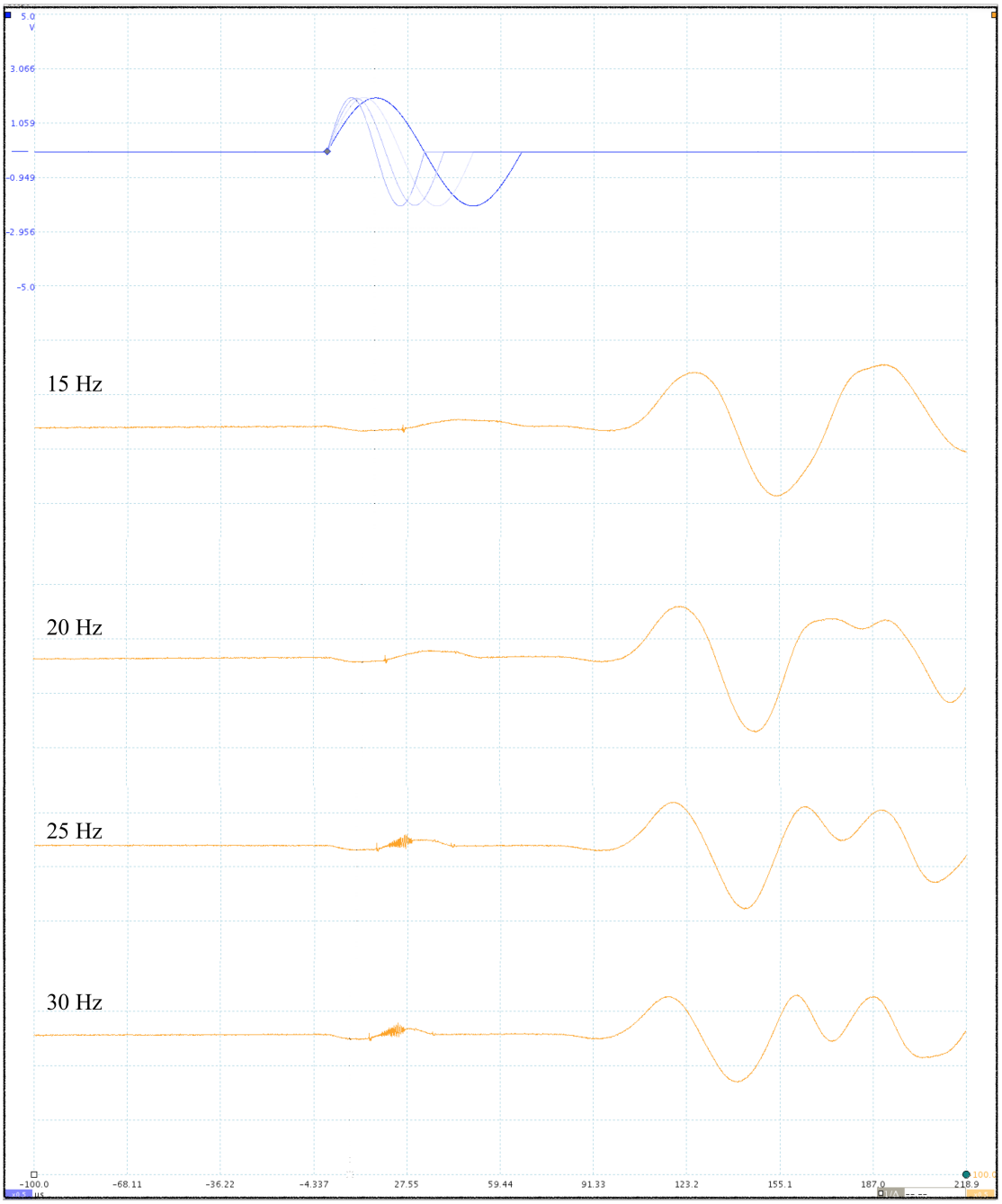

Figure 5.33: Frequency screening for bender readings for specimen 18-5-0-80-II

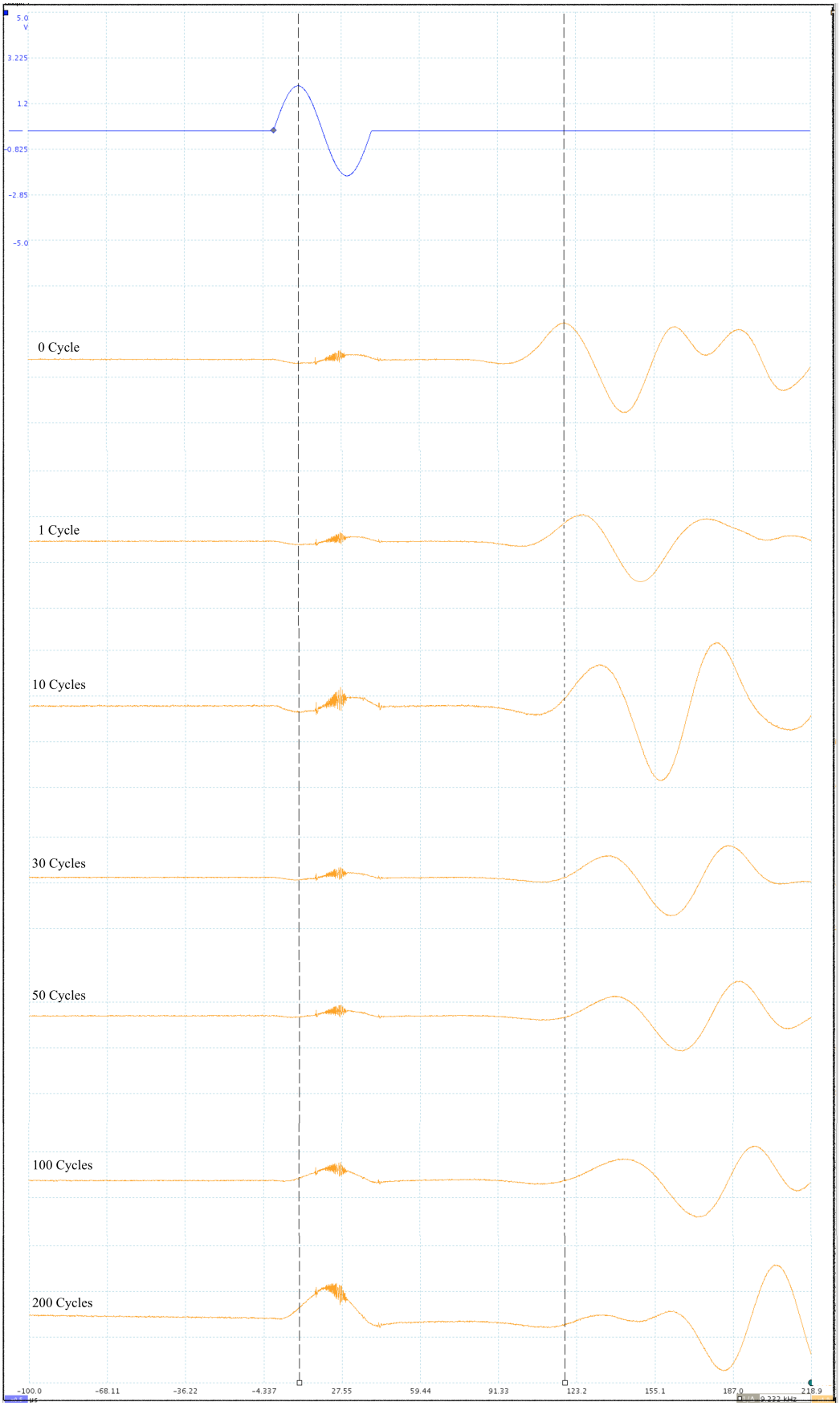

Figure 5.34: Bender readings during cycling for 18-5-0-80-II

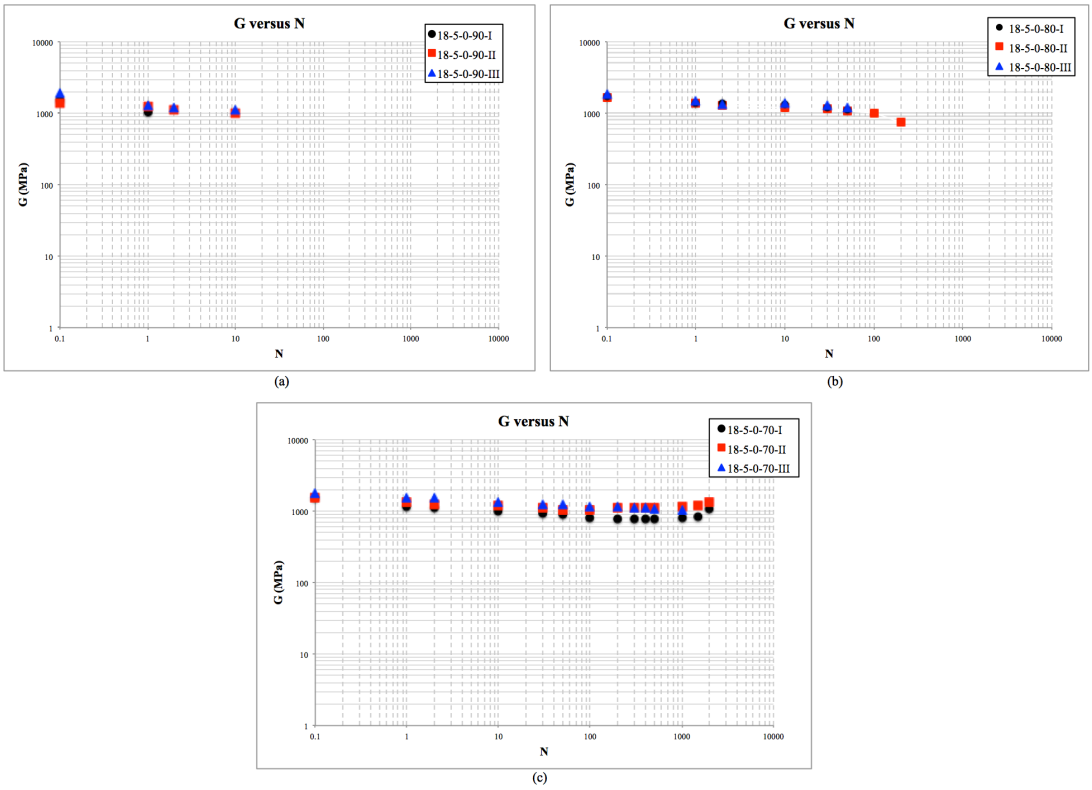

Figure 5.35: Shear modulus versus number of cycles for benchmark specimens at (a) 90% loading (b) 80% loading (c) 70% loading

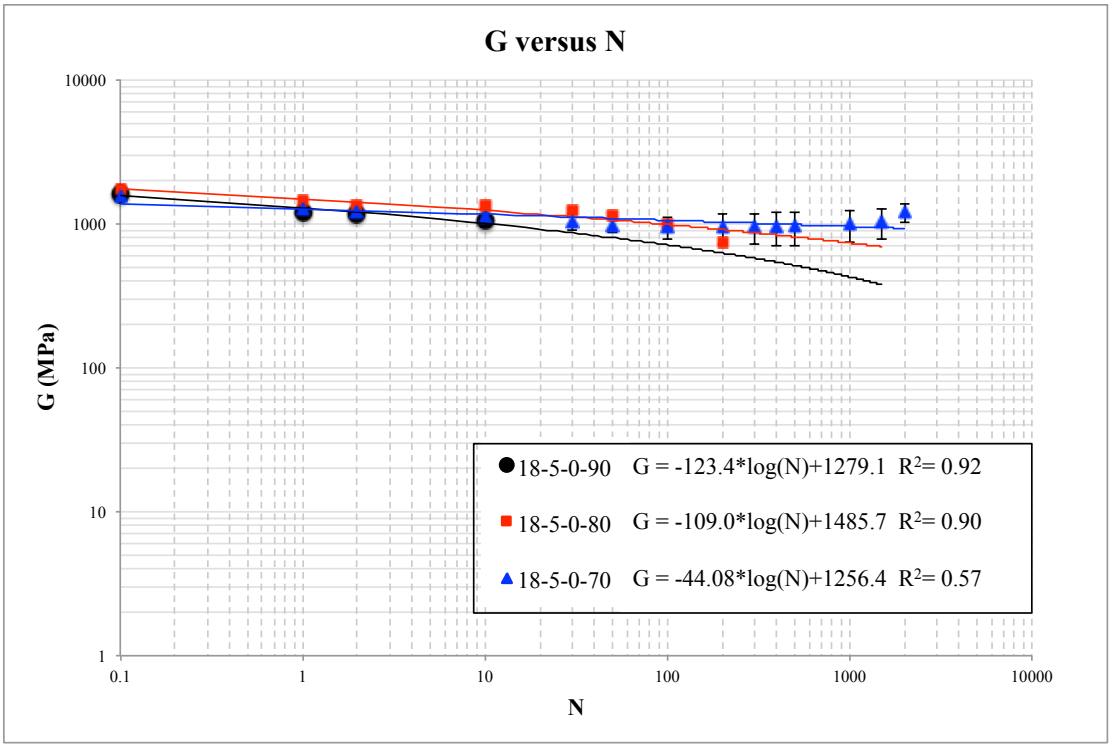

Figure 5.36: Shear modulus versus number of cycles for benchmark specimens

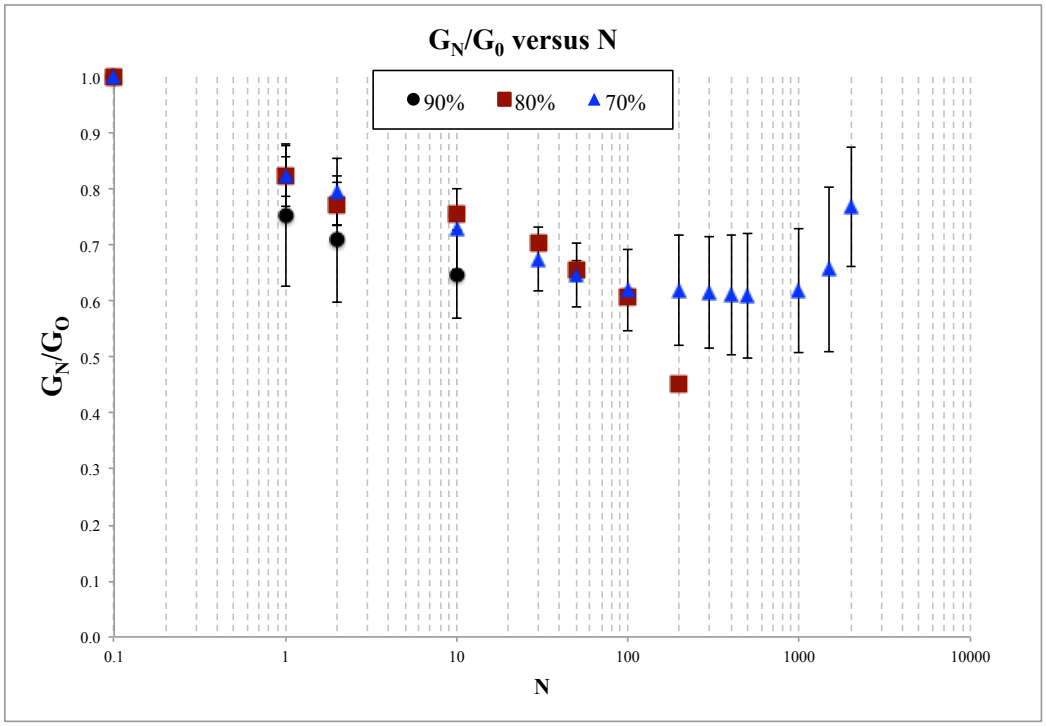

Figure 5.37: G_N/G_0 versus number of cycles for benchmark specimens

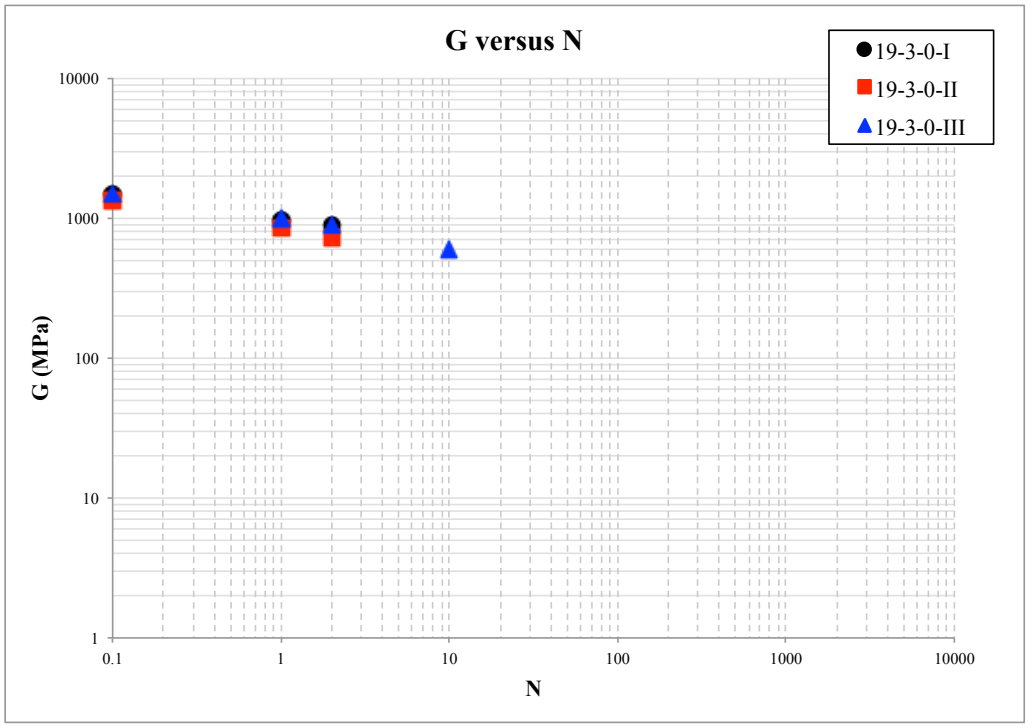

Figure 5.38: Shear modulus versus number of cycles for 19-3-0 specimens at 80% loading

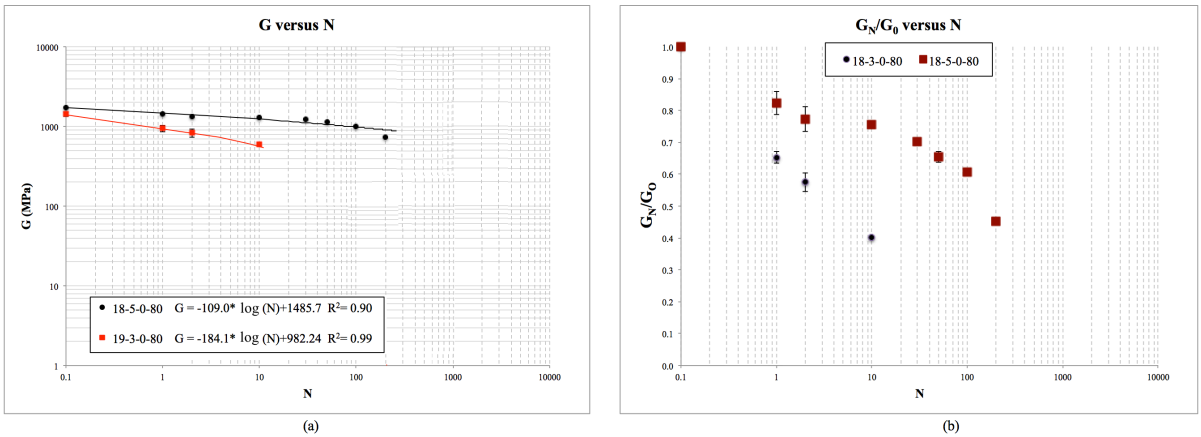

Figure 5.39: (a) Shear modulus versus number of cycles and (a) G_N/G_0 versus number of cycles for benchmark and 19-3-0 specimens at 80% loading

5.2 SOIL-CEMENT-FIBRE

In this topic it is presented the results of the tests carried out for the benchmark mixture (18 kN/m^3; 5% cement; 0.5% fibre) for the stipulated load percentages (90, 80 and 70%). Also, for 80% of the maximum load, it was tested a different mixture combination with the same $\eta/C_{iv}^{0.28}$ (19 kN/m^3; 3% cement; 0.5% fibre). Besides these combinations, further tests were made for the benchmark mixture for a modified load (same as the specimens without fibre) maintaining the same applied load percentages (90, 80 and 70%). Because it is an unconfined test, three repetitions of each point were done, except for the modified loads that only two repetitions were made due to material restraints. During testing, bender elements were used to assess the shear modulus under small strain. This data is also presented in this section.

The value of the maximum load for each specimen studied was derived from the equation of q_u *versus* $\eta/C_{iv}^{0.28}$ presented by Festugato (2011) (Figure 4.1), as mentioned previously. The $\eta/C_{iv}^{0.28}$ of each specimen was calculated after moulding of the specimen and through the fitted formula (equations 4.1 and 4.2), its corresponding q_u value assessed. Table 5.6 presents the values attained for the moulded specimens.

Table 5.6: Soil-cement-fibre mixtures: loading determination for cyclic unconfined compression tests

Mixture	Ideal Load %	Repetition	$\eta/C_{IV}^{0.28}$	Theoretical Load (kPa)	Theoretical Load (N)	% Load (kPa)	% Load (N)	Applied Load (N)	Actual %
18 kN/m³ - 5% cement - 0.5% Fibre	90	I	25.29	1443.74	2861.68	1299.37	2628.10	2506.15	87.58
	90	II	24.09	1641.83	3234.91	1477.65	2911.42	2824.08	87.30
	90	III	23.82	1691.46	3336.24	1522.31	3002.62	2961.90	88.78
	80	I	24.12	1636.32	3220.08	1472.68	2576.07	2530.12	78.57
	80	II	23.72	1710.06	3375.41	1539.06	2700.33	2682.59	79.47
	80	III	23.92	1672.75	3294.75	1505.48	2635.80	2591.73	78.66
	70	I	23.96	1665.51	3276.77	1498.96	2293.74	2230.26	68.06
	70	II	24.39	1588.92	3140.46	1430.03	2198.32	2151.93	68.52
	70	III	24.30	1604.63	3167.30	1444.17	2217.11	2160.41	68.21
18 kN/m³ - 5% cement - 0.5% Fibre - Modified Load	90	I	24.03	1173.42	2319.85	1056.08	2087.87	2149.50	92.66
	90	II	23.68	1228.36	2427.49	1105.52	2184.75	2221.93	91.53
	80	I	24.00	1177.77	2323.50	942.21	1858.80	1876.39	80.76
	80	II	24.30	1134.18	2256.30	907.34	1805.04	1876.55	83.17
	70	I	23.72	1220.75	2418.87	854.52	1693.21	1740.66	71.96
	70	II	24.02	1174.61	2322.20	822.22	1625.54	1675.40	72.15
19 kN/m³ - 3% cement - 0.5% Fibre	80	I	24.14	1632.51	3229.62	1306.01	2583.70	2422.87	75.02
	80	II	24.58	1556.72	3096.69	1245.38	2477.35	2461.85	79.50
	80	III	24.54	1562.75	3093.87	1250.20	2475.10	2608.72	84.32

The acquired data is presented in the form of graphs. Each test has two figures, one for the external data and another for the internal. Each figure has three graphs: q_u *versus* ε_a; $\varepsilon_{a\ max}$ *versus* N; and E *versus* N. For the modified loads the results were very similar, so only the internal data for the repetitions are presented. There is also the data for the shear modulus (G) that is presented on its own item, where the relationship between G and N is presented for the different load percentages.

For fibre-reinforced specimens the definition of failure is very important, since the specimens continue to withstand loading even at very high deformations, also known as ductile behaviour (CONSOLI *et* al., 2009). Given this necessity, it was stipulated that failure occurred at 2% of the maximum axial strain. In order to take into account the initial deformation due to specimen accommodation, it was considered that the 2% strain limited began at half the maximum strain of the first cycle for the internal data.

5.2.1 Applied load percentage: 90%

Figures 5.40 and 5.41, present the data results for the external and internal data of the first specimen, respectively. Followed by figures 5.42 and 5.43 that show respectively the values for the external and internal data for second specimen. Finally, figures 5.44 and 5.45 illustrate the results attained for the external and internal LVDTs of the third specimen, respectively.

The summary of the tests is shown in table 5.7. It presents of cycles until rupture (N), initial shear modulus (G_0), and the estimated value of the initial Young's modulus at small strains (E from G_0), again, the E values are just a estimative. From the presented data, it is possible to infer that the dispersion of $\eta/C_{iv}^{0.28}$ for the replicas is less than 4%. The dispersion of data for the G_0 is less than 14%. The dispersion of G values for the fibre-reinforced specimens was higher than for the unreinforced specimens. However, given that the measurement of bender elements proved more difficult for fibre-reinforced materials, a higher dispersion threshold (of 15% variation) was allowed. Thus, the repetitions for this combination were considered similar.

Table 5.7: Summary of Cyclic UC tests for 90% of estimated maximum loading for benchmark mixtures with fibres

Mixture	Ideal Load %	Repetition	$\eta/C_{IV}^{0.28}$	Applied Load (N)	Actual %	Number of Cycles	Numeber of Cycles Rupture	Initial Bender (μs)	G_0 (MPa)	E from G_0 (MPa)
18 kN/m³ 5% cement 0.5% fibre	90	I	25.29	2506.15	87.58	17	12	169.70	600.53	1513.34
	90	II	24.09	2824.08	87.30	50	25	159.60	684.43	1724.76
	90	III	23.82	2961.90	88.78	55	49	174.30	528.35	1331.45

There was variability in the number of cycles until rupture. However, the results are in the same order of magnitude, and all the moulding indicators – $\eta/C_{iv}^{0.28}$; actual loading percentage in respect to its estimated maximum load; G_0 – suggest that the specimens have similar initial conditions.

The first specimen withstood 12 cycles of the 17 cycles tested. From the external data (figure 5.40) it was observed a high strain during the first cycle of around 1.117%, after which there was a steady increase in strain until rupture around 2.495% (figure 5.40 (b)). This initial strain, which was almost 50% of the total strain, was partly due to equipment accommodation. The Young's modulus (figure 5.40 (c)) presented a 7% decline between the first and tenth

cycles – ratio of E loss of 0.79% per cycle. During the last two cycles there was a 56% decrease in E (28% of E loss per cycle), reaching failure at the 12th cycle.

Observing the internal data for the same specimen, a much lower overall strain is observed and the overall stiffness of the specimen was higher. However, it is important to note that the overall values of E for fibre-reinforced specimens were substantially lower than the values observed by soil-cement mixtures, this is also corroborated by the G values attained from these group of specimens. Once again indicating a much more ductile behaviour.

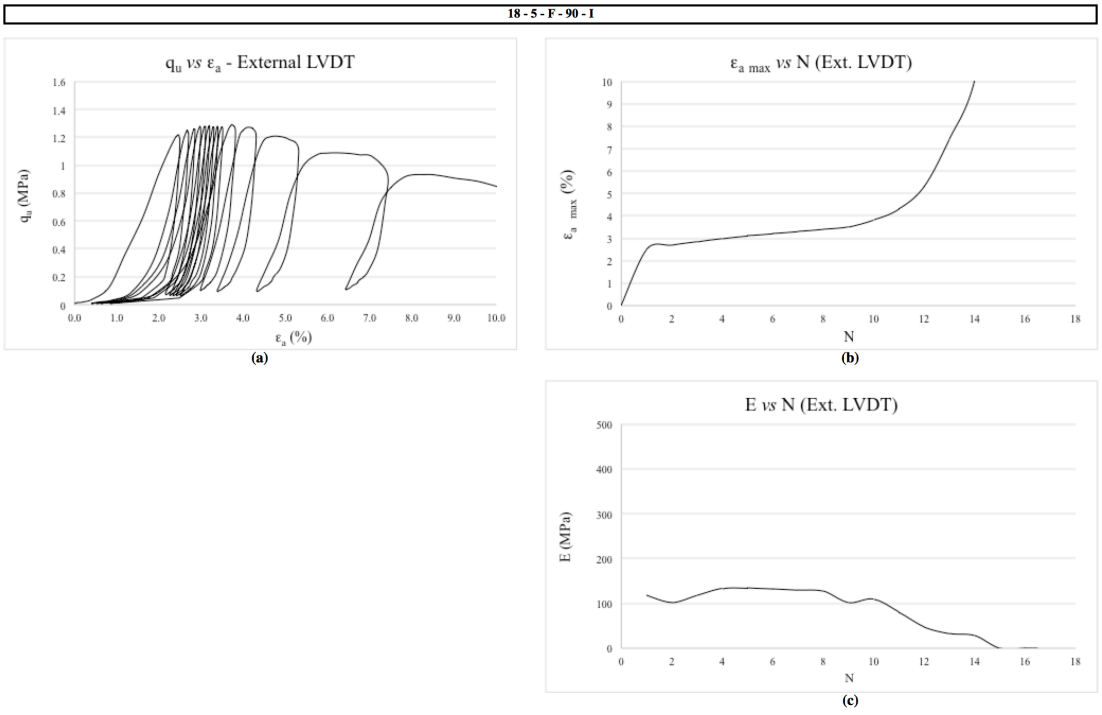

Figure 5.40: External data from specimen 19-5-F-I (a) q_u *versus* ε_a (b) $\varepsilon_{a\ max}$ *versus* N (c) E *versus* N

Figure 5.41 (b) shows that there was an initial strain of 0.5118%, thus the failure threshold for this specimen was of 2.256%. This initial strain was followed by an 85% increase in strain values over the next seven cycles – rate of axial strain gain of 12.2%. Over the last 4 cycles the values of $\varepsilon_{a\ max}$ increased very rapidly at a rate of 53.26% increase per cycle surpassing the stipulated threshold at the 12th cycle with a $\varepsilon_{a\ max}$ of 2.971%. As for the Young's modus (figure 5.41 (c)), the initial E value was of 310.76 MPa. The specimen presented a 15.5% increase in E over the next seven cycles, reaching 359 MPa. After this increase, the values of E rapidly decreased over the next 4 cycles, reaching 36.42 MPa at the twelfth cycle – a loss rate of 22.46% per cycle. The behaviour presented by this specimen indicates a consistent

degradation of the cementitious bonds with cycling leading to a constant increase in the accumulated plastic deformation, resulting in an slight increase in E until a critical number of bonds fail, leaving almost exclusively the fibres responsible for the absorption of load, resulting in high deformations and low Young's modulus.

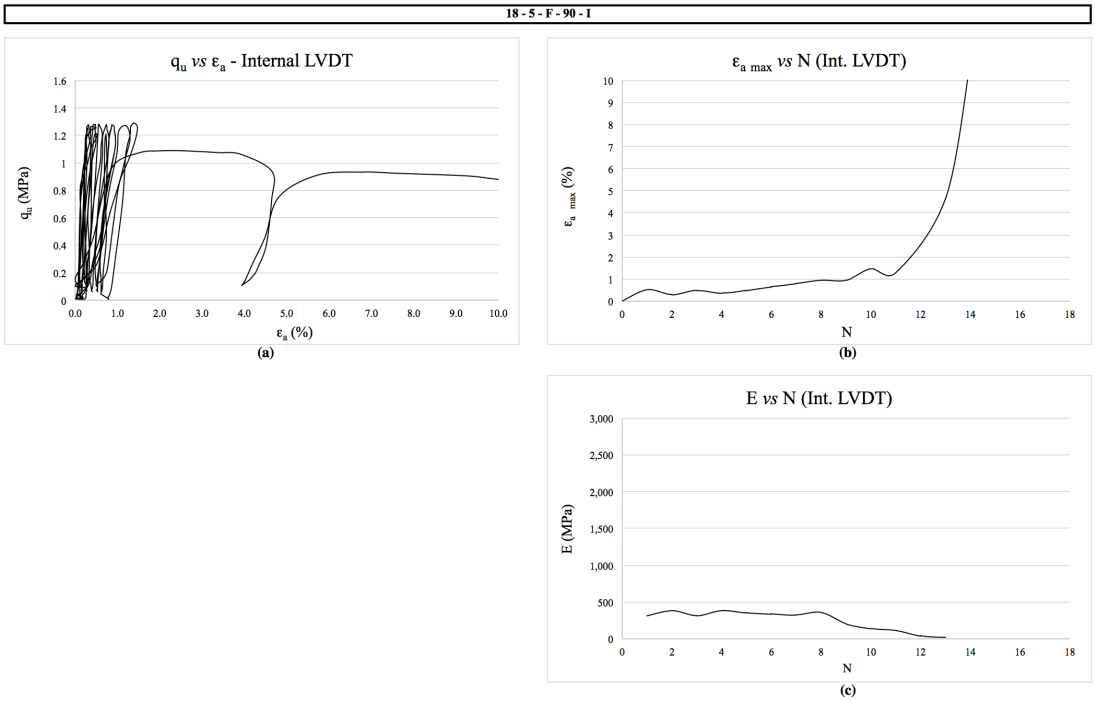

Figure 5.41: Internal data from specimen 19-5-F-I (a) q_u *versus* ε_a (b) $\varepsilon_{a\ max}$ *versus* N (c) E *versus* N

Specimen number two failed at the 25th of the total of 50 cycles tested. From the external data (figure 5.42) it was observed a high strain during the first cycle of around 1.690%, after which there was a steady increase in strain until rupture around 3.337% (figure 5.42 (b)). This initial strain, which was double of the total strain, was partly due to equipment accommodation. The Young's modulus (figure 5.42 (c)) presented a 51.5% increase between the first and third cycles – ratio of E gain of 25.76% per cycle. During the next 22 cycles there was a 21% decrease in E – 0.96% of E loss per cycle), reaching failure at the 25th cycle.

Figure 5.43 (b) shows that there was an initial strain of 1.194%, thus the failure threshold for this specimen was of 2.597%. This initial strain was followed by an 35.18% increase in strain values over the next seven cycles – rate of axial strain gain of 5.025%. Over the next 17 cycles the values of $\varepsilon_{a\ max}$ increased very rapidly at a rate of 3.69% increase per cycle (62.76% total increase) surpassing the stipulated threshold at the 25th cycle with a $\varepsilon_{a\ max}$ of 2.627%. As

for the Young's modus (figure 5.43 (c)), the initial E value was of 213.26 MPa. The specimen presented a 513,16% increase in E over the next seven cycles, reaching 1307.6 MPa. After this increase, the values of E decreased over the next 17 cycles, reaching 418 MPa at the twenty-fifth cycle – a loss rate of 4% per cycle. The behaviour presented by this specimen indicates an initial increase in specimen stiffness, probably due the mobilization of the weaker cement bonds that rapidly failed after eight cycles. These higher values of Young's modulus presented could be due to a higher initial Young's modulus, which is indicated by the G_0 values measured at the beginning of testing.

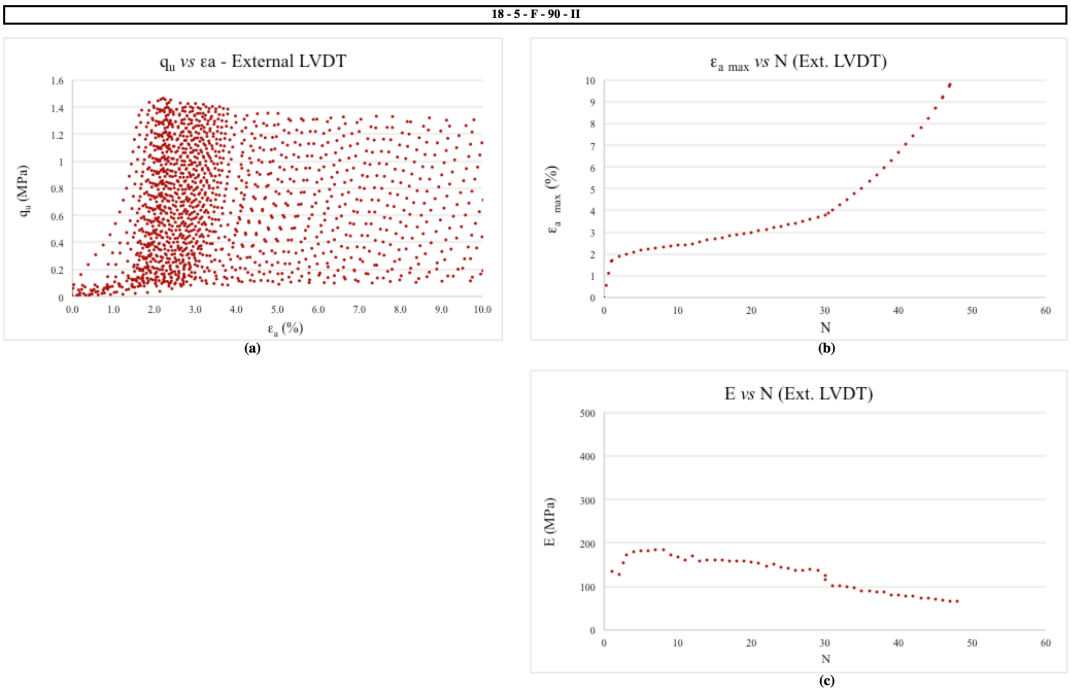

Figure 5.42: External data from specimen 19-5-F-II (a) q_u *versus* ε_a (b) $\varepsilon_{a\ max}$ *versus* N (c) E *versus* N

The last specimen of this combination failed at the 49th of the total of 55 cycles tested. From the external data (figure 5.44) it was observed a strain during the first cycle of around 1.713%, after which there was a steady increase in strain until rupture around 7.156% (figure 5.44 (b)). This value of external strain at failure is very high when compared to the other two specimens. However, when the internal data is taken into consideration, the progression of strain gain is considerably slower. So, it was assumed that the higher external values were probably attributed to an increase in relaxation of the ram during low pressures. This effect does not affect the internal data, since the variation in displacements of the two LVDTs would remain constant. As for the Young's modulus (figure 5.44 (c)) there was an 8.92% decline

between the second and tenth cycles – ratio of E loss of 0.32% per cycle. During the last 19 cycles there was a 44.72% decrease in E (2.35% of E loss per cycle), reaching failure at the 49th cycle.

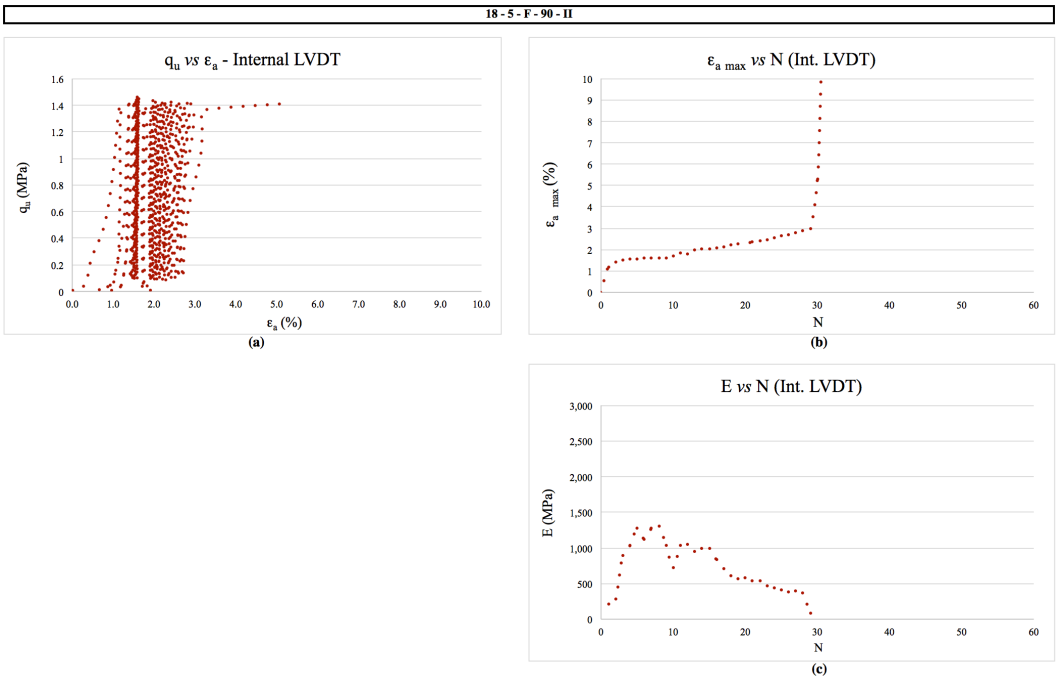

Figure 5.43: Internal data from specimen 19-5-F-II (a) q_u *versus* ε_a (b) $\varepsilon_{a\ max}$ *versus* N (c) E *versus* N

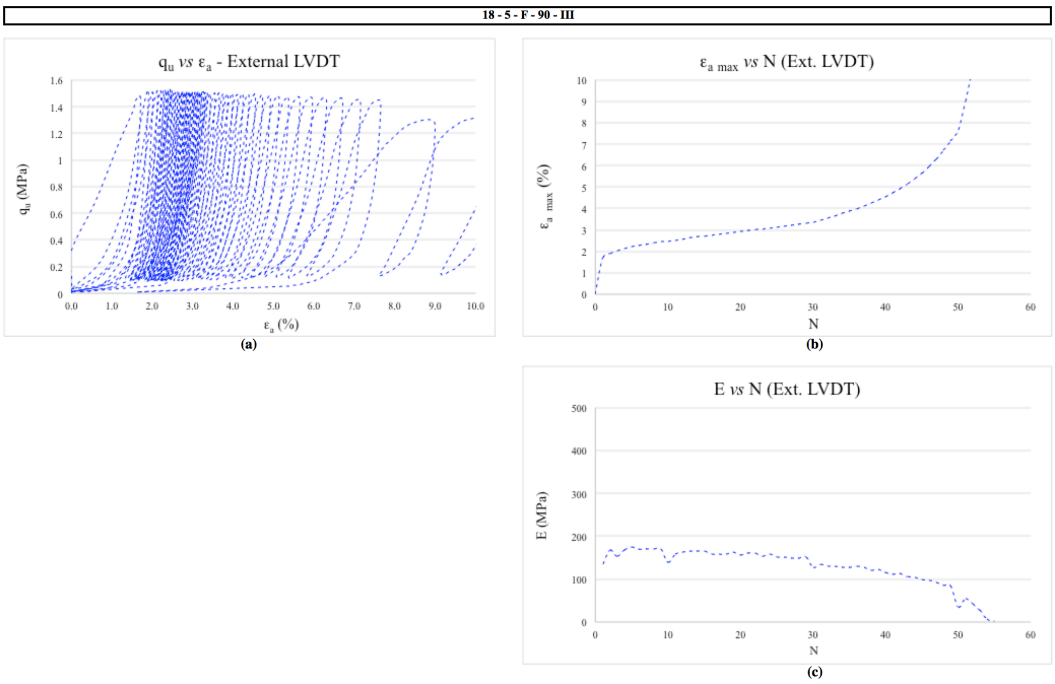

Figure 5.44: External data from specimen 19-5-F-III (a) q_u *versus* ε_a (b) $\varepsilon_{a\ max}$ *versus* N (c) E *versus* N

Figure 5.45 (b) shows that there was an initial strain of 1.878%, thus the failure threshold for this specimen was of 2.939%. This initial strain was followed by a 24.92% increase in strain values over the next 39 cycles – rate of axial strain gain of 0.639%. Over the last 9 cycles the values of $\varepsilon_{a\ max}$ increased at a higher rate of 3.27% increase per cycle surpassing the stipulated threshold at the 49th cycle with a $\varepsilon_{a\ max}$ of 3.037%. As for the Young's modus (figure 5.45 (c)), the initial E value was of 174.34 MPa. The specimen presented an 18.6% increase in E over the next 39 cycles, reaching 206.77 MPa. After this increase, the values of E began to decrease over the next 9 cycles, reaching 143.48 MPa at the 49th cycle – a loss rate of 3.4% per cycle. The behaviour presented by this specimen indicates a consistent degradation of the cementitious bonds with cycling leading to an increase in the accumulated plastic deformation, resulting in an slight increase in E due to the reduction of the difference between $\varepsilon_{a\ max}$ and $\varepsilon_{a\ min}$, until a critical number of bonds fail, leaving almost exclusively the fibres responsible for the absorption of load, resulting in high deformations and low Young's modulus.

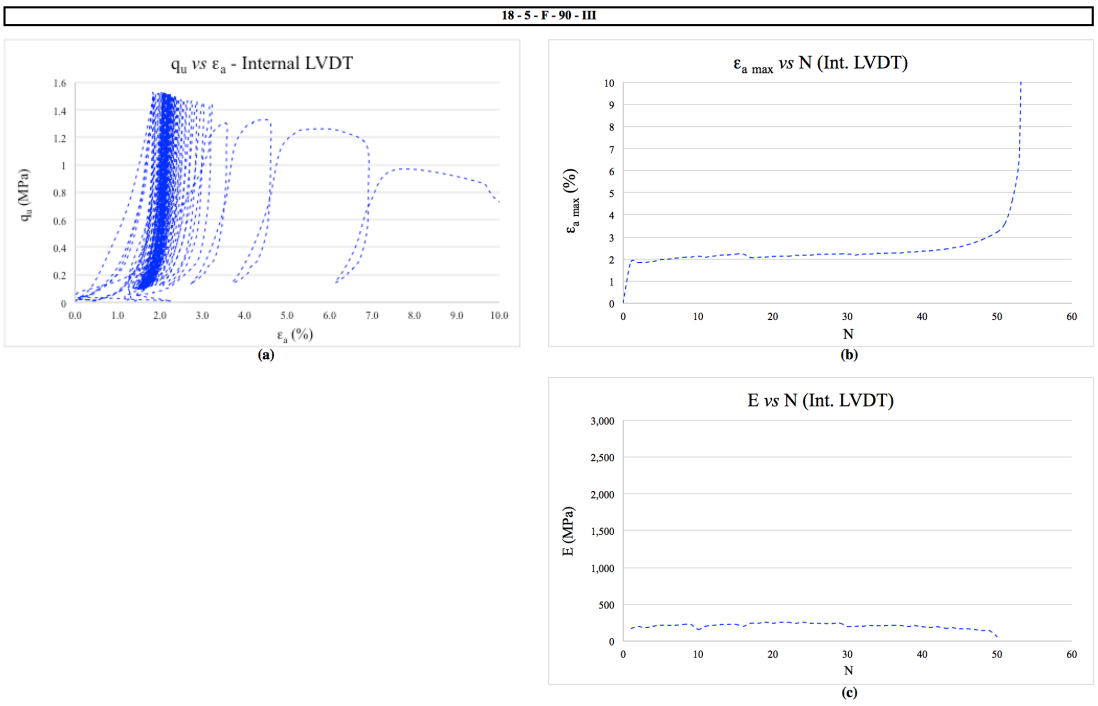

Figure 5.45: Internal data from specimen 19-5-F-III (a) q_u *versus* ε_a (b) $\varepsilon_{a\ max}$ *versus* N (c) E *versus* N

Figure 5.46 presents the superimposed graphs of the external data for the three repetitions. From figure 5.46 (b), it was possible to observe a similar trend of increase in axial strain after the initial deformation, especially for the second and third repetition. The same conclusion

could be drawn about the Young's modulus (figure 5.46 (c)). The first specimen failed earlier than the other two. This might be attributed to the higher $\eta/C_{iv}^{0.28}$ ratio presented by this specimen, even though the specimen was subjected to a lower load that reflected this variation.

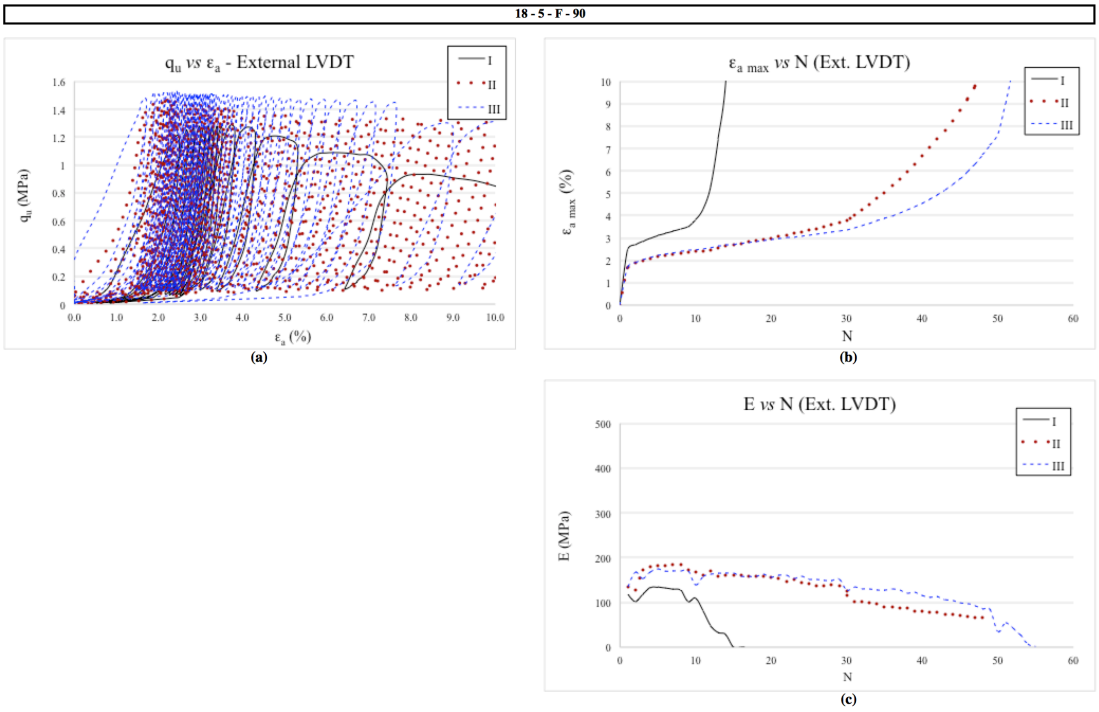

Figure 5.46: External data from specimen 19-5-F-I, II and III (a) q_u *versus* ε_a (b) $\varepsilon_{a\ max}$ *versus* N (c) E *versus* N

Figure 5.47 presents the superimposed graphs of the internal data for the three repetitions. From figure 5.47 (b), it was possible to observe a similar trend for the development of axial strain after the initial deformation, especially for the second and third repetition. For Young's modulus (figure 5.47 (c)) however, there was a significant change in trend for the second repetition when compared to the other two. The second specimen had a more rigid response to cycling, presenting higher values of E throughout testing. This phenomenon might be attributed to a higher value of G_0 (13.23% higher than the average for the repetitions). The reason for this higher initial shear modulus is not apparent in the moulding data, possibly being due to variability in the cementation process of the specimen. The opposite was observed for the third specimen. Its response was very similar to the values for the external LVDT. This response also might be attributed to its G_0 value. Even though the $\eta/C_{iv}^{0.28}$ of this specimen is lower than the other two, its initial shear modulus is also lower, when an increase in cementation and/or decrease in porosity should lead to higher G_0 values. The behaviour

shown by specimen 18-5-F-90-III might also be due to variability in the cementation process of the specimen, as observed for the second specimen.

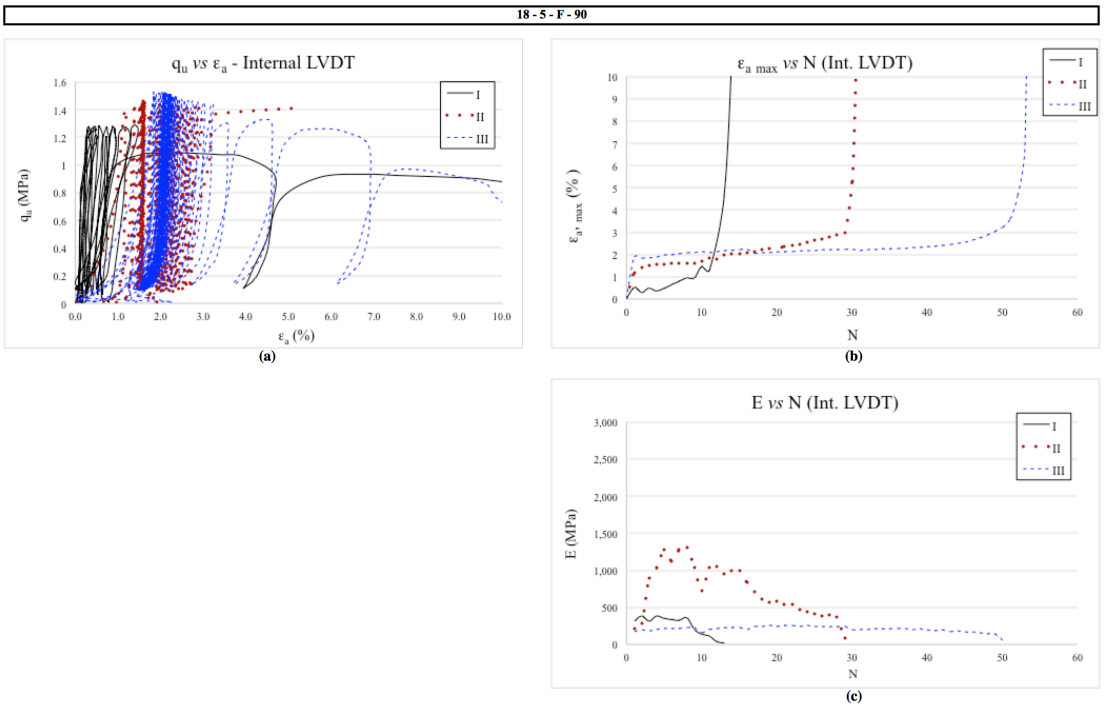

Figure 5.47: Internal data from specimen 19-5-F-I, II and III (a) q_u *versus* ε_a (b) $\varepsilon_{a\ max}$ *versus* N (c) E *versus* N

5.2.2 Applied load percentage: 80%

For this load percentage there were two different mixtures made, as mentioned previously. The first is the benchmark combination – figures 5.48 through 5.55, and the second is the 18 kN/m^3, 3 % cement content specimens – figures 5.56 through 5.63. Both mixtures have the same $\eta/C_{iv}^{0.28}$ and the data from their tests is presented in the following two topics.

5.2.2.1 Benchmark mixture

Figures 5.48 and 5.49, present the data results for the external and internal data of the first specimen, respectively. Followed by figures 5.50 and 5.51 that show respectively the values for the external and internal data for second specimen. Finally, figures 5.52 and 5.53 illustrate the results attained for the external and internal LVDTs of the third specimen, respectively.

The summary of the tests is shown in Table 5.8. It presents of cycles until rupture (N), initial shear modulus (G_0), and the estimated value of the initial Young's modulus at small strains (E from G_0), again, the E values are just an estimative. From the presented data, it is possible to

infer that the dispersion of $\eta/C_{iv}^{0.28}$ for the replicas is less than 1%. The dispersion of data for the G_0 is less than 14%. Given this data, the repetitions for this combination were considered similar.

Table 5.8: Summary of Cyclic UC tests for 80% of estimated maximum loading for benchmark mixtures with fibres

Mixture	Ideal Load %	Repetition	$\eta/C_{IV}^{0.28}$	Applied Load (N)	Actual %	Number of Cycles	Numeber of Cycles Rupture	Initial Bender (μs)	G_0 (MPa)	E from G_0 (MPa)
18 kN/m³ 5% cement 0.5% fibre	80	I	24.12	2530.12	78.57	105	75	169.10	694.67	1750.56
	80	II	23.72	2682.59	79.47	154	80	142.20	824.82	2078.56
	80	III	23.92	2591.73	78.66	68	52	139.40	889.43	2241.37

There was variability in the number of cycles until rupture. However, the results are in the same order of magnitude, and all the moulding indicators – $\eta/C_{iv}^{0.28}$; actual loading percentage in respect to its estimated maximum load; G_0 – suggest that the specimens have similar initial conditions.

The first specimen withstood 75 cycles of the total of 105 cycles tested. From the external data (figure 5.48) it was observed a high strain during the first cycle of around 2.368%, after which there was an increase in strain until rupture around 9.329% (figure 5.48 (b)). This value of external strain at failure is very high when compared to the other two specimens. However, when the internal data is taken into consideration, the progression of strain gain is considerably slower. So, it was assumed that the higher external values were probably attributed to an increase in relaxation of the ram during low pressures. This effect does not affect the internal data, since the variation in displacements of the two LVDTs would remain constant. The Young's modulus (figure 5.48 (c)) presented a 58.28% increase between the first and third cycles – ratio of E gain of 29.14% per cycle. Then, over the next 37 cycles there was a 22.1% decrease in the Young's modulus of the specimen at a rate of 0.60% per cycle. During the last 35 cycles there was a 49.2% decrease in E (1.41% of E loss per cycle), reaching failure at the 75th cycle.

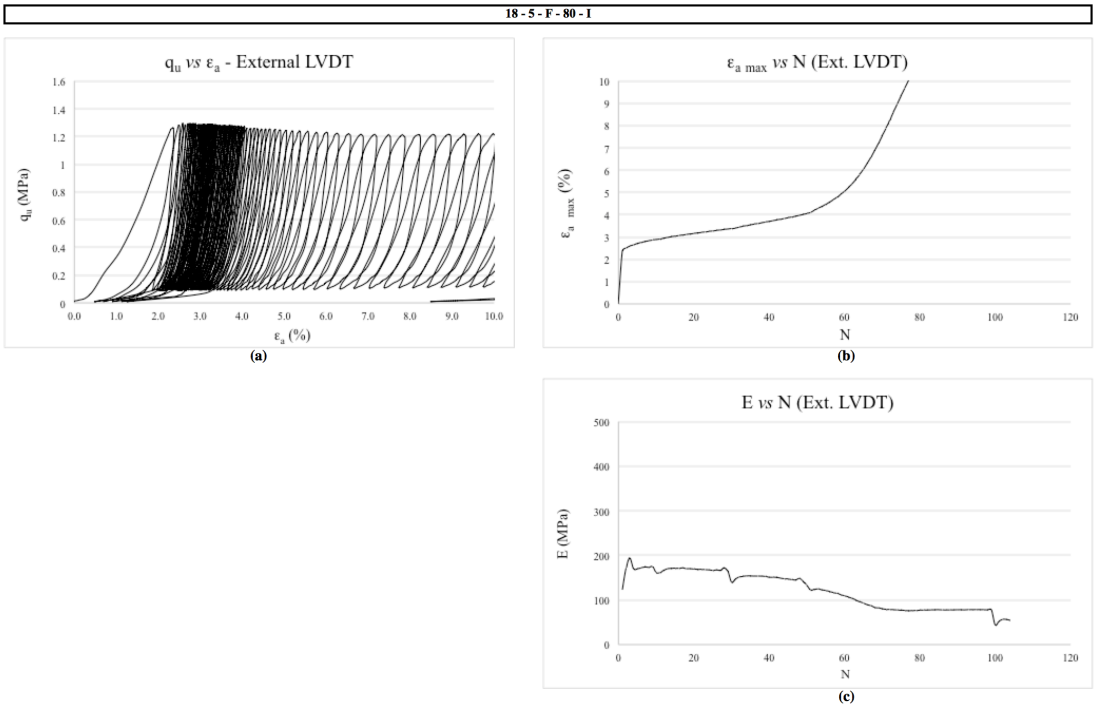

Figure 5.48: External data from specimen 19-5-F-80-I (a) q_u *versus* ε_a (b) $\varepsilon_{a\ max}$ *versus* N (c) E *versus* N

The internal data is presented in figure 5.49. Figure 5.49 (b) shows that there was an initial strain of 1.373%, thus the failure threshold for this specimen was of 2.686%. This initial strain was followed by a 13% increase in strain values over the next thirty-seven cycles – rate of axial strain gain of 0.33%. Over the last 35 cycles the values of $\varepsilon_{a\ max}$ increased at a rate of 2.15% increase per cycle reaching the 75th cycle with a $\varepsilon_{a\ max}$ of 2.716%. As for the Young's modus (figure 5.49 (c)), the initial E value was of 302.27 MPa. The specimen presented a 92% increase in E over the next 37 cycles, reaching 580.22 MPa. After this increase, the values of E decreased over the next 35 cycles, reaching 135.08 MPa at the 75th cycle – a loss rate of 2.19% per cycle. The behaviour presented by this specimen indicates a consistent degradation of the cementitious bonds with cycling leading to a constant increase in the accumulated plastic deformation, resulting in an slight increase in E until a critical number of bonds fail, leaving almost exclusively the fibres responsible for the absorption of load, resulting in high deformations and low Young's modulus.

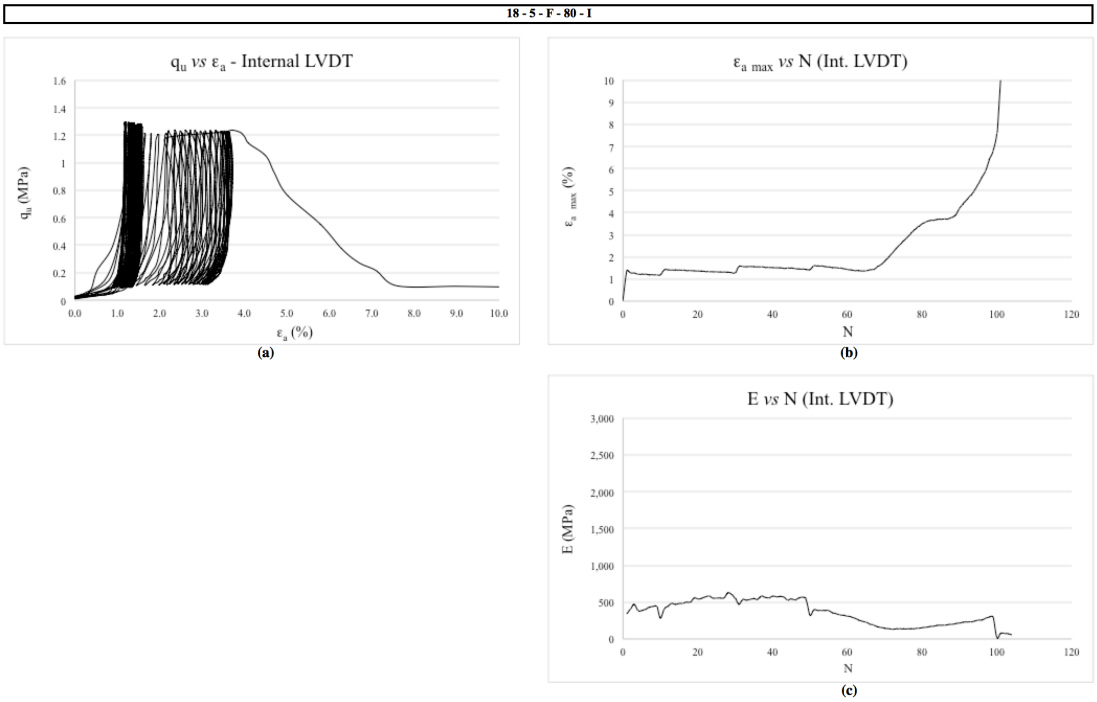

Figure 5.49: Internal data from specimen 19-5-F-80-I (a) q_u *versus* ε_a (b) $\varepsilon_{a\ max}$ *versus* N (c) E *versus* N

The second repetition withstood 80 cycles of the total of 154 cycles tested. From the external data (figure 5.50) it was observed a high strain during the first cycle of around 2.654%, after which there was an increase in strain until rupture around 4.372% (figure 5.50 (b)). The Young's modulus (figure 5.50 (c)) presented a 25.22% increase between the first and twentieth cycles – ratio of E gain of 1.327% per cycle. Then, over the next 60 cycles there was a 19% decrease in the Young's modulus of the specimen at a rate of 0.32% per cycle, reaching failure at the 80th cycle.

The internal data is presented in figure 5.51. Figure 5.51 (b) shows that there was an initial strain of 2.179%, thus the failure threshold for this specimen was of 3.09%. This initial strain was followed by a 17% increase in strain values over the next nineteen cycles – rate of axial strain gain of 0.92%. Over the last 60 cycles the values of $\varepsilon_{a\ max}$ increased at a slower rate of 0.34% increase per cycle surpassing the stipulated threshold at the 80th cycle with a $\varepsilon_{a\ max}$ of 3.091%. As for the Young's modus (figure 5.51 (c)), the initial E value was of 237.36 MPa. The specimen presented a 74% increase in E over the next 19 cycles, reaching 413.28 MPa. After this increase, the values of E decreased over the next 60 cycles, reaching 321.16 MPa at the 80th cycle – a loss rate of 0.37% per cycle. The behaviour presented by this specimen indicates a consistent degradation of the cementitious bonds with cycling leading to a constant

increase in the accumulated plastic deformation, resulting in an slight increase in E until a critical number of bonds fail, leaving almost exclusively the fibres responsible for the absorption of load, resulting in high deformations and low Young's modulus.

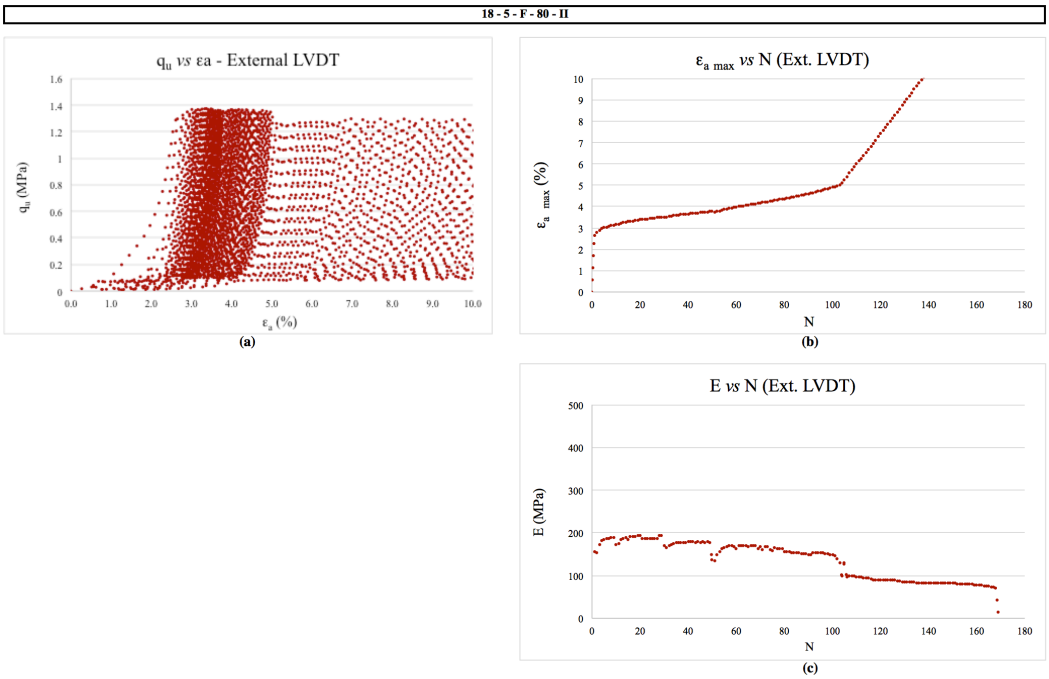

Figure 5.50: External data from specimen 19-5-F-80-II (a) q_u *versus* ε_a (b) $\varepsilon_{a\ max}$ *versus* N (c) E *versus* N

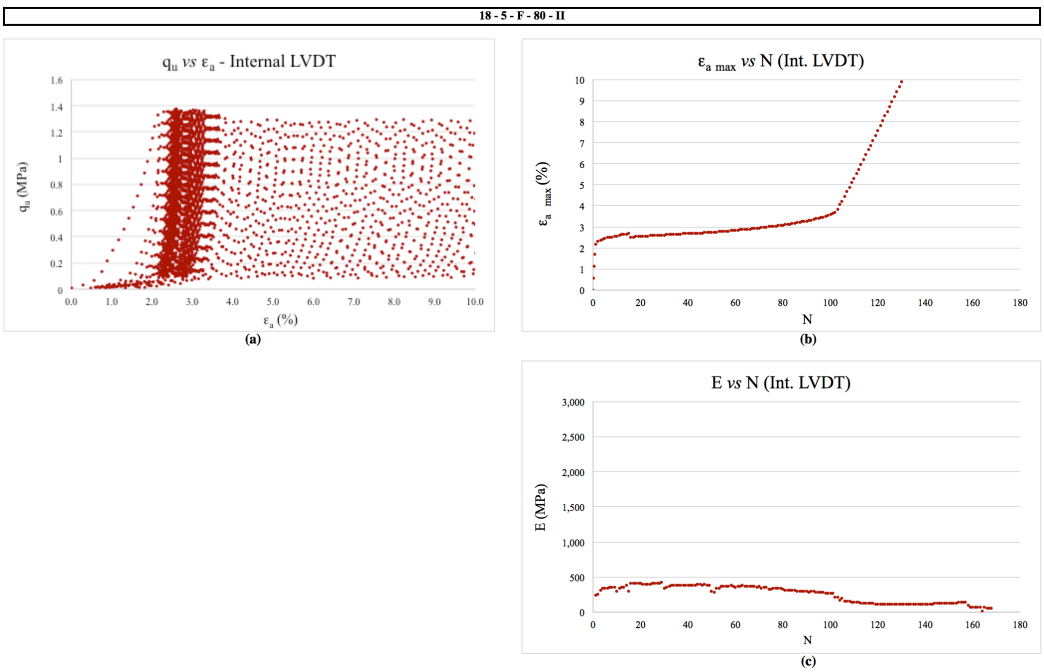

Figure 5.51: Internal data from specimen 19-5-F-80-II (a) q_u *versus* ε_a (b) $\varepsilon_{a\ max}$ *versus* N (c) E *versus* N

As for the third specimen the number of cycles until rupture was 52 of a total of 68 cycles tested. From the external data (figure 5.52) it was observed a strain during the first cycle of around 2.034%, after which there was an increase in strain until rupture around 4.120% (figure 5.52 (b)). The Young's modulus (figure 5.52 (c)) presented a 21.16% increase between the first and twentieth cycles – ratio of E gain of 1.12% per cycle. Then, over the next 32 cycles there was a 32.3% decrease in the Young's modulus of the specimen at a rate of 1.01% per cycle, reaching failure at the 52nd cycle.

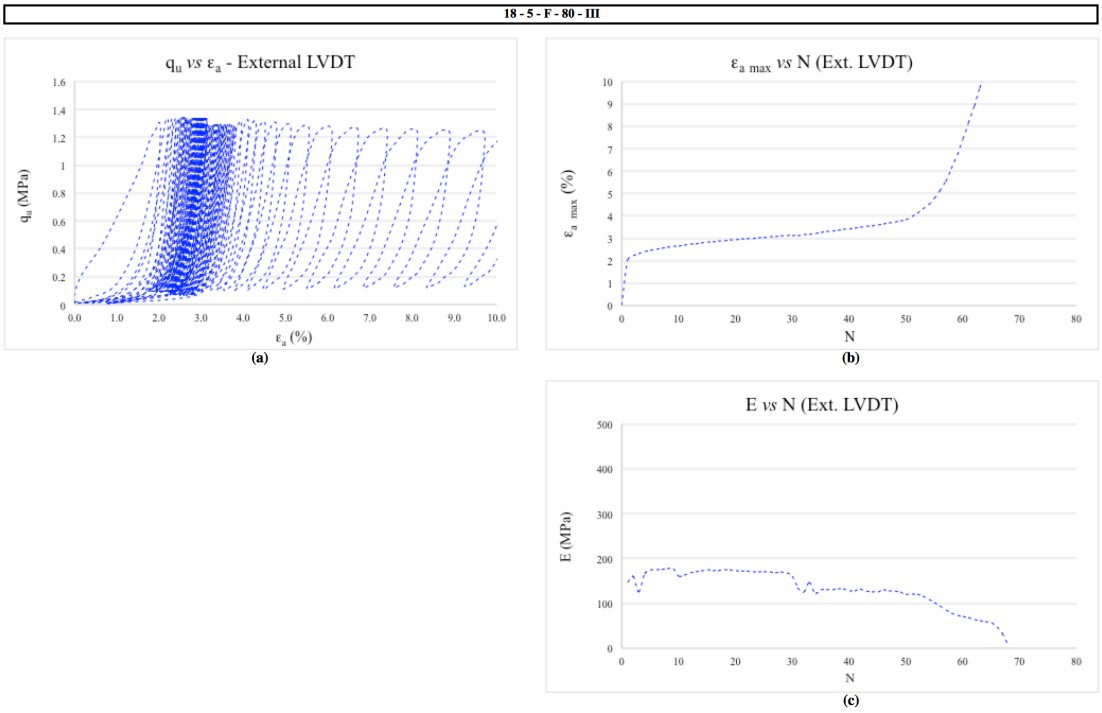

Figure 5.52: External data from specimen 19-5-F-80-III (a) q_u *versus* ε_a (b) $\varepsilon_{a\ max}$ *versus* N (c) E *versus* N

The internal data is presented in figure 5.53. Figure 5.53 (b) shows that there was an initial strain of 1.767%, thus the failure threshold for this specimen was of 2.883%. This initial strain was followed by a 31.75% increase in strain values over the next 19 cycles – rate of axial strain gain of 1.671% per cycle. Over the last 32 cycles the values of $\varepsilon_{a\ max}$ increased at a slower rate of 0.776% increase per cycle surpassing the stipulated threshold at the 52nd cycle with a $\varepsilon_{a\ max}$ of 2.906%. As for the Young's modus (figure 5.53 (c)), the initial E value was of 160.62 MPa. The specimen presented a 56.9% increase in E over the next 19 cycles, reaching 252.08 MPa. After this increase, the values of E decreased over the next 32 cycles, reaching 179.22 MPa at the 52nd cycle – a loss rate of 0.90% per cycle. The behaviour presented by this specimen indicates a consistent degradation of the cementitious bonds with cycling leading to

a constant increase in the accumulated plastic deformation, resulting in an slight increase in E until a critical number of bonds fail, leaving almost exclusively the fibres responsible for the absorption of load, resulting in high deformations and low Young's modulus.

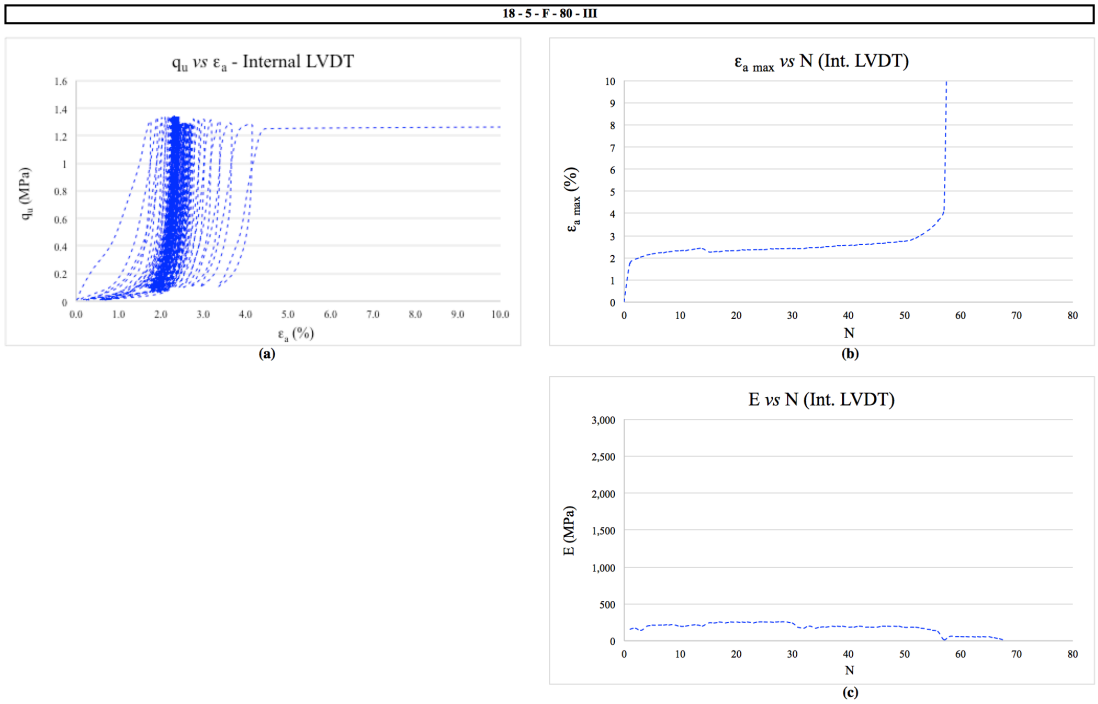

Figure 5.53: Internal data from specimen 19-5-F-80-III (a) q_u *versus* ε_a (b) $\varepsilon_{a\ max}$ *versus* N (c) E *versus* N

Figure 5.54 presents the superimposed graphs of the external data for the three repetitions. From figure 5.54 (b), it was possible to observe a similar trend of increase in axial strain after the initial deformation for all repetitions. The same conclusion could be drawn about the Young's modulus (figure 5.54 (c)). The third specimen failed earlier than the other two even though the specimen had the highest initial shear modulus. Therefore, it could be concluded that this difference was due to variability in the cementation process of the specimen.

Figure 5.55 presents the superimposed graphs of the internal data for the three repetitions. From figure 5.55 (b), it was possible to observe a similar trend for the development of axial strain after the initial deformation for the second and third repetition. The first repetition presented a more rigid response, having lower increase rate of $\varepsilon_{a\ max}$ up until 10 cycles before rupture, which is not expected, given that its G_0 value is l5% lower than the average value for the other two specimens. Once more it is speculated that this behaviour is due to variability in the cementation process of the specimen.

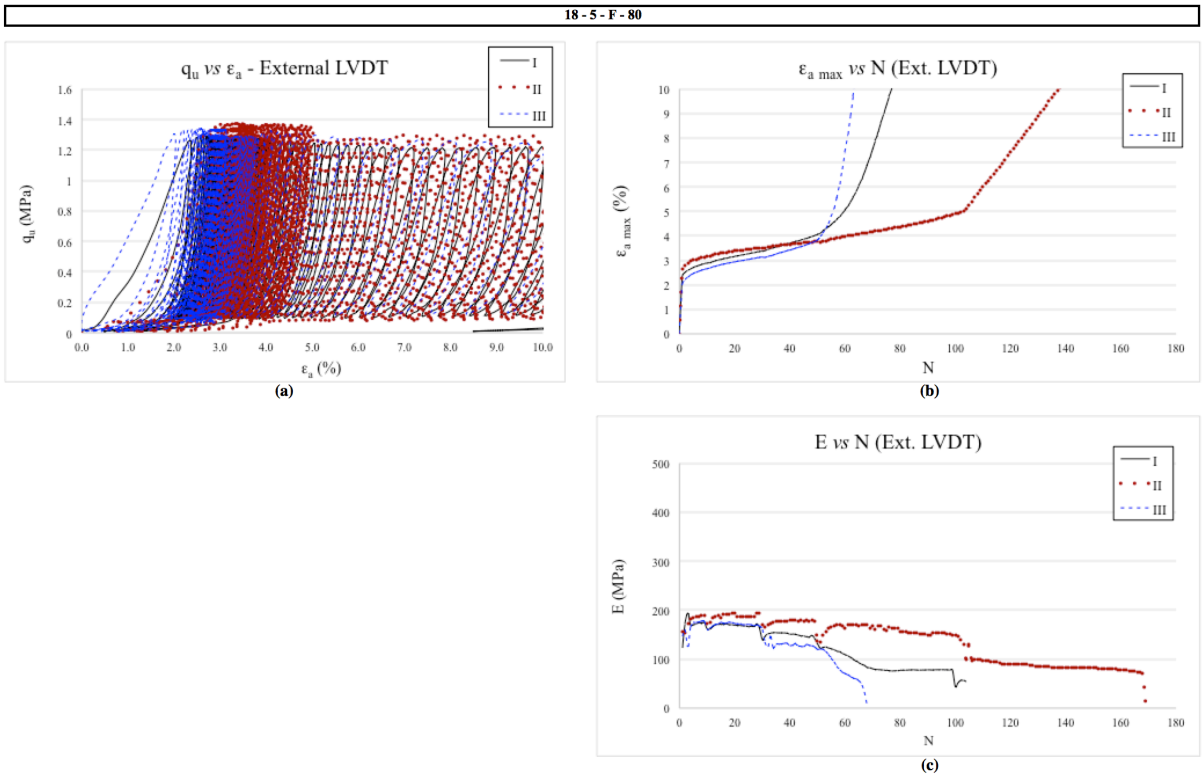

Figure 5.54: External data from specimen 19-5-F-80-I, II and III (a) q_u *versus* ε_a (b) $\varepsilon_{a\ max}$ *versus* N (c) E *versus* N

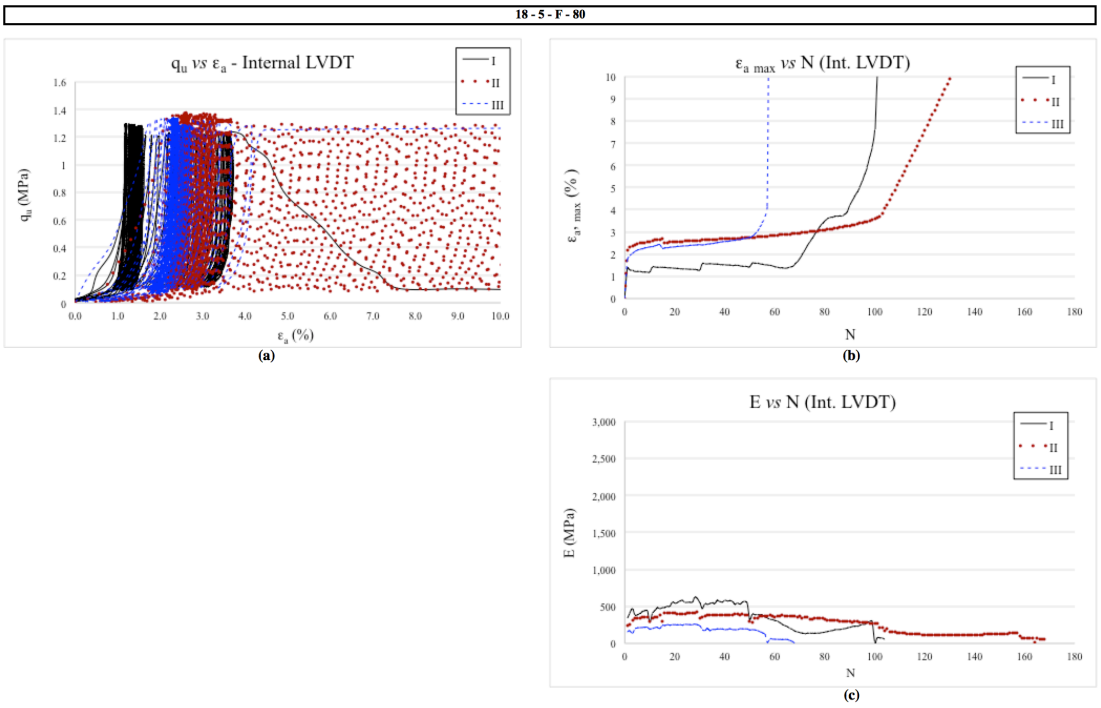

Figure 5.55: Internal data from specimen 19-5-F-80- I, II and III (a) q_u *versus* ε_a (b) $\varepsilon_{a\ max}$ *versus* N (c) E *versus* N

As for Young's modulus (figure 5.55 (c)), the first specimen had a more rigid response to cycling, presenting higher values of E throughout testing, being consistent to the trend observed for $\varepsilon_{a\ max}$. The opposite was observed for the third specimen. Its response was very similar to the values for the external LVDT despite its G_0 and $\eta/C_{iv}^{0.28}$ values being higher than the other specimens, leading to a lower N. The behaviour shown by specimen 18-5-F-80-III might also be due to variability in the cementation process of the specimen, as observed for the first specimen.

5.2.2.2 Alternative mixture

Figures 5.56 and 5.57, present the data results for the external and internal data of the first specimen, respectively. Followed by figures 5.58 and 5.59 that show respectively the values for the external and internal data for second specimen. Finally, figures 5.60 and 5.61 illustrate the results attained for the external and internal LVDTs of the third specimen, respectively.

The summary of the tests is shown in Table 5.9. It presents of cycles until rupture (N), initial shear modulus (G_0), and the estimated value of the initial Young's modulus at small strains (E from G_0), again, the E values are just an estimative. From the presented data, it is possible to infer that the dispersion of $\eta/C_{iv}^{0.28}$ for the replicas is less than 2%. The dispersion of data for the G_0 is less than 3%. Given this data, the repetitions for this combination were considered similar.

Table 5.9: Summary of Cyclic UC tests for 80% of estimated maximum loading for 19 kN/m^3 – 3% mixtures with fibres

Mixture	Ideal Load %	Repetition	$\eta/C_{IV}^{0.28}$	Applied Load (N)	Actual %	Number of Cycles	Numeber of Cycles Rupture	Initial Bender (μs)	G_0 (MPa)	E from G_0 (MPa)
19 kN/m^3 3% cement 0.5% fibre	80	I	24.14	2422.87	75.02	45	4	161.00	751.54	1893.88
	80	II	24.58	2461.85	79.50	37	9	148.50	776.86	1957.70
	80	III	24.54	2608.72	84.32	61	10	147.80	786.81	1982.76

The first specimen withstood 4 cycles of the total of 45 cycles tested. From the external data (figure 5.56) it was observed a strain during the first cycle of around 1.373%, after which there was an increase in strain until rupture around 2.811% (figure 5.56 (b)). The Young's modulus (figure 5.56 (c)) presented a 34.91% increase between the first and fourth cycles – ratio of E gain of 34.91% per cycle, reaching failure at the 4th cycle.

The internal data is presented in figure 5.57. Figure 5.57 (b) shows that there was an initial strain of 0.989%, thus the failure threshold for this specimen was of 2.945%. This initial strain was followed by a 206% increase in strain values over the next three cycles – rate of axial strain gain of 69% – reaching a value of $\varepsilon_{a\ max}$ of 3.035%. As for the Young's modus (figure 5.57 (c)), the initial E value was of 135.18 MPa. The specimen presented a 74.41% increase in E over the next three cycles, reaching 235.77 MPa. The behaviour presented by this specimen indicates a consistent degradation of the cementitious bonds with cycling leading to a constant increase in the accumulated plastic deformation. A gradual failure of cement bonds results in a decrease in porosity as well as slow transference of the burden of the absorption of load from the cementation structures to the fibres, resulting in higher deformation that accumulated lead to failure due to large strains even though the values of E continued to increase.

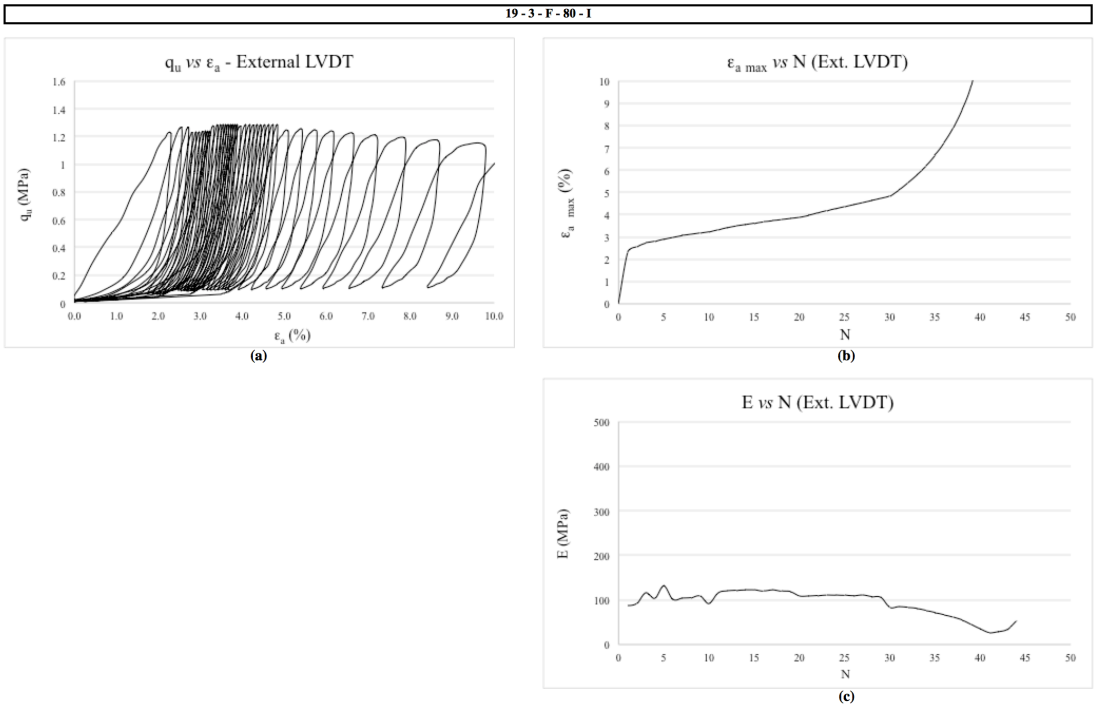

Figure 5.56: External data from specimen 19-3-F-80-I (a) q_u *versus* ε_a (b) $\varepsilon_{a\ max}$ *versus* N (c) E *versus* N

The second repetition ruptured at 9 cycles of the total of 37 cycles tested. From the external data (figure 5.58) it was observed a strain during the first cycle of around 3.859%, after which there was an increase in strain until rupture around 4.853% (figure 5.58 (b)). The Young's modulus (figure 5.58 (c)) presented a 9.34% increase between the first and ninth cycles – ratio of E gain of 1.17% per cycle, reaching failure at the 9th cycle.

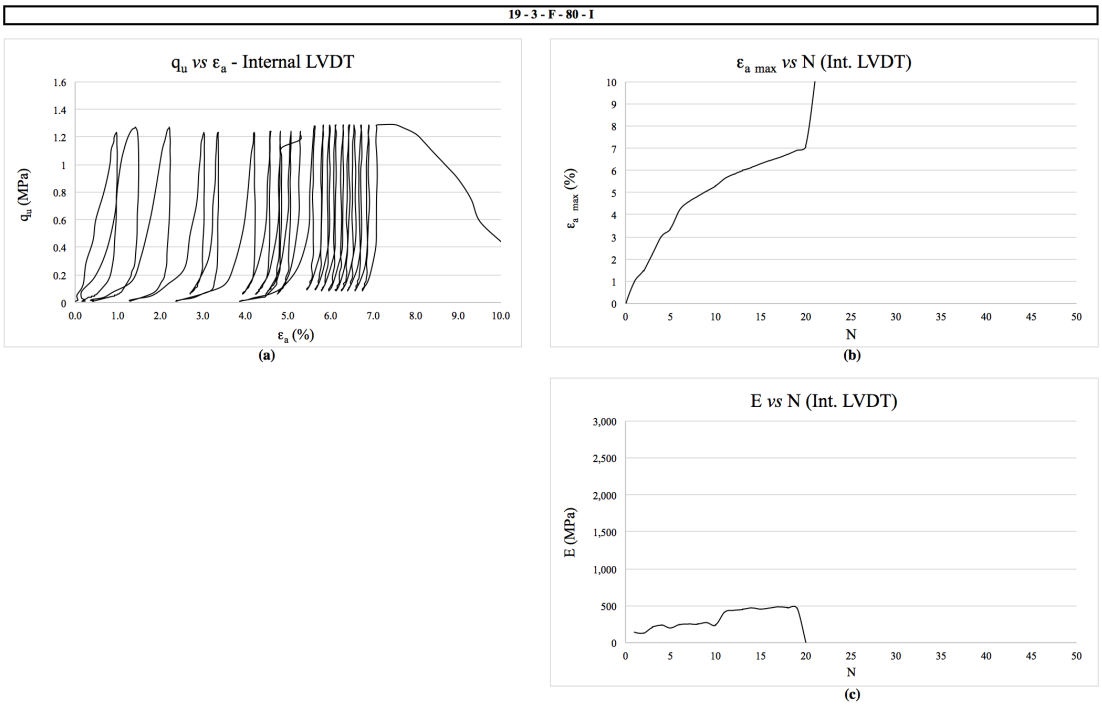

Figure 5.57: Internal data from specimen 19-3-F-80-I (a) q_u *versus* ε_a (b) $\varepsilon_{a\ max}$ *versus* N (c) E *versus* N

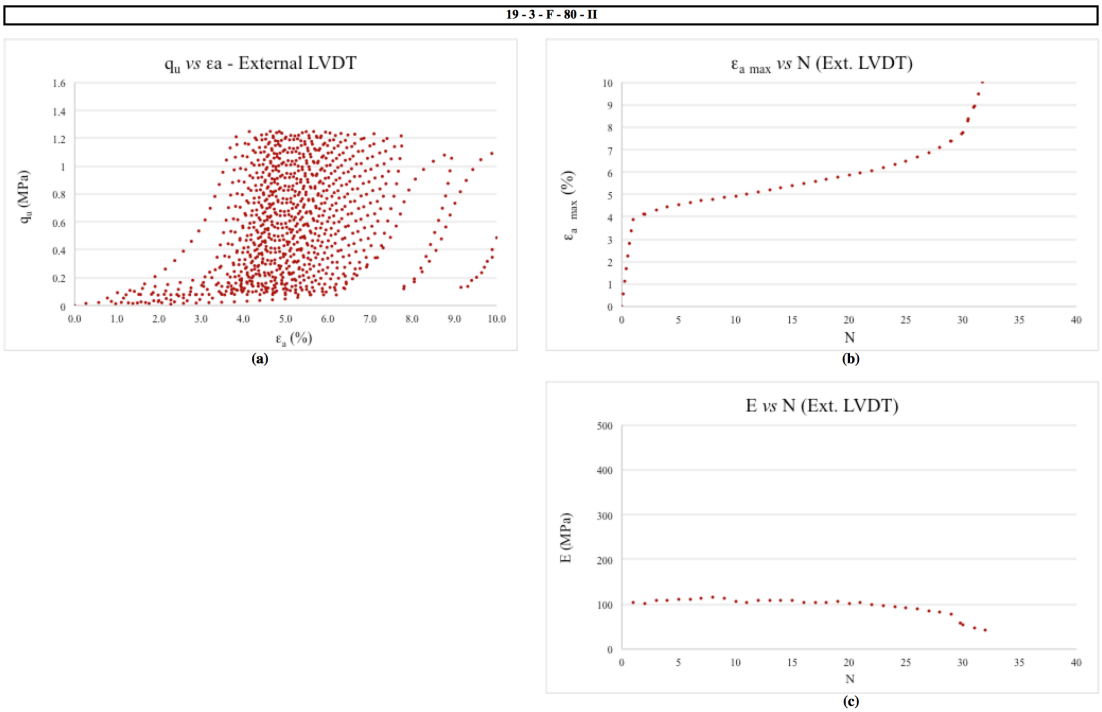

Figure 5.58: External data from specimen 19-3-F-80-II (a) q_u *versus* ε_a (b) $\varepsilon_{a\ max}$ *versus* N (c) E *versus* N

The internal data is presented in figure 5.59. Figure 5.59 (b) shows that there was an initial strain of 2.083%, thus the failure threshold for this specimen was of 3.041%. This initial strain was followed by a 46.09% increase in strain values over the next eight cycles – rate of axial strain gain of 5.76% – reaching a value of $\varepsilon_{a\ max}$ of 3.043%. As for the Young's modus (figure 5.59 (c)), the initial E value was of 127 MPa. The specimen presented a 42.83% increase in E over the next eight cycles, reaching 181.39 MPa. The behaviour presented by this specimen indicates a consistent degradation of the cementitious bonds with cycling leading to a constant increase in the accumulated plastic deformation. A gradual failure of cement bonds results in a decrease in porosity as well as slow transference of the burden of the absorption of load from the cementation structures to the fibres, resulting in higher deformation that accumulated lead to failure due to large strains even though the values of E continued to increase.

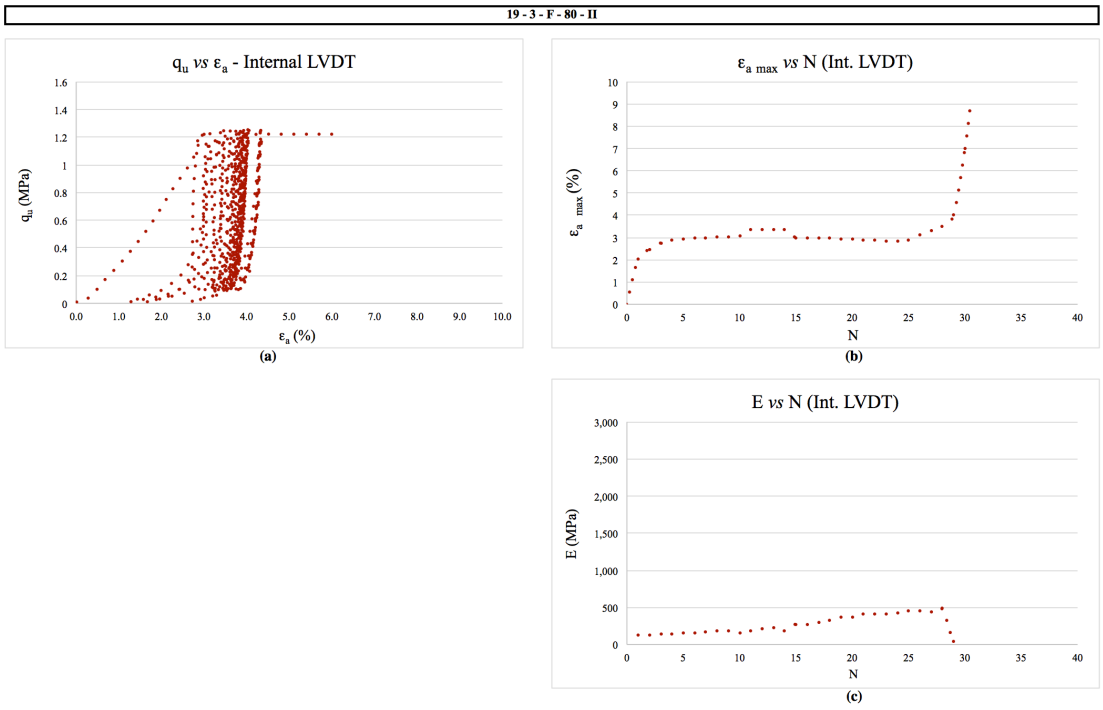

Figure 5.59: Internal data from specimen 19-3-F-80-II (a) q_u *versus* ε_a (b) $\varepsilon_{a\ max}$ *versus* N (c) E *versus* N

The last repetition of this combination ruptured at 10 cycles of the total of 61 cycles tested. From the external data (figure 5.60) it was observed a strain during the first cycle of around 3.073%, after which there was an increase in strain until rupture around 3.920% (figure 5.60 (b)). The Young's modulus (figure 5.60 (c)) presented a 6.48% increase between the first and tenth cycles – ratio of E gain of 0.72% per cycle, reaching failure at the 10th cycle.

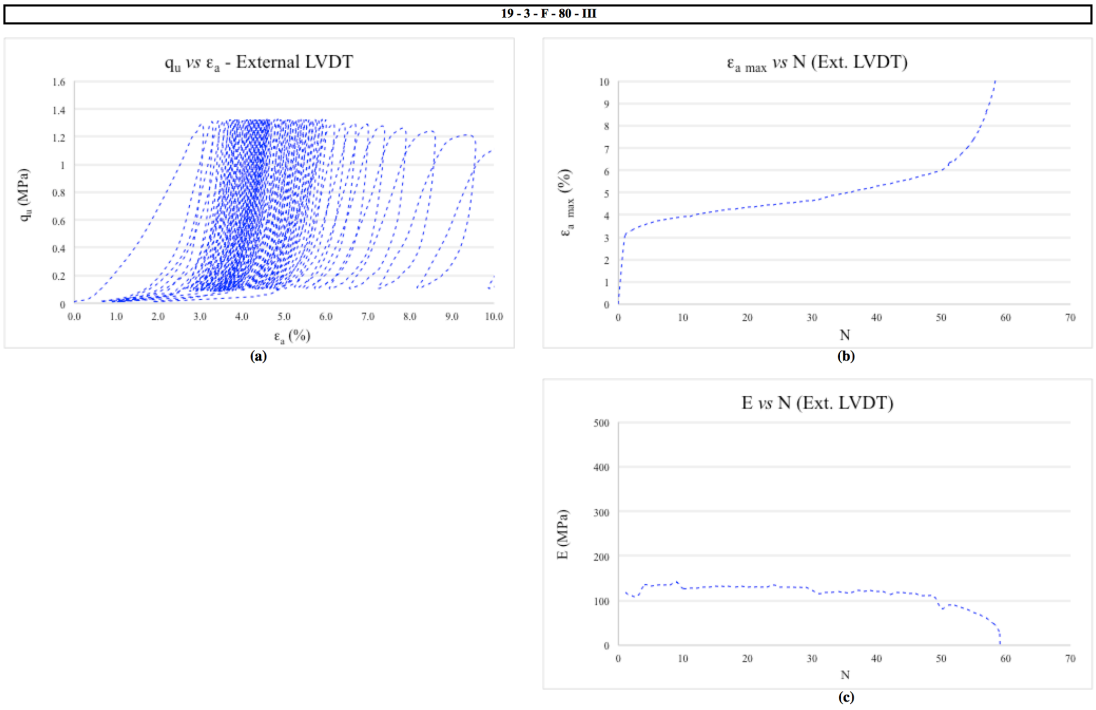

Figure 5.60: External data from specimen 19-3-F-80-III (a) q_u *versus* ε_a (b) $\varepsilon_{a\ max}$ *versus* N (c) E *versus* N

The internal data is presented in figure 5.61. Figure 5.61 (b) shows that there was an initial strain of 3.498%, because the initial strain was very high, it was decided assume that the deformation due to equipment accommodation was higher (two-thirds of the initial value). In being so, the threshold stipulated for this specimen was 4.332%. This initial strain was followed by a 27.27% increase in strain values over the next nine cycles – rate of axial strain gain of 2.69% – reaching a value of $\varepsilon_{a\ max}$ of 4.347% at the10th cycle. As for the Young's modus (figure 5.61 (c)), the initial E value was of 141.66 MPa. The specimen presented a 30.9% increase in E over the next nine cycles, reaching 185.43 MPa. The behaviour presented by this specimen indicates a consistent degradation of the cementitious bonds with cycling leading to a constant increase in the accumulated plastic deformation. A gradual failure of cement bonds results in a decrease in porosity as well as slow transference of the burden of the absorption of load from the cementation structures to the fibres, resulting in higher deformation that accumulated lead to failure due to large strains even though the values of E continued to increase.

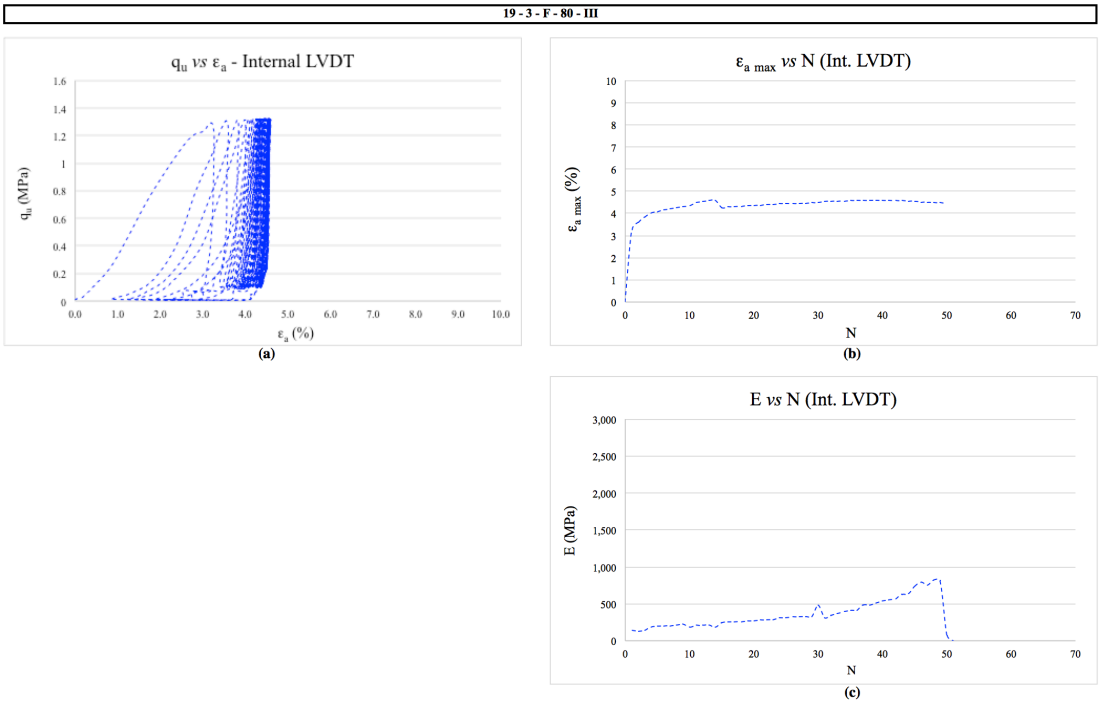

Figure 5.61: Internal data from specimen 19-3-F-80-III (a) q_u *versus* ε_a (b) $\varepsilon_{a\ max}$ *versus* N (c) E *versus* N

Figure 5.62 presents the superimposed graphs of the external data for the three repetitions. From figure 5.62 (b), it was possible to observe a similar trend of increase in axial strain after the initial deformation for all repetitions. The same conclusion could be drawn about the Young's modulus (figure 5.62 (c)).

Figure 5.63 presents the superimposed graphs of the internal data for the three repetitions. From figure 5.63 (b), it was possible to observe a similar trend for the development of axial strain after the initial deformation for the second and third repetition. The first specimen failed earlier than the other two. This might have occurred because the G_0 value for this specimen is lower than the others. However, it is possible that this difference was due to variability in the cementation process of the specimen. As for Young's modulus (figure 5.63 (c)), all specimens presented similar trends and the values were similar to the attained for the external data.

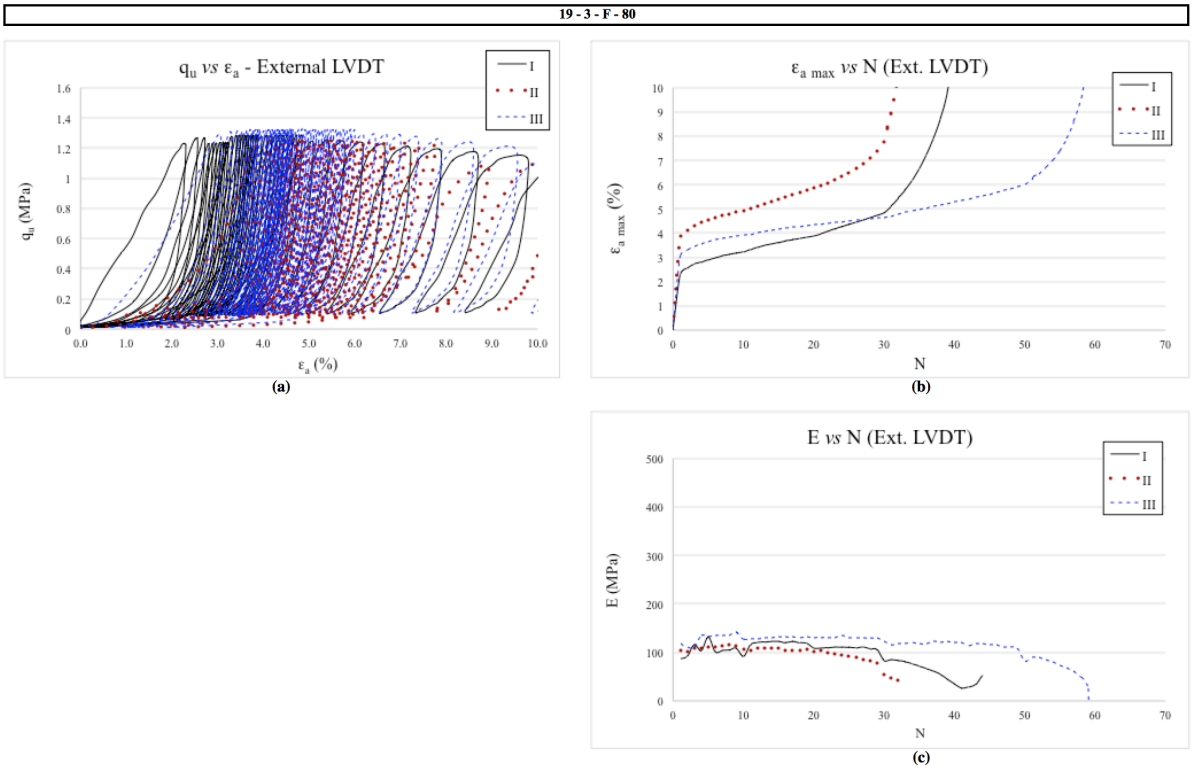

Figure 5.62: External data from specimen 19-3-F-80-I, II and III (a) q_u *versus* ε_a (b) $\varepsilon_{a\ max}$ *versus* N (c) E *versus* N

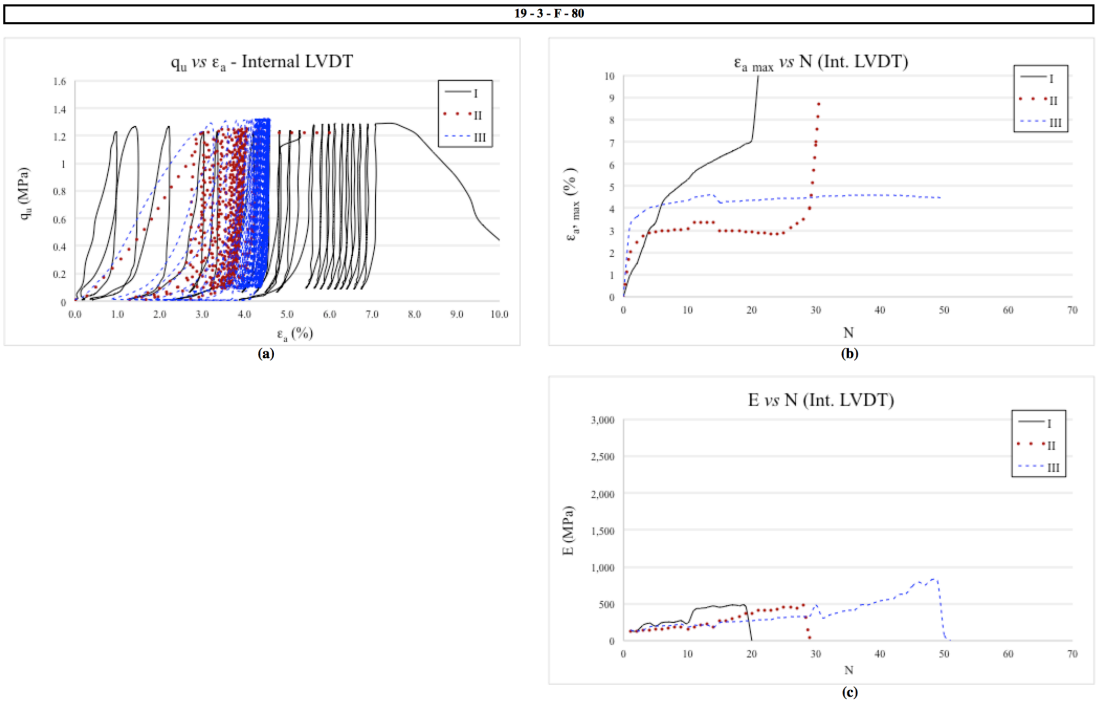

Figure 5.63: Internal data from specimen 19-3-F-80- I, II and III (a) q_u *versus* ε_a (b) $\varepsilon_{a\ max}$ *versus* N (c) E *versus* N

5.2.3 Applied load percentage: 70%

Figures 5.64 and 5.65, present the data results for the external and internal data of the first specimen, respectively. Followed by figures 5.66 and 5.67 that show respectively the values for the external and internal data for second specimen. Finally, figures 5.68 and 5.69 illustrate the results attained for the external and internal LVDTs of the third specimen, respectively.

The summary of the tests is shown in Table 5.10. It presents of cycles until rupture (N), initial shear modulus (G_0), and the estimated value of the initial Young's modulus at small strains (E from G_0), again, the E values are just an estimative. From the presented data, it is possible to infer that the dispersion of $\eta/C_{iv}^{0.28}$ for the replicas is less than 2%. The dispersion of data for the G_0 is less than 9%. Given this data, the repetitions for this combination were considered similar.

Table 5.10: Summary of Cyclic UC tests for 70% of estimated maximum loading for benchmark mixtures with fibres

Mixture	Ideal Load %	Repetition	$\eta/C_{IV}^{0.28}$	Applied Load (N)	Actual %	Number of Cycles	Numeber of Cycles Rupture	Initial Bender (μs)	G_0 (MPa)	E from G_0 (MPa)
18 kN/m³ 5% cement 0.5% fibre	70	I	23.96	2230.26	68.06	346	157	164.00	751.66	1894.17
	70	II	24.39	2151.93	68.52	253	100	162.00	626.09	1577.75
	70	III	24.30	2160.41	68.21	270	203	154.30	699.16	1761.87

The first repetition withstood 157 cycles of the total of 346 cycles tested. From the external data (figure 5.64) it was observed a strain during the first cycle of around 2.457%, after which there was an increase in strain until rupture around 3.940% (figure 5.64 (b)). The Young's modulus (figure 5.64 (c)) presented a 34.93% increase between the first and thirtieth cycles – ratio of E gain of 1.204% per cycle. Then, over the next 127 cycles there was a 21.1% decrease in the Young's modulus of the specimen at a rate of 0.167% per cycle, reaching failure at the 157th cycle.

The internal data is presented in figure 5.65. Figure 5.65 (b) shows that there was an initial strain of 0.542%, thus the failure threshold for this specimen was of 2.271%. This initial strain was followed by a 152% increase in strain values over the next twenty-nine cycles – rate of axial strain gain of 5.25%. Over the last 127 cycles the values of $\varepsilon_{a\ max}$ increased at a rate of 0.524% increase per cycle reaching the 157^{h} cycle with a $\varepsilon_{a\ max}$ of 2.277%. As for the

Young's modus (figure 5.65 (c)), the initial E value was of 289.76 MPa. The specimen presented a 34.3% increase in E over the next 29 cycles, reaching 389.16 MPa. After, the values of E continued to increase over the next 127 cycles, reaching 468.71 MPa at the 157th cycle – an increase rate of 0.161% per cycle. The behaviour presented by this specimen indicates a consistent degradation of the cementitious bonds with cycling leading to a constant increase in the accumulated plastic deformation. A gradual failure of cement bonds results in a decrease in porosity as well as slow transference of the burden of the absorption of load from the cementation structures to the fibres, resulting in higher deformation that accumulated lead to failure due to large strains even though the values of E continued to increase.

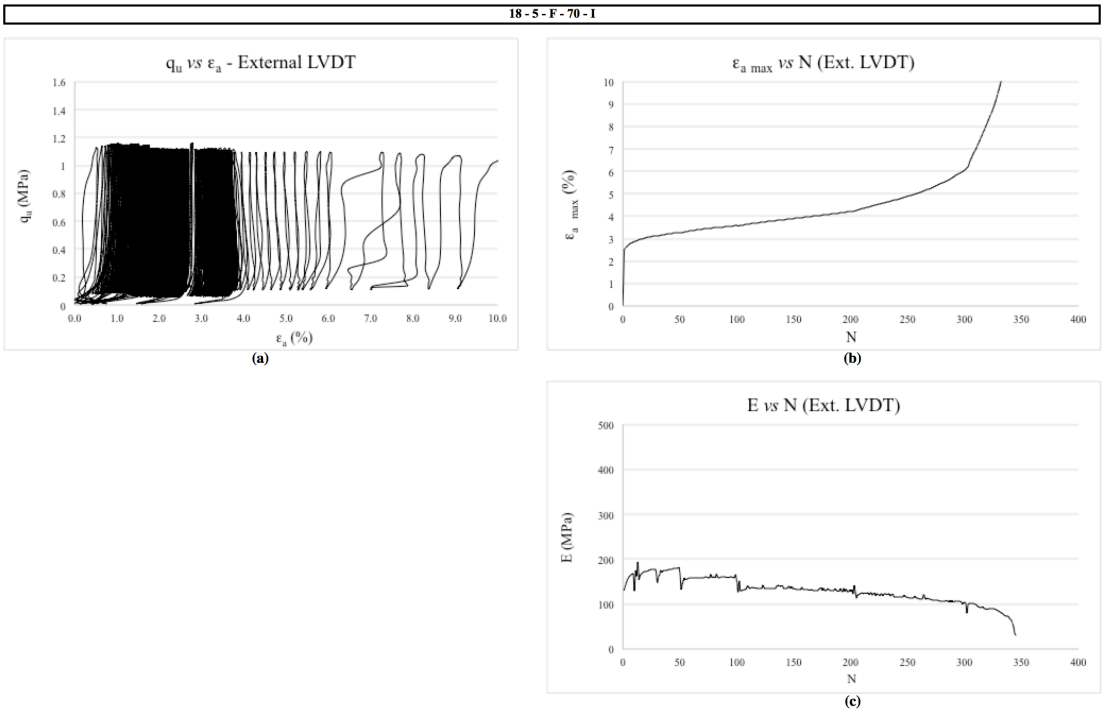

Figure 5.64: External data from specimen 18-5-F-70-I (a) q_u *versus* ε_a (b) $\varepsilon_{a\ max}$ *versus* N (c) E *versus* N

The second specimen of this combination failed 100 cycles of the total of 253 cycles tested. From the external data (figure 5.66) it was observed a strain during the first cycle of around 1.162%, after which there was an increase in strain until rupture around 2.965% (figure 5.66 (b)). The Young's modulus (figure 5.66 (c)) presented a 111.7% increase between the first and thirtieth cycles – ratio of E gain of 3.852% per cycle. Then, over the next 69 cycles there was a 20.53% decrease in the Young's modulus of the specimen at a rate of 0.293% per cycle, reaching failure at the 100th cycle.

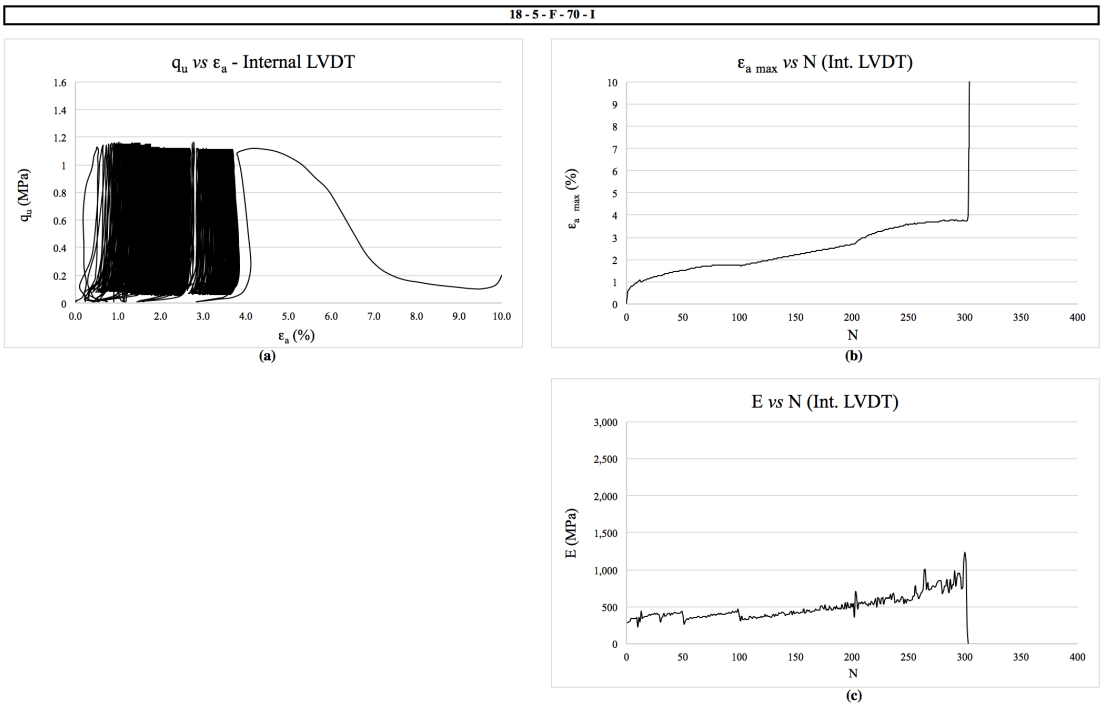

Figure 5.65: Internal data from specimen 18-5-F-70-I (a) q_u *versus* ε_a (b) $\varepsilon_{a\ max}$ *versus* N (c) E *versus* N

The internal data is presented in figure 5.67. Figure 5.67 (b) shows that there was an initial strain of 1.845%, thus the failure threshold for this specimen was of 3.476%. This initial strain was followed by a 35.23% increase in strain values over the next twenty-nine cycles – rate of axial strain gain of 1.215%. Over the last 69 cycles the values of $\varepsilon_{a\ max}$ increased at a rate of 0.577% increase per cycle reaching the 100th cycle with a $\varepsilon_{a\ max}$ of 3.502%. As for the Young's modus (figure 5.67 (c)), the initial E value was of 157.72 MPa. The specimen presented a 18.53% increase in E over the next 29 cycles, reaching 186.94 MPa. After, the values of E continued to increase over the next 69 cycles, reaching 222.7 MPa at the 100th cycle – an increase rate of 0.273% per cycle. The behaviour presented by this specimen indicates a consistent degradation of the cementitious bonds with cycling leading to a constant increase in the accumulated plastic deformation. A gradual failure of cement bonds results in a decrease in porosity as well as slow transference of the burden of the absorption of load from the cementation structures to the fibres, resulting in higher deformation that accumulated lead to failure due to large strains even though the values of E continued to increase.

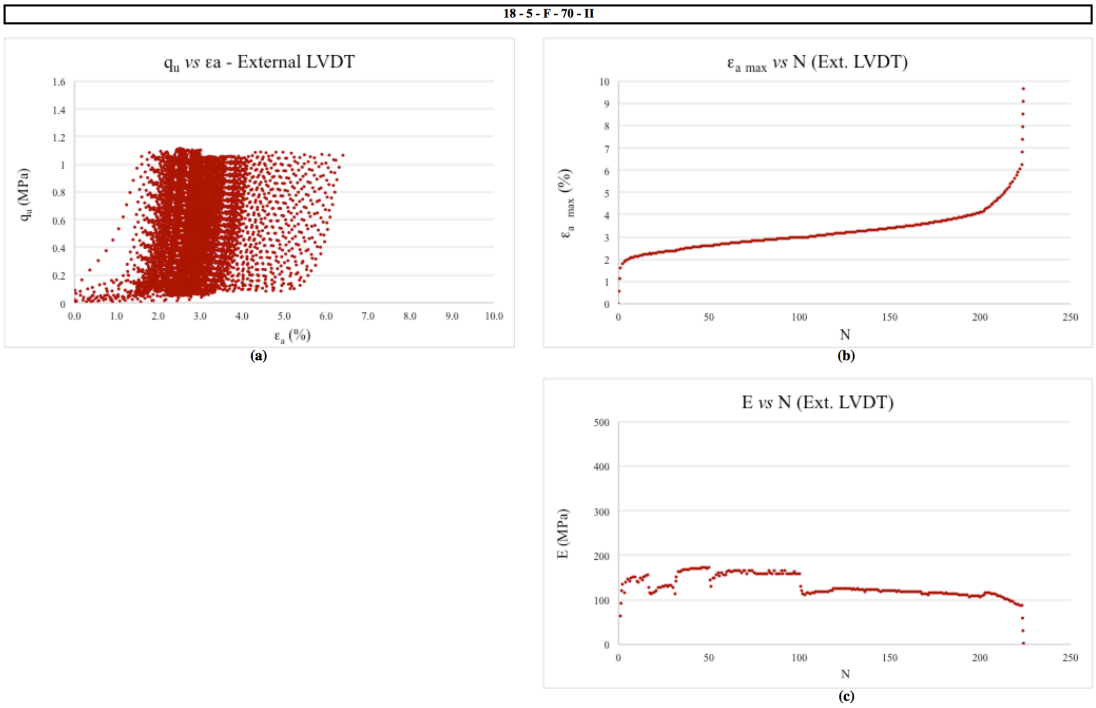

Figure 5.66: External data from specimen 18-5-F-70-II (a) q_u *versus* ε_a (b) $\varepsilon_{a\ max}$ *versus* N (c) E *versus* N

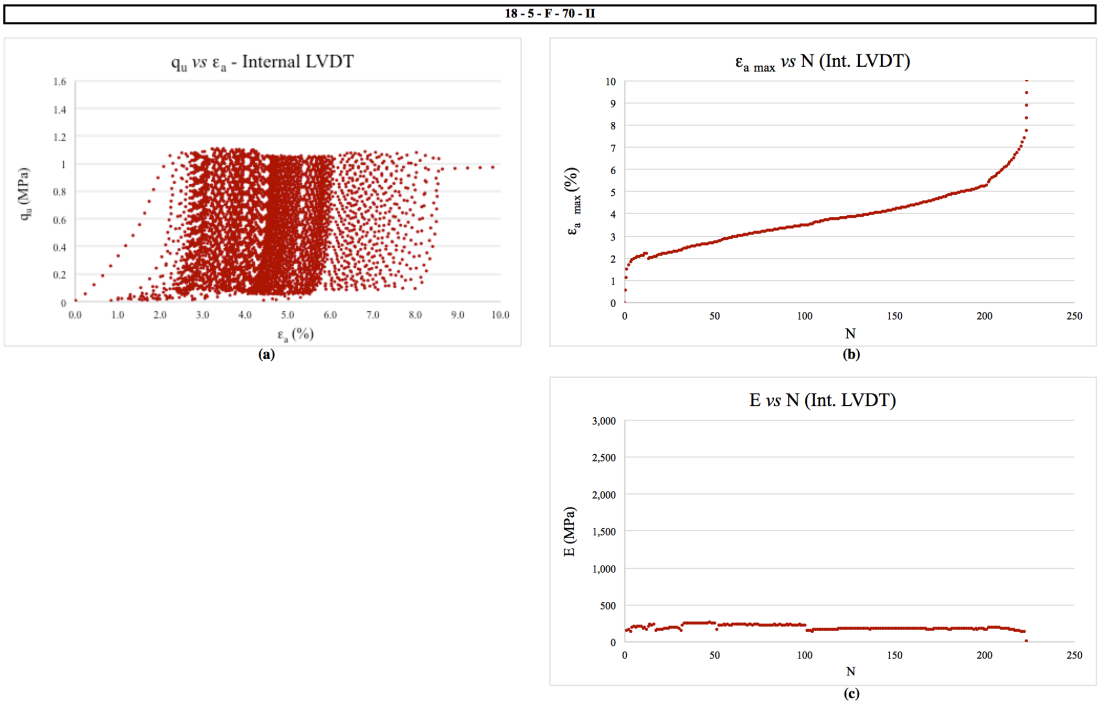

Figure 5.67: Internal data from specimen 18-5-F-70-II (a) q_u *versus* ε_a (b) $\varepsilon_{a\ max}$ *versus* N (c) E *versus* N

The last repetition for this combination failed 203 cycles of the total of 270 cycles tested. From the external data (figure 5.68) it was observed a strain during the first cycle of around 2.077%, after which there was an increase in strain until rupture around 3.747% (figure 5.68 (b)). The Young's modulus (figure 5.68 (c)) presented a 23.21% increase between the first and thirtieth cycles – ratio of E gain of 0.800% per cycle. Then, over the next 173 cycles there was an 8.6% decrease in the Young's modulus of the specimen at a rate of 0.05% per cycle, reaching failure at the 203rd cycle.

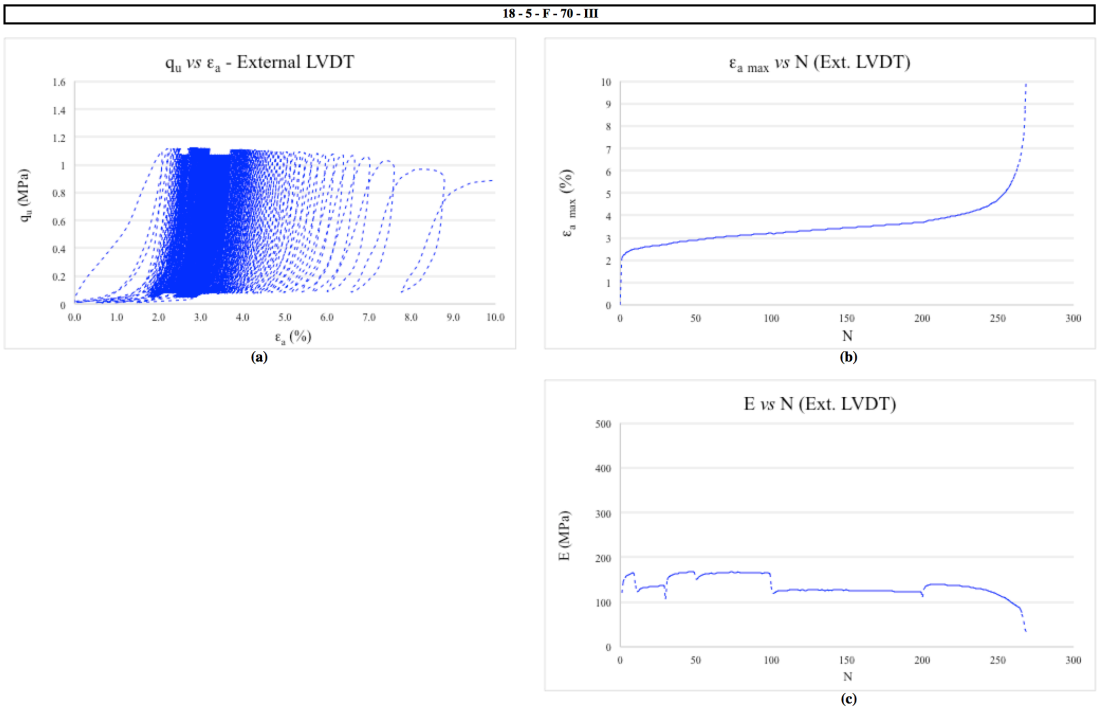

Figure 5.68: External data from specimen 18-5-F-70-III (a) q_u *versus* ε_a (b) $\varepsilon_{a\ max}$ *versus* N (c) E *versus* N

The internal data is presented in figure 5.69. Figure 5.69 (b) shows that there was an initial strain of 2.633%, therefore the failure threshold for this specimen was of 3.31%. This initial strain was followed by a 17.81% increase in strain values over the next twenty-nine cycles – rate of axial strain gain of 0.614%. Over the last 173 cycles the values of $\varepsilon_{a\ max}$ increased at a rate of 0.041% increase per cycle reaching the 203rd cycle with a $\varepsilon_{a\ max}$ of 3.323%. As for the Young's modus (figure 5.69 (c)), the initial E value was of 139.17 MPa. The specimen presented an 80.58% increase in E over the next 29 cycles, reaching 251.32 MPa. After, the values of E continued to increase over the next 173 cycles, reaching 376.90 MPa at the 203rd cycle – an increase rate of 0.289% per cycle. The behaviour presented by this specimen indicates a consistent degradation of the cementitious bonds with cycling leading to a constant

increase in the accumulated plastic deformation. A gradual failure of cement bonds results in a decrease in porosity as well as slow transference of the burden of the absorption of load from the cementation structures to the fibres, resulting in higher deformation that accumulated lead to failure due to large strains even though the values of E continued to increase.

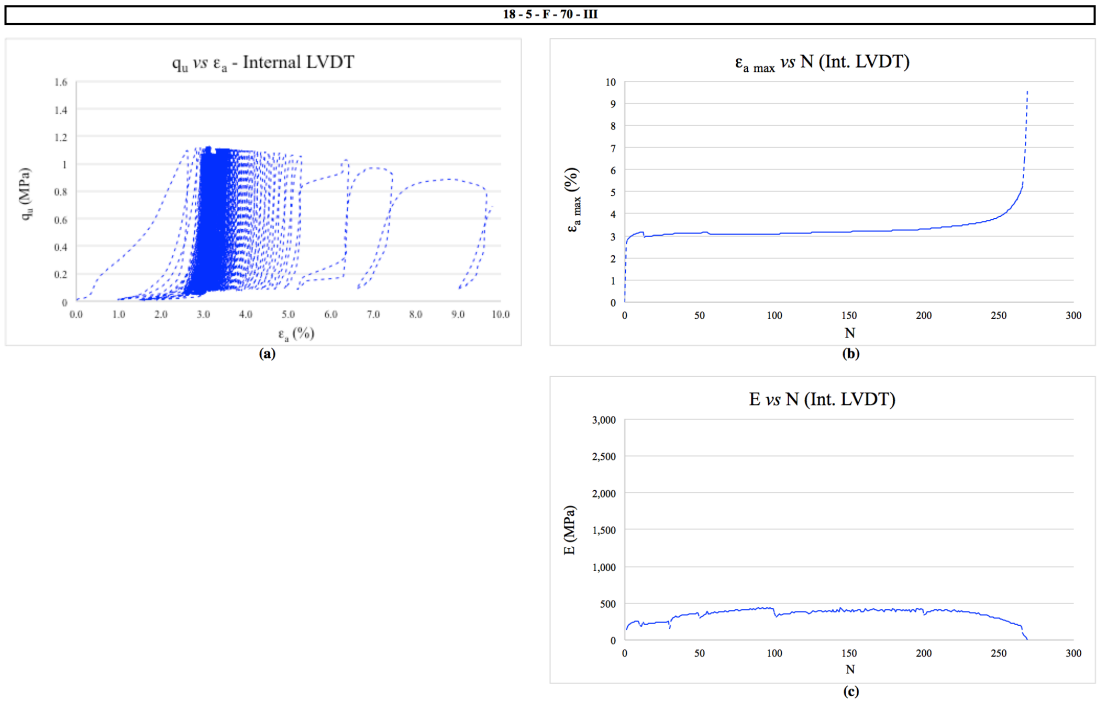

Figure 5.69: Internal data from specimen 18-5-F-70-III (a) q_u *versus* ε_a (b) $\varepsilon_{a\ max}$ *versus* N (c) E *versus* N

Figure 5.70 presents the superimposed graphs of the external data for the three repetitions. From figure 5.70 (b), it was possible to observe a similar trend of increase in axial strain after the initial deformation for all repetitions. The same conclusion could be drawn about the Young's modulus (figure 5.70 (c)).

Figure 5.71 presents the superimposed graphs of the internal data for the three repetitions. From figure 5.71 (b), it was possible to observe a similar development of axial strain after the initial deformation trend for specimens I and II. However, the rate in strain gain for the second repetition was higher than the first specimen. This indicates that the specimen accumulated higher plastic deformations being less stiff than the others. The aforementioned assumption is corroborated by the lower value in G_0 compared to the other two repetitions. As for the third repetition presented a much stiffer response to loading having a low increase rate of maximum axial strain, leading to lower plastic deformations over time, thus withstanding

high N values. When analysing the initial specimen conditions, no explication for this difference in behaviour was found. It is possible that this difference was due to variability in the cementation process of the specimen. As for Young's modulus (figure 5.71 (c)), all specimens presented similar trends and the values were similar to the attained for the external data until rupture was reached.

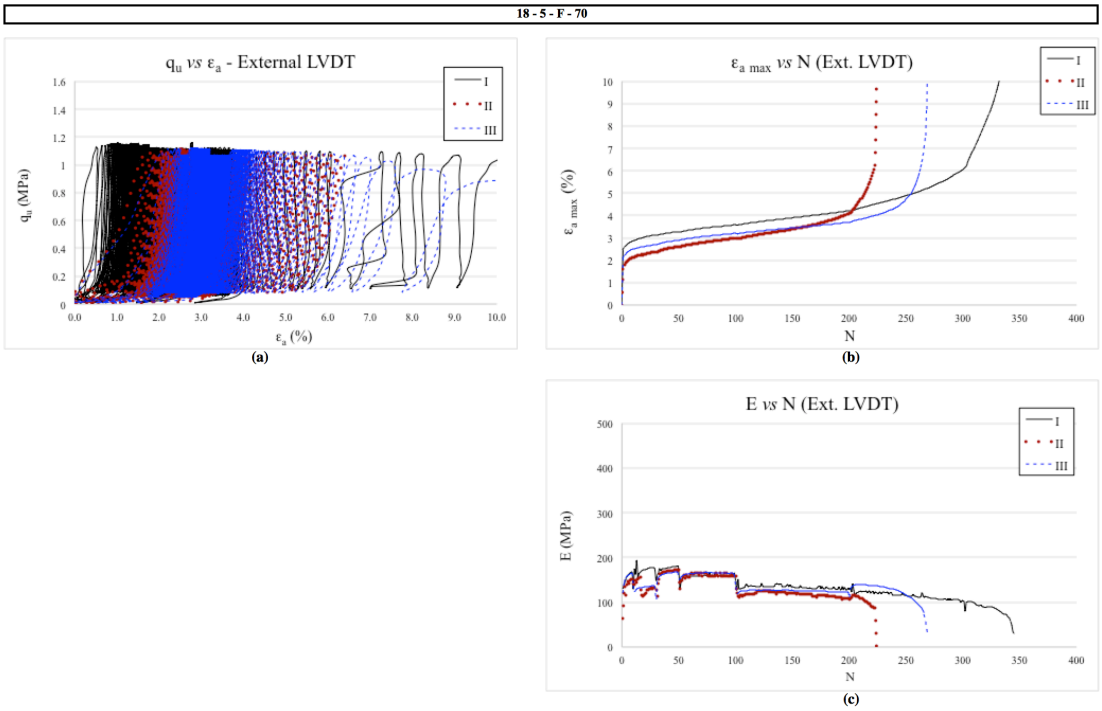

Figure 5.70: External data from specimen 18-5-F-70-I, II and III (a) q_u *versus* ε_a (b) $\varepsilon_{a\ max}$ *versus* N (c) E *versus* N

5.2.4 Shear Modulus

During testing bender element tests were carried out at pre-established intervals – 0, 1, 2, 10, 30, 50, 100, 200, 300, 400, 500, 1000, 1500, and 2000 cycles. For every reading the cyclic test was stopped and 10% of the tested load was applied in order for the measurements to be able to be made. The values attained are presented in appendices B. As stated in item 3.2.10.2, at the beginning of every test a frequency screening was made in order to assess the best one to conduct the tests.

From the data presented thus far it is observed that the fibre-reinforce combinations failed earlier than the non-reinforced ones, which could be attributed to the fact that the applied load was on average 48% higher. The cementation bonds in the fibre-reinforced specimen might be affected by the presence of the fibres in the matrix, then, when a high percentage of the maximum q_u value

is applied, the cementation bond degrade more rapidly, leading to high strains at a lower number of cycles, as it was observed for monotonic tests by Consoli *et* al. (2009). Therefore, the combinations with added fibres were tested for the same load values attained form the unreinforced curves. This data is presented in the next topic. This lower number of cycles observed was translated to the shear modulus values as a continued degradation of G_N values with cycling. Even though failure was stipulated at 2% of $\varepsilon_{a\ max}$, the values of G were measured until much higher strains in order to assess the shear modulus behaviour of the specimens.

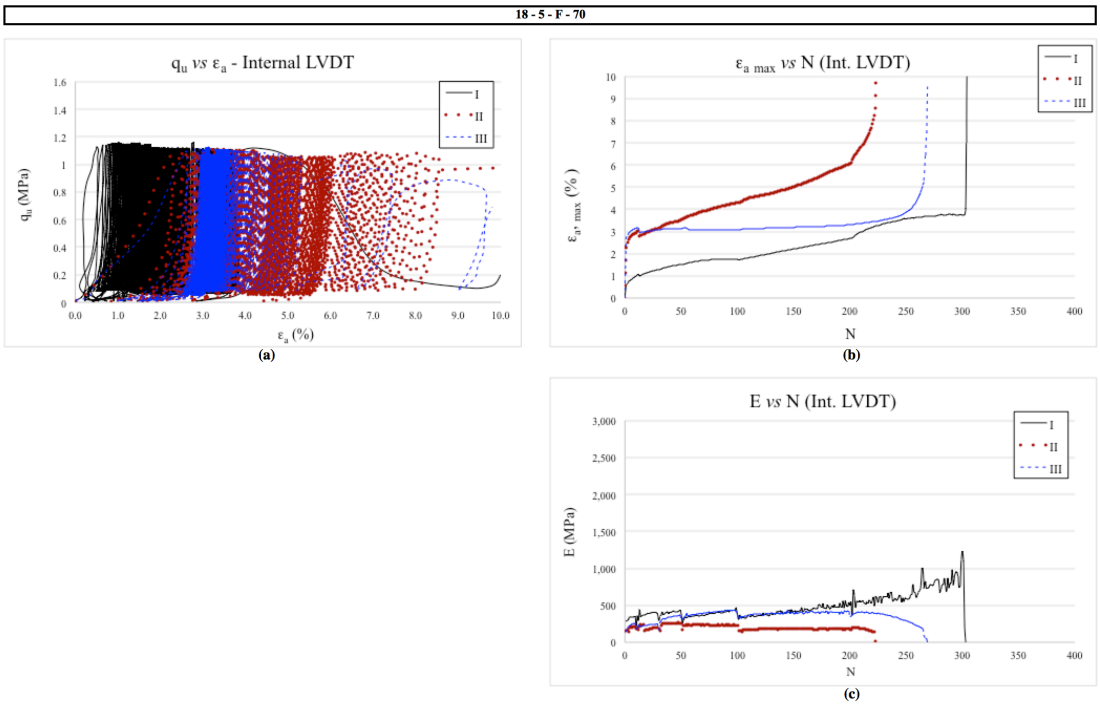

Figure 5.71: Internal data from specimen 18-5-F-70- I, II and III (a) q_u *versus* ε_a (b) $\varepsilon_{a\ max}$ *versus* N (c) E *versus* N

Figure 5.72 presents the values of shear modulus *versus* number of cycles for all the repetitions for the 19-5-F combinations. It is possible to conclude that the values of G obtained for all repetitions are within the same order of magnitude and have similar tendencies. Figure 5.72 (a) presents the values of shear modulus *versus* the number of cycles for the fibre-reinforced benchmark mixtures at 90% of the estimated maximum load. A decreasing in G trend can be observed for all repetitions. The same trend can be observed in figure 5.72 (b) where the fibre-reinforced benchmark mixtures were tested for 80% of the estimated maximum load. Figure 5.72 (c) presents the fibre-reinforced benchmark mixtures tested for 70% of the estimated maximum load. From these graphs it is possible to note a plateau between cycles 10 and 100. Over the next 200 cycles the decrease in e G_N values resumes. It is important to note

the failure threshold adopted resulted in specimens failing before complete degradation on stiffness occurred. This trend was also observed for the E data from the internal measurements.

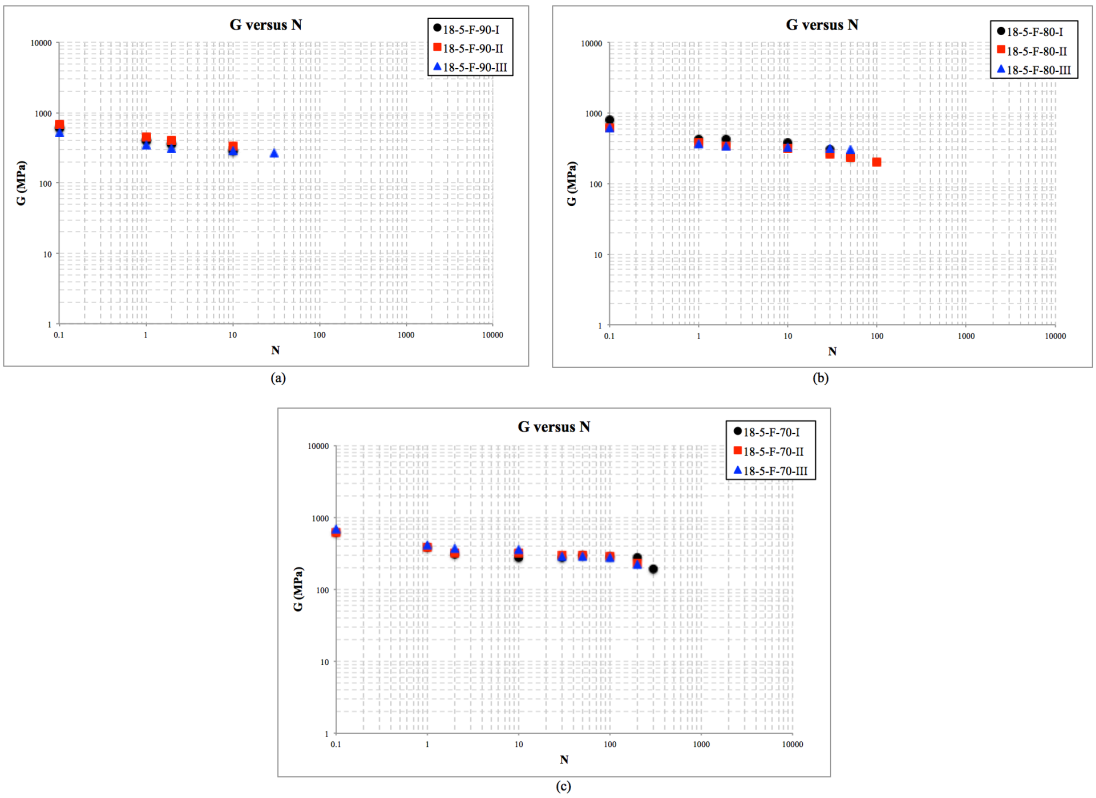

Figure 5.72: Shear modulus versus number of cycles for fibre-reinforced benchmark specimens at (a) 90% loading (b) 80% loading (c) 70% loading

Plotting the average values of the repetitions, figure 5.73 displays the relationships between G and N for the three percentages of applied loads studied and their respective fitted equations. It is possible to infer form the presented data that the G_N values withstood a lower decrease rate as the applied load decreased, as it should be expected, lower applied load resulted in less damage to the structure for a given number of cycles. For the all applied loads there was a consistent degradation of stiffness with cycling.

The G_N values were normalised by the G_0 values of the mixtures, as shown in figure 5.74. From these graphs it is easier to differentiate the aforementioned trends. The G_N values presented a similar decrease rates until the 10^{th} cycle. Then, there was a more pronounced degradation of G_N for the 80% load over the next 90 cycles (when cycling stopped for this load percentage) than the

observed for the 70% applied load. Over the next 200 cycles the 70% specimens reached the same G_N/G_0 ratio as the observed for 80% specimens at 100 cycles.

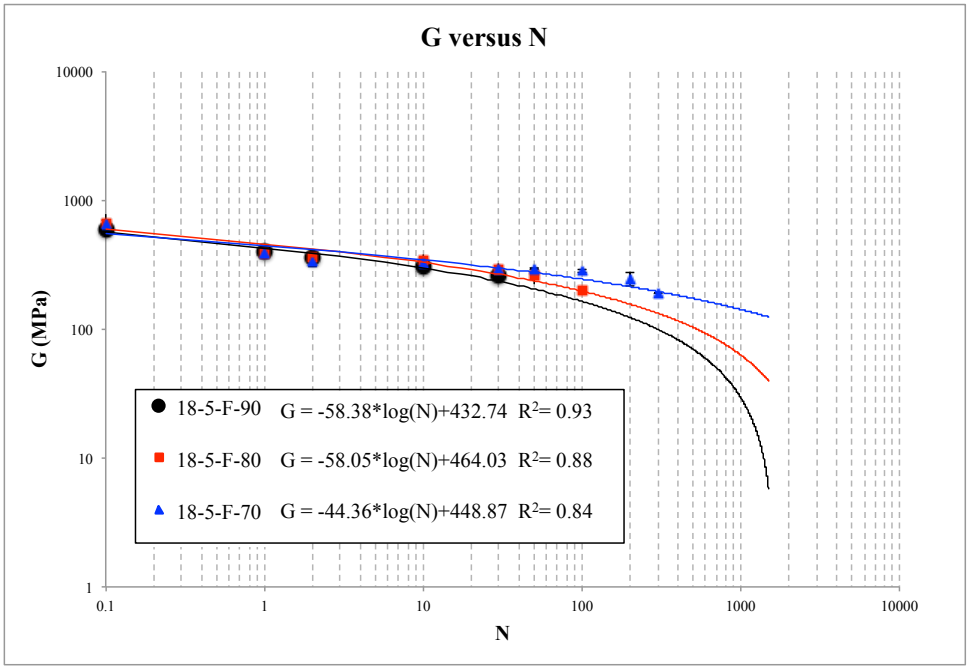

Figure 5.73: Shear modulus versus number of cycles for fibre-reinforced benchmark specimens

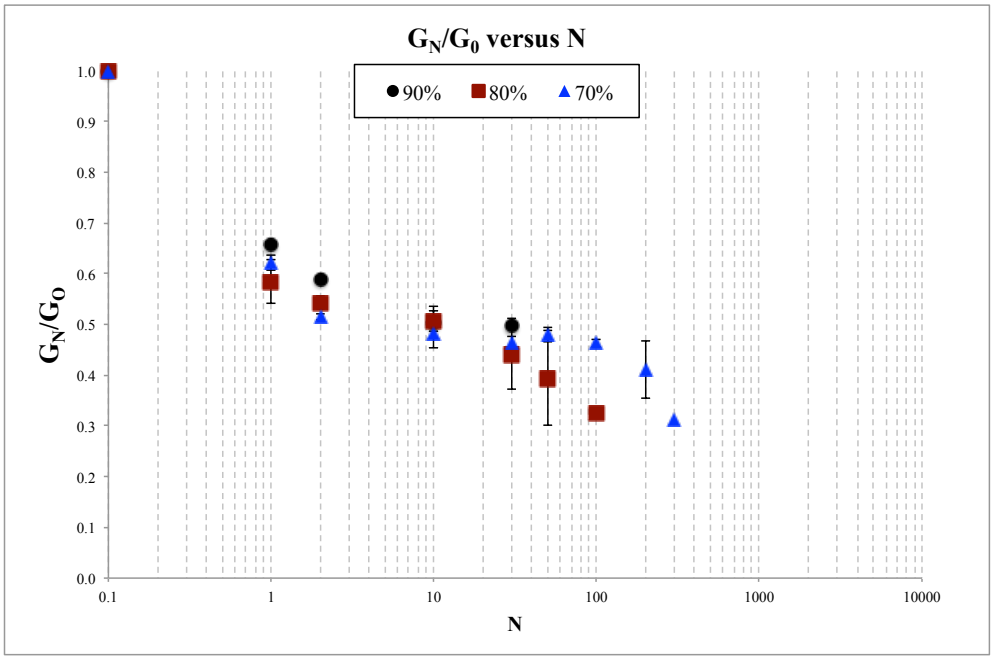

Figure 5.74: G_N/G_0 versus number of cycles for fibre-reinforced benchmark specimens

Figure 5.75 presents the values of shear modulus *versus* number of cycles for all the repetitions for the 19-3-F-80 combinations. It is possible to conclude that the values of G obtained for all repetitions are within the same order of magnitude and have similar tendencies. When observing figure 5.76, that compares it data to the one from the benchmark mixture at the same applied load percentage, it is possible to conclude that there is a much more pronounced degradation of shear stiffness for the specimen with lower cementation, even though the present similar $\eta/C_{iv}^{0.28}$. When comparing the fitted equation of the 19-3-F-80 from figure 5.76 (a) to the equation for 18-5-F-90 specimens (figure 5.73) it was observed a higher degradation rate for the material with lower cementation. Suggesting that the amount of cementation bonds (cement content) might play a larger role in cyclic loading than its porosity for the studied materials, as observed for unreinforced specimens.

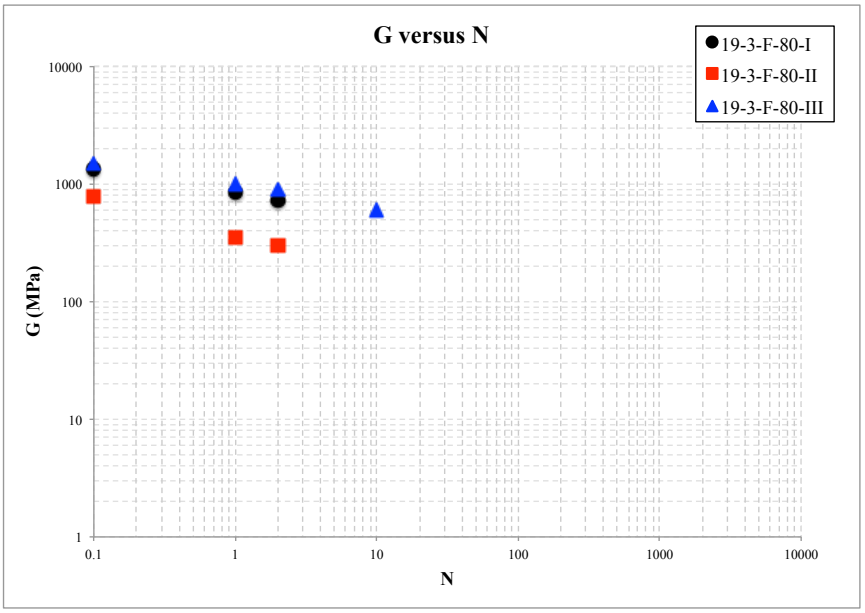

Figure 5.75: Shear modulus versus number of cycles for 19-3-F specimens at 80% loading

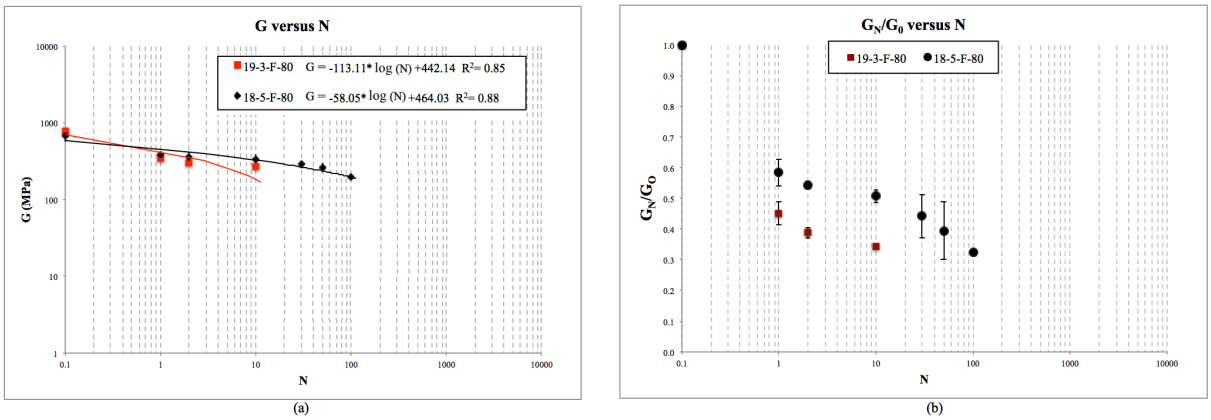

Figure 5.76: (a) Shear modulus versus number of cycles and (a) G_N/G_O versus number of cycles for fibre-reinforced benchmark and 19-3-F specimens at 80% loading

5.2.5 Modified load

As mentioned previously, the response under cyclic loading of the fibre-reinforced specimens for the applied load (from the fitted equation from unconfined compression tests) was not better than the response of the unreinforced specimens. However, the magnitude of the unconfined compression strength values for reinforced specimens were on average 48% higher. Leading to the conclusion that even though under monotonic loading the cemented matrix of the reinforced specimens hold higher loads, when a high percentage of this load is applied, the cementitious bonds degraded faster. Therefore, the same loads applied on the benchmark soil-cement specimens were used on the soil-cement-fibre specimens in order to evaluate if this of rate degradation with applied load would continue to happen.

For this part of the experiment program only two repetitions were made due to restraints on the availability of the studied materials at the University of Bristol. The results between the repetitions at the three different loading conditions were very similar, in being so, it was decided that only presenting the superimposed internal data for each loading percentage would suffice to present the results.

The summary of the tests is shown in Table 5.11. It presents of cycles until rupture (N), initial shear modulus (G_0), and the estimated value of the initial Young's modulus at small strains (E from G_0), again, the E values are just a estimative. From the presented data, it is possible to infer that the dispersion of $\eta/C_{iv}^{0.28}$ for the replicas is less than 1%. The dispersion of data for the G_0 is less than 11%.

No specimen reached the failure threshold and all the moulding indicators – $\eta/C_{iv}^{0.28}$; actual loading percentage in respect to its estimated maximum load; G_0 – suggest that the specimens have similar initial conditions.

Table 5.11: Summary of Cyclic UC tests for modified loading conditions for benchmark mixtures with fibres

Mixture	Ideal Load %	Repetition	$\eta/C_{IV}^{0.28}$	Applied Load (N)	Actual %	Number of Cycles	Numeber of Cycles Rupture	Initial Bender (μs)	G_0 (MPa)	E from G_0 (MPa)
18 kN/m³ - 5% cement 0.5% fibre - Modified Load	90	I	24.03	2149.50	92.66	2000	-	151.90	711.55	1793.10
	90	II	23.68	2221.93	91.53	2000	-	145.80	773.24	1948.56
	80	I	24.30	1876.39	80.76	2000	-	171.00	539.78	1360.25
	80	II	24.00	1876.55	83.17	2000	-	155.90	672.17	1693.87
	70	I	23.72	1740.66	71.96	2000	-	158.90	634.65	1599.32
	70	II	24.02	1675.40	72.15	2000	-	171.50	543.56	1369.78

5.2.5.1 Applied load percentages: 90, 80 and 70%

Figure 5.77, present the results from the internal data for both repetitions under 90% of the modified load. Followed by figure 5.78 that shows the results from the internal data for both repetitions under 80% of the modified load. Finally, figure 5.79 illustrate the results attained for the internal data for both repetitions under 70% of the modified load.

The internal data for both repetitions under 90% applied modified load (figure 5.77) showed similar trends over the 2000 applied cycles. When analysing the first specimen (figure 5.77 (b)), it was observed that for the first repetition there was an initial strain of 1.579%. Thus, the failure threshold for this specimen was of 2.79%. This initial strain was followed by a 45.68% increase in strain values over the next two thousand cycles – rate of axial strain gain of 0.036% – with a $\varepsilon_{a\ max}$ of 2.30%. Therefore, the failure threshold was not met. As for the Young's modus (figure 5.77 (c)), the initial E value was of 292.08 MPa. The specimen presented an 87% increase in E over the next two thousand cycles reaching 546.2 MPa – an increase rate of 0.044% per cycle. The behaviour presented by this specimen indicates a consistent degradation of the cementitious bonds with cycling leading to a constant increase in the accumulated plastic deformation. A gradual failure of cement bonds results in a decrease in porosity as well as slow transference of the burden of the absorption of load from the cementation structures to the fibres. Therefore, values of E continued to increase.

Focusing on the second specimen (figure 5.77 (b)), it was observed that there was an initial strain of 1.726%. Leading to a failure threshold of 2.863%. This initial strain was followed by a 20.80% increase in strain values over the next two thousand cycles ending the test at a $\varepsilon_{a\ max}$ of 2.086% – rate of axial strain gain of 0.018%. Therefore, the failure threshold was not met. As for the Young's modus (figure 5.77 (c)), the initial E value was of 150.23 MPa. The specimen presented a 59.5% increase in E over the next two thousand cycles reaching 239.7 MPa – an increase rate of 0.03% per cycle. The behaviour presented by this specimen indicates a consistent degradation of the cementitious bonds with cycling leading to a constant increase in the accumulated plastic deformation. A gradual failure of cement bonds results in a decrease in porosity as well as slow transference of the burden of the absorption of load from the cementation structures to the fibres. Therefore, values of E continued to increase.

The first specimen presented a total maximum axial deformation of 0.721% which is double the total value observed for the second (0.359%). A similar trend was also observed for the Young's modulus. The first specimen presented an increase in E 2.85 times higher than the second. It is plausible to conceive that the higher deformation of the first specimen led to a higher Young's modulus. This higher deformation of the first repetition might be attributed to the lower G_0 values observed before testing. And a lower G_0 could also explain the reason for the higher rate of increase of E during testing for the first specimen.

Another important observation to be made is that the applied load values for the 18-5-F-90-ML specimens were extremely similar to the values applied for the 18-5-F-70 specimens. However, the total number of cycles did not have the same order of magnitude. This might be caused by a slight variation in $\eta/C_{iv}^{0.28}$ achieved after moulding, G_0 values observed before testing, or even a possible mistake during moulding. However, discrepancies in N values for slight differences in the matrix are observed in cyclic testing. When testing the cyclic behaviour of a cemented calcareous soil under triaxial tests, Sharma and Fahey (2003) observed a variation of over 13000 cycles for a variation of 3% in applied load. The authors also an increase in the number of cycles with the increase in confining stress up to 200 kPa.

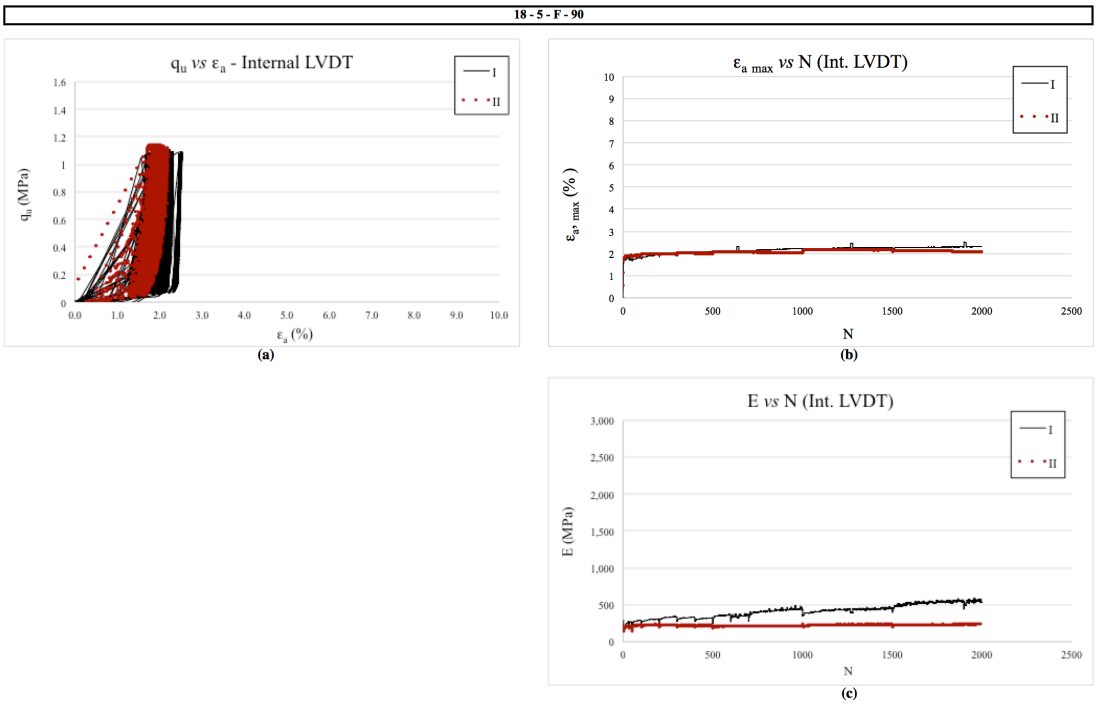

Figure 5.77: Internal data from specimen 18-5-F-90-ML I and II (a) q_u *versus* ε_a (b) $\varepsilon_{a\ max}$ *versus* N (c) E *versus* N

The internal data for both repetitions under 80% applied modified load (figure 5.78) showed similar trends over the 2000 applied cycles. When analysing the first specimen (figure 5.78 (b)), it was observed that for the first repetition there was an initial strain of 1.054%. Thus, the failure threshold for this specimen was of 2.53%. This initial strain was followed by an 11.08% increase in strain values over the next two thousand cycles – rate of axial strain gain of 0.006% – with a $\varepsilon_{a\ max}$ of 1.170%. Therefore, the failure threshold was not met. As for the Young's modus (figure 5.78 (c)), the initial E value was of 207.39 MPa. The specimen presented a 159% increase in E over the next two thousand cycles reaching 537.2 MPa – an increase rate of 0.08% per cycle. The behaviour presented by this specimen indicates a consistent degradation of the cementitious bonds with cycling leading to a constant increase in the accumulated plastic deformation. Since the increase in $\varepsilon_{a\ max}$ did not present a high increase rate, but presented a high E, the $\varepsilon_{a\ min}$ of the test increased at a high pace, and therefore of plastic deformation. A gradual failure of cement bonds results in a decrease in porosity as well as slow transference of the burden of the absorption of load from the cementation structures to the fibres with the continuous increase in E values.

Focusing on the second specimen (figure 5.78 (b)), it was observed that there was an initial strain of 1.243%. Leading to a failure threshold of 2.621%. This initial strain was followed by

a 45.6% increase in strain values over the next two thousand cycles ending the test at a $\varepsilon_{a\ max}$ of 1.810% – rate of axial strain gain of 0.023%. Therefore, the failure threshold was not met. As for the Young's modus (figure 5.78 (c)), the initial E value was of 113.87 MPa. The specimen presented a 98% increase in E over the next two thousand cycles reaching 225.20 MPa – an increase rate of 0.049% per cycle. The behaviour presented by this specimen indicates a consistent degradation of the cementitious bonds with cycling leading to a constant increase in the accumulated plastic deformation. A gradual failure of cement bonds results in a decrease in porosity as well as slow transference of the burden of the absorption of load from the cementation structures to the fibres with the continuous increase in E values.

The first specimen presented a total maximum axial deformation of 0.117% which is a fifth of the total value observed for the second (0.567%). An opposite trend was observed for the Young's modulus. The first specimen presented an increase in E three times higher than the second. As mentioned before, rate of increase of $\varepsilon_{a\ max}$ was not high, but presented a high rate of increase of E, which means that the $\varepsilon_{a\ min}$ during testing increased at a higher pace and therefore so did the plastic deformation. It can be inferred buy this that the major plastic deformation occurred in the lower two-thirds of the specimen. It is plausible to conceive that the higher deformation of the first specimen led to a higher Young's modulus. This higher Young's modulus increase of the first repetition might be attributed to the lower G_0 values observed before testing.

The internal data for both repetitions under 70% applied modified load (figure 5.79) showed similar trends over the 2000 applied cycles. When analysing the first specimen (figure 5.79 (b)), it was observed that for the first repetition there was an initial strain of 2.396%. Thus, the failure threshold for this specimen was of 3.198%. This initial strain was followed by a 23.55% increase in strain values over the next two thousand cycles – rate of axial strain gain of 0.012% – with a $\varepsilon_{a\ max}$ of 2.961%. Therefore, the failure threshold was not met.

As for the Young's modus (figure 5.79 (c)), the initial E value was of 113.84 MPa. The specimen presented a 103% increase in E over the next two thousand cycles reaching 231.29 MPa – an increase rate of 0.052% per cycle. The behaviour presented by this specimen indicates a consistent degradation of the cementitious bonds with cycling leading to a constant increase in the accumulated plastic deformation. Since the increase in $\varepsilon_{a\ max}$ did not present a high increase rate, but presented a higher increase in E, the $\varepsilon_{a\ min}$ of the test increased at a

higher pace, and so did the accumulated plastic deformation. A gradual failure of cement bonds results in a decrease in porosity as well as slow transference of the burden of the absorption of load from the cementation structures to the fibres. Therefore, values of E continued to increase.

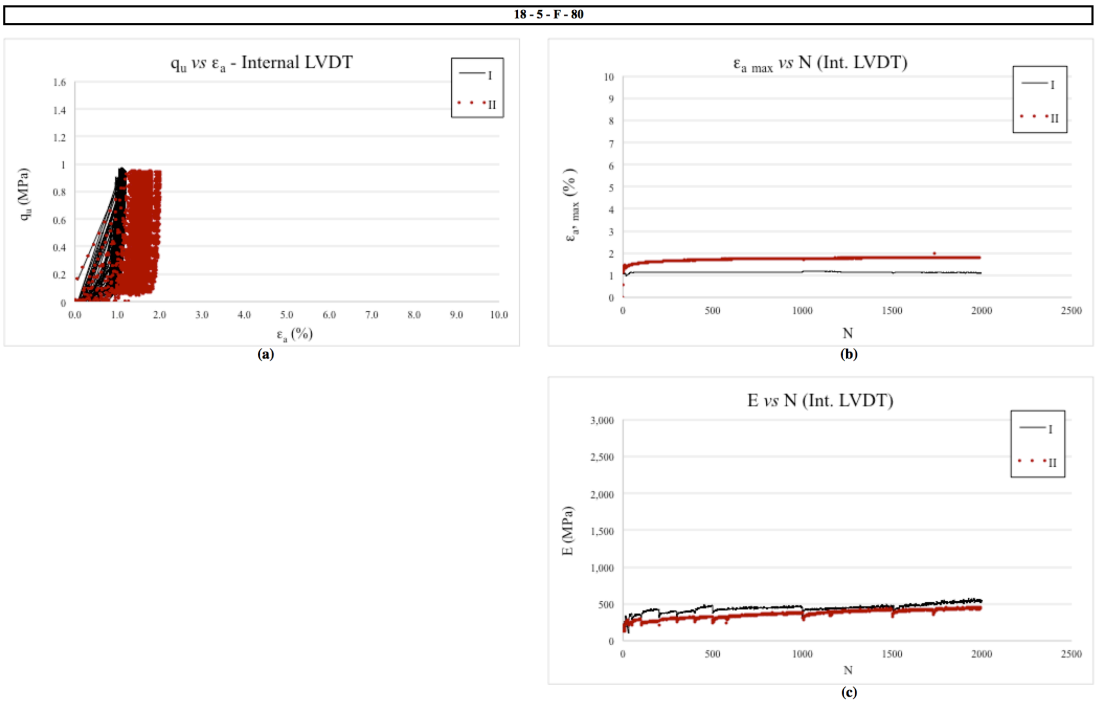

Figure 5.78: Internal data from specimen 18-5-F-80-ML I and II (a) q_u *versus* ε_a (b) $\varepsilon_{a\ max}$ *versus* N (c) E *versus* N

Focusing on the second specimen (figure 5.79 (b)), it was observed that there was an initial strain of 2.595%. Leading to a failure threshold of 3.297%. This initial strain was followed by an 8.3% increase in strain values over the next two thousand cycles ending the test at a $\varepsilon_{a\ max}$ of 2.810% – rate of axial strain gain of 0.004%. Therefore, the failure threshold was not met. As for the Young's modus (figure 5.79 (c)), the initial E value was of 238.78 MPa. The specimen presented a 119% increase in E over the next two thousand cycles reaching 521.88 MPa – an increase rate of 0.059% per cycle. The behaviour presented by this specimen indicates a consistent degradation of the cementitious bonds with cycling leading to a constant increase in the accumulated plastic deformation. A gradual failure of cement bonds results in a decrease in porosity as well as slow transference of the burden of the absorption of load from the cementation structures to the fibres. Therefore, values of E continued to increase.

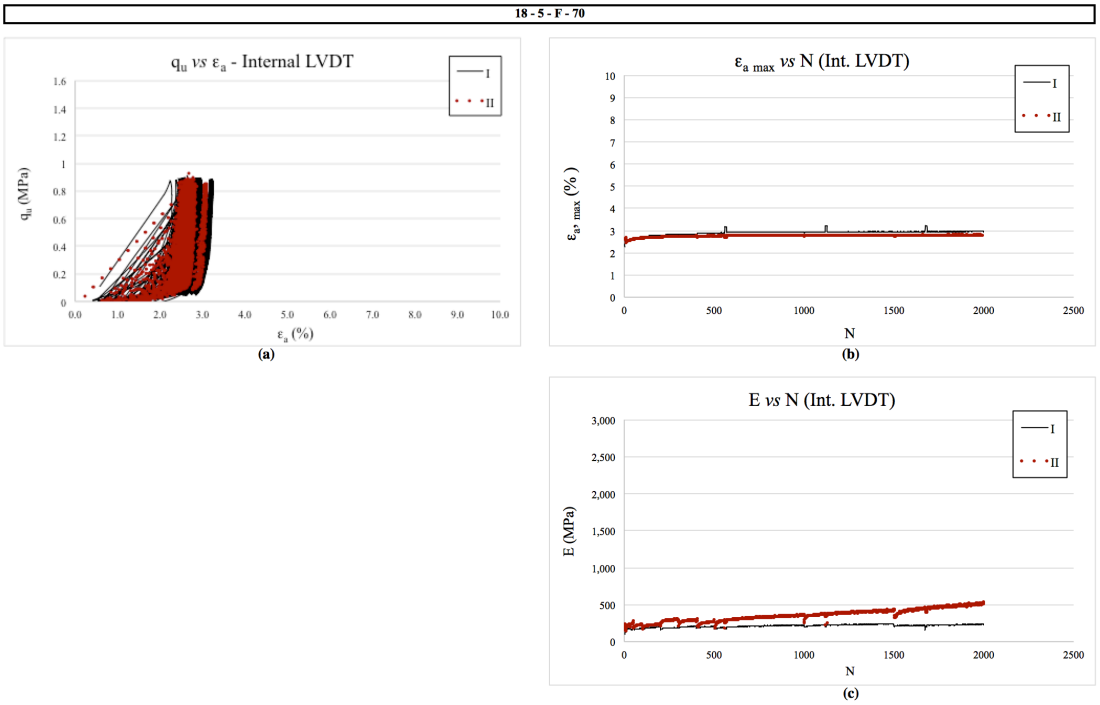

Figure 5.79: Internal data from specimen 18-5-F-70-ML I and II (a) q_u *versus* ε_a (b) $\varepsilon_{a\ max}$ *versus* N (c) E *versus* N

The first specimen presented a total maximum axial deformation of 0.564% which is a double of the total value observed for the second (0.215%). A similar trend was also observed for the Young's modulus. The first specimen presented an increase in E 2.85 times higher than the second. As mentioned before, rate of increase of $\varepsilon_{a\ max}$ was not high, but presented a higher rate of increase of E, which means that the $\varepsilon_{a\ min}$ of the test increased at a higher pace and therefore so did the accumulated plastic deformation. It can be inferred buy this that the majority of plastic deformation occurred in the lower two-thirds of the specimen. It is plausible to conceive that the higher deformation of the second specimen led to a higher Young's modulus. This higher deformation of the first repetition might be attributed to the lower G_0 values observed before testing. And a lower G_0 could also explain the higher rate of increase of E during testing for the first specimen.

5.2.5.2 Shear modulus

During testing bender element tests were carried out at pre-established intervals – 0, 1, 2, 10, 30, 50, 100, 200, 300, 400, 500, 1000, 1500, and 2000 cycles. For every reading the cyclic test was stopped and 10% of the tested load was applied in order for the measurements to be able to be made. The values attained are presented in appendices B. As stated in item 3.2.10.2, at the

beginning of every test a frequency screening was made in order to assess the best one to conduct the tests.

From the data presented thus far it is observed that the fibre-reinforce combinations failed earlier than the non-reinforced ones. So, the combinations with added fibres were tested for the same load values attained form the unreinforced curves. For this lower applied load, none of the specimens failed. This translated to the shear modulus values as an initial degradation of G_N that reach a plateau, following an increase on G_N until the test was stopped.

Figure 5.80 presents the values of shear modulus *versus* number of cycles for all the repetitions for the 18-5-F-ML combinations. It is possible to conclude that the values of G obtained for all repetitions are within the same order of magnitude and have similar tendencies. Figure 5.80 (a) presents the values of shear modulus *versus* the number of cycles for the fibre-reinforced benchmark with modified load mixtures at 90% of the estimated maximum load, it can be observed an initial decreasing in the G_N trend followed by stabilization in values for all repetitions. In figure 5.80 (b) the fibre-reinforced benchmark mixtures were tested for 80% of the estimated maximum load. An initial degradation of G_N was observed for the first 50 cycles, followed by stabilization in values over the next 145 cycles. Throughout the last 1000 cycles it was observed a slight increase in shear modulus values for all repetitions. Figure 5.80 (c) presents the fibre-reinforced benchmark mixtures tested for 70% of the estimated maximum load. The same trend was observed for this combination than the presented by the previous. An initial degradation of G_N was observed for the first 10 cycles, followed by stabilization in values over the next 190 cycles. Throughout the last 1800 cycles it was observed a slight increase in shear modulus values for all repetitions.

Plotting the average values of the repetitions, figure 5.81 displays the relationships between G and N for the three percentages of applied loads studied and their respective fitted equations. It is possible to infer form the presented data that the G_N values withstood a lower decrease rate as the applied load decreased, as it should be expected, lower applied load resulted in less damage to the structure for a given number of cycles.

The G_N values were normalised by the G_0 values of the mixtures, as shown in figure 5.82. From these graphs it is easier to differentiate the aforementioned trends. For the 90% load specimens a more pronounced initial degradation of G_N was observed for the first 50 cycles followed by stabilization in values for all repetitions. As for the 80% load, there was an initial degradation

of G_N was observed for the first 50 cycles, but less pronounced than the previous load percentage one. This was followed by the stabilization in values over the next 145 cycles. Throughout the last 1000 cycles it was observed a slight increase in shear modulus values for all repetitions. For the last percentage of applied load (70%), an initial degradation of G_N was observed for the first 10 cycles, similarly to the one observed for the 80% load, followed by stabilization in values over the next 190 cycles. Throughout the last 1800 cycles it was observed an increase in shear modulus values for all repetitions, reaching similar values to the ones observed at the 10^{th} cycle.

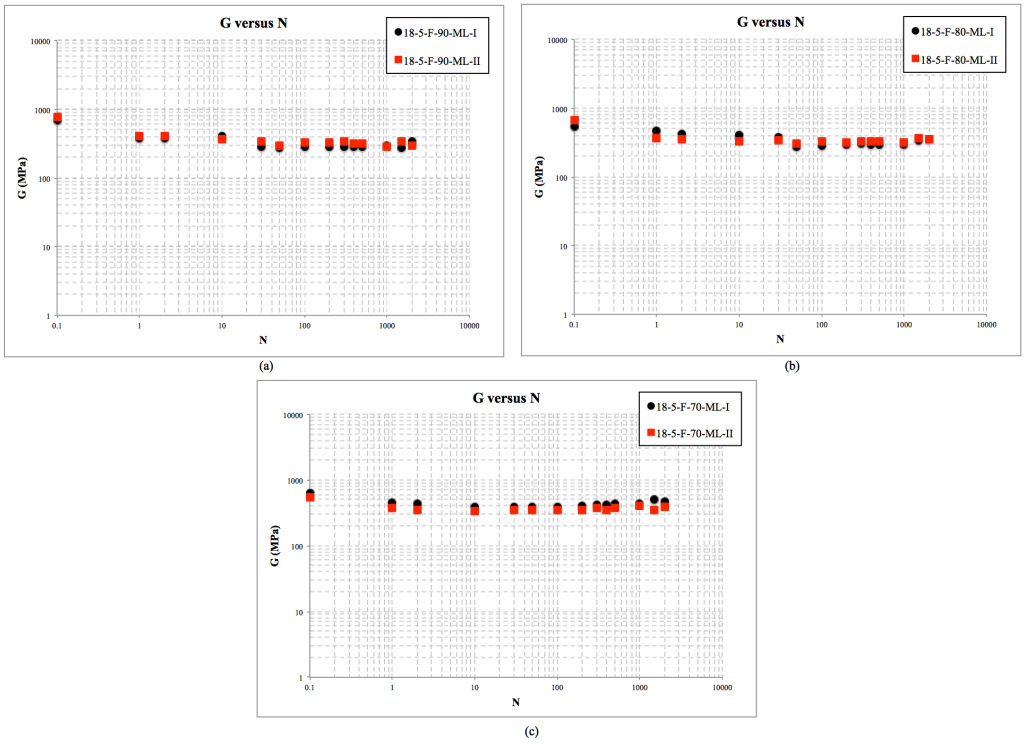

Figure 5.80: Shear modulus versus number of cycles for fibre-reinforced benchmark for modified loading specimens at (a) 90% loading (b) 80% loading (c) 70% loading

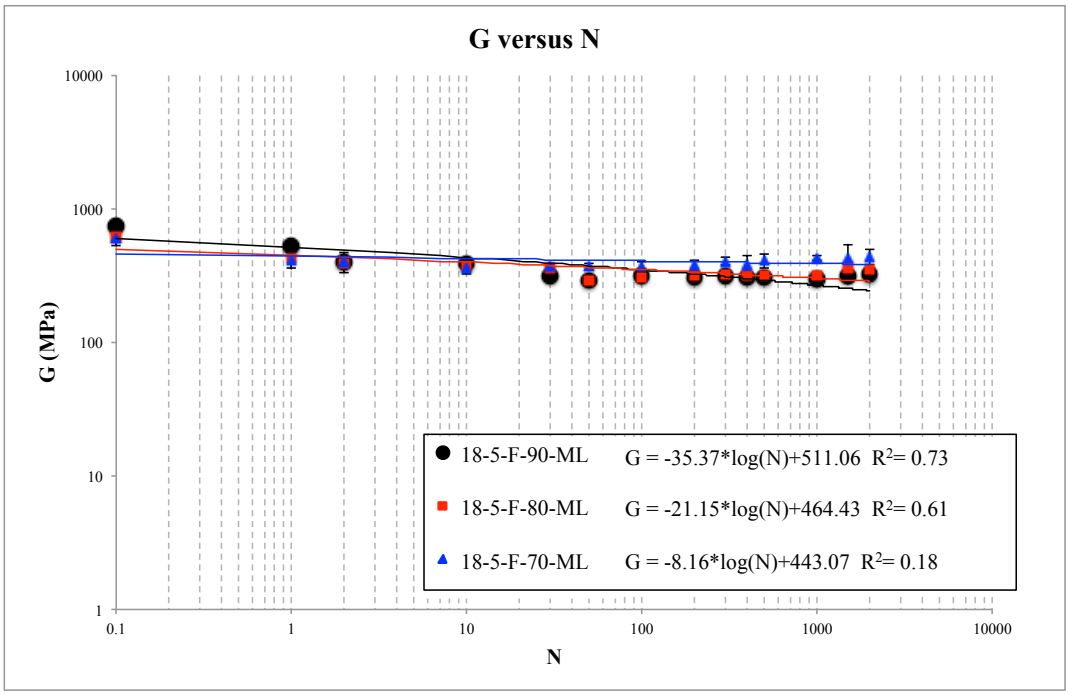

Figure 5.81: Shear modulus versus number of cycles for fibre-reinforced benchmark specimens for modified loading

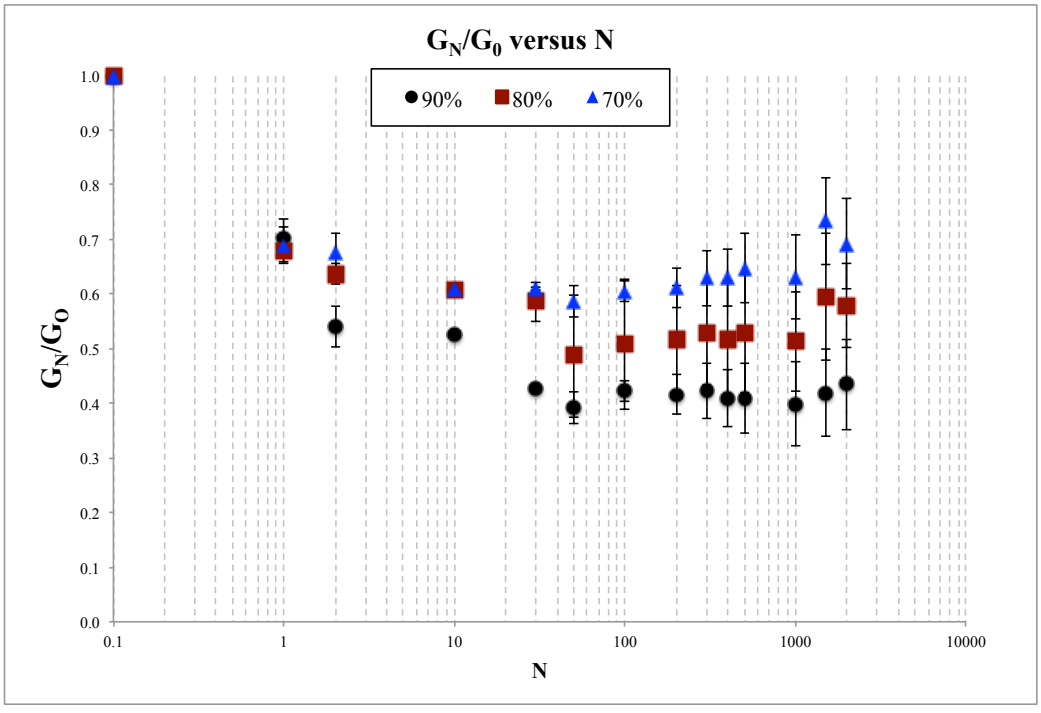

Figure 5.82: G_N/G_0 versus number of cycles for fibre-reinforced benchmark specimens for modified loading

5.3 DISCUSSION

In this topic it will be discussed the data presented in this chapter. The result analysis was divided in four items were the implication of fibre insertion and different mixtures was assessed. Firstly, the influence of load percentage applied was discussed. Then, an analysis of the maximum axial strain was shown. Followed by an analysis of the Young's modulus. Finally, the progress of the shear modulus with number of cycles for the studied variables was evaluated.

5.3.1 Percentage of load applied

From the data presented in this chapter it is possible to conclude that the number of cycles increased with the decrease of percentage of load applied. Even if the insertion of fibres disrupted the results, this trend was observed for all combination, which is consistent with the data from other authors (GÁLVEZ, 2017; MAHER; HO, 1993; YE, 1989).

Figure 5.83 presents the average values of the number of cycles against the applied load percentage (LP) for soil-cement specimens. A power function relationship was the best fit for the data. Figure 5.84 presents the average values of the number of cycle against the applied load percentage (LP) for soil-cement-fibre specimens. Also for this set o data a power function relationship was the best fit for the data.

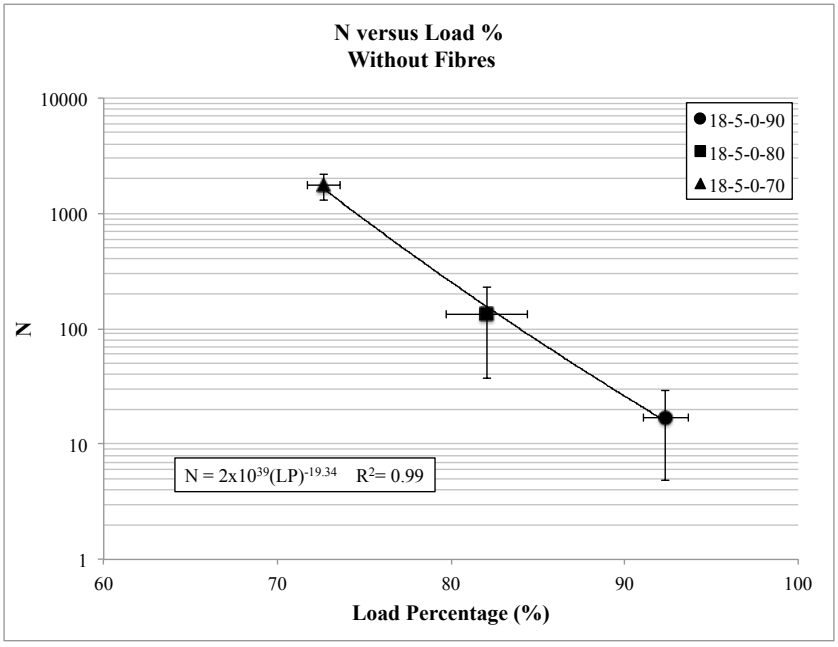

Figure 5.83: Number of cycles *versus* percentage of applied load for soil-cement mixtures

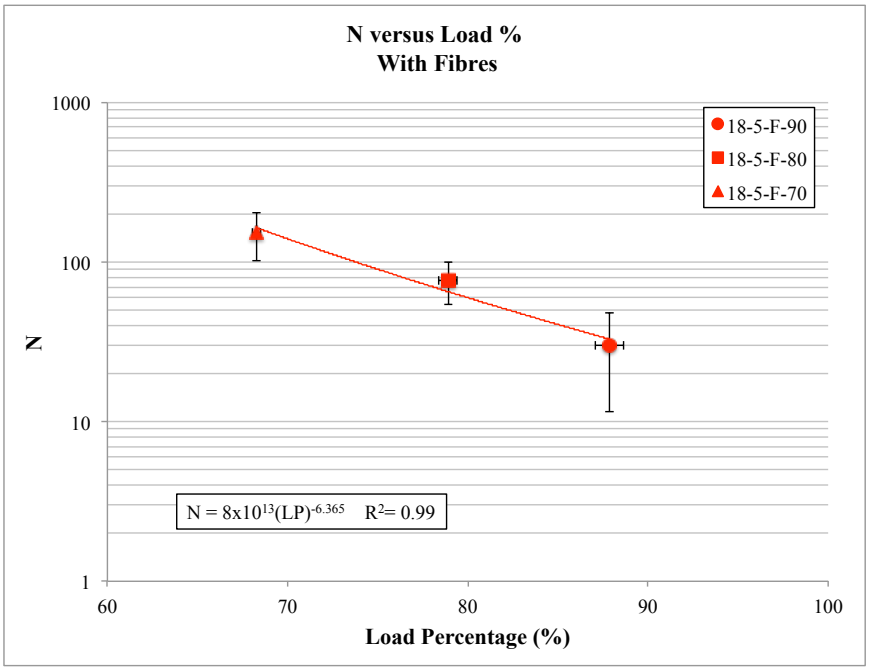

Figure 5.84: Number of cycles *versus* percentage of applied load for soil-cement-fibre mixtures

For every combination at least 5 specimens were made (with exception of the modified load specimens) but only the ones that had the least variability in the initial conditions were chosen to be presented in this research. Even with this prior screening there was still variability in the number of cycles. As mentioned before, the same load was applied for the 18-5-F-70 specimens as for the 18-5-F-ML-90. However, the response to the number of cycles was different. This might be caused by a slight variation in $\eta/C_{iv}^{0.28}$, G_0 values, or even a possible mistake during moulding. However, is not uncommon to observe discrepancies in N values for slight differences in the matrix during cyclic testing, i.e. Sharma and Fahey (2003) that observed a variation of four times the number of cycles for a variation of 3% in applied load. For the present study, the values attained for the 18-5-F-ML-90 specimens were more congruent with the data obtained from the unreinforced specimens. In being so, all following discussion will take the data from the modified load into consideration over the data for the original applied load for this combination.

Figure 5.85 presents the relationship between load applied (LA) and the number of cycles for the average values and their standard deviation. As mentioned before, the maximum load values used were attained through the fitted equation of unconfined compression versus $\eta/C_{iv}^{0.28}$. Given this, there was a variation of applied load for a same load percentage given its initial $\eta/C_{iv}^{0.28}$. Considering the data from the modified load (18-5-F-90-ML) as the 70% of the fibre-reinforced

specimens (instead of 18-5-F-70), it is possible to conclude that fibre insertion did improve the behaviour of the composite for the studied mixture since for the highest applied load the number of cycles until failure was far greater than the observed for soil-cement specimens, the same behaviour was observed by Heineck *et* al., 2005 and Maher and Ho, 1993. It is important to observe that even for the original values of the 70% of the load, reinforced specimens presented a nine times higher number of cycles for an applied load 100 kPa higher than the load applied for the 90% of the unreinforced specimen.

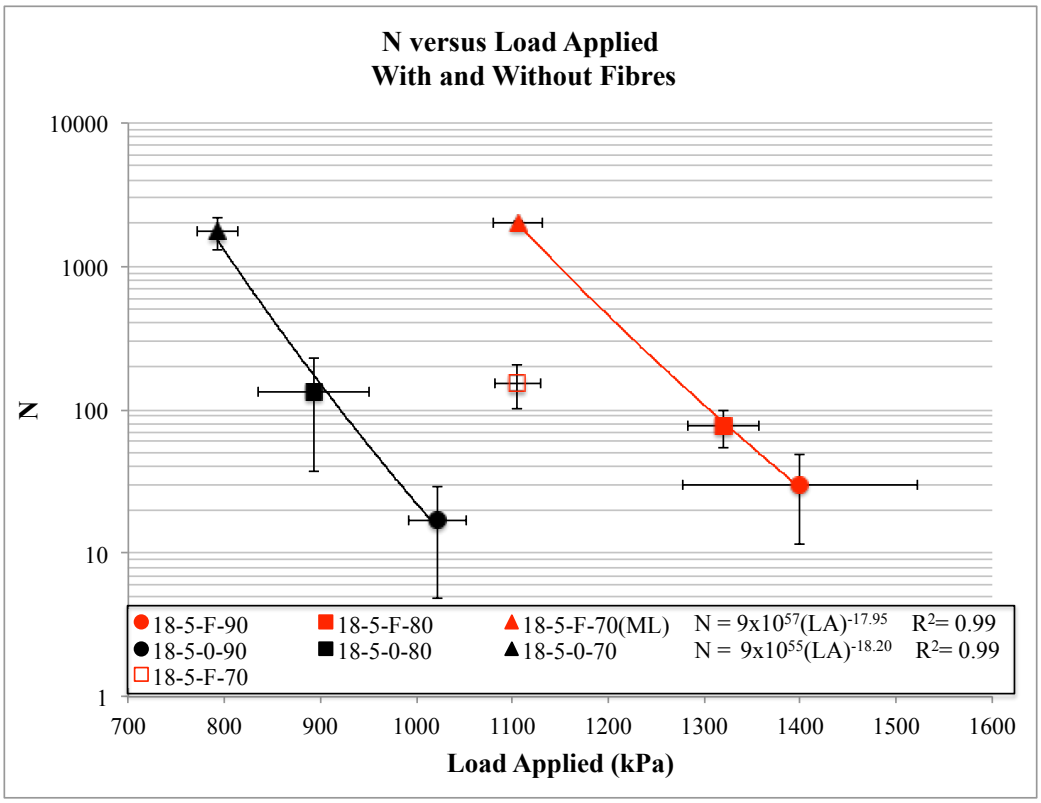

Figure 5.85: Number of cycles *versus* applied load for soil-cement and soil-cement-fibre mixtures

Taking into account all the data for the benchmark specimens, form figure 5.86 it is possible to infer that fibre insertion improves the behaviour of the studied material under unconfined cyclic testing. For the same loading range (800 to 1100 kPa) unreinforced specimens reached failure, whist unreinforced did not within the stipulated maximum number of cycles.

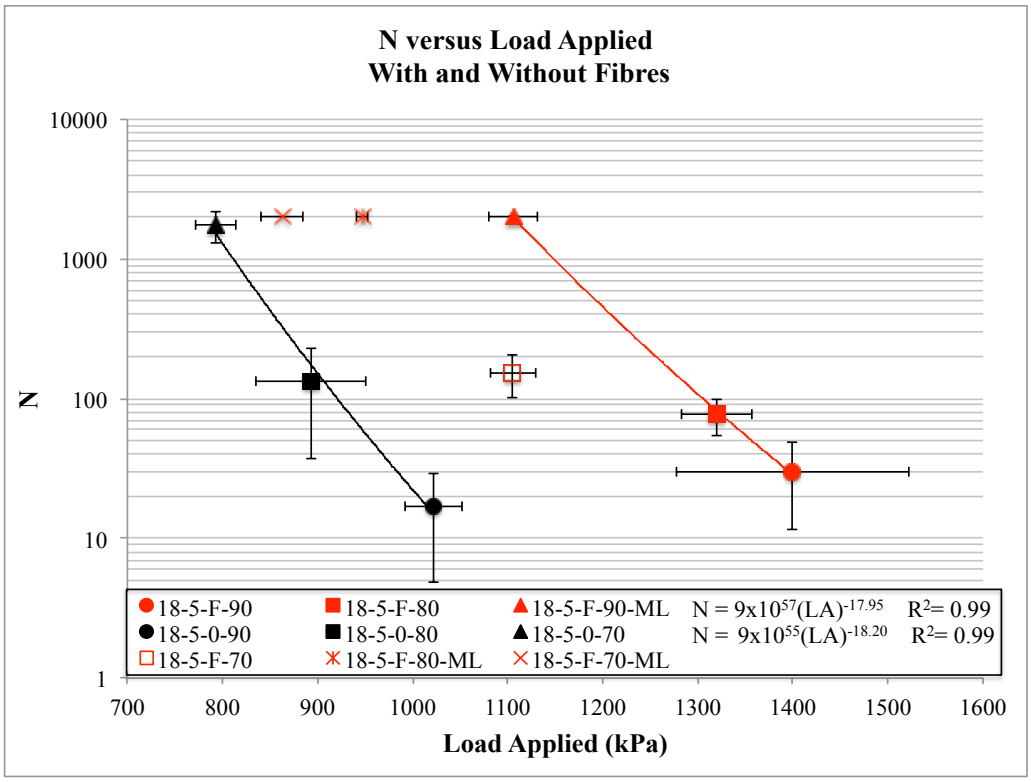

Figure 5.86: Number of cycles *versus* applied load for soil-cement and soil-cement-fibre mixtures for original and modified loading

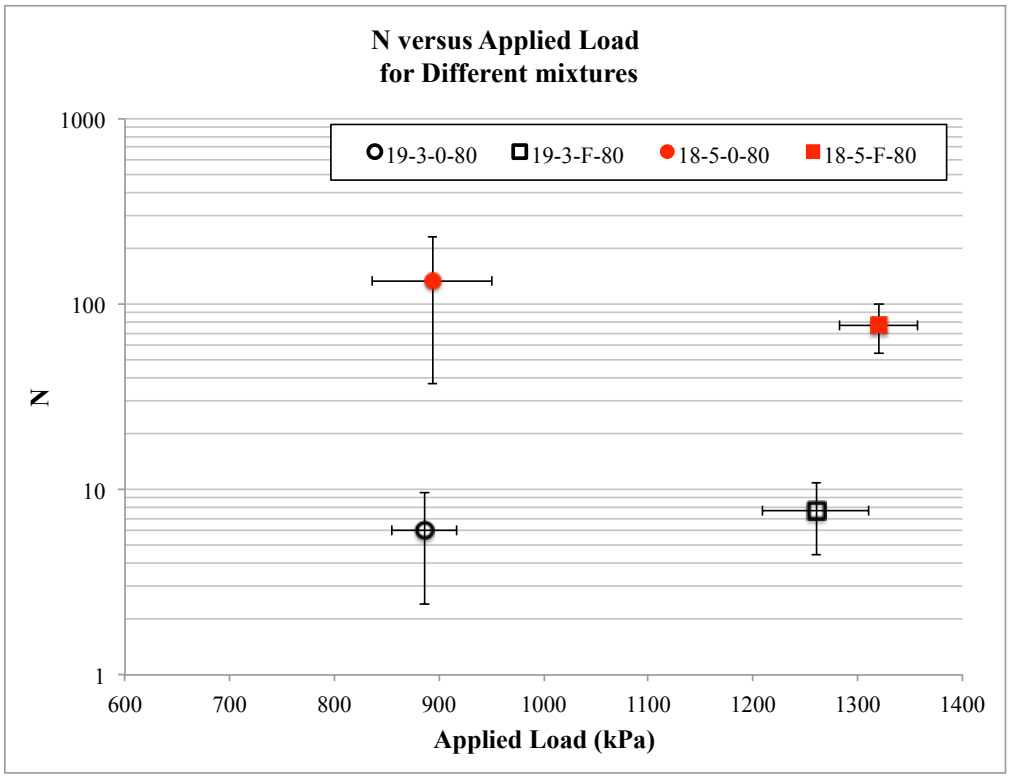

Figure 5.87: Number of cycles *versus* applied load for benchmark mixtures and 19-3 mixtures

Regarding the specimens with similar $\eta/C_{iv}^{0.28}$ but higher density and lower cementation, when compared the number of cycles against applied load, it is possible to observe (figure 5.87) that the number of cycles reduced for the 19 kN/m^3 - 3% cement specimens for unreinforced and reinforced mixtures. These results point to a higher influence of the cementation ratio in the behaviour of cemented and fibre-reinforced cemented composites. However, further research should be done to assess the influence of cementation and porosity on the cyclic behaviour of composite materials.

5.3.2 Axial strain

Besides the difference in the number of cycles when the insertion of fibres is concerned, there was a difference in the maximum axial strain for the specimens with and without fibres. For this analysis the values of $\varepsilon_{a\ max}$ were the maximum value at the last cycle before rupture occurred minus half of the $\varepsilon_{a\ max}$ for the first cycle (an estimative of the strain due to accommodation), similarly to the approach used to assess rupture. The average values for the benchmark specimens are presented in figure 5.88. This figure indicates that for the unreinforced specimens failure was reached at a $\varepsilon_{a\ max}$ of approximately 0.5%. As for the soil-cement specimens that did not fail for the stipulated maximum number of cycles the axial strain at 2000 cycles was around 0.17% indicating that there were still these specimens at the stage of constant accumulation of plastic strain. As for the fibre-reinforced specimens, the $\varepsilon_{a\ max}$ for the cycle just before rupture occurred was a little lower than the stipulated 2%, as expected since it was the stipulated failure condition. When considering the values for the modified load specimen as 70% applied load, is observed that it still had on average 0.6% of axial deformation until failure, the rate in which failure might occur is hard to predict, but it is possible to presume failure is not eminent.

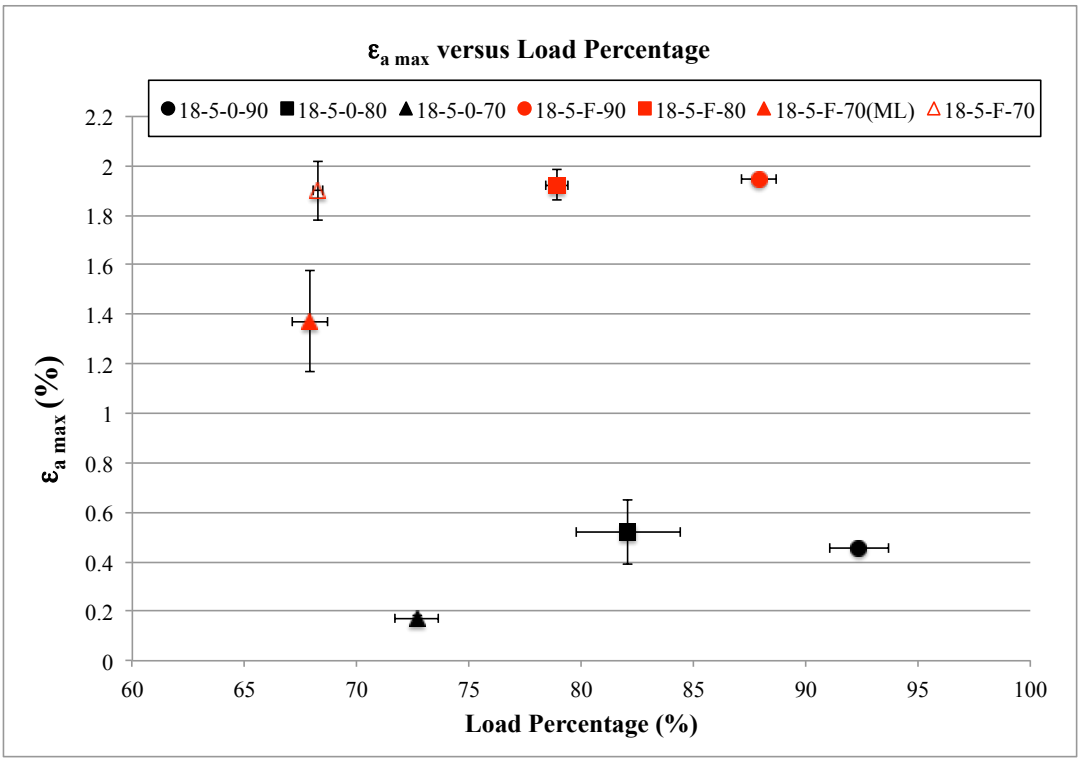

Figure 5.88: Maximum axial strain *versus* load percentage for benchmark mixtures

Given the difficulty to measure the axial strain due to initial accommodation, figure 5.89 presents the data for the difference between $\varepsilon_{a\ max}$ for the last cycle and for the first (disregarding initial strain). This way it is easier to assess the development of axial strain during cycling. It is possible to infer from this data that specimens reinforced with fibres present higher axial deformation before rupture, which is expected given the elastic nature of the fibres that confers a greater capacity to absorb loading under higher strains. From this graph is possible to infer the relevance of the strain during the first cycle over the next cycles. For the unreinforced specimens the first cycle represented on average 32% of the total strain. As for the reinforced, the first cycle represented on average 46% of the total strain. The greatest impact was for the modified loads, where the deformation during the first cycle accounted for on average 69% of the total strain. Of course, it has to be taken into account that since the modified load specimens did not reach failure a significant portion of the total mobilized strain until failure is not being taken into consideration.

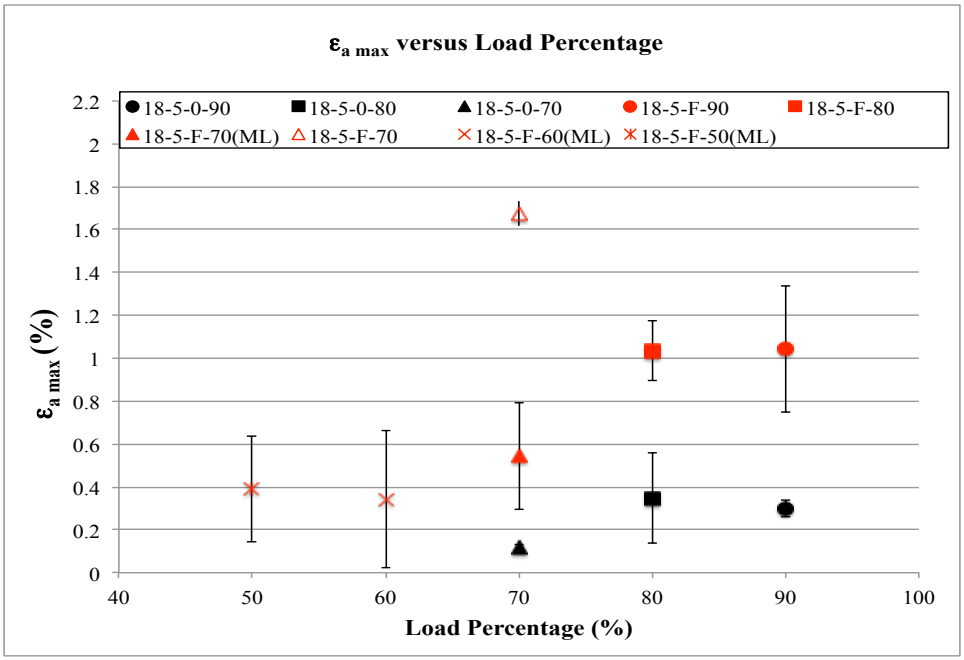

Figure 5.89: Maximum axial strain after first cycle *versus* load percentage for benchmark mixtures for original and modified loading

Figure 5.90 presents the data for the difference between $\varepsilon_{a\ max}$ for the last cycle and for the first (disregarding initial strain) against the applied load. This way it is easier to assess the development of axial strain regarding the stress imposed to the specimen. Maher and Ho (1993) observed an increase of strain at failure for fibre-reinforced specimens. It is possible to infer from the data for the present study that specimens that are within the same range of applied load (18-5-0-80, 18-5-F-80-ML, 18-5-F-70-ML and 18-5-0-90) presented similar values of $\varepsilon_{a\ max}$, however, the modified load specimens did not reach failure, which indicates that as observed by Maher and Ho (1993), the axial strain at failure is higher for fibre-reinforced specimens for the same range of applied load.

Considering the specimens with similar $\eta/C_{iv}^{0.28}$ but higher density and lower cementation, it is possible to observe (figure 5.91) that the $\varepsilon_{a\ max}$ was lower for the 19 kN/m^3 - 3% cement specimens for unreinforced mixtures than for the benchmark mixtures. As for the reinforced specimens, the $\varepsilon_{a\ max}$ at failure was similar to the values of the benchmark mixture. These results suggest that there is a higher influence of the cementation ratio in the behaviour of cemented composites, but the insertion of fibres mitigates this influence. This might be related to the more ductile behaviour of fibre-reinforced specimens. However, further research should be done to assess the influence of cementation and porosity on the cyclic behaviour of composite materials

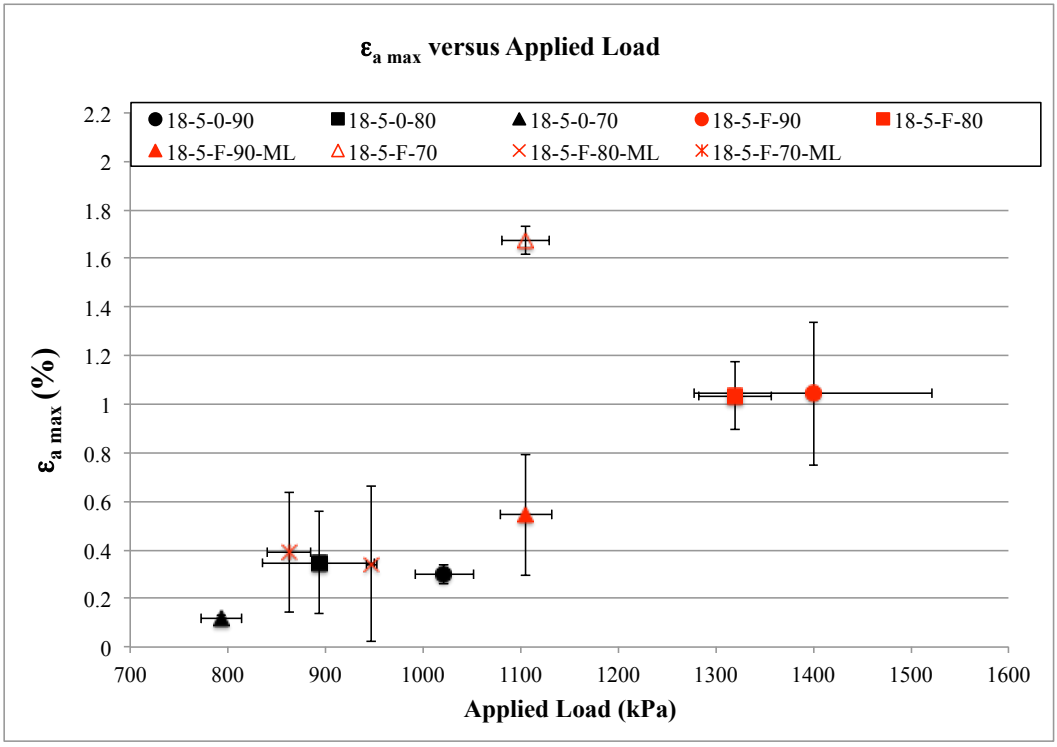

Figure 5.90: Maximum axial strain after first cycle *versus* applied load for benchmark mixtures for original and modified loading

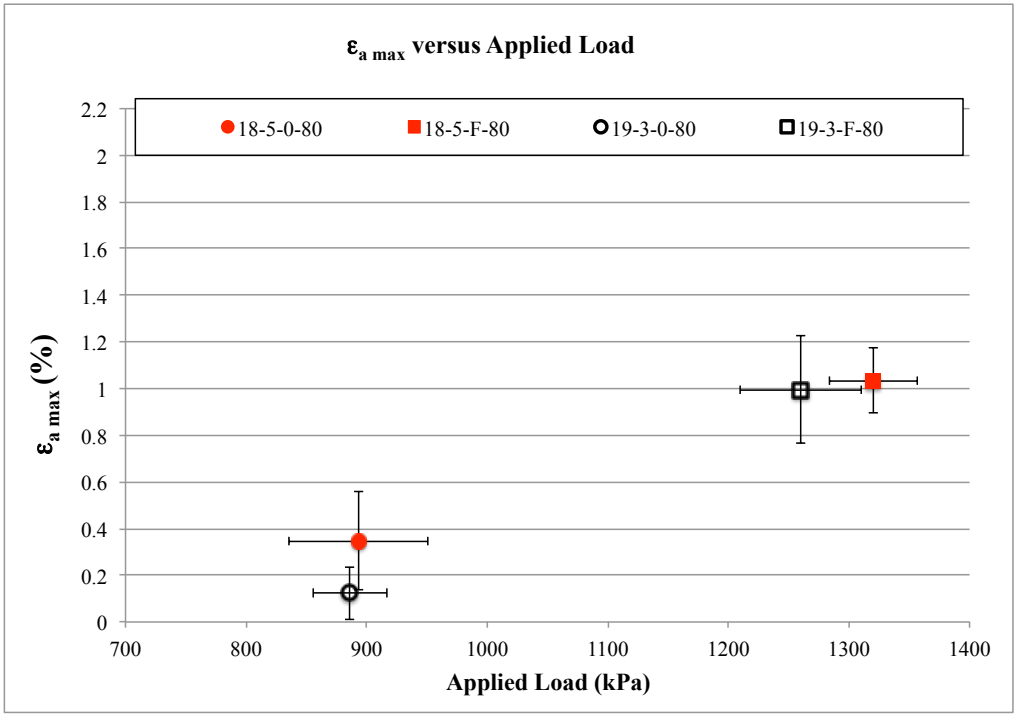

Figure 5.91: Maximum axial strain after first cycle *versus* applied load for benchmark and 19-3 mixtures

5.3.3 Young's modulus

When considering the Young's modulus attained through the unloading-reloading loop of the stress-strain graph during cycling, two main points can be highlighted from the data. The first is the difference in the magnitude of values between soil-cement and soil-cement-fibre composites. Even though there was fluctuation on the values of Young's modulus during the cycling process, it is possible to assume that the E values remained somewhat constant during the largest bulk of cycling for all specimen combinations.

For soil-cement mixtures the values of E according to the internal data were on average around 2200 MPa. Which is very different from the data from the external measurements that were on average 350 MPa. But, as mentioned during the presentation of the data, the values from the external LVDT did not reflect accurately the behaviour of the specimens due to important losses in accuracy from the accumulated strain of a series of parts of the equipment. As for the fibre-reinforced specimens, the Young's modulus values were on average around 380 MPa from the internal data, and 160 MPa from the external. The values from the internal data of E for reinforced mixture might be obscured due to a greater deformation of the specimen during testing. Figure 5.92 exemplifies the difference in rupture mode of soil-cement and soil-cement-fibres. After a certain deformation the plastic extensions could distort, obscuring the data for the last cycles. Even taking these factors into consideration, it is possible to conclude that fibre insertion lead to a decrease in the Young's modulus. This is also exemplified by the fact that the rupture mode went from brittle for the cemented specimens, to ductile for the fibre-reinforced cemented specimens.

Li and Ding (2002) observed an increase of shear modulus under CU triaxial testing with an increase in fibre content and an increase in confining pressure. This trend was not observed in the present research. However, it is important to note that the testing in this research is unconfined, which might be the reason for the lower Young's modulus values for fibre-reinforced specimens. The absence of a confining pressure allows the specimen to expand radially freely, leading to higher axial deformations in the unloading-reloading loop and therefore lower E values.

The second important observation to be made from the Young's modulus data is the progression of the E values with the cycles. The specimens that were more rigid presented a peak in E values at the beginning of testing, which could be attributed to the mobilization of

the weaker cementation bonds, followed by a degradation of stiffness until a plateau of constant plastic strain is reached. After which, a second peak in E is observed right before failure. This second peak might be caused by a collapse in the cemented matrix, leading to a decrease in void ratio and in turn an increase in E culminating in failure. This last peak could be considered a fictional increase in E, since it is the product of the eminent collapse of the matrix. As for the less rigid specimens, it was observed a constant increase of the Young's modulus that could be attributed by gradual mobilization of the cementitious bonds with the decrease of void ratio of the matrix, this trend continues until the degradation of the bonds reach a critical point. After this subtle peak, the values of E decrease until failure.

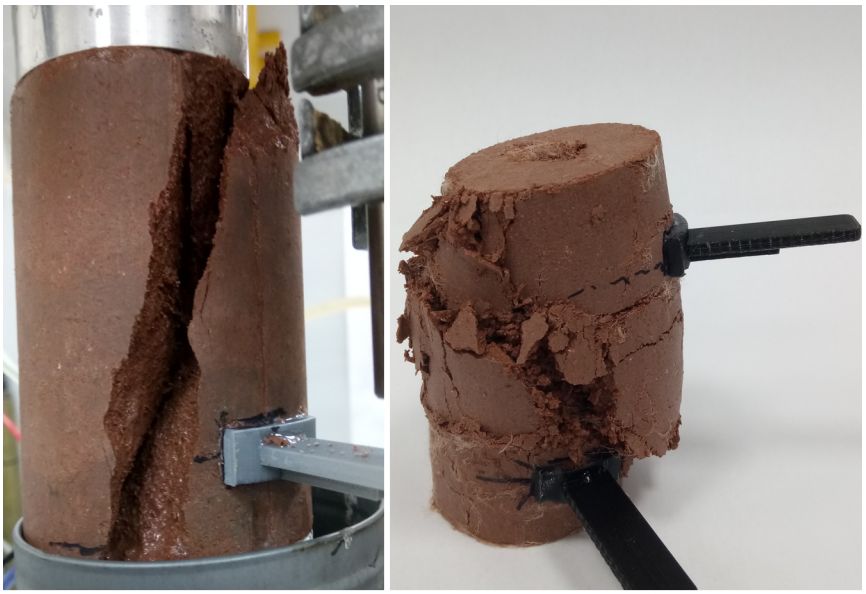

Figure 5.92: Rupture mode for (a) soil-cement mixtures (b) soil-cement-fibre mixtures

The 19-3 specimens presented lower E values for soil-cement mixture, but similar values of E for fibre-reinforced cemented mixture when compared to the corresponding benchmark specimens. This might indicate, as observed for axial strain, a greater importance of the cementation percentage for soil-cement mixtures that is mitigated for soil-cement-fibre mixture due to the disruption on the formation of cement bonds due to fibre insertion. However, as also was mentioned before, further research should be done to assess the influence of cementation and porosity on the cyclic behaviour of composite materials.

5.3.4 Shear modulus

The shear modulus measured through bender elements at the specified interval of cycles showed that, similarly to the trend observed for the Young's modulus, the values of G were higher for soil-cement specimens then the observed for soil-cement-fibre mixtures. This trend can be observed in figure 5.93. This trend is different than the observed in literature. Heineck *et* al. (2005) concluded that fibre insertion did not alter the very-small strain values of shear modulus for the same material studied in this research when subjected to isotropic compression. The very-small strain measurements in this research were done at very low axial stresses, which might be the reason for the lower shear modulus at very-small strains values for fibre-reinforced specimens. The absence of axial and radial stresses means that the matrix has higher void ratio during very-small strain testing, leading to less contact between the particles and a dispersion of the shear waves when fibres are encountered.

A logarithmic relationship was found for the deterioration of small-strain G with the number of cycles, a similar relationship was proposed by Yasuhara *et* al. (1998). The relationship could be described as equation 5.2.

$$G_N = -B \cdot log_{10}(N) + G_1 \tag{5.2}$$

Where B is the rate of rate of degradation due to influence of load percentage adopted during testing. Table 5.12 presents the values attained by the fitted equation from the experimental data.

Observing table 5.12 it is possible to conclude from the B values that the rate of stiffness degradation decreases with the decrease in the applied load. Also, that the difference on the rate of degradation is higher for unreinforced specimens for the applied loads then the observed for reinforced specimens. However, the coefficient of determination drastic decreases for the specimens that did not reach rupture. This is due to the observed increase in G values over the last 1500 cycles which might be attributed to a slow densification of the specimens over continued repetitive cycling that happened alongside the slow degradation of cemented bonds. The values predicted by the equation for the very-small strain shear modulus after the first cycle were similar to the average values attained from the measured specimens.

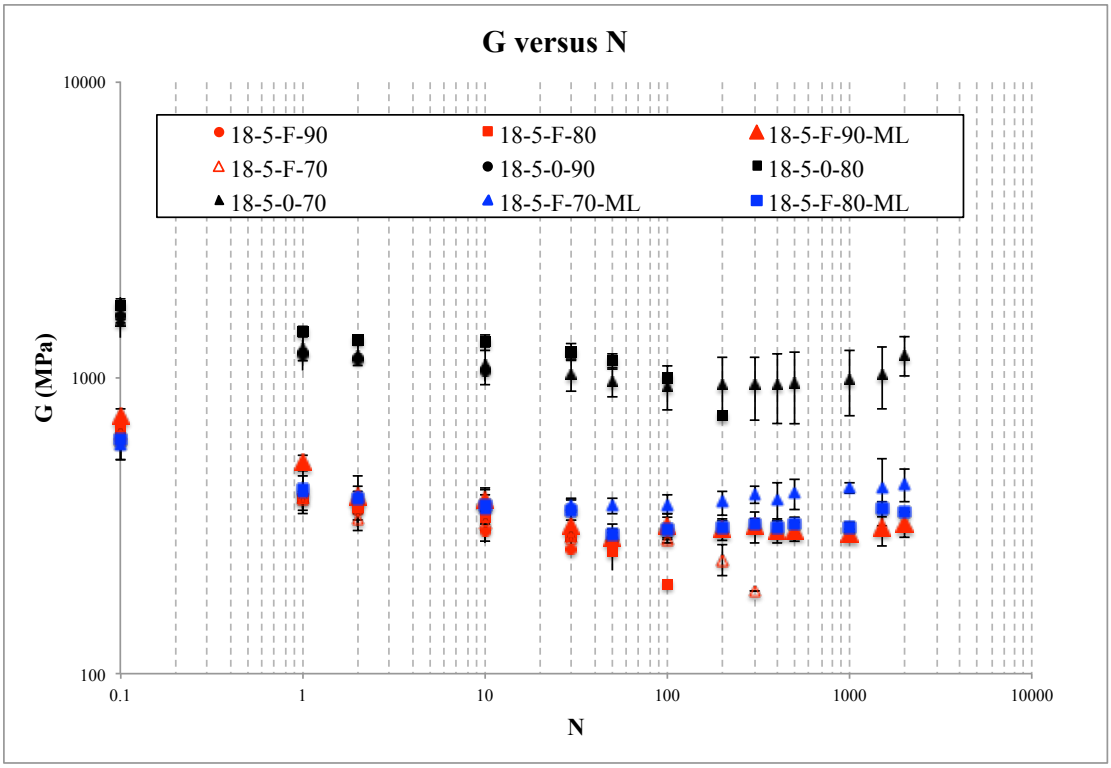

Figure 5.93: Shear modulus versus number of cycles for soil-cement and soil-cement-fibre benchmark specimens under original and modified loading

It is also possible to assess from the data presented in this table that degradation rates of G_N for the 19 kN/m^3 and 3% cement with and without fibres were higher than the observed by the correspondent benchmark specimens. The values of the ratio for cemented specimens were 69% higher than the observed for benchmark specimens and 95% higher for the fibre-reinforced specimens.

Table 5.12: Values for the fitted equation from empirical data

Mixture	Ideal Load %	B	G_1 (MPa)	R^2	Average Measured G_1 (MPa)	Measured/ Predicted G_1
18 kN/m^3; 5% cement	90	123.4	1279.10	0.92	1200.85	0.94
	80	109	1485.70	0.90	1431.68	0.96
	70	44.08	1256.40	0.57	1251.51	1.00
18 kN/m^3; 5% cement; 0.5% fibre	90	58.38	432.74	0.93	397.28	0.92
	80	58.05	464.03	0.88	389.68	0.84
	70	44.36	448.87	0.84	393.77	0.88
18 kN/m^3; 5% cement; 0.5% fibre; Modified load	90	37.37	511.06	0.73	520.04	1.02
	80	21.25	464.43	0.61	416.31	0.90
	70	8.16	443.07	0.18	411.90	0.93
19 kN/m^3; 3% cement	80	184.1	982.54	0.99	919.46	0.94
19 kN/m^3; 3% cement; 0.5% fibre	80	113.1	442.14	0.85	348.34	0.79

Figure 5.94 presents the average values for the relation between G_0 and G_1 for the studied mixtures against the applied load for the studied benchmark combinations. It is possible to observe that for same loading levels there was a higher initial degradation of stiffness for the fibre-reinforced mixtures, varying between 1.4 and 1.5. As for the unreinforced specimens, the values are G_0/G_1 ranged between 1.2 and 1.3. This corroborates the findings that point to a more rigid behaviour for cemented specimens and a ductile behaviour for fibre-reinforced cemented mixtures. Also, a higher initial degradation was observed for specimens subjected to higher loads for unreinforced and reinforced mixtures.

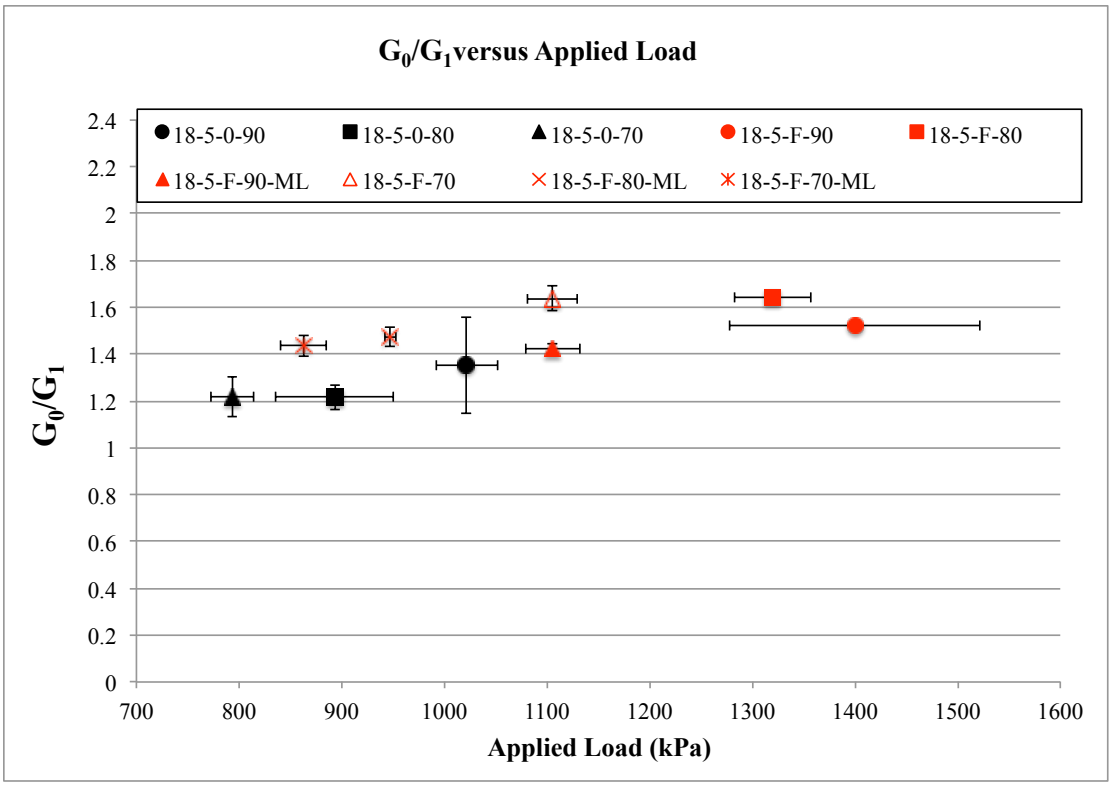

Figure 5.94: Initial shear modulus degradation *versus* applied load for soil-cement and soil-cement-fibre benchmark specimens under original and modified loading

6 FATIGUE TESTS

This chapter presents the results for the fatigue tests carried out during this research. Firstly, it is presented the data for the soil-cement tests, analysing the influence of percentage of applied load on the number of cycles and radial displacement. Then, the data for soil-cement-fibre admixtures is presented, where the same variables are analysed for the stipulated load. Finally, the results and analysis are discussed as a whole. The moulding data of the following tests are presented in Appendices C.

Initially, the stipulated experimental program for fatigue testing included flexural tensile (FT) tests as well as split tensile (ST). However, the maximum load for FT tests ranged from 0.3 to 0.8 kN whilst the maximum load spectrum for ST tests range from 0.7 to 1.75 kN. The equipment used presented an intrinsic variability of applied load peaks of on average 4.5% of the targeted load (from 20 to 95 N). When it was attempted to apply lower loads, the equipment would struggle to work at such low air pressures, leading to a greater variability of loading between peaks, which led to specimen failure very quickly due to application of a peak load higher than the maximum baring load of the specimen. Various attempts were made to remediate this issue, the pressure regulator valve was recalibrated; the routine was checked and altered; the load cell was exchanged; the wiring redone and voltage amplitude of acquisition board altered. Nothing helped with this issue, thus, it was decided to only carry out the tests for ST since the load range was higher and this issue would not interfere so much with the results.

For the same reason, it was decided that rather than maintaining a fixed load percentage (90%) whilst varying the $\eta/C_{iv}^{0.28}$ used, it more consistent results would be observed by evaluating the progression of number of cycles due to fatigue (N_f) for three different loading conditions (90. 80 and 70% of the predicted maximum load) for a benchmark mixture – 18 kN/m^3, 5% cement content, 0 and 0.5% of fibre insertion, similarly to what was done for the CUC tests. Besides these tests, fatigue tests were carried out for two other mixtures for 80% of the estimated maximum load. The first had a higher $\eta/C_{iv}^{0.28}$ than the benchmark (18 kN/m^3; 3% cement content; 0 and 0.5% of fibre), and the second a lower $\eta/C_{iv}^{0.28}$ (19 kN/m^3; 5% cement content; 0 and 0.5% of fibre).

The measurement of displacement is carried out at the faces of the radius and not at the centre of the disk – which would be extremely difficult to do in this kind of test. Given this, the displacement measured is not the actual strain, but the displacement at the radius that is dumped by the loss of energy from the centre of the specimen until its surface.

For each test, data was acquired from two LVDTs and load cell. The response variables were: radial displacement – ε_r [%]; applied load (LA) [kPa]; and number of cycles – N_f. It was stipulated that the maximum N_f would be of 260 000 cycles, which represents around 36 h of testing.

6.1 SOIL-CEMENT

In this topic it is presented the results for soil-cement mixtures. The value of the maximum load for each specimen studied was attained from the data presented in item 4.1.2. The $\eta/C_{iv}^{0.28}$ of each specimen was calculated after moulding of the specimen. Table 6.1 presents the values attained for the moulded specimens.

Table 6.1: Soil-cement mixtures: loading determination for fatigue tests

Mixture	Rep.	Ideal Load (%)	$\eta/Civ^{0,28}$	Average Static Load (N)	Average Static q_t (kPa)	% of load	% Static q_u (kPa)	Applied q_t (kPa)	Std. Dev. Peaks	Percentage of Peak Var. (%)	Applied Percentage (%)
18 kN/m³ - 3% cement	I	80	28.22	699.61	88.94	559.69	71.15	70.23	2.83	4.03	78.96
	II	80	29.07					68.10	2.71	3.98	76.57
	III	80	28.02					70.34	3.63	5.16	79.09
18 kN/m³ - 5% cement	I	90	25.35	1143.33	144.53	1029.00	130.08	133.25	6.52	4.89	92.20
	II	90	25.57					128.03	6.46	5.05	88.58
	III	90	25.81					127.76	7.68	6.01	88.40
	I	80	25.94	1143.33	144.46	914.67	115.57	120.91	5.02	4.15	83.70
	II	89	25.03					111.98	3.84	3.43	77.51
	III	80	25.45					116.66	3.80	3.26	80.75
	I	70	24.78	1143.33	145.83	800.33	102.08	102.78	4.05	3.94	70.48
	II	70	25.24					96.84	6.84	7.06	66.40
	III	70	24.92					101.50	4.25	4.19	69.60
19 kN/m³ - 5% cement	I	80	21.25	1744.79	221.71	1395.83	177.37	170.69	7.39	4.33	76.99
	II	80	21.85					171.09	9.61	5.62	77.17
	III	80	22.24					167.10	3.51	2.10	75.37

The acquired data is presented in the form of graphs. Each combination is presented in the form of two graphs. The first presents the ε_r *versus* N_f data for the three repetitions. The second presents the q_t *versus* N_f data for the three repetitions. Due to large number of data only the data for specified intervals of cycles are presented in the graphs (1, 10, 100, 500, 1000, 5000, 10000, 30000, 50000, 10000, 150000, 200000, 260000) until rupture occurred.

6.1.1 Applied load percentage: 90%

A summary of the results for specimens tested at 90% of its maximum estimated load is presented in table 6.2. From the presented data, it is possible to infer that the dispersion of $\eta/C_{iv}^{0.28}$ for the replicas is less than 0.9%. The dispersion of data for the applied load is less than 2.5%. Indicating similar initial and loading conditions for the studied specimens. Dispersion on the number of cycles was observed, the second specimen presented higher N_f, however, the values were within the same order of magnitude.

Figures 6.1 and 6.2 present the data for tensile strength and radial displacement in, respectively. In figure 6.1 it is observed a stable average of load peaks through cycling for all repetitions and an abrupt loss in strength, indicating a fragile rupture. From figure 6.2 it is also observed a stable radial deformation through cycling, nevertheless, the values for the repetitions varied slightly. The first specimen presented an average ε_r of 0.5% whilst the second and third presented an average ε_r of 0.3% until rupture. The higher ε_r might be due to a higher overall applied load (3.5% higher).

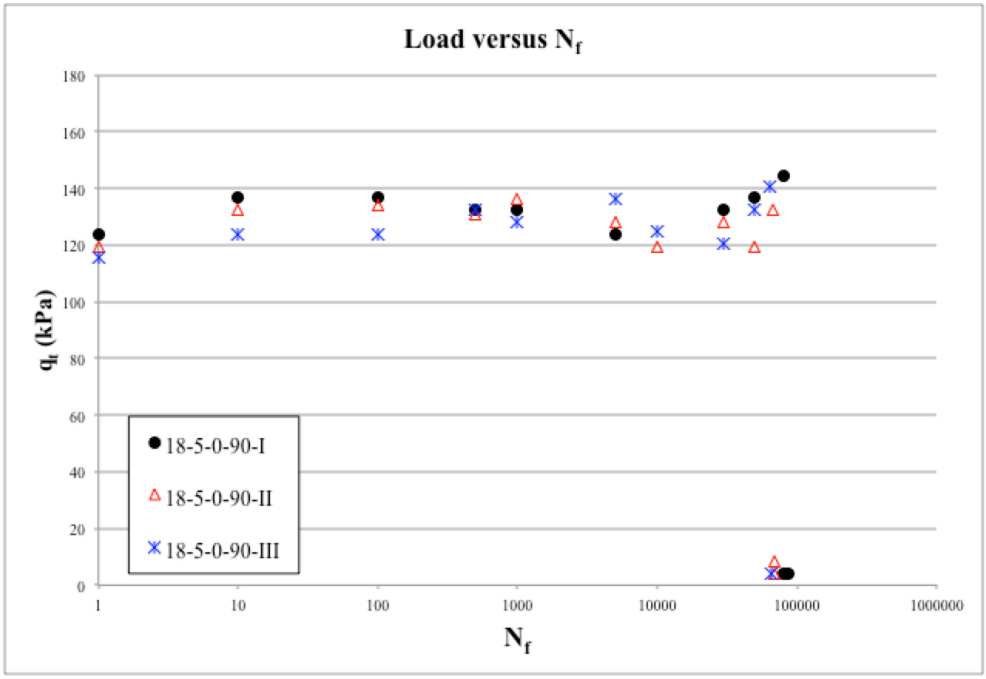

Figure 6.1: Tensile strength *versus* N_f for fatigue testing for specimens 18-5-0-90-I, II and III

Table 6.2: Soil-cement mixtures: loading determination for benchmark mixtures at 90% of loading fatigue tests

Mixture	Rep.	Ideal Load (%)	$\eta/Civ^{0,28}$	Applied q_t (kPa)	Applied Percentage (%)	Numebr of cycles
18 kN/m^3 - 5% cement	I	90	25.35	133.25	92.20	68200
	II	90	25.57	128.03	88.58	80160
	III	90	25.81	127.76	88.40	64590

6.1.2 Applied load percentage: 80%

For this load percentage there were three different mixtures made, as mentioned previously. The first was the benchmark combination – figures 6.3 and 6.4. The second was the 18 kN/m^3, 3% cement content specimens – figures 6.5 and 6.6 – that have higher $\eta/C_{iv}^{0.28}$ values than the benchmark mixture. The third were lower $\eta/C_{iv}^{0.28}$ specimens (19 kN/m^3, 5% cement content) – figures 6.7 and 6.8. The results for these tests are presented in the following two topics.

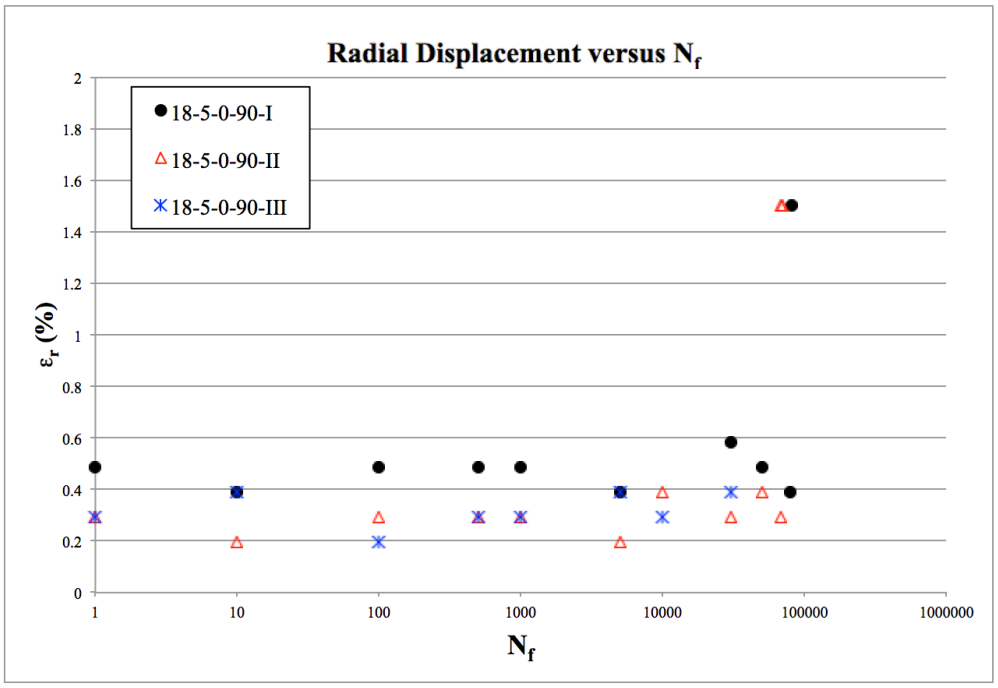

Figure 6.2: Radial displacement *versus* N_f for fatigue testing for specimens 18-5-0-90-I, II and III

6.1.2.1 Benchmark mixtures

A summary of the results for benchmark specimens tested at 80% of its maximum estimated load is presented in table 6.3. From the presented data, it is possible to infer that the dispersion of $\eta/C_{iv}^{0.28}$ for the replicas is less than 1.8%. The dispersion of data for the applied load is less than 3.9%. Indicating similar initial and loading conditions for the studied specimens. As observed from the previous loading percentage, dispersion on the number of cycles was observed, however, the values were within the same order of magnitude.

Table 6.3: Soil-cement mixtures: loading determination for benchmark mixtures at 80% of loading fatigue tests

Mixture	Rep.	Ideal Load (%)	$\eta/Civ^{0,28}$	Applied q_t (kPa)	Applied Percentage (%)	Numebr of cycles
18 kN/m^3 - 5% cement	I	80	25.94	120.91	83.70	94157
	II	89	25.03	111.98	77.51	90870
	III	80	25.45	116.66	80.75	86282

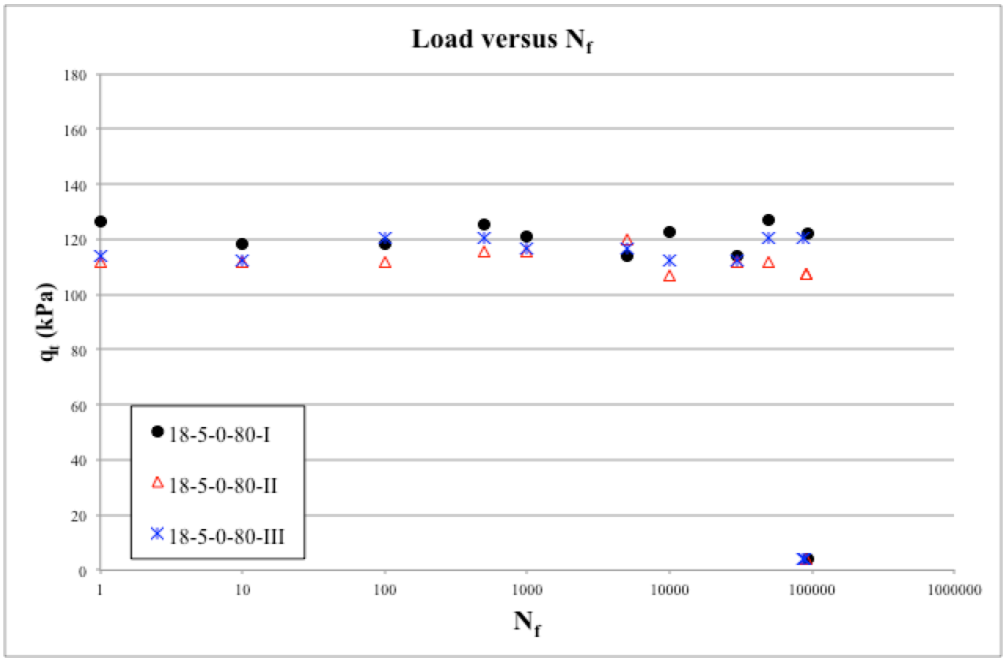

Figure 6.3: Tensile strength *versus* N_f for fatigue testing for specimens 18-5-0-80-I, II and III

Figures 6.3 and 6.4 present the data for tensile strength and radial displacement in, respectively. In figure 6.3 it is observed a stable average of load peaks through cycling for all repetitions and an abrupt loss in strength, indicating a fragile rupture. From figure 6.4 it is also observed a stable radial deformation through cycling. All repetitions presented an average ε_r of 0.4% until rupture. This indicates consistent results from the repetitions.

6.1.2.2 Alternative mixtures

As mentioned at the beginning of this chapter, two different mixtures were made in order to assess the impact of $\eta/C_{iv}^{0.28}$ in the fatigue life. Firstly, it is presented the data for the mixture with higher $\eta/C_{iv}^{0.28}$ values than the established benchmark, meaning that the specimen has a higher porosity and/or less cementation. For this mixture the porosity was kept constant and the cementation level was reduced. Then, it is presented the data for the mixture with lower $\eta/C_{iv}^{0.28}$ values than the established benchmark, meaning that the specimen has a lower porosity and/or higher cementation. For this mixture the cementation was kept constant and the porosity was reduced.

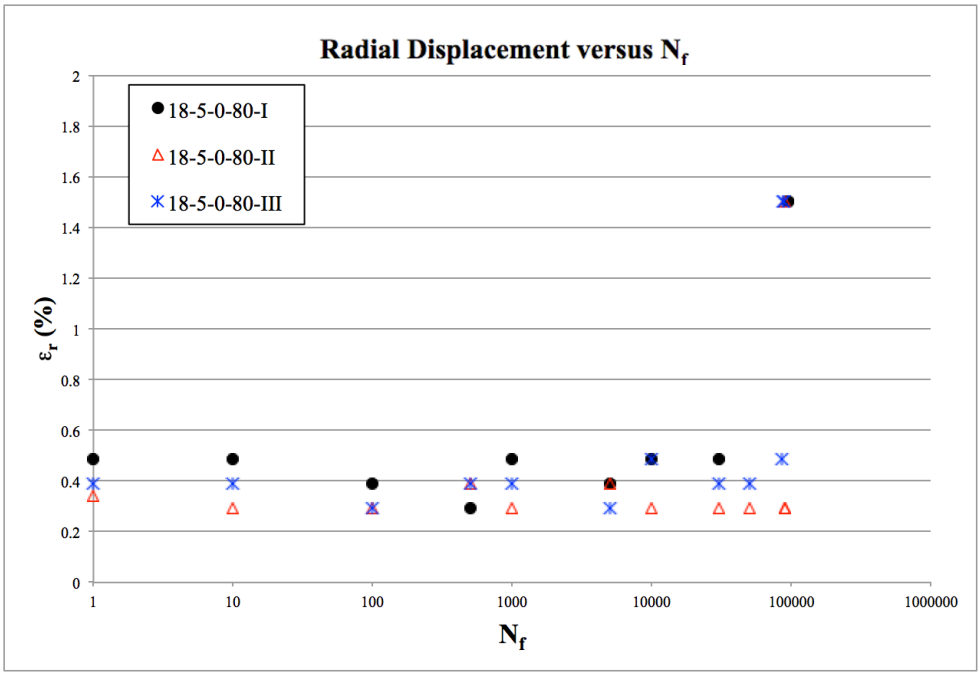

Figure 6.4: Radial displacement *versus* N_f for fatigue testing for specimens 18-5-0-80-I, II and III

A summary of the results for 18-3-0 specimens tested at 80% of its maximum estimated load is presented in table 6.4. From the presented data, it is possible to infer that the dispersion of $\eta/C_{iv}^{0.28}$ for the replicas is less than 2%. The dispersion of data for the applied load is less than 2%. Indicating similar initial and loading conditions for the studied specimens. As observed from the previous data, dispersion on the number of cycles was observed. For the second specimen the N_f was lower than the other two and not in the same order of magnitude. This might be due to a higher a $\eta/C_{iv}^{0.28}$ than the attained for the other two.

Table 6.4: Soil-cement mixtures: loading determination for 18-3-0 mixtures at 80% of loading fatigue tests

Mixture	Rep.	Ideal Load (%)	$\eta/Civ^{0,28}$	Applied q_t (kPa)	Applied Percentage (%)	Numebr of cycles
18 kN/m^3 - 3% cement	I	80	28.22	70.23	78.96	72877
	II	80	29.07	68.10	76.57	9659
	III	80	28.02	70.34	79.09	49700

Figures 6.5 and 6.6 present the data for tensile strength and radial displacement in, respectively. In figure 6.5 it is observed a stable average of load peaks through cycling for all

repetitions and an abrupt loss in strength, indicating a fragile rupture. From figure 6.6 it is also observed a stable radial deformation through cycling. The second specimen presented a lower average ε_r (0.2%), which is lower than the observed for the other repetitions. The first presented an average ε_r of 0.4%, whilst the third presented an average ε_r of 0.3%, until rupture. The lower ε_r for the second repetition suggests a more rigid specimen than the other two.

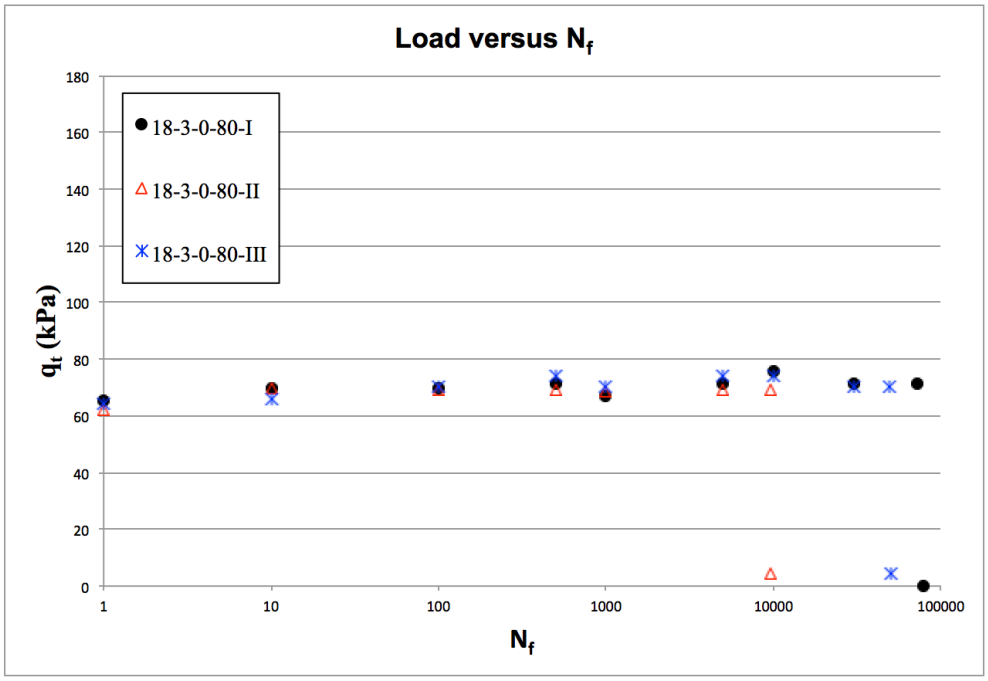

Figure 6.5: Tensile strength *versus* N_f for fatigue testing for specimens 18-3-0-80-I, II and III

A summary of the results for 19-5-0 specimens tested at 80% of its maximum estimated load is presented in table 6.5. From the presented data, it is possible to infer that the dispersion of $\eta/C_{iv}^{0.28}$ for the replicas is less than 2.3%. The dispersion of data for the applied load is less than 1.3%. Indicating similar initial and loading conditions for the studied specimens. As observed from previous data, dispersion on the number of cycles was observed. However, the values were within the same order of magnitude.

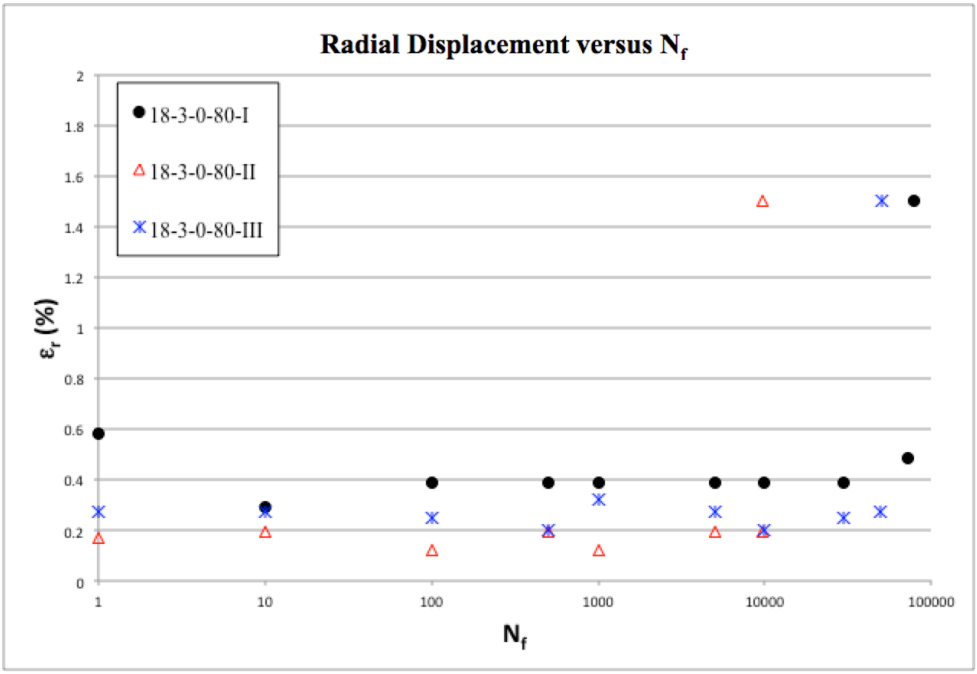

Figure 6.6: Radial displacement *versus* N_f for fatigue testing for specimens 18-3-0-80-I, II and III

Figures 6.7 and 6.8 present the data for tensile strength and radial displacement in, respectively. In figure 6.7 it is observed a stable average of load peaks through cycling for all repetitions and an abrupt loss in strength, indicating a fragile rupture. From figure 6.8 it is also observed a stable radial deformation through cycling. All repetitions presented an average ε_r of 0.1% until rupture. The lower values of radial displacement indicate that this mixture is more rigid than the other ones presented thus far, which was expected since the specimen has a lower void ratio than the other mixtures.

Table 6.5: Soil-cement mixtures: loading determination for 19-5-0 mixtures at 80% of loading fatigue tests

Mixture	Rep.	Ideal Load (%)	$\eta/Civ^{0,28}$	Applied q_t (kPa)	Applied Percentage (%)	Numebr of cycles
19 kN/m^3 - 5% cement	I	80	21.25	170.69	76.99	123300
	II	80	21.85	171.09	77.17	120000
	III	80	22.24	167.10	75.37	109000

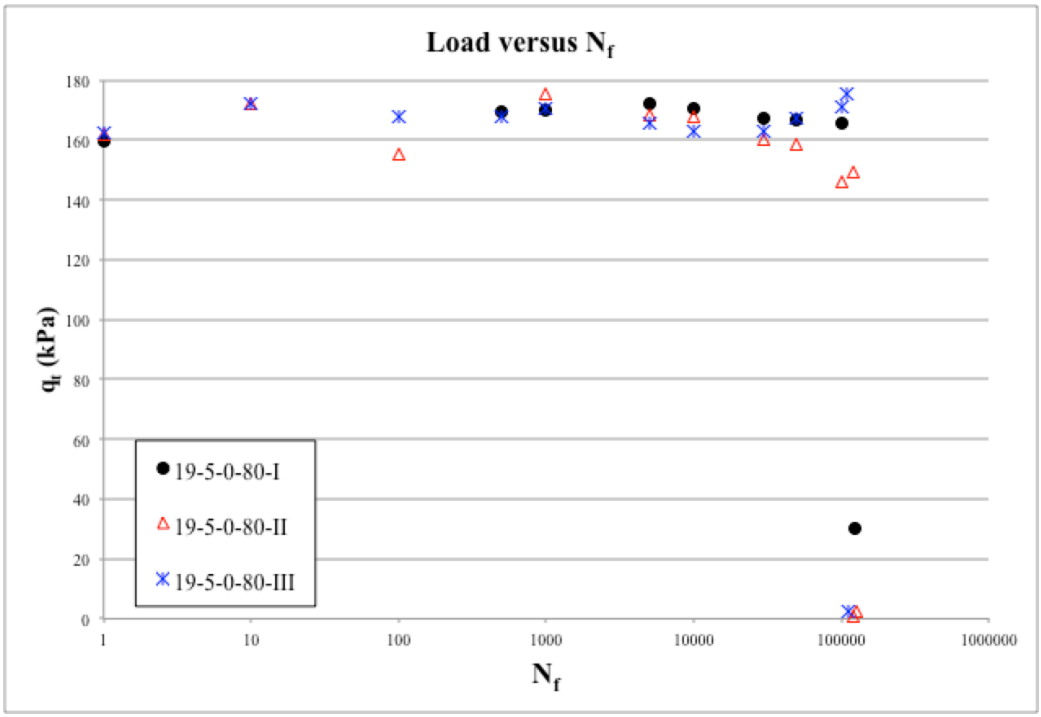

Figure 6.7: Tensile strength *versus* N_f for fatigue testing for specimens 19-5-0-80-I, II and III

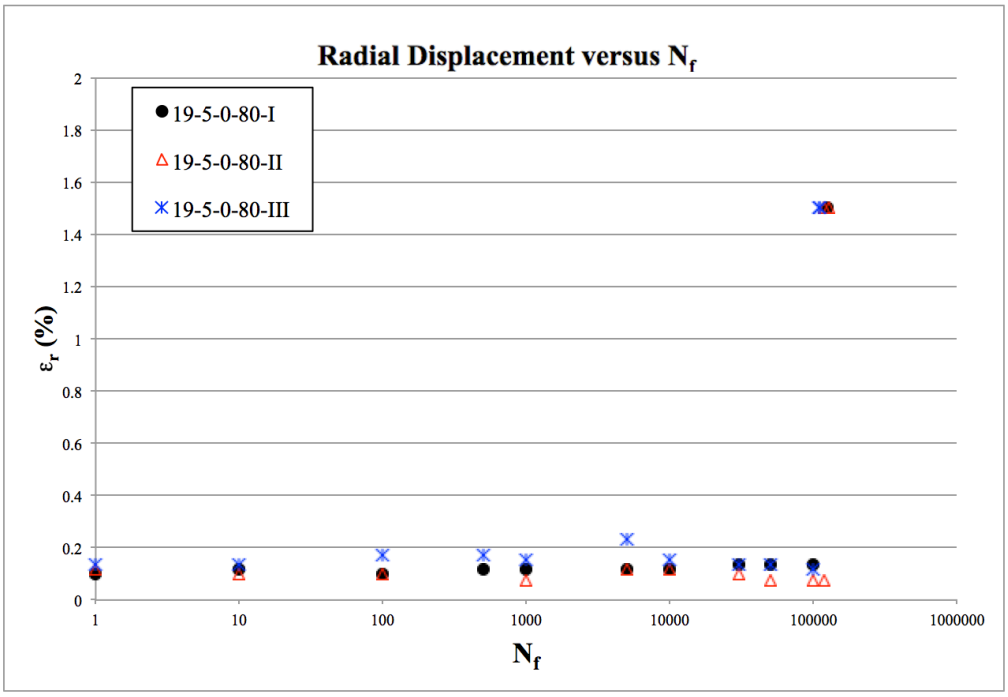

Figure 6.8: Radial displacement *versus* N_f for fatigue testing for specimen 19-5-0-80-I, II and III

6.1.3 Applied load percentage: 70%

A summary of the results for benchmark specimens tested at 70% of its maximum estimated load is presented in table 6.6. From the presented data, it is possible to infer that the dispersion of $\eta/C_{iv}^{0.28}$ for the replicas is less than 1%. The dispersion of data for the applied load is less than 3.2%. Indicating similar initial and loading conditions for the studied specimens. For this load percentage none of the repetitions failed within the established maximum number of cycles (260000), which is consistent with the data presented for 90 and 80% of applied loading.

Table 6.6: Soil-cement mixtures: loading determination for benchmark mixtures at 70% of loading fatigue tests

Mixture	Rep.	Ideal Load (%)	$\eta/Civ^{0,28}$	Applied q_t (kPa)	Applied Percentage (%)	Numeber of cycles
18 kN/m^3 - 5% cement	I	70	24.78	102.78	70.48	267100
	II	70	25.24	96.84	66.40	263050
	III	70	24.92	101.50	69.60	260300

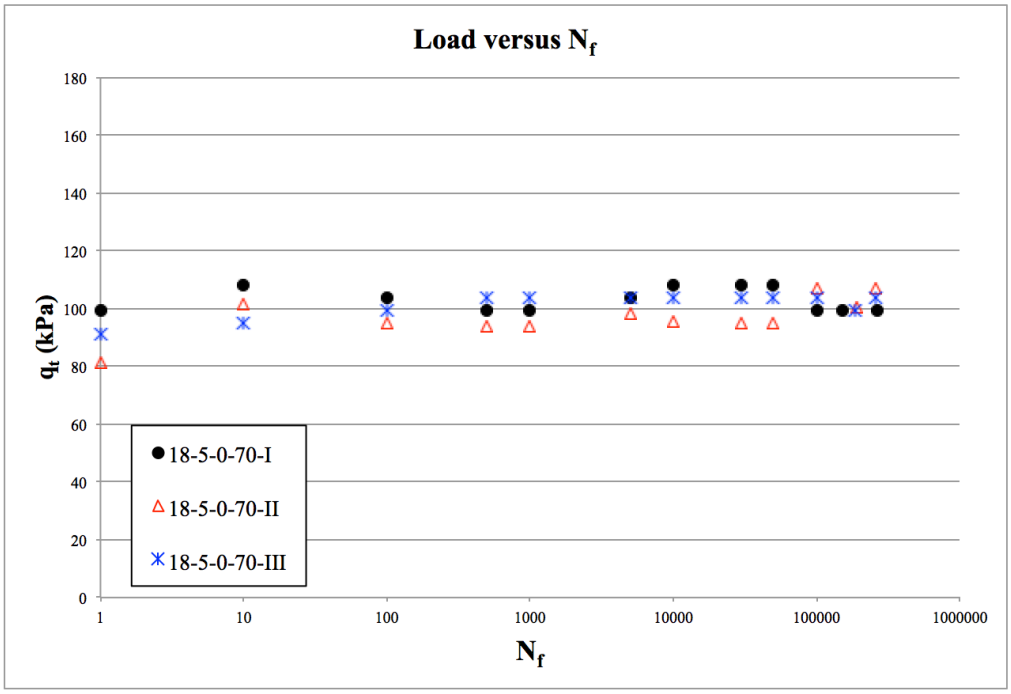

Figure 6.9: Tensile strength *versus* N_f for fatigue testing for specimens 18-5-0-70-I, II and III

Figures 6.9 and 6.10 present the data for tensile strength and radial displacement in, respectively. In figure 6.9 it is observed a stable and consistent average of load peaks through cycling for all repetitions. From figure 6.10 it is also observed a stable radial deformation through cycling. The first specimen presented a lower average ε_r (0.2%), which is lower than the observed for the other repetitions. The second presented more variability through cycles and the other two but with an average ε_r of 0.4%. The third presented an average ε_r of 0.3%. The lower ε_r for the first repetition suggests a more rigid specimen than the other two.

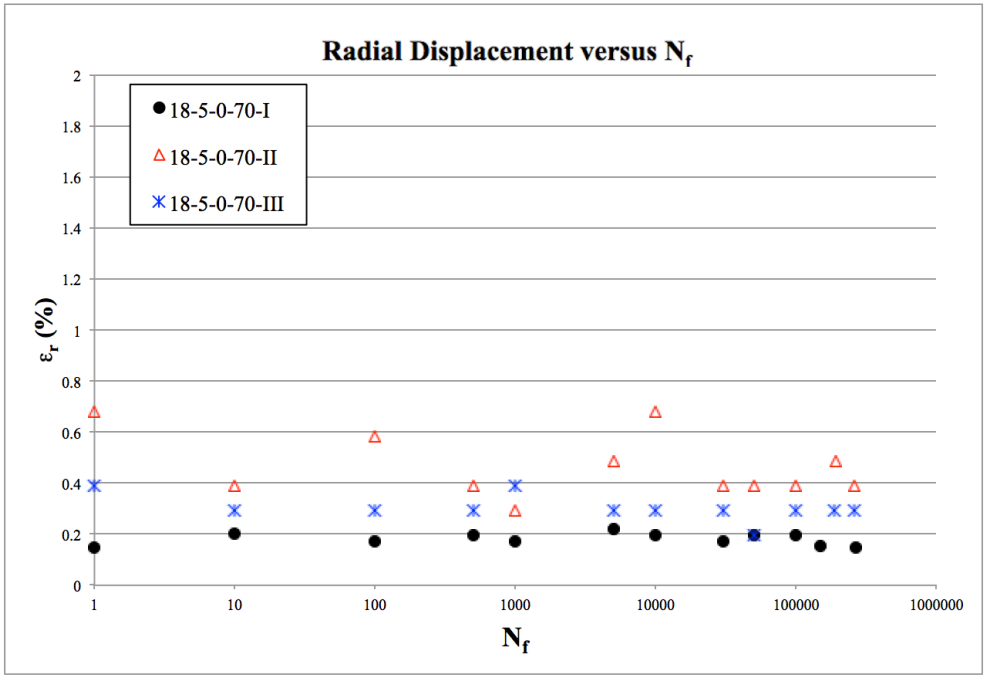

Figure 6.10: Radial displacement *versus* N_f for fatigue testing for specimens 18-5-0-70-I, II and III

6.2 SOIL-CEMENT-FIBRE

In this topic it is presented the results for soil-cement-fibre admixtures. The value of the maximum load for each specimen studied was attained from the data presented in item 4.1.2. The $\eta/C_{iv}^{0.28}$ of each specimen was calculated after moulding of the specimen. Table 6.7 presents the values attained for the moulded specimens a dash was used when the specimens did not last enough cycles to assess the standard deviation of the loading peaks.

The acquired data is presented in the form of graphs. Each combination is presented in the form of two graphs. The first presents the q_t *versus* N_f data for the three repetitions. The second presents the ε_r *versus* N_f data for the three repetitions. Since fibre-reinforced

specimens did not withstand many cycles, all cycles are presented until rupture occurred. As expected, fibre-reinforced mixtures presented a more ductile failure mode, thus a maximum radial deformation should be used to determine failure. For the present research, given that for tensile tests radial deformation are lower than the observed by axial compression tests, a ε_r of 0.8% was chosen as the failure parameter.

Table 6.7: Soil-cement-fibre mixtures: loading determination for fatigue tests

Mixture	Rep.	Ideal Load (%)	$\eta/Civ^{0.28}$	Average Static Load (N)	Average Static q_t (kPa)	% of load	% Static q_u (kPa)	Applied q_t (kPa)	Std. Dev. Peaks	Percentage of Peak Var. (%)	Applied Percentage (%)
18 kN/m³ - 3% cement - 0.5% fibre	I	80	29.30	698.65	87.95	558.92	70.36	65.07	3.63	5.58	73.99
	II	80	29.50					73.76	2.54	3.44	83.87
	III	80	29.34					72.13	3.55	4.92	82.02
18 kN/m³ - 5% cement - 0.5% fibre	I	90	25.45	989.57	124.24	890.61	111.81	113.36	-	-	91.25
	I	90	26.01					115.65	5.65	4.89	93.09
	II	90	25.54					115.78	6.12	5.29	93.19
	I	80	25.88	989.57	124.61	791.65	99.69	103.02	2.77	2.69	82.68
	II	80	25.72					104.37	2.69	2.58	83.76
	III	80	25.97					96.41	-	-	77.37
	I	70	25.75	989.57	124.62	692.70	87.23	92.34	3.50	3.79	74.10
	II	70	25.93					92.58	4.01	4.33	74.29
	III	70	26.07					90.36	3.56	3.94	72.51
19 kN/m³ - 5% cement - 0.5% fibre	I	80	24.85	1833.07	226.41	1466.46	181.13	177.71	11.48	6.46	78.49
	II	80	24.11					155.02	-	-	68.47
	III	80	23.53					164.55	7.01	4.26	72.68

6.2.1 Applied load percentage: 90%

A summary of the results for reinforced specimens tested at 90% of its maximum estimated load is presented in table 6.8. From the presented data, it is possible to infer that the dispersion of $\eta/C_{iv}^{0.28}$ for the replicas is less than 1.2%. The dispersion of data for the applied load is also less than 1.2%. Indicating similar initial and loading conditions for the studied specimens. Dispersion on the number of cycles was observed. The first specimen only lasted two cycles. The remaining two specimens were within the same order of magnitude. The lower number of cycles in fatigue testing for fibre-reinforced mixtures might be due to an imposed anisotropy of the specimen after moulding the specimen with fibre insertion. This will be discussed in the discussion section of this chapter.

Table 6.8: Soil-cement-fibre mixtures: loading determination for benchmark mixtures at 90% of loading fatigue tests

Mixture	Rep.	Ideal Load (%)	$\eta/Civ^{0,28}$	Applied q_t (kPa)	Applied Percentage (%)	Numeber of cycles
18 kN/m^3 - 5% cement - 0.5% fibre	I	90	25.45	113.36	91.25	2
	II	90	26.01	115.65	93.09	11
	III	90	25.54	115.78	93.19	10

Figures 6.11 and 6.12 present the data for tensile strength and radial displacement in, respectively. In figure 6.11 it is observed a stable average of load peaks through cycling for the second and third repetitions that had a more sizable number of cycles for any assessments to be made. There was a gradual loss in strength with loading for all specimens, indicating a ductile rupture. From figure 6.12 it is also observed a stable radial deformation through cycling for repetitions II and III until rupture at cycles 11 and 10, respectively. The first repetition reached 0.8% of radial deformation at the second cycle. It is important to note that the radial displacement remained somewhat constant after rupture occurred for specimens I and III even though their load bearing capacity decreased with the progression of load application. The second repetition presented a more pronounced increase in displacement after rupture.

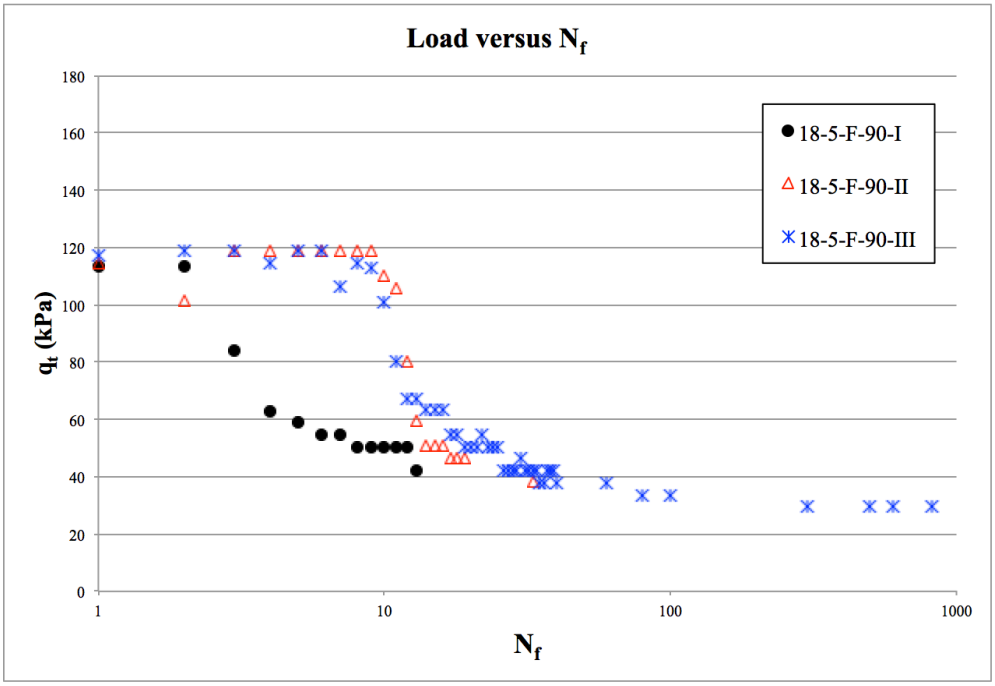

Figure 6.11: Tensile strength *versus* N_f for fatigue testing for specimens 18-5-F-90-I, II and III

6.2.2 Applied load percentage: 80%

Similarly to the tests carried out without fibre, for this load percentage three different mixtures made. The first was the fibre reinforced benchmark combination – figures 6.13 and 6.14. The second was the 18 kN/m^3, 3% cement content, 0.5% fibre addition specimens – figures 6.15 and 6.16 – that have higher $\eta/C_{iv}^{0.28}$ values than the benchmark mixture. The third were lower $\eta/C_{iv}^{0.28}$ specimens (19 kN/m^3, 5% cement content, 0.5% fibre addition) – figures 6.17 and 6.18. The results for these tests are presented in the following two topics.

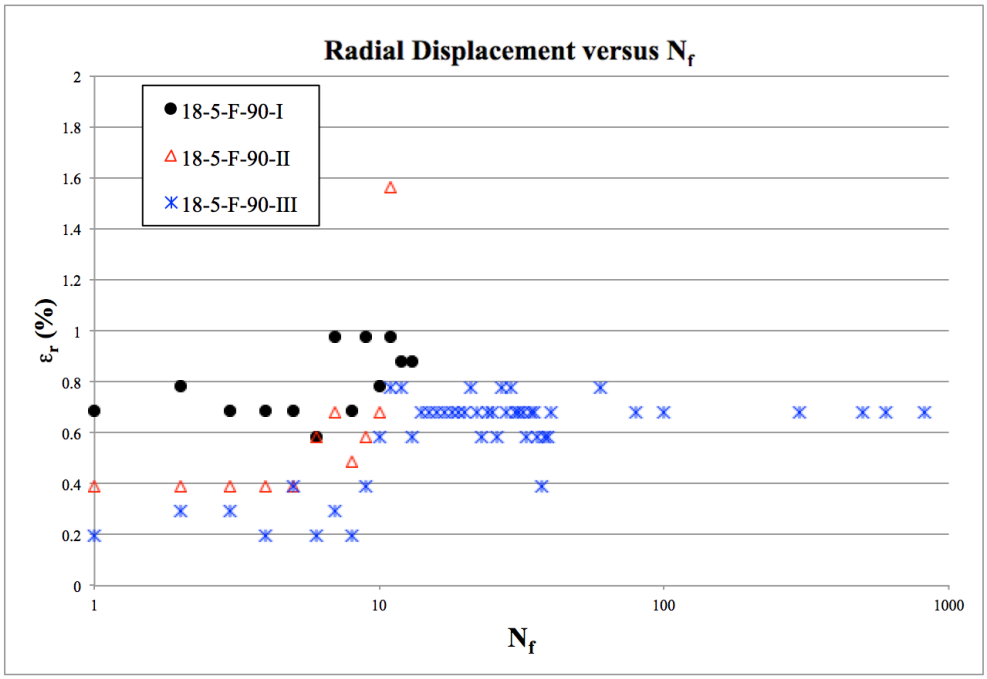

Figure 6.12: Radial displacement *versus* N_f for fatigue testing for specimens 18-5-F-90-I, II and III

6.2.2.1 Benchmark mixture

A summary of the results for the fibre-reinforce benchmark specimens tested at 80% of its maximum estimated load is presented in table 6.9. From the presented data, it is possible to infer that the dispersion of $\eta/C_{iv}^{0.28}$ for the replicas is less than 0.5%. The dispersion of data for the applied load is less than 4.2%. Thus, it was considered that there were equal initial and loading conditions for the studied specimens. However, it is important to note that specimen number three failed after three cycles and did not bear the stipulated load, this might be due a variation in the specimen caused by a less cemented matrix or a matrix with weaker

cementitious bonds. If the third specimen is not taken into account, de dispersion of data for applied load is of less than 1%. Once again, dispersion on the number of cycles was observed.

Figures 6.13 and 6.14 present the data for tensile strength and radial displacement in, respectively. In figure 6.13 it is observed a stable average of load peaks through cycling for the first and second repetitions that presented a more sizable number of cycles for any assessments to be made. There was a gradual loss in strength with loading for all specimens, reinforcing the observation made previously of a ductile rupture. From figure 6.14 it is observed more disperse data from radial deformation through cycling for the first repetition. For the first cycle a high deformation was measured, almost reaching the failure criteria, this might have been cause by a remnant accommodation of the specimen even after the 10 accommodation cycles, or even an initial deformation that led to a reduction of voids in the matrix. After this initial displacement there were lower overall values, especially after 10 cycles where ε_r was around 0.3%. This might be due to a better absorption of the imposed load by the specimen structure after the initial deformation. At the 28th cycle the specimen reached the failure threshold established. The second specimen reached failure after the 15th cycle after maintaining stable ε_r values around 0.5%. As for the third specimen, as mentioned previously, it did not bear the stipulated load and failed after three cycles, after a slight decrease in ε_r for the second cycle, probably caused by the collapse of the cemented structure, the specimen reached failure after the third cycle.

Table 6.9: Soil-cement-fibre mixtures: loading determination for benchmark mixtures at 80% of loading fatigue tests

Mixture	Rep.	Ideal Load (%)	$\eta/Civ^{0,28}$	Applied q_t (kPa)	Applied Percentage (%)	Numeber of cycles
18 kN/m^3 - 5% cement - 0.5% fibre	I	80	25.88	103.02	82.68	28
	II	80	25.72	104.37	83.76	15
	III	80	25.97	96.41	77.37	3

6.2.2.2 Alternative mixtures

As the presented for soil-cement tests, two different fibre-reinforced mixtures were made in order to assess the impact of $\eta/C_{iv}^{0.28}$ in the fatigue life. Firstly, it is presented the data for the mixture with higher $\eta/C_{iv}^{0.28}$ values than the established benchmark, meaning that the specimen

has a higher porosity and/or less cementation. For this mixture the porosity was kept constant and the cementation level was reduced. Then, it is presented the data for the mixture with lower $\eta/C_{iv}^{0.28}$ values than the established benchmark, which means that the specimen has a lower porosity and/or higher cementation. For this mixture the cementation was kept constant and the porosity was reduced.

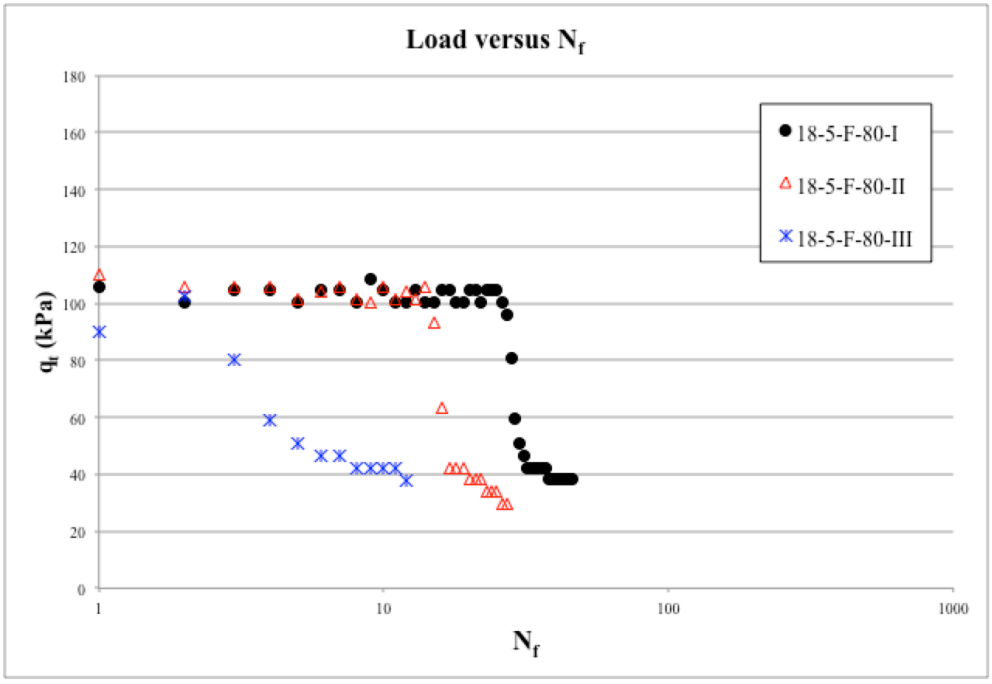

Figure 6.13: Tensile strength *versus* N_f for fatigue testing for specimens 18-5-F-80-I, II and III

A summary of the results for 18-3-F specimens tested at 80% of its maximum estimated load is presented in table 6.10. From the presented data, it is possible to infer that the dispersion of $\eta/C_{iv}^{0.28}$ for the replicas is less than 0.5%. The dispersion of data for the applied load is less than 7%. Indicating similar initial and loading conditions for the studied specimens. However, it is important to note that specimen number one failed after eleven cycles and did not bear the stipulated load this might be due a variation in the specimen caused by a less cemented matrix or a matrix with weaker cementitious bonds. If the first specimen is not taken into account, de dispersion of data for applied load is of less than 1.6%. Once again, dispersion on the number of cycles was observed.

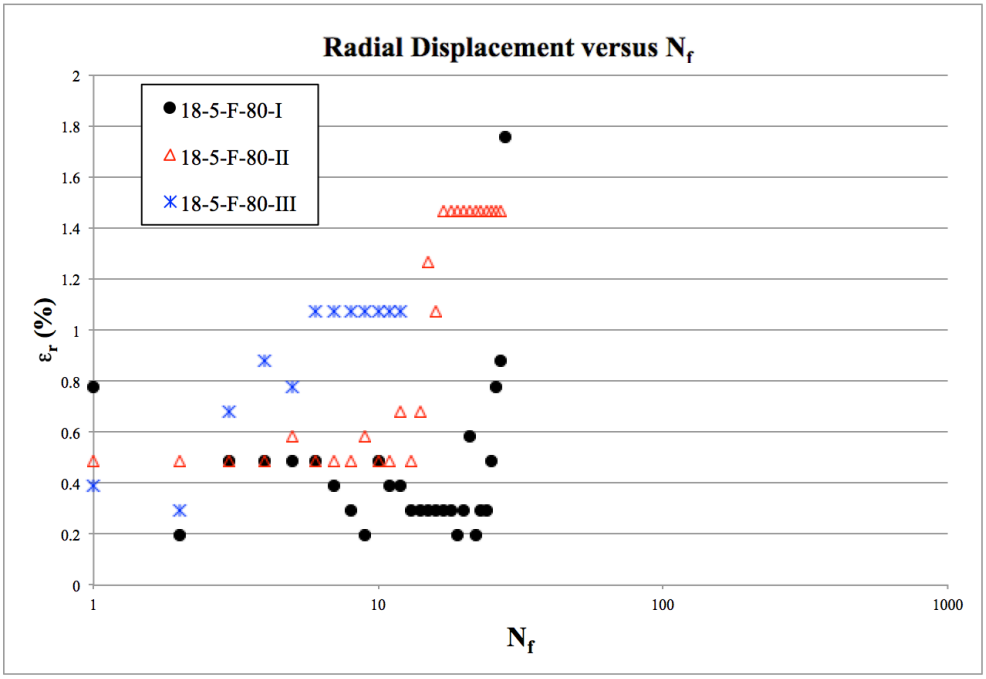

Figure 6.14: Radial displacement *versus* N_f for fatigue testing for specimens 18-5-F-80-I, II and III

Figures 6.15 and 6.16 present the data for tensile strength and displacement in, respectively. In figure 6.15 it is observed a stable average of load peaks through cycling for the second and third, the first specimen presented lower values, slowly increasing with cycling. This indicates a decrease in the void ratio of the mixture, possibly caused by the break of weaker cement bonds, leading to an increase in bearing capacity until a collapse of the structure. There was a gradual loss in strength with loading for all specimens, reinforcing the observation made previously of a ductile rupture.

Table 6.10: Soil-cement-fibre mixtures: loading determination for 18-3-F mixtures at 80% of loading fatigue tests

Mixture	Rep.	Ideal Load (%)	$\eta/Civ^{0,28}$	Applied q_t (kPa)	Applied Percentage (%)	Numeber of cycles
18 kN/m^3 - 3% cement - 0.5% fibre	I	80	29.30	65.07	73.99	11
	II	80	29.50	73.76	83.87	21
	III	80	29.34	72.13	82.02	37

From figure 6.16 it is observed more disperse data from radial deformation through cycling for all repetitions. This might be due to the lower applied load when compared to the other

mixtures or the lower cementation rate of the matrix. The first repetition presented a high deformation for the first couple of cycles almost reaching the failure criteria. This might have been cause by a remnant accommodation of the specimen even after the 10 accommodation cycles, or even an initial deformation that led to a reduction of voids in the matrix caused by the failure of the weaker cement bonds of the structure. After this initial displacement, there were lower overall displacements at around 0.6%. This might be due to a better absorption of the imposed load by the specimen structure after the initial deformation, reaching the failure threshold established at the 11th cycle. The other two specimens presented similar trends but at lower overall displacement. The second specimen reached failure after the 21st cycle with ε_r values around 0.5%. The third specimen reached failure after the 21st cycle with ε_r values around 0.4%. It is important to note that the lower were overall displacement, higher were the number of cycles, indicating that specimens that best absorbed the applied loads within the matrix had higher fatigue life.

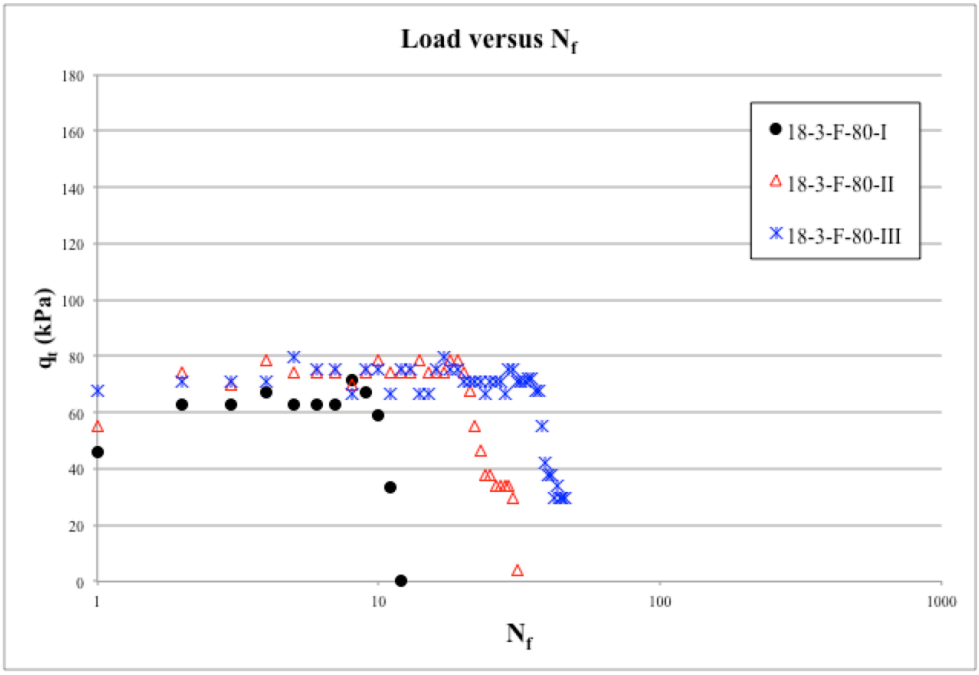

Figure 6.15: Tensile strength *versus* N_f for fatigue testing for specimens 18-3-F-80-I, II and III

A summary of the results for 19-5-F specimens tested at 80% of its maximum estimated load is presented in table 6.11. From the presented data, it is possible to infer that the dispersion of $\eta/C_{iv}^{0.28}$ for the replicas is less than 0.5%. The dispersion of data for the applied load is less

than 7%. Indicating similar initial and loading conditions for the studied specimens. For this mixture the number of cycles observed were very similar.

Figures 6.17 and 6.18 present the data for tensile strength and displacement in, respectively. In figure 6.17 it is observed a consistent average of peak values for the first specimen. For specimens II and III a slow increase in strength with cycling over a couple of cycles, leading to rupture. This indicates a decrease in the void ratio of the mixture, possibly caused by the break of weaker cement bonds, leading to an increase in bearing capacity until a collapse of the structure. There was a gradual loss in strength with loading for all specimens, again indicating a ductile rupture.

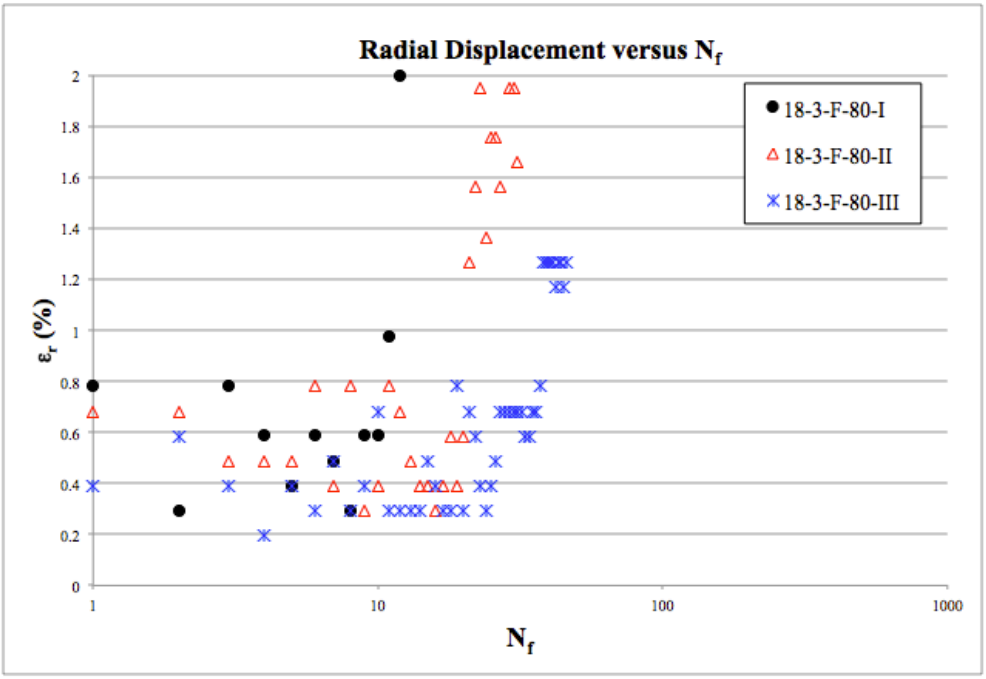

Figure 6.16: Radial displacement *versus* N_f for fatigue testing for specimens 18-3-F-80-I, II and III

Table 6.11: Soil-cement-fibre mixtures: loading determination for 19-5-F mixtures at 80% of loading fatigue tests

Mixture	Rep.	Ideal Load (%)	$\eta/Civ^{0,28}$	Applied q_t (kPa)	Applied Percentage (%)	Numeber of cycles
19 kN/m^3 - 5% cement - 0.5% fibre	I	80	22.84	177.71	78.49	6
	II	80	22.73	155.02	68.47	3
	III	80	22.62	164.55	72.68	4

From figure 6.18 it was observed a stable radial deformation through cycling for all repetitions until rupture at cycles 6, 3 and 4, respectively. The first repetition presented an average ε_r of 0.3% surpassing the threshold at the seventh cycle. The second repetition had an average ε_r of 0.5% for the first two cycles, reaching the radial deformation threshold at the third cycle. The third repetition presented an average ε_r of 0.4% reaching failure at the fourth cycle. Again, the lower the overall displacements, higher were the number of cycles, indicating that specimens that best absorbed the applied loads within the matrix had higher fatigue life.

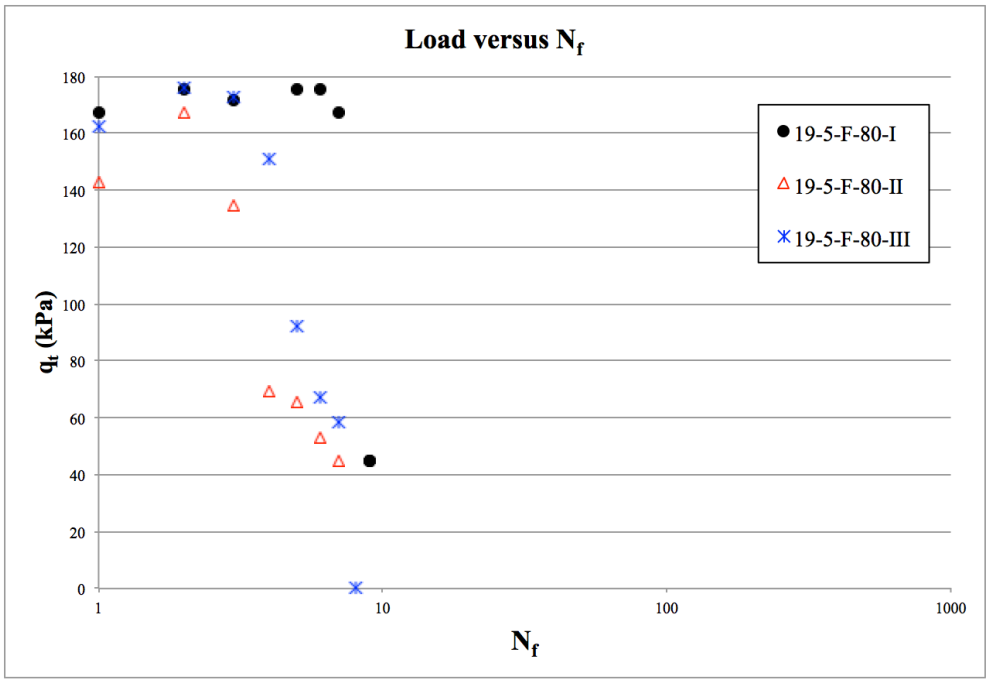

Figure 6.17: Tensile strength *versus* N_f for fatigue testing for specimens 19-5-F-80-I, II and III

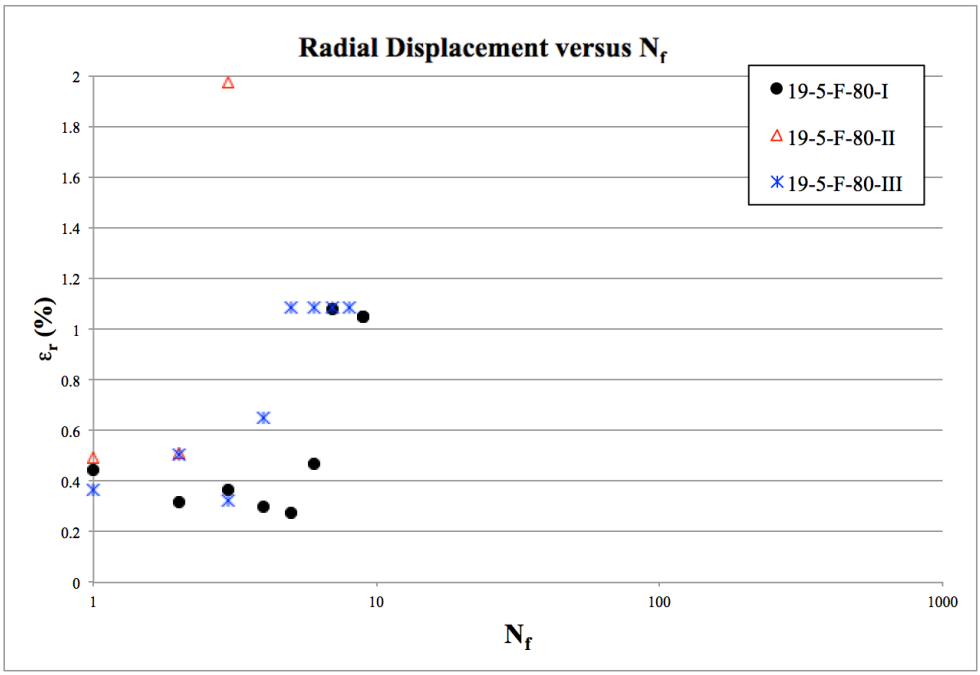

Figure 6.18: Radial displacement *versus* N_f for fatigue testing for specimens 19-5-F-80-I, II and III

6.2.3 Applied load percentage: 70%

A summary of the results for reinforced specimens tested at 70% of its maximum estimated load is presented in table 6.12. From the presented data, it is possible to infer that the dispersion of $\eta/C_{iv}^{0.28}$ for the replicas is less than 1%. The dispersion of data for the applied load is also less than 2%. Indicating similar initial and loading conditions for the studied specimens. Dispersion on the number of cycles was observed. The first specimen lasted 220 cycles whereas the others presented less than a quarter of the number of cycles within the same order of magnitude. This might have happened because the first specimen had a lower $\eta/C_{iv}^{0.28}$, however, the difference between the highest and lowest values was only 1.2%. Therefore, the difference in N_f might be due to intrinsic variability of the moulding and testing process. It is important to highlight that as observed for the unreinforced specimens the N_f increased with the decrease of applied load as expected, even though reinforced specimens had drastically lower fatigue lives.

Table 6.12: Soil-cement-fibre mixtures: loading determination for benchmark mixtures at 70% of loading fatigue tests

Mixture	Rep.	Ideal Load (%)	$\eta/Civ^{0,28}$	Applied q_t (kPa)	Applied Percentage (%)	Numeber of cycles
18 kN/m^3 - 5% cement - 0.5% fibre	I	70	25.75	92.34	74.10	220
	II	70	25.93	92.58	74.29	37
	III	70	26.07	90.36	72.51	49

Figures 6.19 and 6.20 present the data for tensile strength and radial displacement in, respectively. In figure 6.19 it is observed a stable average of load peaks through cycling for all repetitions. There was a gradual loss in strength with loading for all specimens, indicating a ductile rupture. From figure 6.20 it is observed a stable range and average value of radial deformation through cycling for all repetitions until rupture. The only difference from the testing data between the from specimen and the other two is a higher initial ε_r, this initial higher deformation might have reduced the void ratio of the specimen, decreasing its porosity and leading to a higher fatigue life.

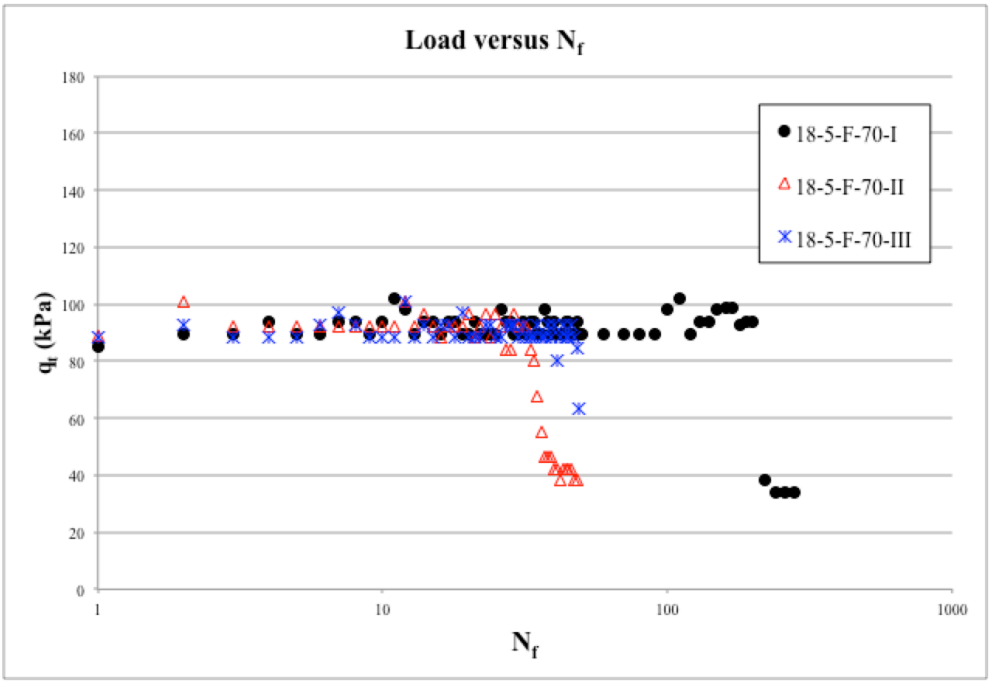

Figure 6.19: Tensile strength *versus* N_f for fatigue testing for specimens 18-5-F-70-I, II and III

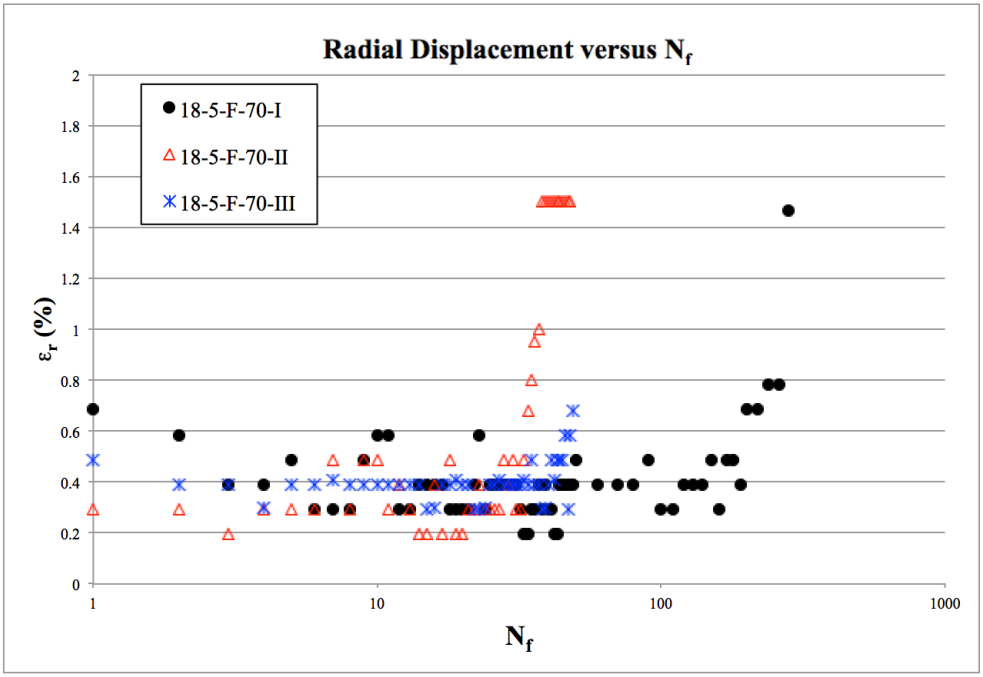

Figure 6.20: Radial displacement *versus* N_f for fatigue testing for specimens 18-5-F-70-I, II and III

6.3 DISCUSSION

In this topic it will be discussed the results presented in this chapter. The result analysis was divided in three items were the implication of fibre insertion was assessed. Firstly, the influence of load percentage applied was discussed. Followed by an analysis of the rupture mode. Finally, the influence of the porosity/volumetric cement content ratio was evaluated.

6.3.1 Rupture mode

From the results obtained for this section of the experimental program it was observed a drastic difference in fatigue life for unreinforced and fibre-reinforced mixtures. Most assessments of fatigue life in literature were made for flexural tensile fatigue (four-point tensile fatigue; direct tensile fatigue) testing (SPECHT, 2000; ZHANG; LI, 2002; SOBHAN; DAS, 2007; DISFANI *et* al., 2014; FEDRIGO *et* al. 2018, 2019; ARULRAJAH *et* al. 2020) since it evaluates the behaviour of the studied material purely under tensile strength, which closer to the behaviour observed for sub-base layers in pavement design. For these tests the aforementioned authors found an increase in fatigue life with fibre insertion. When cyclic split tensile tests (or indirect tensile cyclic tests) are performed in literature, it is usually to evaluate the resilient modulus of the material (MOHAMMAD *et* al., 2000; GASPARD,

MOHAMMAD; WU, 2003; KHATTAK; ALRASHIDI, 2006; TAKAIKAEW *et* al., 2018). This process follows the procedures of the ASTM D 4123, where there it is advised the use of 10 to 50% the maximum split tensile strength over 50 to 200 cycles. The authors mentioned previously found stability or increase in resilient modulus with the addition of fibres. However, these tests aimed to maintain the analysis of the behaviour of the specimen in the elastic rage. As for the tests performed in the present research higher loads are imposed to the specimen (70 to 90%), thus evaluating the behaviour of the specimen on the plastic realm. Little literature was found on the behaviour of split tensile fatigue testing for soil composites (VENSON, 2015; MIGUEL, 2020). Venson (2015) studied the fatigue life for cemented sand under 90% of maximum loading, concluding that fatigue life increased exponentially with the decrease of η/C_{iv}. As for Miguel (2020), the author studied fatigue life of a sulphated dispersive soil treated with pozzolan, carbide lime and glass fibres. The author found a decrease in fatigue life with fibre insertion, but attributed the phenomenon to the fragility of the glass fibres and did not note any unexpected differences in the rupture mode.

Besides the difference in number of cycles, it was observed an unexpected rupture mode of the specimen that can be seen in figure 6.21. The typical failure mode for split tensile tests is a vertical fracture alongside the diameter of the specimen. This typical behaviour was observed for unreinforced specimens (figure 3.4 (a) and (c)). From figure 6.21 it can be observed that besides the expected vertical fracture alongside the diameter there were numerous cracks alongside the height (surface parallel to the loading beam). The developments of this cracks might be responsible for the decrease in bearing capacity for monotonic tests and fatigue life in cyclic testing.

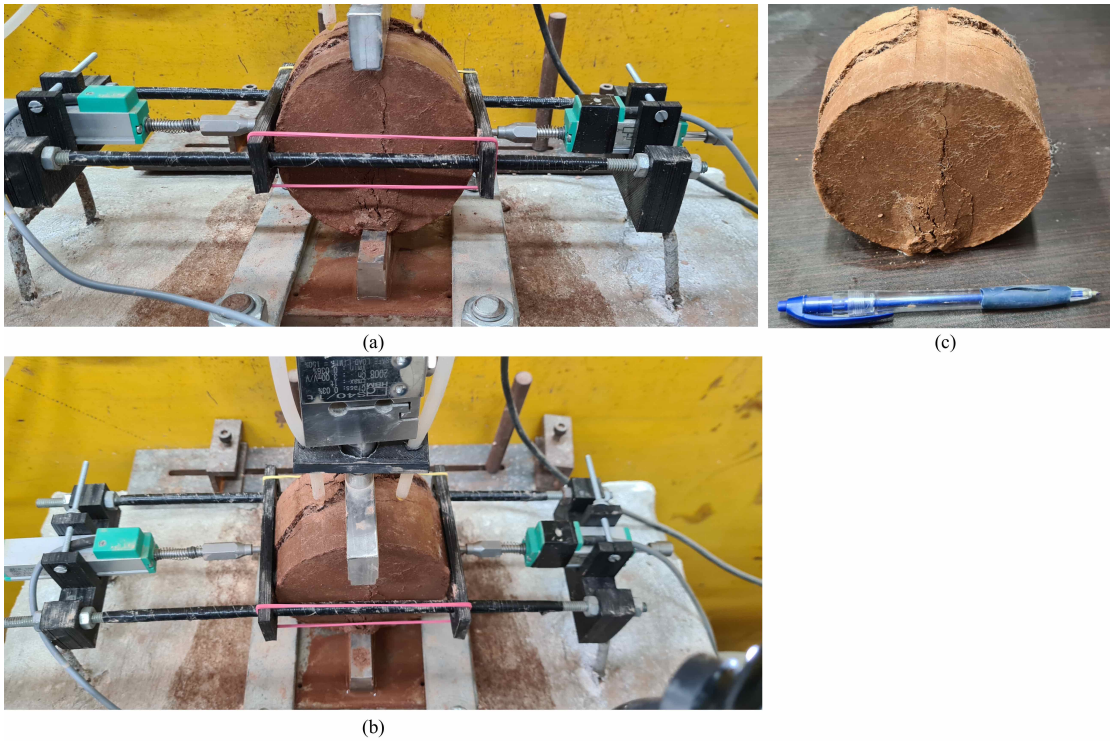

(a) (c)

(b)

Figure 6.21: Rupture mode of fibre-reinforced fatigue specimens (a) front view right after failure (b) upper view right after failure (c) ruptured specimen

Michalowski and Cérmak (2002) and Diambra *et* al. (2007), found that the fibres are distributed anisotropically due to the compaction layers of the reinforced composite, with 97% of the fibres oriented between -45^{o} to +45^{o} of the horizontal plane (perpendicular to compaction). Figure 6.22 shows the typical orientation of fibres of the ruptures specimen in this research, form the pictures presented it is observed that the orientation of the fibres are mostly alongside the horizontal plane in respect to the compaction effort as described by the previously mentioned authors. Taking this into consideration and that plain strain across the height axis can no longer be assumed, it is possible that the fibre insertion imposed an anisotropy to the composite where most of the fibres were on the horizontal plane in respect to the compaction. Usually, the majority of fibre orientation is perpendicular to the applied load. For split tensile tests fibres are mostly oriented parallel to the applied load. Then, when loading is applied, the fibre-reinforced specimens absorb more of the energy allowing higher deformations in all planes. Since there is much lower percentage of fibres in the plane of the height of the specimen (perpendicular to the compaction effort), fibres are not aiding in the absorption of stresses as they are in the other plane. This leads to a break of the cement bonds that cannot withstand the higher tensile stresses impose resulting in a lower fatigue life. Besides this possible cause for the lower fatigue life, as observed by Consoli *et* al (2009), the addition of fibres also disrupts the formation of cementitious bonds,

which could be also a contributor on the reduction of the number of cycles until rupture in fibre-reinforced soils. This phenomenon needs to be studied further in order to assess the parameters (e.g. diameter/height ratio; cement ratio; fibre type, length and percentage) that influence on the observed behaviour.

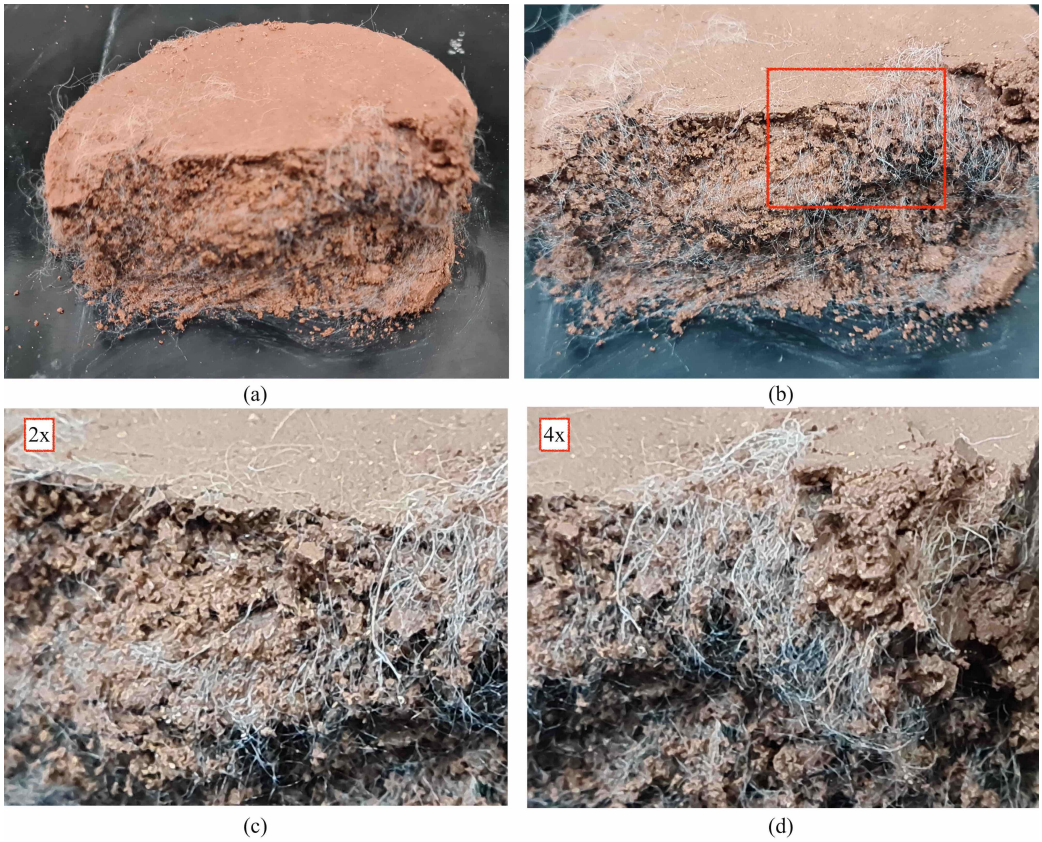

Figure 6.22: Fibre orientation inside ruptured fatigue specimens (a) ruptured specimen (b) full vertical rupture surface (c) two-times zoom (d) four-times zoom

6.3.2 Percentage of load applied

Differently to what was observed for the cyclic unconfined compression tests, the values of load applied to the fibre-reinforced mixtures were similar to the applied for the unreinforced ones. However, instead of observing an improvement in the cyclic behaviour of the composite due to fibre insertion, there was a significant decrease in N_f values, this phenomenon might be due to the disruption of the formation of cementitious bonds due to the fibre additions and/or anisotropy imposed on the specimen because of fibre insertion, as mentioned in the previous topic. Figure 6.23 illustrates this trend by plotting the average applied load for each combination against the average number of cycles until failure or the maximum number of cycles established for the same combinations. For the data presented in this graph the

repetitions that did not result in N_f values on the same order of magnitude of the other ones were not taken into consideration. A logarithmic relationship between applied load and the number of cycles was observed with a good coefficient of determination.

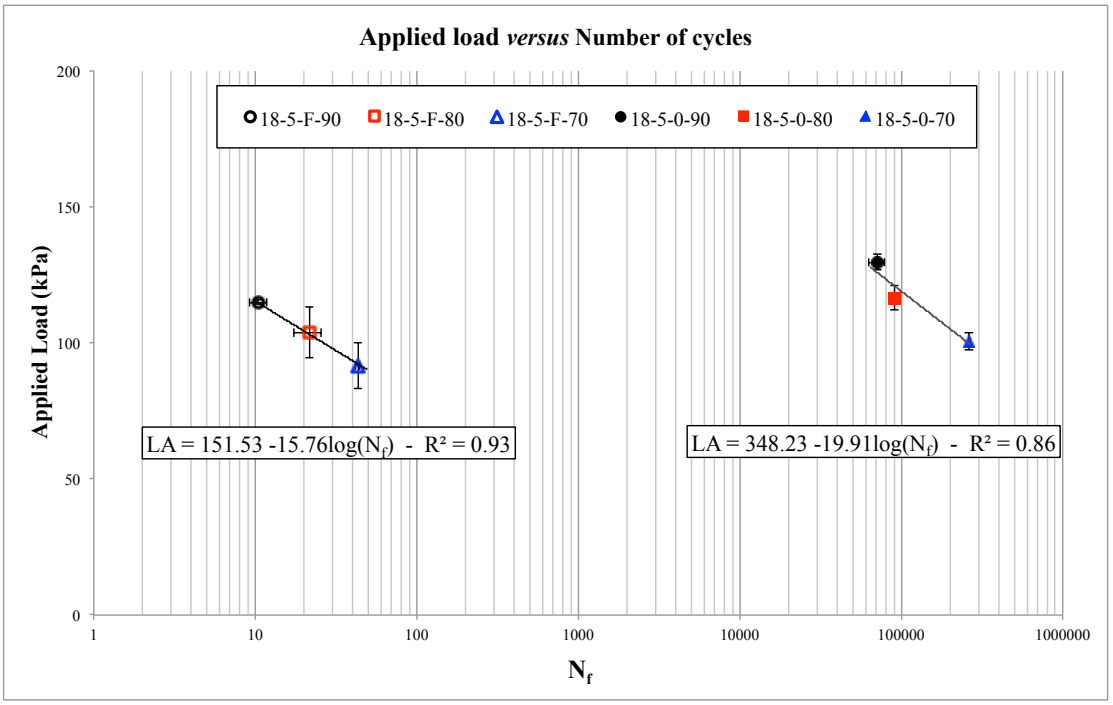

Figure 6.23: Influence of a load on fatigue life for all benchmark specimens

6.3.3 Porosity/volumetric cement content ratio

The data comparing the different porosity/ volumetric cement content for the same percentage of load application (80%) with the number of cycles until failure is presented in figure 6.24. Similarly to what was observed for the different load applied, fibre-reinforced specimens also presented much lower fatigue life than the observed for the unreinforced specimens. Again, this trend might be due to an anisotropy imposed by fibre insertion. For soil-cement mixtures a decrease in $\eta/C_{iv}^{0.28}$ lead to higher values of N_f following a power function relationship. For fibre-reinforced mixtures, there was another difference in trends besides the lower number of cycles until rupture due to fibre insertion. A decrease in fatigue life was observed for the 19-5-F specimen in respect to the other two mixtures with fibres. As mentioned previously, the cementation bonds in the fibre-reinforced specimens might be affected by the presence of the fibres in the matrix, then, when a higher maximum q_t value is applied for the 19-5-F specimens, the cementation bond degrade more rapidly than for the other mixtures, leading to lower number

of cycles, Consoli *et* al. (2009) observed similar trends for monotonic tests when cementation rate was increased for fibre-reinforced specimens.

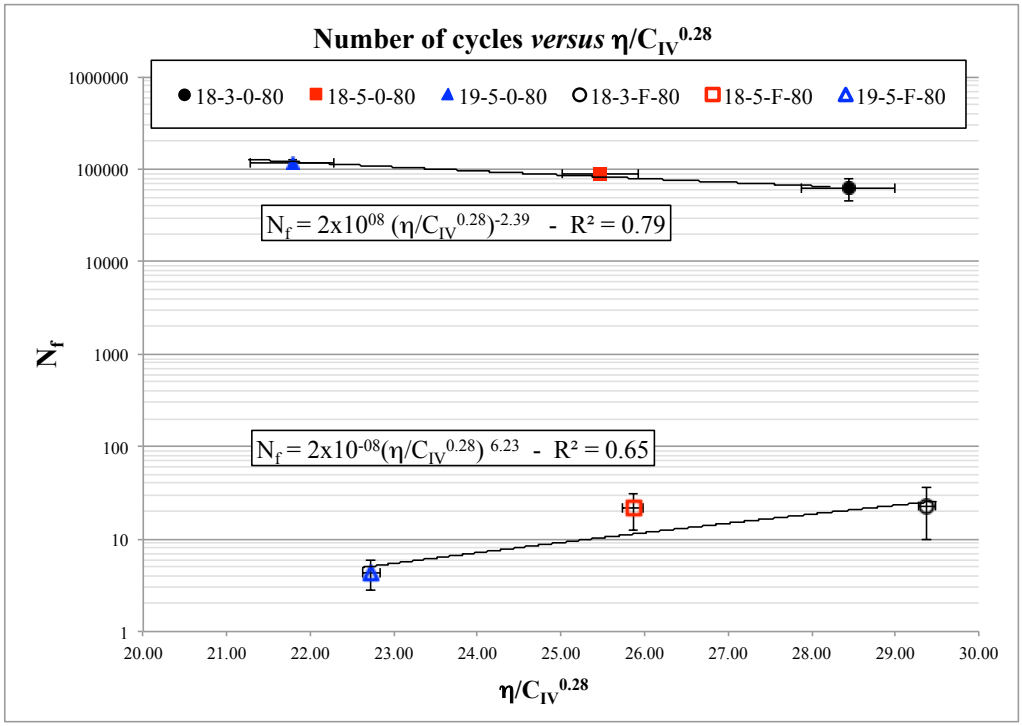

Figure 6.24: Influence of $\eta/C_{iv}^{0.28}$ on fatigue life for 80% of the maximum load

7 QUALITATIVE MODEL

This chapter presents a qualitative model that aims to reproduce the behaviour of a cemented soil under cyclic unconfined compression. Firstly, a theoretical model is proposed aiming represent the degradation of the matrix leading to failure of the cemented materials. Then, the data from the experimental program is used to conduct a parametric analysis.

7.1 THEORETICAL MODEL

This model is based on a one-dimensional approach of a cemented sand when subjected to unconfined cyclic loading. During unconfined cyclic loading the cemented matrix is subjected to tension that promotes a gradual break of the cementation bonds, leading to a degradation of the shear modulus and a reduction in the void ratio of the matrix. On the present research, the models found in literature that best fitted the proposed qualitative model were developed for clays. It is important to highlight that there are few researches on literature of theoretical models for cyclic loading on cemented sands (e.g. IMAM, 1999; IMAM; CHAN, 2008; TARIQ; TAKESHI, 2012; WENG, 2014; RAHIMI *et* al., 2018), however, most do not fit the scope of the present research. It should also be highlighted that the researches on models for cyclic loading on cemented sands is relatively new, reinforcing the gap of knowledge on the subject by the scientific community.

When considering this test on υ-ln(p') plane, the NCL for the uncemented material can be described as equation (7.1). As for the cemented material there is a new NCL. These lines are considered parallel. The cemented NCL usually presents a shift of the line upwards, that is considered to be only dependent of the cement content (RIOS *et* al., 2012; ROTTA *et* al., 2003; CONSOLI; FOPPA, 2014, DIAMBRA *et* al., 2019). The cemented equation for the cemented NCL is presented in equation (7.2). A schematic representation of the υ-ln(p') plane and the pertinent data is presented in figure 7.1.

$$\upsilon = T_U + \lambda \cdot \ln(p') \tag{7.1}$$

$$\upsilon = T_C + \lambda \cdot \ln(p') \tag{7.2}$$

where:

υ = specific volume (m^3/kg);

T_U = displacement of the uncemented NCL;

T_C = displacement of the cemented NCL;

l = inclination of the NCL;

p'= mean effective stress (q_u/3) (MPa).

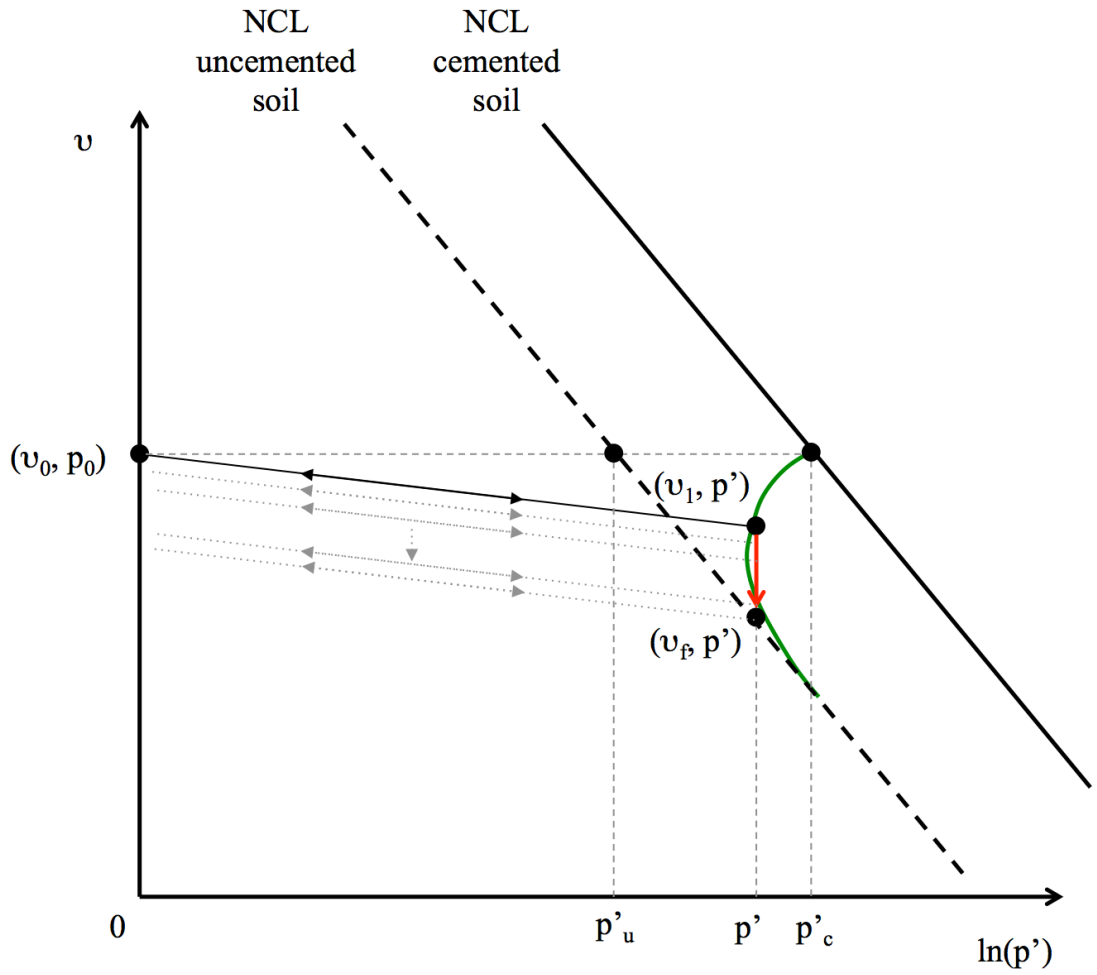

Figure 7.1: Schematic representation of the proposed model

Considering that the NCL for the cemented soil is a displacement of the NCL for the uncemented material depended solely on cement content, T_C can be written as equation 7.3

$$T_C = T_U + k_1 \cdot C \tag{7.3}$$

where:

κ_1 = constant dependent on the cementation ratio;

C = degradation of cementation parameter.

The parameter C that represents the rate of degradation of cementation can be defined as function dependent on the axial strain and degradation of stiffness of the mixture. Idriss *et* al. (1978) proposed a stress-strain non-linear degradation model for soft clay through triaxial cyclic testing. The model proposed that the amplitude of the cyclic strain controls the rate of degradation. Thus equation 7.4 is proposed.

$$C = e^{-K_2 \cdot \delta\varepsilon_{a,N}} \tag{7.4}$$

where:

κ_2 = constant dependent on the load applied;

$\delta\varepsilon_{a,\,N}$ = increment in axial strain at the N^{th} cycle.

Substituting equation 7.4 and 7.3 in equation 7.2, the NCL for cemented soils can be rewritten as equation 7.5.

$$v = T_U + k_1 \cdot e^{-K_2 \cdot \delta\varepsilon_{a,N}} + \lambda \cdot \ln(p') \tag{7.5}$$

Considering that the axial deformation at a given cycle is composed by an elastic deformation and a plastic deformation, $\delta\varepsilon_a$ can be written as equation 7.6.

$$\delta\varepsilon_{a,N} = {\delta\varepsilon_{a,N}}^{E} + {\delta\varepsilon_{a,N}}^{P} \tag{7.6}$$

where

$\delta\varepsilon_{a,\,N}{}^{E}$ = elastic portion on the increment in axial strain at the N^{th} cycle;

$\delta\varepsilon_{a,\,N}{}^{P}$ = plastic portion on the increment in axial strain at the N^{th} cycle.

Muir Wood (2009) states that for an elastic medium ${\delta\varepsilon_{a,N}}^{E}$ follows equation 7.7. Even though this is a theoretical model, the use of fitting parameters such as k_3 is necessary for a future parametric analysis. This parameter accounts for possible necessary adjustments to the trend.

$${\delta\varepsilon_{a,N}}^{E} = \frac{\Delta\sigma'}{G_0} = k_3 \cdot \frac{q_u}{G_0} \tag{7.7}$$

where

k_3 = fitting parameter;

G_0 = initial shear modulus;

q_u = applied load.

As for the plastic deformation portion of the strain increment, Cai *et* al. (2018) proposed the relationship shown in equation 7.8 when studying the behaviour of a clay under cyclic loading for hollow cylinder tests.

$$\delta\varepsilon_{a,N}{}^{P} = e^{a+b\cdot\delta D} \tag{7.8}$$

where

δ_D = stiffness degradation;

a = intercept of the degradation line in semilog;

b = slope of the degradation line in semilog.

Idriss *et* al. (1978) stated that degradation index represents an irreversible degradation process in the structure of the soil and can be correlated with N. The authors proposed equation 7.9, considering that the Poisson's ratio remains constant during testing.

$$\delta_D = \frac{E_N}{E_1} \cong \frac{G_N}{G_1} = N^{-d} \tag{7.9}$$

where:

E_N = Young's modulus at the N^{th} cycle;

E_1 = Young's modulus at the 1^{st} cycle;

G_N = Shear modulus at the N^{th} cycle;

G_1 = Shear modulus at the 1^{st} cycle;

N = number of cycles;

d = inclination of the slope of E_N/E_1 (or G_N/G_1) versus N, both on logarithmic scale.

However, for the values attained for this research did not present a linear trend when the data was plotted as suggested. Yasuhara *et* al. (1998), following the model proposed by Idriss *et* al. (1978) whilst studying cyclic stiffness of a plastic clay found that a better fit to the data would be equation 7.10.

$$\delta_D = \frac{E_N}{E_1} \cong \frac{G_N}{G_1} = 1 - A \cdot log_{10}(N) \tag{7.10}$$

where A = gradient of the line of G_N/G_1 versus N on a semi log scale.

This proposed correlation presented a better fit to the data from this research. Through mathematical manipulation equation 7.10 can be rewritten as equation 7.11, which has the same format as observed for the empirical data in equation 5.2.

$$\delta_D \cdot G_1 = -B \cdot log_{10}(N) + G_1 \tag{7.11}$$

where B is equal to the product of A times G_1 and reflects the rate of degradation due to influence of load percentage adopted during testing.

Then, equation 7.8 can be rewritten as equation 7.12.

$$\delta\varepsilon_{a,N}{}^{P} = e^{a+b\cdot(1-B/G_1\cdot log_{10}(N))} \tag{7.12}$$

However, for the present study, a better fit to the data was found for equation 7.13.

$$\delta\varepsilon_{a,N}{}^{P} = e^{a-\cdot(1-B/G_1\cdot log_{10}(N))^b} \tag{7.13}$$

Then, equation 7.6 can be rewritten as equation 7.14.

$$\delta\varepsilon_{a,N} = \mathrm{k}_3 \cdot \frac{\mathrm{q}_u}{G_0} + e^{a-\cdot(1-B/G_1\cdot log_{10}(N))^b} \tag{7.14}$$

Finally, equation 7.5 can be rewritten as equation 7.15.

$$v = T_U + k_1 \cdot e^{-K_2\left(\mathrm{k}_3\frac{\mathrm{q}_u}{G_0}+e^{a-\cdot(1-B/G_1\cdot log_{10}(N))^b}\right)} + \lambda \cdot \ln(p') \tag{7.15}$$

It is important to mention that the same proposed logic of stiffness degradation could be used on a qualitative model on the p'- q plane, where the cycling process would promote a degradation of the cemented soil until the stress path reached the failure envelope of the uncemented material, reaching failure.

7.2 PARAMETRIC ANALYSIS

A parametric analysis was carried out for four specimens (18-5-0-90-II; 18-5-0-80-III; 18-5-0-70-I; 19-3-0-80-III) in order to assess the proposed model for the data from unreinforced CUC tests. Firstly, equation 7.14 was used to attempt to reproduce the relationship between ε_a versus N. With the values of $\delta\varepsilon_{a,N}$, it was estimated loss of specific volume with loading.

The values of the constants of equation 7.14 for the analysed specimens are presented in table 7.1. From the presented data, it is possible to conclude that *a* is equal to unity; b is almost constant and around 2; k_3 adjusts the variation of the ratio q_u/E_0 regarding the fist cycle; B represents the rate of degradation of the specimen, being higher for higher applied load.

Table 7.1: Constants of equation 7.14 for the analysed specimens

Sample	k_3	q_u (kPa)	E_0 (MPa)	E_1 (MPa)	B	a	b
18-5-0-90-II	0.201879	1052.49	3555.372	1845.9	539.59	1	2
18-5-0-80-III	0.786099	827.8525	4648.386	385.52	385.52	1	2
18-5-0-70-II	0.308643	815.8313	3873.862	1380	148.8	1	2.7
19-3-0-80-III	0.39138	853.5	3340.432	1139.83	185	1	2

Figure 7.2 show the model equation of $\delta\varepsilon_{a,N}$ *versus* N compared to the actual values from the experimental program for the specimen 18-5-0-90-II. The graph presents the equation for total strain and plastic strain. The elastic strain is a constant – the difference between the two. Form the presented graph it is observed that the proposed equation replicates quite well the beginning of the development of strain with N, However, the proposed equation fails to accurately depict the behaviour of the axial strain when the cementation deteriorates, leading to failure. Indicating that further studies should be carried out in order to better assess the collapse of the matrix leading to rupture.

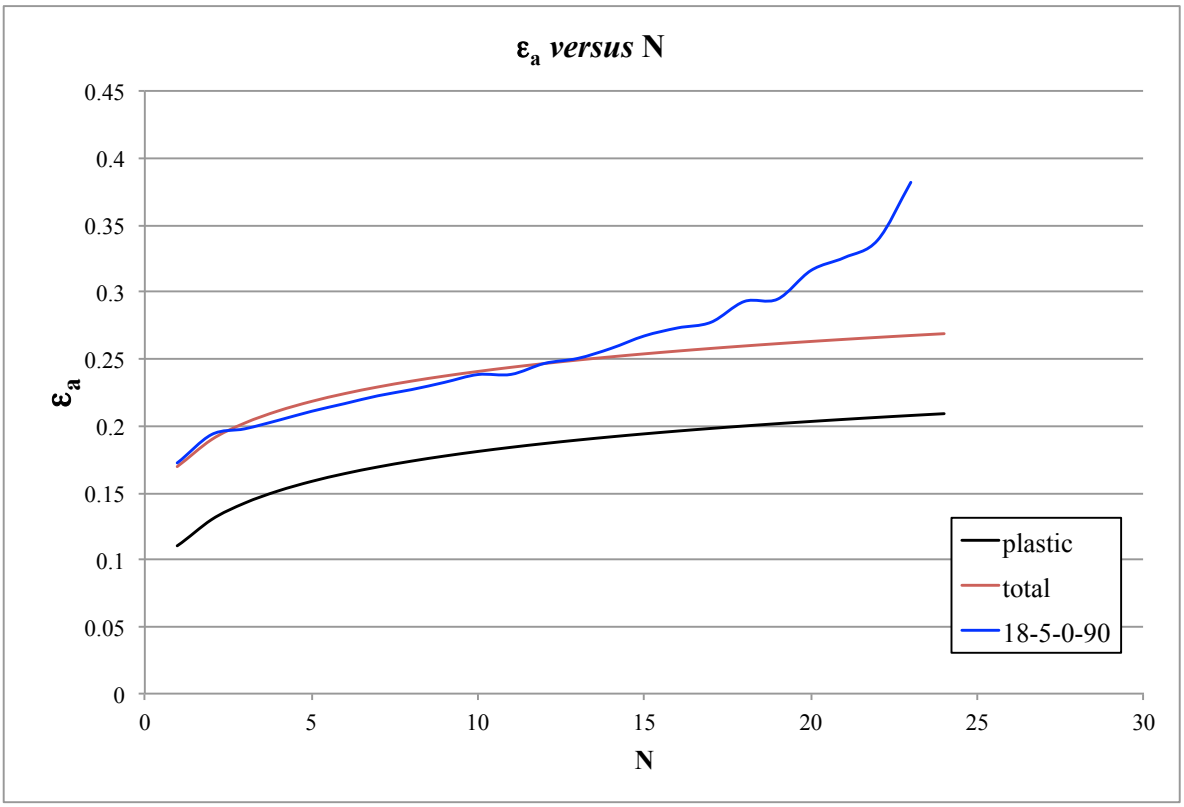

Figure 7.2: $\delta\varepsilon_{a,\,N}$ *versus* N compared to ε_a versus N for specimen 18-5-0-90-II

Figure 7.3 show the model equation of $\delta\varepsilon_{a,\,N}$ *versus* N compared to the actual values from the experimental program for the specimen 18-5-0-80-III. The graph presents the equation for total strain and plastic strain. The elastic strain is a constant – the difference between the two. From the presented graph it is possible to infer that the proposed equation replicates quite well the development of strain with N, differently to what was observed in figure 7.2, there was not a increase in the rate of strain gain before rupture for this specimen, thus the proposed equation was able to describe more accurately the observed ε_a versus N relationship.

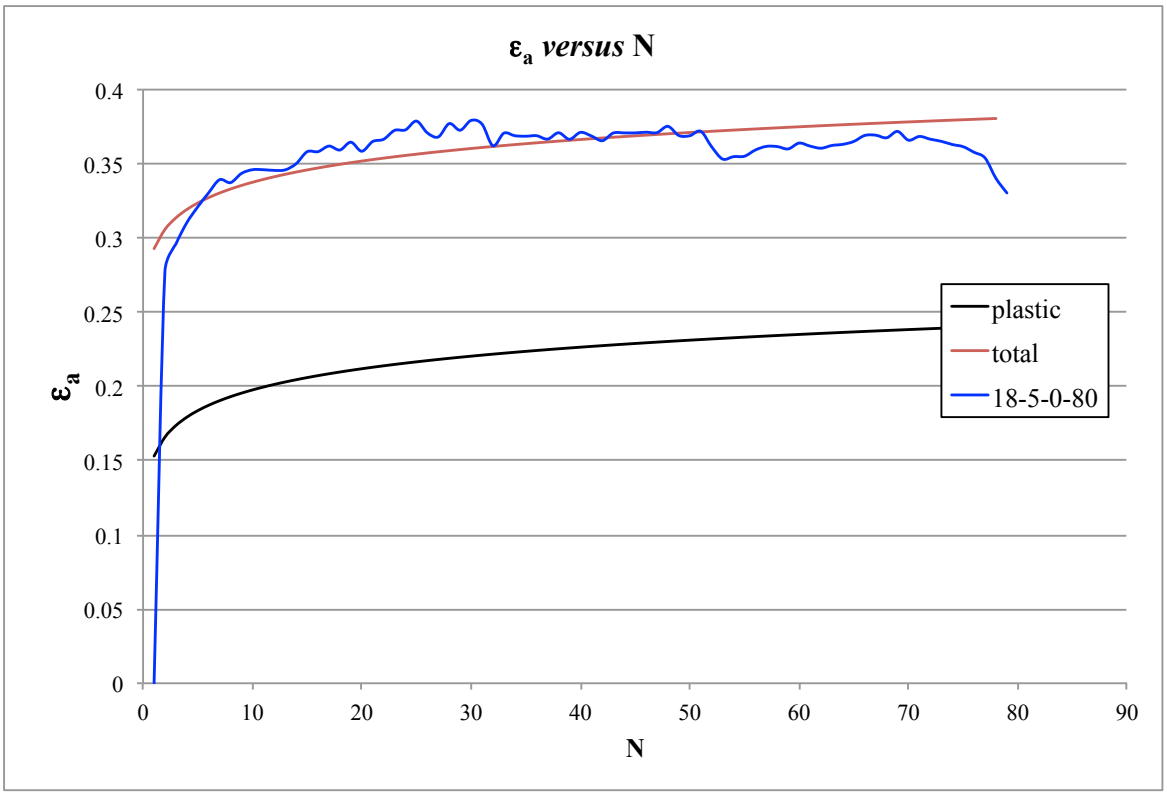

Figure 7.3: $\delta\varepsilon_{a,N}$ *versus* N compared to ε_a versus N for specimen 18-5-0-80-III

Figure 7.4 show the model equation of $\delta\varepsilon_{a,N}$ *versus* N compared to the actual values from the experimental program for the specimen 18-5-0-70-II. The graph presents the equation for total strain and plastic strain. The elastic strain is a constant – the difference between the two. From the presented graph it is observed that the proposed equation replicates quite well the development of strain with N for values of N greater than 500. Increase in the rate of strain gain at beginning of cycling was not accurately captured by equation 7.14. Nevertheless, it can be concluded that the equation accurately represented the majority of studied test.

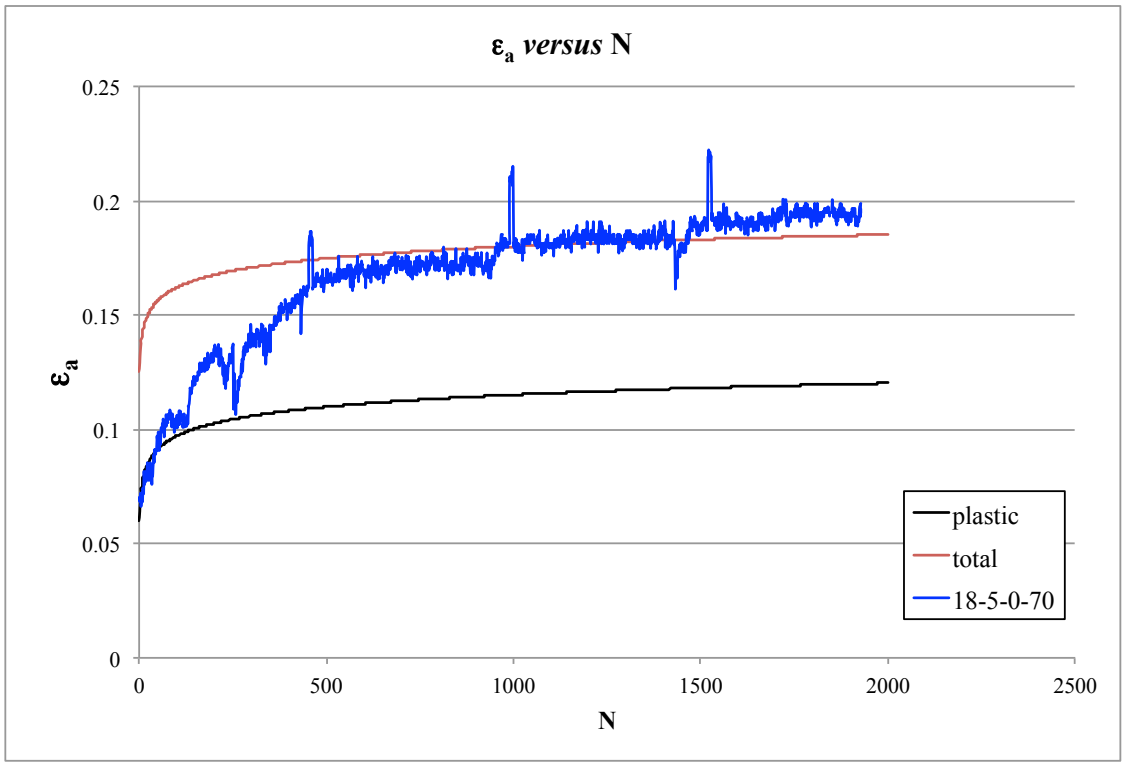

Figure 7.4: $\delta\varepsilon_{a,\,N}$ *versus* N compared to ε_a versus N for specimen 18-5-0-70-II

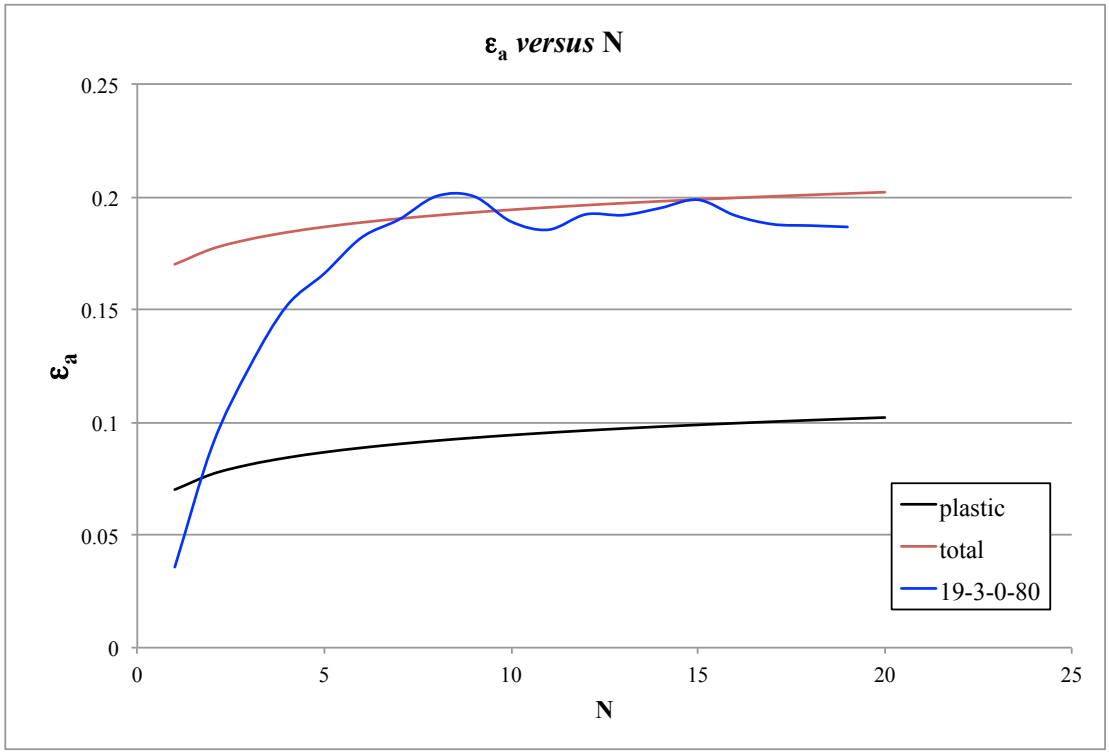

Figure 7.5: $\delta\varepsilon_{a,\,N}$ *versus* N compared to ε_a versus N for specimen 19-3-0-80-III

Figure 7.5 show the proposed equation of $\delta\varepsilon_{a,N}$ *versus* N compared to the actual values from the experimental program for the specimen 19-3-0-80-III. Similarly to what was observed in figure 7.4, equation 7.14 replicates quite well the development of strain with N for values of N greater than 6. The increase rate of strain gain at beginning of cycling was not accurately captured by the equation. Nevertheless, it can be concluded that the equation accurately represented the majority of studied test.

From the data presented so far in this chapter it is possible to conclude that equation 7.14 can accurately represent the increase in axial strain with loading for specimens that do not present a high rate of increase in axial strain with cycling.

Based on the results presented, it was calculated the decrease in specific volume due to uniaxial unconfined cyclic loading for the studied cemented sand. The values of λ, T_U and T_C used in order plot the NCL lines were obtained from the work of Prietto (2004) and are presented in table 7.2.

The values of the constants of equation 7.15 for the analysed specimens are presented in table 7.3. From the presented data, it is possible to conclude that k_1 is equal to T_C and that k_2 is influenced by the percentage of load applied.

Table 7.2: NCL paramenters for Botucatu sandstone residual soil (PRIETTO, 2004)

Material	λ	T_U	T_C
Uncemented	-0.068	1.973	-
3% cement content	-	-	2.069727
5% cement content	-	-	2.114433

Figure 7.6 show the proposed equation of u *versus* ln(p') for the specimen 18-5-0-90-II. The decrease in specific volume of the specimen due to unconfined compression cycling occurs as expected for the proposed model. There was a steady decrease in υ values until rupture. For this specimen rupture occurred before the specific value reached the NCL for the uncemented material.

Table 7.3: Constants of equation 7.15 for the analysed specimens

Sample	k_1	k_2
18-5-0-90-II	2.114433	20
18-5-0-80-III	2.114433	30
18-5-0-70-II	2.114433	40
19-3-0-80-III	2.069727	30

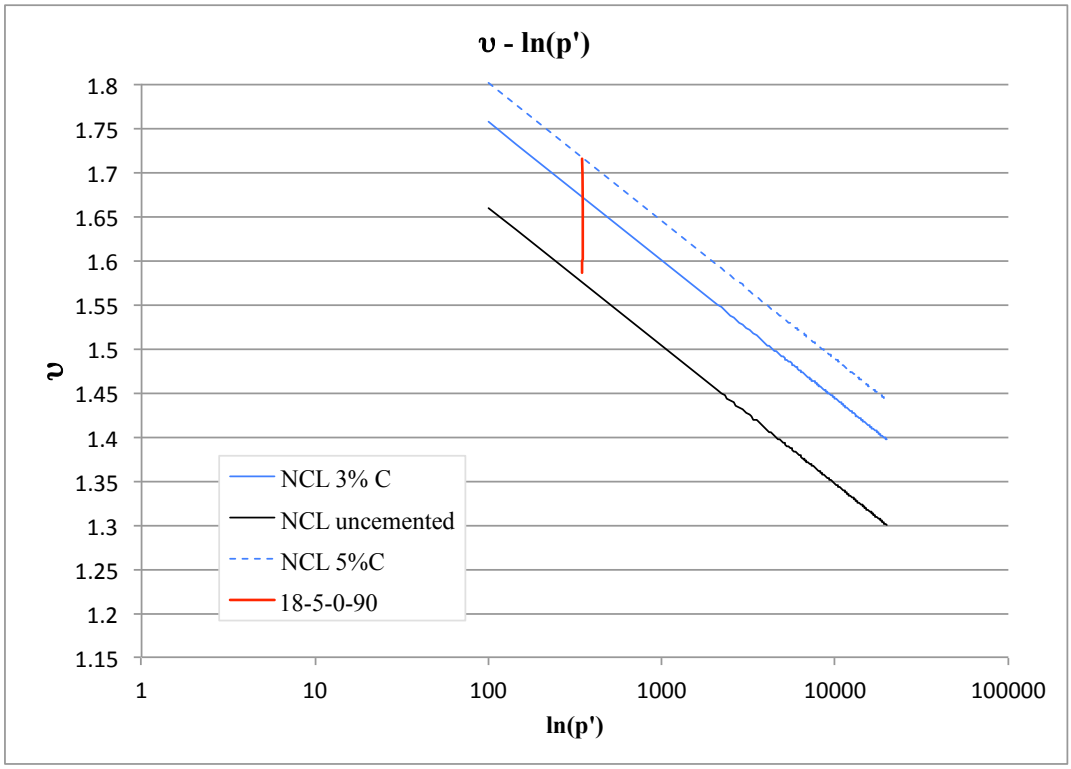

Figure 7.6: υ *versus* ln(p') for specimen 18-5-0-90-II

Figure 7.7 show the proposed equation of u *versus* ln(p') for the specimen 18-5-0-80-III. The decrease in specific volume of the specimen due to unconfined compression cycling occurs as expected for the proposed model. There was a steady decrease in υ values until rupture. For this specimen rupture occurred when the specific value reached the NCL for the uncemented material.

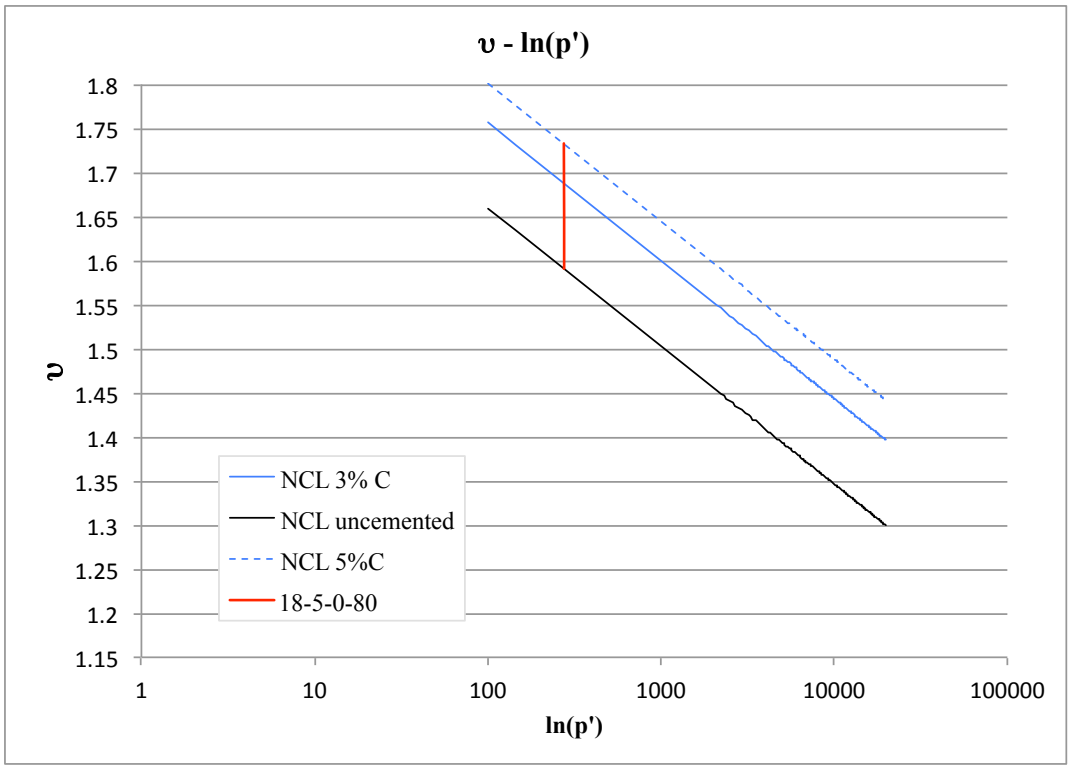

Figure 7.7: υ *versus* ln(p') for specimen 18-5-0-80-III

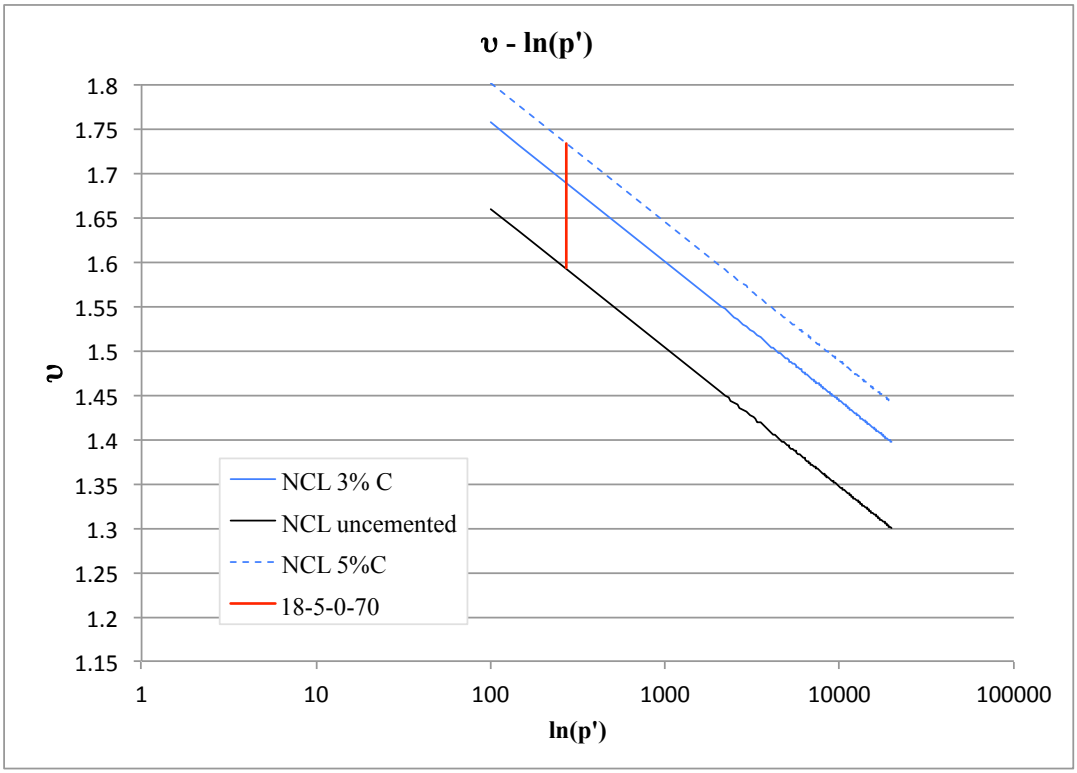

Figure 7.8: υ *versus* ln(p') for specimen 18-5-0-70-II

Figure 7.8 show the proposed equation of u *versus* ln(p') for the specimen 18-5-0-70-III. Similarly to what was observed for the previous specimen, the decrease in specific volume of the specimen due to unconfined compression cycling occurs as expected for the proposed model. There was a steady decrease in υ values until rupture. For this specimen rupture occurred when the specific value reached the NCL for the uncemented material.

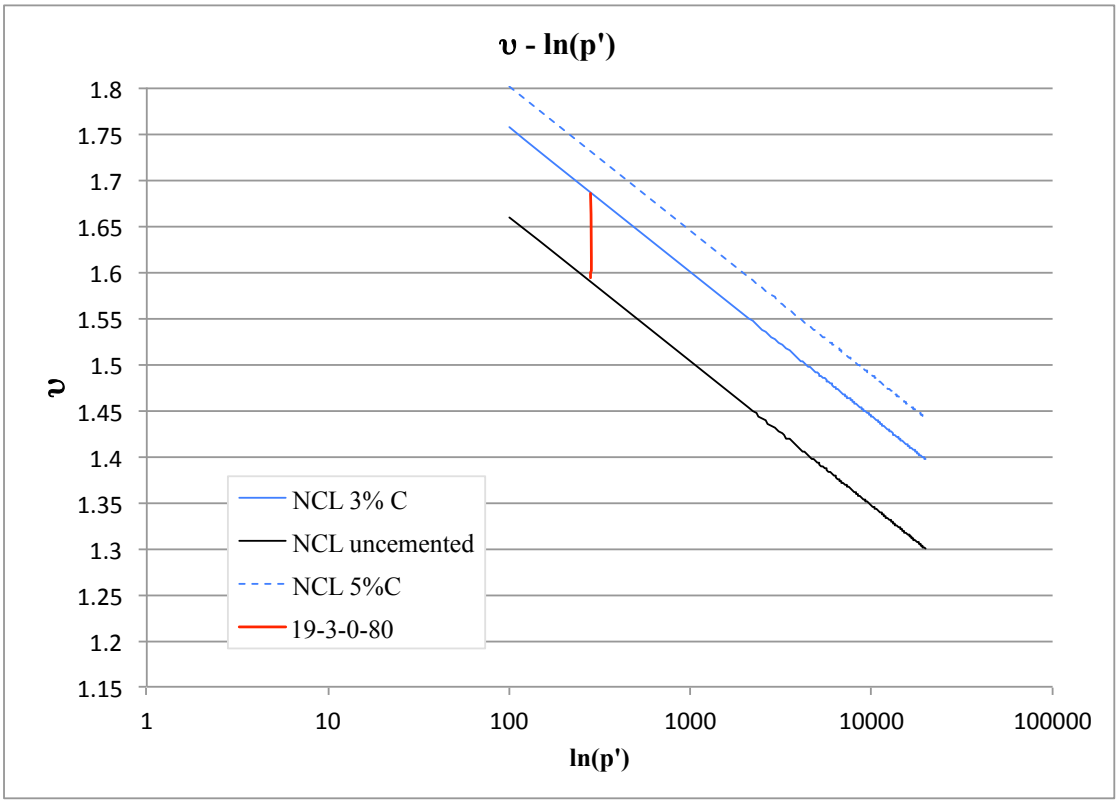

Figure 7.9: υ *versus* ln(p') for specimen 19-3-0-80-III

Figure 7.9 show the proposed equation of u *versus* ln(p') for the specimen 19-3-0-80-II. The decrease in specific volume of the specimen due to unconfined compression cycling occurs as expected for the proposed model. There was a steady decrease in υ values until rupture. For this specimen the cemented NCL was different due to its lower cement content, but rupture also occurred when the specific value reached the NCL for the uncemented material.

From the data presented, it is possible to conclude that for loads of 80% and lower the specimen reaches failure when the specific volume of the specimen reaches the NCL for the uncemented material. For 90% the specimen reached failure before all the cementitious bonds degraded. It is also possible to conclude that within its boundary conditions the qualitative model proposed can accurately describe the observed behaviour during the CUC experimental program. However, a more complete analysis should be made in order to validate the model.

8 CONCLUSIONS AND SUGGESTION FOR FUTURE RESEARCHES

This chapter presents the conclusions that can be drawn from the work realized on the doctorate thesis that was conducted. It also presents suggestions for future researches based on the points that this research reviewed.

8.1 CONCLUSIONS

From the experimental program presented and the tests carried out until this moment in this doctorate thesis it is possible to draw a series of conclusions. Since there are many drawn conclusions from this research, the most relevant findings were condensed and are presented below.

(1) for CUC tests:

- a power function relationship was found to be the best fit for the number of cycles against the applied load percentage (LP) all studied specimens;
- fibre insertion did improve the behaviour of the composite for the studied mixtures;
- there was a higher influence of the cementation rate in the behaviour of cemented and fibre-reinforced cemented composites;
- fibre-reinforced specimens presented higher axial deformation before rupture;
- within the same range of load applied, similar values of $\varepsilon_{a\ max}$ were observed;
- there is a higher influence of the cementation ratio in the behaviour of soil-cement composites, however the insertion of fibres mitigates this influence;
- fibre insertion leads to a decrease in the Young's modulus;
- the values of shear modulus at very-small strains were higher for soil-cement specimens then the observed for soil-cement-fibre mixtures;

- a logarithmic relationship was found for the deterioration of small-strain G with the number of cycles;
- for same loading levels there was a higher initial degradation of stiffness for the fibre-reinforced mixtures than the observed for the unreinforced specimen;

(2) for fatigue tests: there was a significant decrease in N_f values for fibre-reinforced mixtures;

(3) for qualitative model: a qualitative model was proposed to describe the degradation of specific volume of a cemented sand with cyclic unconfined compression leading to failure. A parametric study was made in order to assess the efficacy of the model, it was possible to conclude that equation 7.14 can accurately represent the increase in axial strain with loading for specimens that do not present a high rate of increase in axial strain with cycling.

A more detailed presentation of the conclusions from the hole experimental program and qualitative model are presented on the following topics.

(a) regarding the studied soil:

The characterizations tests carried out showed that the Botucatu sandstone residual soil sample collected from the reservoir has grain size distribution, Atterberg limits and compaction curve similar to previously studied samples from the literature;

(b) regarding unconfined monotonic tests:

The unconfined compression carried out to validate the use of the data presented by Festugato (2011) concluded that the strength values were on the same order of magnitude as the presented in the previous study. Therefore, it could be used as reference the data for the cyclic unconfined compression tests.

From split tensile tests the data presented by Festugato (2011) and the one attained by this research for cylindrical specimens of 5 x 10 cm (D x H) were within the same level of magnitude, as observed with the unconfined compression.

It was observed that the maximum values of q_t attained for the 5 x 10 cm (D x H) were different than the q_t values obtained for 10 x 5 cm (D x H). For the 10 x 5 cm specimens' values of q_t were similar for mixtures with and without fibres. However, the difference in q_t values between unreinforced and fibre-reinforced specimens increased with the decrease of $\eta/C_{iv}^{0.28}$. Indicating that fibre addition leads to disruption of the formation of cementitious bonds with the increase of cementation and/or decrease in porosity.

The q_t values for the 10 x 5 specimens without fibres are higher than the 5 x 10 specimens, especially for specimens for higher $\eta/C_{iv}^{0.28}$. For the mixtures with fibres, there was a decrease in q_t for 10 x 5 specimens in respect to the values observed for 5 x 10. This phenomenon could be attributed to the difference in the diameter/height ratio. For the 10 x 5 cm specimens, plain strain across the height axis can no longer be assumed. Also, there is an anisotropy imposed during the moulding process for the fibre-reinforced specimens and a disruption in the formation of cementation bonds due to fibre insertion.

Specimens subjected to flexural tests presented an expressive increase in tensile strength due to the increase in cement content. However, the increase in dry unit weight did not confer the mixtures the same level of strength gain observed by the increase in cement content.

The addition of randomly oriented fibres increased the tensile strength mainly for lower density specimen. As the density of the specimen increased, the fibre contribution in tensile strength gain decreased. This can be attributed to the increase in entanglement and stretch of fibres on the denser specimens.

The use of the porosity/volumetric cement content ratio can be used as methodology for predicting tensile strength on flexural tests. There was a good fit of the data when an exponent of 0.28 is used on the volumetric cement content, with high coefficient of determination for cemented soil and fibre-reinforced cemented soil. By comparing the results from the literature for different tests of the same mixtures, the strength observed for flexural strength follow the same exponential trend as the other tests, and the values are higher than the attained for split tensile tests, but lower than the observed for unconfined compression tests;

(c) regarding cyclic unconfined compression tests:

The number of cycles increased with the decrease of percentage of load applied, regardless of fibre insertion. A power function relationship was found to be the best fit for the number of cycles against the applied load percentage (LP) all studied specimens. Even for similar initial conditions, variability in the number of cycles was observed, regardless of fibre insertion.

Fibre insertion did improve the behaviour of the composite for the studied mixtures. When comparing applied loads, the number of cycles until failure for soil-cement-fibre composites was far greater than the observed for soil-cement specimens.

The number of cycles reduced for the specimens with similar $\eta/C_{iv}^{0.28}$ but higher density and lower cementation for unreinforced and reinforced mixtures indicating to a higher influence of the cementation ratio in the behaviour of cemented and fibre-reinforced cemented composites.

Fibre-reinforced specimens presented higher axial deformation before rupture, which was expected given the elastic nature of the fibres that confers a greater capacity to absorb loading under higher strains.

Within the same range of load applied, similar values of $\varepsilon_{a\ max}$ were observed. However, the fibre-reinforced specimens did not reach failure for this load range, indicating that the axial strain at failure is higher for fibre-reinforced specimens for the same range of applied load.

Considering the specimens with similar $\eta/C_{iv}^{0.28}$ but higher density and lower cementation, $\varepsilon_{a\ max}$ was lower for the for unreinforced mixtures than the observed for unreinforced benchmark specimens. As for the reinforced specimens, the $\varepsilon_{a\ max}$ at failure was similar to the values observed for benchmark mixtures, indicating that there is a higher influence of the cementation ratio in the behaviour of cemented composites, however the insertion of fibres mitigates this influence.

Fibre insertion lead to a decrease in the Young's modulus. Testing in this research was unconfined, which might be the reason for the lower Young's modulus values for fibre-reinforced specimens. The absence of a confining pressure allows the specimen to expand radially freely, leading to higher axial deformations in the unloading-reloading loop and therefore lower E values.

The specimens that were more rigid presented a peak in E values at the beginning of testing, followed by a degradation of stiffness until a plateau of constant plastic strain is reached then, it is observed a second peak in E caused by a collapse in the cemented matrix, leading to a decrease in void ratio and in turn an increase in E culminating in failure. This last peak could be considered a fictional increase in E, since it is the product of the eminent collapse of the matrix.

The less rigid specimens presented a constant increase of the Young's modulus that could be attributed by gradual mobilization of the cementitious bonds with the decrease of void ratio of the matrix continuing until the degradation of the bonds reached a critical point. Then, the values of E decrease until failure.

The specimens with similar $\eta/C_{iv}^{0.28}$ but higher density and lower cementation presented lower E values for soil-cement mixture, but similar values of E for fibre-reinforced cemented mixture when compared to the corresponding benchmark specimens, indicating a greater importance of the cementation percentage for soil-cement mixtures that is mitigated for soil-cement-fibre mixture due to the disruption on the formation of cement bonds due to fibre insertion.

The values of shear modulus at very-small strains were higher for soil-cement specimens then the observed for soil-cement-fibre mixtures. The absence of axial and radial stresses during bender reading means that the matrix has higher void ratio during very-small strain testing, leading to less contact between the particles and a dispersion of the shear waves when fibres are encountered.

A logarithmic relationship was found for the deterioration of small-strain G with the number of cycles, a similar relationship was proposed by Yasuhara *et* al. (1998). However, the coefficient of determination drastic decreases for the specimens that did not reach rupture due to the observed increase in G values over the last 1500 cycles which might be attributed to a slow densification of the specimens over continued repetitive cycling that happened alongside the slow degradation of cemented bonds.

For specimens with similar $\eta/C_{iv}^{0.28}$ but higher density and lower cementation, degradation rates of G_N were higher than the observed by the correspondent benchmark specimens with and without fibres.

For same loading levels there was a higher initial degradation of stiffness for the fibre-reinforced mixtures than the observed for the unreinforced specimens. Corroborating that a more rigid behaviour for cemented specimens and a more ductile behaviour for fibre-reinforced cemented mixtures. Also, a higher initial degradation was observed for specimens subjected to higher loads for unreinforced and reinforced mixtures;

(d) regarding fatigue tests:

Regarding rupture mode, besides the expected vertical fracture alongside the diameter there were numerous cracks alongside the height (surface parallel to the loading beam). The developments of this cracks might be responsible for the decrease in bearing capacity for monotonic tests and fatigue life in cyclic testing.

The values of load applied to the fibre-reinforced mixtures were similar to the applied for the unreinforced ones. However, there was a significant decrease in N_f values for fibre-reinforced mixtures. This phenomenon might be due to the disruption of the formation of cementitious bonds due to the fibre additions and/or anisotropy imposed on the specimen because of fibre insertion allied to the fact that that plain strain across the height axis can no longer be assumed for the 10 x 5 cm specimens.

For soil-cement mixtures a decrease in $\eta/C_{iv}^{0.28}$ lead to higher values of N_f following a power function relationship. For fibre-reinforced mixtures, there was lower number of cycles until rupture due to fibre insertion. Also, a decrease in fatigue life was observed for the lower $\eta/C_{iv}^{0.28}$ specimen in respect to the other two mixtures with fibres. The cementation bonds in the fibre-reinforced specimens might be affected by the presence of the fibres in the matrix, then, when a higher maximum q_t value were applied, the cementation bond degraded more rapidly than for the other mixtures, leading to lower number of cycles;

(e) regarding the qualitative model:

A qualitative model was proposed to describe the degradation of specific volume of a cemented sand with cyclic unconfined compression leading to failure. A parametric study was made in order to assess the efficacy of the model, it was possible to

conclude that equation 7.14 can accurately represent the increase in axial strain with loading for specimens that do not present a high rate of increase in axial strain with cycling;

It was possible to conclude that for loads of 80% and lower the specimen reaches failure when the specific volume of the specimen reaches the NCL for the uncemented material. For loads of 90% the specimen reached failure before all the cementitious bonds degraded. It is also possible to conclude that within its boundary conditions the qualitative model proposed can accurately describe the observed behaviour during the CUC experimental program. However, a more complete analysis should be made in order to validate the model.

8.2 SUGGESTIONS FOR FUTURE RESEARCHES

Based on the data presented by the present research the following suggestions can be made for future works:

(a) Test other soils and additions under CUC tests in order to have a broader understating of the test and its applications;

(b) Measure the radial deformation on CUC tests in order to better evaluate the tri-dimensional deformations of the composite materials under unconfined cyclic loading;

(c) Attempt to measure bender elements continuously through cycling in order to observe the evolution of shear strain at very-small strains when the specimen is experiencing high strains;

(d) Assess the influence of cementation and porosity on the influence of loading percentages on $\varepsilon_{a\,max}$ for CUC tests of composite materials;

(e) Test other soils and additions under split tensile tests in order to have a broader understating of the test and its applications;

(f) Assess the parameters – diameter/height ratio; cement ratio; fibre type, length and percentage – that govern the behaviour of 10 x 5 cm specimens for monotonic and fatigue testing;

(g) Develop a constitutive model that represents the behaviour of cemented and fibre-reinforced cemented soils composites under cyclic unconfined compression testing;

(h) Develop a constitutive model that represents the behaviour of cemented and fibre-reinforced cemented soil composites under split tensile fatigue testing.

9 REFERENCES

AMERICAN ASSOCIATION OF STATE HIGHWAYS AND TRANSPORTATION OFFICIALS. **AASHTO/T307-99**: Standard method of test for determining the resilient modulus of soils and aggregate materials. v. 99, 2007.

ANDERSEN, K. H.; PUECH, A. A.; JARDINE, R. J. Cyclic resistant geotechnical design and parameter selection for offshore engineering and other applications. In: TC 209 WORKSHOP 18TH ICSMGE: DESING FOR CYCLIC LOADING: PILES AND OTHER FOUNDATIONS, 2013, Paris. **Proceedings**. Paris, 2013, p. 9–44.

ARULRAJAH, A.; PERERA, S.; WONG, Y. C.; HORPIBULSUK, S.; MAGHOOL, F. Stiffness and flexural strength evaluation of cement stabilized PET blends with demolition wastes. **Construction and Building Materials**, v. 239, 117819, 2020.

ASSOCIAÇÃO BRASILEIRA DE NORMAS TÉCNICAS. **NBR 12.533**: Solo-cimento – dosagem para emprego como camada de pavimento. Rio de Janeiro, 7p .1992.

_____. **NBR 7222**: Concreto e argamassa — Determinação da resistência à tração por compressão diametral de corpos de prova cilíndricos. Rio de Janeiro, 5 p. 2011.

_____. **NBR 6457**: Amostras de solo - Preparação para ensaios de compactação e ensaios de caracterização. Rio de Janeiro, 8 p. 2016 a.

_____. **NBR 6458**: Grãos de pedregulho retidos na peneira de abertura 4,8 mm - Determinação da massa específica, da massa específica aparente e da absorção de água. Rio de Janeiro, 10 p. 2016 b.

_____. **NBR 6459**: Solo - Determinação do limite de liquidez. Rio de Janeiro, 5 p. 2016 c.

_____. **NRB 7180**: Solo - Determinação do limite de plasticidade. Rio de Janeiro, 3 p. 2016 d.

_____. **NBR 7181**: Solo - Análise granulométrica. Rio de Janeiro, 12 p. 2016 e.

_____. **NBR 7182**: Solo - Ensaio de compactação. Rio de Janeiro, 9 p. 2016 f.

_____. **NBR 16605**: Cimento Portland e outros materiais em pó — Determinação da massa específica. 2017.

AMERICAN SOCIETY FOR TESTING AND MATERIALS. **ASTM D 4123**: Standard test method for indirect tension test for resilient modulus of bituminous mixtures. 1995

_____. **ASTM D3999**: Standard test methods for the determination of the modulus and damping properties of soils using the cyclic triaxial apparatus. 2011a.

_____. **ASTM D5311**: Standard test method for load controlled cyclic triaxial strength of soil. 2011 b.

_____. **ASTM D1635**: Standard test method for flexural strength of soil-cement using simple beam with third-point loading, 2012.

_____. **ASTM E1823**: Standard terminology relating to fatigue and fracture testing. 2013.

ATKINSON, J. H. **An introduction to the mechanics of soils and foundations**. London: McGraw-Hill, 337 p., 1993.

ATKINSON, J. H., BRANSBY, P. L. **The mechanics of soils – an introduction to critical state soil mechanics**. London: McGraw-Hill, 375p., 1978.

BEEN, K.; JEFFERIES, M. G. A state parameter for sands. **Géotechnique**, v. 35, n. 2, p. 99-112, 1985.

BORTOLOTTO, M. S. **Bender elements, ultrasonic pulse velocity, and local gauges for the analysis of stiffness degradation of an artificially cemented soil**. 2017. 171 p. Dissertation (Master in Engineering) – Post-Graduate Program in Civil Engineering, Federal University of Rio Grande do Sul, Porto Alegre, 2017.

BRITISH STANDARD METHODS OF TEST. **BS EN 12697-24**: Bituminous mixtures – Test methods for hot mix asphalt – Part 24: Resistance to fatigue. 2004.

BRITTO, A. M.; GUNN, M. J. **Critical state soil mechanics via finite elements**. Chichester: Ellis Horwood Limited, 488p., 1987.

BUILDING RESEARCH ESTABLISHMENT. **Design Guide: soft soil stabilization – development of design and construction methods to stabilize soft organic soils – soft soil stabilization**. 1st ed. Watford: IHS BRE Press, 2002.

BURROUGHS, V. S. **Quantitative criteria for the selection and stabilisation of soils for rammed earth wall construction**. 2001. 296 p. Thesis (Doctor in Philosophy) – Faculty of the Built Environment, University of New South Wales, Sydney, 2001.

CAI, Y.; WU, T.; GUO, L.; WANG, J. Stiffness degradation and plastic strain accumulation of clay under cyclic load with principal stress rotation and deviatoric stress variation. **Journal of Geotechnical and Geoenvironmental Engineering**, v. 144, n. 5, 04018021, 2018.

CASAGRANDE, M. D. T. **Estudo do comportamento de um solo reforçado com fibras de polipropileno visando o uso como base de fundações superficiais**. 2001, 95 p. Dissertation (Master in Engineering) – Post-Graduate Program in Civil Engineering, Federal University of Rio Grande do Sul, Porto Alegre, 2001.

CASAGRANDE, M. D. T. **Comportamento de solos reforçados com fibras submetidos a grandes deformações**. 2005. 217p. Thesis (Doctor in Engineering) – Post-Graduate Program in Civil Engineering, Federal University of Rio Grande do Sul, Porto Alegre, 2005.

CASAGRANDE, M. D. T.; COOP, M. R.; CONSOLI, N. C. Behavior of a fiber-reinforced bentonite at large shear displacements. **Journal of Geotechnical and Geoenvironmental Engineering**, v. 132, n. 11, p. 1505-1508, 2006.

CLAYTON, C. R. I. Stiffness at small strain: research and practice. **Géotechnique**, v. 61, n. 1, p. 5–37, 2011.

CLOUGH, G. W.; SITAR, N.; BACHUS, R. C.; RAD, N. S. Cemented Sands Under Static Loading. **Journal of Geotechnical Engineering Division**, v. 107, n. ASCE 16319 Proceeding, p. 799-817, 1981.

CONSOLI, N. C.; BASSANI, M. A., FESTUGATO, L. Effect of fiber-reinforcement on the strength of cemented soils. **Geotextiles and Geomembranes**. v. 28, n. 4, p. 344-351, 2010b.

CONSOLI, N. C., CASAGRANDE, M. D. T., COOP, M. R. The effect of fiber-reinforcement on the isotropic compression behavior of a sand. **Journal of Geotechnical and Geoenvironmental Engineering**, v. 131, n. 11, p. 1434-1436, 2005.

CONSOLI, N. C.; CASAGRANDE, M. D. T.; COOP, M. R. Performance of a fibre-reinforced sand at large shear strains. **Géotechnique**, v. 57, n. 9, p. 751-756, 2007b.

CONSOLI, N. C.; CONSOLI, B. S.; FESTUGATO, L. A practical methodology for the determination of failure envelopes of fiber-reinforced cemented sands. **Geotextiles and Geomembranes**, v. 41, p. 50-54, 2013a.

CONSOLI, N. C.; CRUZ, R. C., FLOSS, M. F., FESTUGATO, L. Parameters controlling tensile and compressive strength of artificially cemented sand. **Journal of Geotechnical and Geoenvironmental Engineering**, v. 136, n. 5, p. 759-763, 2010a.

CONSOLI, N. C.; DA FONSECA, A. V.; CRUZ, R. C.; SILVA, S. R. Voids/cement ratio controlling tensile strength of cement-treated soils. **Journal of Geotechnical and Geoenvironmental Engineering**, v. 137, n. 11, p. 1126-1131, 2011b.

CONSOLI, N. C.; DA SILVA, K.; RIVOIRE, A. B. Compacted clay-industrial wastes blends: Long term performance under extreme freeze-thaw and wet-dry conditions. **Applied Clay Science**, v. 146, p. 404-410, 2017b.

CONSOLI, N. C.; DE MORAES, R. R.; FESTUGATO, L. Parameters controlling tensile and compressive strength of fiber-reinforced cemented soil. **Journal of Materials in Civil Engineering**, v. 25, n. 10, p. 1568-1573. 2013b.

CONSOLI, N. C.; FOPPA, D.; FESTUGATO, L.; HEINECK, K. S. Key parameters for strength control of artificially cemented soils. **Journal of Geotechnical and Geoenvironmental Engineering**, v. 133, n. 2, p. 197-205, 2007a.

CONSOLI, N. C.; FOPPA, D. Porosity/cement ratio controlling initial bulk modulus and incremental yield stress of an artificially cemented soil cured under stress. **Géotechnique Letters**, v. 4, n. 1, p. 22-26, 2014.

CONSOLI, N. C.; MORAES, R. R., FESTUGATO, L. Split tensile strength of monofilament polypropylene fiber-reinforced cemented sandy soils. **Geosynthetics International**, v. 18, n. 2, p. 57-62, 2011a.

CONSOLI, N. C.; NIERWINSKI, H. P.; DA SILVA, A. P.; SOSNOSKI, J. Durability and strength of fiber-reinforced compacted gold tailings-cement blends. **Geotextiles and Geomembranes**, v. 45, n. 2, p. 98-102, 2017a.

CONSOLI, N. C.; PRIETTO, P. D. M.; ULBRICH, L. A. The behavior of a fiber-reinforced cemented soil. **Ground Improvement**, v. 3, n. 3, p. 21-30, 1998.

CONSOLI, N. C.; TOMASI, L.F. The impact of dry unit weight and cement content on the durability of sand–cement blends. **Proceedings of the Institution of Civil Engineers – Ground Improvement**, p. 1-7, 2017.

CONSOLI, N. C.; ULBRICH, L. A.; PRIETTO, P. D. M. Engineering behavior of randomly distributed fiber-reinforced cement soil. In: INTERNATIONAL SYMPOSIUM ON RECENT DEVELOPMENTS IN SOIL AND PAVEMENT MECHANICS, 1997, Rio de Janeiro. **Proceedings**. Rotterdam: A.A. Balkema, p. 481-486, 1997.

CONSOLI, N. C.; VENDRUSCOLO, M. A.; FONINI, A.; DALLA ROSA, F. Fiber reinforcement effects on sand considering a wide cementation range. **Geotextiles and Geomembranes**, v. 27, n. 3, p. 196-203, 2009.

CONSOLI, N. C.; VENDRUSCOLO, M. A.; PRIETTO, P. D. M. Behavior of plate load tests on soil layers improved with cement and fiber. **Journal of Geotechnical and Geoenvironmental Engineering**, v. 128, n. 1, p. 96-101, 2003.

COOP, M. R.; ATKINSON, J. H. The mechanics of cemented carbonated sands. **Géotechnique**, v. 43, n. 1, p. 53-67, 1993.

CORTI, R. **Hardening memory surface constitutive model for granular soils under cyclic loading conditions**. 2016. 238 p. Thesis (Doctor of Philosophy in the Faculty of Engineering) – Department of Civil Engineering, University of Bristol, Bristol, UK, 2016.

DA FONSECA A. V.; RIOS, S.; AMARAL M. F.; PANICO, F. Fatigue cyclic tests on artificially cemented soil. **Geotechnical Testing Journal**, v. 36, n. 2, p. 227-235, 2013.

DA SILVA, A. P. **Constitutive modelling of fibre-reinforced sands under cyclic loads.** 2017. Dissertation (Master of Engineering) – Postgraduate Program in Civil Engineering, Federal University of Rio Grande do Sul, Porto Alegre, 2017.

DALLA ROSA, A. **Estudo dos parâmetros-chave no controle da resistência de misturas solo-cinza-cal**. 2009. 198 p. Dissertation (Master in Engineering) – Post-Graduate Program in Civil Engineering, Federal University of Rio Grande do Sul, Porto Alegre, 2009.

DASS, R. N.; YEN, S. C.; DAS, B. M.; PURI, V. K.; W RIGHT, M. A. Tensile stress-strain characteristics of lightly cemented sand. **Geotechnical Testing Journal**, v. 17, n. 3, p. 305-314, 1994.

DAVIS, R. O.; SELVADURAI, A. P. S. **Plasticity and geomechanics**. Cambridge, UK: Cambridge University Press, 2002.

DE PAULA, T. M. **Misturas de cinza volante e cal de carbureto: comportamento da resistência à compressão simples frente à moagem da cinza volante**. 2016. 180 p. Dissertation (Master in Engineering) – Post-Graduate Program in Civil Engineering, Federal University of Rio Grande do Sul, Porto Alegre, 2016.

DIAMBRA, A.; RUSSELL, A. R.; IBRAIM, E.; MUIR WOOD, D. Determination of fibre orientation distribution in reinforced sands. **Géotechnique**, v. 57, n. 7, p. 623-628, 2007.

DIAMBRA, A.; IBRAIM, E.; MUIR WOOD, D.; RUSSEL, A. R. Fibre reinforced sands: experiments and modelling. **Geotextiles and Geomembranes**, v. 28, n. 3, p. 238-250, 2010.

DIAMBRA, A.; IBRAIM, E.; RUSSEL, A. R.; MUIR WOOD, D. Modelling the undrained response of fibre reinforced sands. **Soils and Foundations**, v. 51, n. 4, p. 625-636, 2011

DIAMBRA, A.; IBRAIM, E.; RUSSEL, A. R.; MUIR WOOD, D. Fibre reinforced sands: from experiments to modelling and beyond. **International Journal for Numerical and Analytical Methods in Geomechanics**, v. 37, n. 15, p. 2427-2455, 2013.

DIAMBRA, A.; IBRAIM, E.; PECCIN, A.; CONSOLI, N. C.; FESTUGATO, L. Theoretical derivation of artificially cemented granular soil strength. **Journal of Geotechnical and Geoenvironmental Engineering**, v. 143, n. 5, p. 04017003-1-9, 2017.

DIAMBRA, A.; FESTUGATO, L.; IBRAIM, E.; PECCIN, A.; CONSOLI, N. C. Modelling tensile/compressive strength ratio of artificially cemented clean sand. **Soils and Foundations**, v. 58, n. 1, p. 199-211, 2018.

DING, D.; HARGROVE, S. K. Nonlinear stress-strain relationship of soil reinforced with flexible geofibers. **Journal of Geotechnical and Geoenvironmental. Engineering**, v. 132, n. 6, p. 791-794, 2006.

DISFANI, M. M.; ARULRAJAH, A.; HAGHIGHI, H.; MOHAMMADINIA, A.; HORPIBULSUK, S. Flexural beam fatigue strength evaluation of crushed brick as a supplementary material in cement stabilized recycled concrete aggregates. **Construction and Building Materials**, v. 68, p. 667–676, 2014.

DONATO, M. **Comportamento mecânico de concreto compactado com rolo reforçado com fibras de polipropileno**. 2003. 82p. Dissertation (Master in Engineering) – Post-Graduate Program in Civil Engineering, Federal University of Rio Grande do Sul, Porto Alegre, 2003.

DONATO, M. **Medidas diretas de tensão em solo reforçado com fibras de polipropileno**. 2007. 161 p. Thesis (Doctor in Engineering) – Post-Graduate Program in Civil Engineering, Federal University of Rio Grande do Sul, Porto Alegre, 2007.

DONATO, M.; FOPPA, D.; CERATTI, J. A. P.; CONSOLI, N. C. Fibras de polipropileno como reforço para materiais geotécnicos. **Solos e Rochas**, v. 27, n. 2, p. 161-179, 2004.

DONKOR, P.; OBONYO, E. Compressed soil blocks: Influence of fibers on flexural properties and failure mechanism. **Construction and Building Materials**, v. 121, p. 25-33, 2016.

EL-RAWI, N.M.; HALIBURTON, T. A.; JANES, R. L. Effect of compaction on strength of soil-cement. **Journal of the Soil Mechanics and Foundation Division**, v. 93, n. 6, p. 195-208, 1967.

FEDRIGO, W.; NÚÑEZ, W. P.; LÓPEZ, M. A. C.; KLEINERT, T. R.; CERATTI, J. A. P. A study on the resilient modulus of cement-treated mixtures of RAP and aggregates using

indirect tensile, triaxial and flexural tests. **Construction and Building Materials**, v. 171, p. 161-169, 2018.

FEDRIGO, W.; NÚÑEZ, W. P.; SCHREINERT, G. G.; KLEINERT, T. R.; MATUELLA, M. F.; CASTAÑEDA LÓPEZ, M. A.; CERATTI, J. A. P. Flexural strength, stiffness and fatigue of cement-treated mixtures of reclaimed asphalt pavement and lateritic soil**. Road Materials and Pavement Design**, p. 1-19, 2019.

FELT, E.J.; ABRAMS, M.S. Strength and elastic properties of compacted soil-cement mixtures. In: AMERICAN SOCIETY FOR TESTING AND MATERIALS SPECIAL TECHNICAL PUBLICATION PORTLAND CEMENT ASSOCIATION RESEARCH AND DEVELOPMENT LABORATORY BULLETIN, 1957.

FESTUGATO, L. **Análise do comportamento mecânico de um solo micro-reforçado com fibras de distintos índices aspecto**. 2008. 146 p. Dissertation (Master in Engineering) – Post-Graduate Program in Civil Engineering, Federal University of Rio Grande do Sul, Porto Alegre, 2008.

FESTUGATO, L. **Comportamento de hidratação e resposta cisalhante cíclica de resíduo de mineração cimentado reforçado com fibras**. 2011. 224 p. Thesis (Doctor in Engineering) – Post-Graduate Program in Civil Engineering, Federal University of Rio Grande do Sul, Porto Alegre, 2011.

FESTUGATO, L.; DA SILVA, A. P.; DIAMBRA, A.; CONSOLI, N. C.; IBRAIM, E. Modelling tensile/compressive strength ratio of fibre reinforced cemented soils. **Geotextiles and Geomembranes**, v. 46, n. 2, p. 155-165, 2018.

FEUERHARMEL, M. R. **Comportamento de solos reforçados com fibras de polipropileno**. 2000. 131 p. Dissertation (Master in Engineering) – Post-Graduate Program in Civil Engineering, Federal University of Rio Grande do Sul, Porto Alegre, 2000.

FLOREZ, J. H.; FESTUGATO, L.; CONSOLI, N. C. Efeito da adição de fibras na resposta ante carregamentos cíclicos em areias limpas. In: CONGRESSO BRASILEIRO DE MECÂNICA DOS SOLOS E ENGENHARIA GEOTÉCNICA, 13th, 2016, Belo Horizonte, Brazil. **Proceedings**. ABMS, 2016.

FOPPA, D. **Análise da variáveis-chave no controle da resistência mecânica de solos artificialmente cimentados**. 2005. 144 p. Dissertation (Master in Engineering) – Post-Graduate Program in Civil Engineering, Federal University of Rio Grande do Sul, Porto Alegre, 2005.

FREITAG, D. R. Soil randomly reinforced with fibers. **Journal of Geotechnical Engineering**, v. 112, n. 8, p. 823-826, 1986.

GÁLVEZ, J. H. F. **Efeito da adição de fibras no comportamento de uma areia sob carregamentos cíclicos**. 2017. 188 p. Thesis (Doctor in Engineering) – Post-Graduate Program in Civil Engineering, Federal University of Rio Grande do Sul, Porto Alegre, 2017.

GASPARD, K. J.; MOHAMMAD, L.; WU, Z. Laboratory mechanistic evaluation of soil-cement mixtures with fibrillated polypropylene fibers. In: PROCEEDING OF THE 82ND TRANSPORTATION RESEARCH BOARD ANNUAL MEETING. **Proceedings**, 2003.

GRAY, D. H.; AL-REFEAI, T. Behavior of fabric versus fiber-reinforced sand. Journal of **Geotechnical Engineering**, v. 112, n. 8, p. 804-820, 1986.

GRAY, D. H.; OHASHI, H. Mechanics of fiber reinforcement in sand. **Journal of Geotechnical Engineering**, v. 109, n. 3, p. 335-353, 1983.

HALL, M. R.; NAJIM, K. B.; DEHDEZI, P. K. Soil stabilisation and earth construction: materials, properties and techniques. In: **Modern Earth Buildings**. 2012. p. 222-255.

HANNANT, L. Polymers and polymers composites. In: J.M. ILLSTON**. Construction materials: their nature and behavior**. 2ed., London: J.M. Illston/E & FN Spon, p. 359-403, 1994.

HEINECK, K. S. **Estudo da influência de cimentações introduzidas sob tensão**. 1998. 117 p. Dissertation (Master in Engineering) – Post-Graduate Program in Civil Engineering, Federal University of Rio Grande do Sul, Porto Alegre, 1998.

HEINECK, K. S. **Estudo do comportamento hidráulico e mecânico de materiais geotécnicos para barreiras horizontais impermeáveis**. 2002, 255 p. Thesis (Doctor in Engineering) – Post-Graduate Program in Civil Engineering, Federal University of Rio Grande do Sul, Porto Alegre, 2002.

HEINECK, K. S.; CONSOLI, N. C.; BICA, A.; CASAGRANDE, M. D. T. Comportamento de solos micro-reforçados a pequeníssimas e grandes deformações cisalhantes. **Solos e Rochas**, v. 26, n. 1, p .3-17, 2003.

HEINECK, K. S.; COOP, M. R.; CONSOLI, N. C. Effect of microreinforcement of soils from very small to large shear strains. **Journal of geotechnical and geoenvironmental engineering**, v. 131, n. 8, p. 1024-1033, 2005.

HOLLAWAY, L. Polymers and polymer composites. In: **Construction Materials, their nature and behavior**. London: J. M. Illston/E. & F.N. Spon, 2ed., p. 321-358, 1994.

HUANG J. T.; AIREY D. W. Properties of artificially cemented carbonate sand. **Journal of Geotechnical and Geoenvironmental Engineering**, v. 124, n. 6, p. 492-499, 1998.

IBRAIM, E.; DIAMBRA, A.; MUIR WOOD, D.; RUSSEL, A. R. Static liquefaction of fibre reinforced sand under monotonic loading. **Geotextiles and Geomembranes**, v.28, p. 374-385, 2010.

IDRISS, I. M.; DOBRY, R. U.; SING, R. D. Nonlinear behavior of soft clays during cyclic loading. **Journal of Geotechnical Engineering**, v. 104, p. 1427-1447(ASCE 14265), 1978.

ILLSTON, J. M. **Construction materials: their nature and behavior**. 2ed. London: E & FN Spon, 518 p., 1994.

IMAM, S.M., **Modeling the constitutive behavior of sand for the analysis of static liquefaction**. 1999. Thesis (Doctor in Engineering). Edmonton, AB, Canada: University of Alberta; 1999.

IMAM S.M.R.; CHAN D.H. Application of a critical state model for the cyclic loading of sands. **In: Proceedings of GeoEdmonton: 61st Canadian geotechnical conference**. Edmonton. p. 127-34, 2008.

INGLES, O. G.; METCALF, J. B. **Soil stabilization – principles and practice**. Australia: Butterworths Pty. Limited, 366p., 1972.

JOHNSTON, C. D. Fiber-reinforced cement and concrete. In: **Advances in concrete technology**. 2ed. Ottawa: V. M. Malhorta, p. 603-673. 1994.

JONES, C. J. F. P. **Earth Reinforcement and Soil Structures**. 6th ed. London: Butterworths, 379 p., 1996.

KANIRAJ, S. R.; HAVANAGI, V. G. Behavior of cement-stabilized fiber-reinforced fly ash-soil mixtures**. Journal of Geotechnical and Geoenvironmental Engineering**, v. 127, n. 7, p. 574-584, 2001.

KHATTAK, M. J.; ALRASHIDI, M. Mechanistic characteristics of processed cellulose-fiber reinforced soil-cement mixtures. In: **Advances in Pavement Engineering**, 2005, p. 1-13.

KHATTAK, M. J.; ALRASHIDI, M. Durability and mechanistic characteristics of fiber reinforced soil–cement mixtures. **International Journal of Pavement Engineering**, v. 7, n. 1, p. 53–62, 2006.

LEE, J.S.; SANTAMARINA, J. C. Bender elements: Performance and signal interpretation. Journal of Geotechnical and Geoenvironmental Engineering, v. 131, n. 9, p 1063-1070, 2005.

LEIVA, D. E. **Evolution of stiffness and deformation of Hostun sand under drained cyclic loading**. 2014. 395 p. Thesis (Doctor of Philosophy in the Faculty of Engineering) – Department of Civil Engineering, University of Bristol, Bristol, UK, 2014.

LI, J.; DING, D. W. Nonlinear elastic behavior of fiber-reinforced soil under cyclic loading. **Soil Dynamics and Earthquake Engineering**, v. 22, n. 9-12, p. 977-983, 2002.

LOPES JUNIOR, L. S. **Parâmetros de controle da resistência mecânica de solos tratados com cal, cimento e rocha basáltica pulverizada**. 2007. 147 p. Dissertation (Master in Engineering) – Post-Graduate Program in Civil Engineering, Federal University of Rio Grande do Sul, Porto Alegre, 2007.

MACHADO, S. L.; CARVALHO, M. F.; VILAR, O. M. Constitutive model for municipal solid waste. **Journal of Geotechnical and Geoenvironmental Engineering**, v. 128, n. 11, p. 940-951, 2002.

MAHER, M. H.; GRAY, D. H. Static response of sand reinforced with randomly distributed fibres. **Journal of Geotechnical Engineering**, v. 116, n. 11, p. 1661-1677, 1990.

MAHER, M. H.; HO, Y. C. Behavior of fiber-reinforced cemented sand under static and cyclic loads. **Geotechnical Testing Journal**, v. 16, n. 3, p. 330-338, 1993.

MAHER, M. H.; HO, Y. C. Mechanical properties of kaolinite/fiber soil composite. **Journal of Geotechnical Engineering**, v. 120, n. 8, p. 1387-1393, 1994.

MAHER, M. H.; WOODS, R. D. Dynamic response of sand reinforced with randomly distributed fibers. **Journal of Geotechnical Engineering**, v. 116, n. 7, p. 1116-1131, 1990.

MCGOWN, A.; ANDRAWES, K. Z. Influences of non-woven fabric inclusions on the stress strain behavior of a soil mass. In: **International Conference on the Use of Fabrics in Geotechnics**, Paper and Discussion, Paris, France, 1977, p. 20-22, 1977.

MCGOWN, A.; ANDRAWES, K. Z.; AL-HASANI, M.M. Effect of inclusion properties on the behavior of sand. **Géotechnique**, v. 28, n. 3, p. 327-346, 1978.

MCGOWN, A.; ANDRAWES, K.; HYTIRIS, N.; MERCER F.B. Soil strengthening using randomly distributed mesh elements. In: XI INTERNATIONAL CONFERENCE ON SOIL MECHANICS AND FOUNDATION ENGINEERING, SAN FRANCISCO, 1985. **Proceedings**. Publication of Balkema (AA), 1985.

MEDINA, J.; MOTTA, L. M. G. **Mecânica dos pavimentos**. 1. ed. Rio de Janeiro: COPPE/UFRJ, 380 p., 1997.

MEDINA, J.; MOTTA, L. M. G. **Mecânica dos pavimento**s. 2. ed. Rio de Janeiro: COPPE/UFRJ, 2005. 574 p.

MICHALOWSKI, R. L.; CÉRMAK, J. Strength anisotropy of fiber-reinforced sand. **Computers and Geotechnics**, v. 29, n. 4, p. 279-299, 2002.

MICHALOWSKI, R. L.; ZHAO, A. Failure of fiber-reinforced granular soils. **Journal of Geotechnical Engineering**, v. 122, N. 3, p. 226-234, 1996.

MIGUEL, G. D. **Desempenho e comportamento mecânico de um solo dispersivo e sulfatado tratado com uma pozolana artificial, cal de carbureto e reforçado com fibras de vidro**. 2020. 281 p. Dissertation (Master in Engineering) – Post-Graduate Program in Civil Engineering, Federal University of Rio Grande do Sul, Porto Alegre, 2020.

MITCHELL, J. K.; SOGA, K. Fundamentals of soil behavior. 3rd. ed. [s.l.] John Wiley & Sons, Inc., 2005.

MOREL, J. C.; GOURC, J. P. Mechanical behaviour of sand reinforced with mesh elements. **Geosynthetics International**, v. 4, n. 5, p. 481-508, 1997.

MOHAMMAD, L.; RAGHAVANDRA, A.; HUANG, B. Laboratory performance evaluation of cement-stabilized soil base mixtures. **Transportation Research Record: Journal of the Transportation Research Board**, v. 1721, p. 19–28, 2000.

MUIR WOOD, D. **Soil Behaviour and Critical State Soil Mechanics**. Cambridge: Cambridge University Press, 488 p., 1990.

MUIR WOOD, D. **Geotechnical modelling**. London: CRC Press, v. 2.2, 504 p., 2004.

MUIR WOOD, D. **Soil mechanics: A One-dimensional introduction**. Cambridge: Cambridge University Press, 239 p., 2009.

NATARAJ, M. S.; ADDULA; H. R.; MCMANIS, K. L. Strength and deformation characteristics of fiber reinforced soils. In: III INTERNATIONAL SYMPOSIUM ON ENVIRONMENTAL GEOTECHNOLOGY, San Diego, 1996. **Proceedings**. Pennsylvania: Technomic Publiching Co., Inc, v. 1, p. 826-835, 1996.

NATARAJ M. S.; McMANIS, K. L. Strength and deformation properties of soils reinforced with fibrillated fibers. **Geosynthetics International**, v. 4, n. 1, p. 65-79, 1997.

NÚÑEZ, W. P. **Estabilização físico-química de um solo residual de arenito Botucatu, visando seu emprego na pavimentação**. 1991. 150 p. Dissertation (Master in Engineering) – Post-Graduate Program in Civil Engineering, Federal University of Rio Grande do Sul, Porto Alegre, 1991.

PORBAHA, A; SHIBUYA, S.; KISHIDA, T. State of the art in deep mixing technology: part III – geomaterial characterization. **Ground Improvement, Journal of ISSMGE**, v.4, n.3, p. 91-110, 2000.

PRIETTO, P. D. M. **Estudo do comportamento mecânico de um solo artificialmente cimentado**. 1996. 150 p. Dissertation (Master in Engineering) – Post-Graduate Program in Civil Engineering, Federal University of Rio Grande do Sul, Porto Alegre, 1996.

PRIETTO, P. D. M. **Resistência e dilatância de solos cimentados:.uma abordagem teórico-experimental**. 2004. 230 p. Thesis (Doctor in Engineering) – Post-Graduate Program in Civil Engineering, Federal University of Rio Grande do Sul, Porto Alegre, 2004.

RAHIMI, M.; CHAN, D.; NOURI, A. Constitutive model for monotonic and cyclic responses of loosely cemented sand formations. **Journal of Rock Mechanics and Geotechnical Engineering**, v. 10, n. 4, p.740-752, 2018.

RIOS, S.; VIANA DA FONSECA, A.; BAUDET, B. A. Effect of the porosity/cement ratio on the compression of cemented soil. **Journal of geotechnical and geoenvironmental engineering**, v. 138, n. 11, p. 1422-1426., 2012.

ROSCOE, K. H.; BURLAND, J. B. On the generalized stress-strain behaviour of wet clay. In: CONFERENCE IN ENGINEERING PLASTICITY. **Papers**. Cambridge: Cambridge University Press, 1968, p. 536-609.

ROTTA, G. V.; CONSOLI, N. C.; PRIETTO, P. D. M.; COOP, M. R.; GRAHAM, J. Isotropic yielding in an artificially cemented soil cured under stress. **Géotechnique**, v. 53, n. 5, p. 493-501, 2003.

SALDANHA, R. B. **Misturas cinza volante e cal de carbureto: comportamento da resistência à compressão simples para cura acelerada**. 2014. 170 p. Dissertation (Master in Engineering) – Post-Graduate Program in Civil Engineering, Federal University of Rio Grande do Sul, Porto Alegre, 2014.

SANTAMARINA, J. C.; KLEIN, J. C.; FAM, M. A. Soils and waves: particulate materials behaviour, characterization and process monitoring. [s.l.] John Wiley & Sons Ltd, 2001.

SCHNAID, F.; PRIETTO, P. D. M.; CONSOLI, N. C. Prediction of cemented sand behavior in triaxial compression. **Journal of Geotechnical and Geoenvironmental Engineering**, v. 127, n. 10, p. 857-868, 2001.

SCHOFIELD, A. N.; WROTH, C. P. **Critical state soil mechanics**. London: McGraw-Hill, 218 p. 1968.

SHARMA, S. S.,; FAHEY, M. Degradation of stiffness of cemented calcareous soil in cyclic triaxial tests. **Journal of Geotechnical and Geoenvironmental Engineering**, v. 129, n. 7, p. 619-629, 2003.

SILVANI, C. **Influência da temperatura na cura da mistura areia- cinza volante-cal**. 2013. 106 p. Dissertation (Master in Engineering) – Post-Graduate Program in Civil Engineering, Federal University of Rio Grande do Sul, Porto Alegre, 2013.

SOBHAN, K.; DAS, B. M. Durability of soil–cements against fatigue fracture. **Journal of Materials in Civil Engineering**, v. 19, n. 1, p. 26–32, 2007.

SPECHT, L. P. **Comportamento de misturas de solo-cimento-fibra submetidos a carregamentos estáticos visando à pavimentação**. 2000. 130 p. Dissertation (Master in Engineering) – Post-Graduate Program in Civil Engineering, Federal University of Rio Grande do Sul, Porto Alegre, 2000.

STAUFFER, S. D.; HOLTZ, R. D. Stress-strain and strength behavior of staple fiber and continuous filament-reinforced sand. **Transportations Research Record**, n. 1474, p. 82-95, 1995.

STINCHOMB, W. W.; REIFSNIDER, K. L. Fatigue damage mechanisms in composite materials: a review. In: FATIGUE MECHANISMS – STP675, Kansas City, 1978. **Proceedings**. ASTM International, 1979, p. 762-781.

SUKONTASUKKUL, P.; JAMSAWANG, P. Use of steel and polypropylene fibers to improve flexural performance of deep soil–cement column. **Construction and Building Materials**, v. 29, p. 201-205. 2012.

TAKAIKAEW, T.; TEPSRIHA, P.; HORPIBULSUK, S.; HOY, M.; KALOUSH, K. E.; ARULRAJAH, A. Performance of fiber-reinforced asphalt concretes with various asphalt binders in Thailand. **Journal of Materials in Civil Engineering**, v. 30, n. 8, 04018193, 2018.

TANG, C.; SHI, B.; GAO, W.; CHEN, F.; CAI, Y. Strength and mechanical behavior of short polypropylene fiber reinforced and cement stabilized clayey soil. **Geotextiles and Geomembranes**, v. 25, n. 3, p. 194-202, 2007.

TARIQ, K. A.; TAKESHI M. Cement treated sand as a measure against cyclic loading. **Grouting and Deep Mixing**, p. 1985-1994. 2012.

TEODORO, J. M. **Resistência ao cisalhamento de solos reforçados com fibras plásticas**. 1999. 108 p. Dissertation (Master in Engineering) – São Carlos School, University of São Paulo, São Carlos, 1999.

ULBRICH, L. A. **Aspectos do comportamento mecânico de um solo reforçado com fibras**. 1997. 122 p. Dissertation (Master in Engineering) – Post-Graduate Program in Civil Engineering, Federal University of Rio Grande do Sul, Porto Alegre, 1997.

VAN IMPE, W. F. **Soil improvement techniques and their evolution**. Rotterdam, A. A. Balkema, 125p, 1989.

VENDRUSCOLO, M. A. **Comportamento de ensaios de placa em camadas de solo melhoradas com cimento e fibras de polipropileno**. 2003. 224 p. Thesis (Doctor in Engineering) – Post-Graduate Program in Civil Engineering, Federal University of Rio Grande do Sul, Porto Alegre, 2003.

VENSON, G. I. **Módulo de resiliência e vida de fadiga de areia artificialmente cimentada**. 2015. 142 p. Dissertation (Master in Engineering) – Post-Graduate Program in Civil Engineering, Federal University of Rio Grande do Sul, Porto Alegre, 2015.

VIDAL, H. The principle of reinforced earth. **Highway Research Record**. Washington, D.C., NCR-HRB, n. 282, p. 1-16, 1969.

VILLARD, P.; JOUVE, P. Behaviour of granular materials reinforced by continuous threads. **Computers and Geotechnics**, v. 7, p. 83-98, 1989.

WENG M. C. A generalized plasticity-based model for sandstone considering timedependent behaviour and wetting deterioration. **Rock Mechanics and Rock Engineering v.** 47, n. 4, p.1197-1209, 2014.

YASUHARA, K.; HYDE, A. F. L.; TOYOTA, N.; MURAKAMI, S.. Cyclic stiffness of plastic silt with an initial drained shear stress. In **Pre-failure deformation behaviour of geomaterials**, p. 373-382. Thomas Telford Publishing, 1998.

YE, L. On fatigue damage accumulation and material degradation in composite materials. **Composites science and technology**, n. 36, v. 4, p. 339-350, 1989

YU, H. S. **Plasticity and Geotechnics**. New York: Springer, v. 13, 522 p., 2006.

ZHANG, J.; LI, V. C. Monotonic and fatigue performance in bending of fiber-reinforced engineered cementitious composite in overlay system. **Cement and Concrete Research**, v. 32, n. 3, p. 415–423, 2002.

APPENDICES

APPENDICES A

MOULDING RESULTS FOR CYCLIC UNCONFINED COMPRESSION TESTS

Mixture	Moulding Date	Repetition	% of Load	C (%)	γ_d (g/cm^3)	γ_{di}/γ_{df}	ω_i/ω_f	ω_{av}(%)	W_{SP} (g)	$D_{AVERAGE}$ (cm)	$H_{AVERAGE}$ (cm)	Vspec (cm^3)	γ_n (gf/cm^3)	γ_d (gf/cm^3)	e	η (%)	Civ (%)	η/Civ$^{0.28}$
18-5-0	12/02/19	I	80	5	1.800	0.991	1.029	9.72	393.43	5.01	10.01	197.48	1.99	1.82	0.48	32.49	2.74	24.49
	23/02.19	IV	70	5	1.800	0.988	1.043	9.59	393.51	5.01	10.01	197.13	2.00	1.82	0.48	32.27	2.75	24.30
	25/02/19	II	90	5	1.800	0.993	1.018	9.83	393.15	5.00	10.04	197.46	1.99	1.81	0.48	32.60	2.74	24.58
	26/02/19	II	80	5	1.800	0.990	1.038	9.63	393.77	5.01	10.01	197.52	1.99	1.82	0.48	32.39	2.75	24.40
	07/03/19	IV	90	5	1.800	0.988	1.037	9.64	393.37	4.99	10.07	196.97	2.00	1.82	0.48	32.27	2.75	24.30
	08/03/19	V	90	5	1.800	0.993	1.005	9.95	393.50	5.00	10.05	197.52	1.99	1.81	0.48	32.63	2.74	24.61
	11/03/19	IV	80	5	1.800	1.000	1.033	9.68	392.33	5.01	10.09	198.82	1.97	1.80	0.49	33.10	2.72	25.02
	12/03/19	VI	70	5	1.800	0.996	1.002	9.98	393.11	5.01	10.04	197.81	1.99	1.81	0.49	32.81	2.73	24.77
	14/03/19	V	70	5	1.800	0.996	1.026	9.74	393.30	5.01	10.05	198.31	1.98	1.81	0.49	32.81	2.73	24.76
19-3-0	06/03/19	I	80	3	1.900	1.002	1.024	9.77	414.99	5.01	10.10	199.37	2.08	1.90	0.41	29.29	1.75	25.03
	13/03.19	III	80	3	1.900	0.994	1.025	9.75	415.02	5.01	10.02	197.77	2.10	1.91	0.40	28.70	1.77	24.47
	14/03/19	IV	80	3	1.900	1.001	0.983	10.17	415.19	5.01	10.06	198.57	2.09	1.90	0.41	29.23	1.75	24.97
18-5-F	01/03/19	I	90	5	1.800	1.018	0.962	10.39	393.22	5.04	10.11	201.38	1.95	1.77	0.50	33.31	2.67	25.29
	04/03/19	II	90	5	1.800	0.997	1.041	9.61	393.38	5.01	10.09	198.74	1.98	1.81	0.47	31.91	2.73	24.09
	07/03/19	III	80	5	1.800	0.997	1.001	9.99	393.02	5.01	10.06	197.98	1.99	1.80	0.47	31.95	2.73	24.12
	09/03/19	III	70	5	1.800	0.995	1.041	9.60	393.47	5.01	10.08	198.35	1.98	1.81	0.47	31.76	2.74	23.96
	16/03/19	IV	70	5	1.800	1.002	1.012	9.88	393.38	5.02	10.08	199.28	1.97	1.80	0.48	32.26	2.72	24.39
	17/03/19	V	70	5	1.800	1.000	1.048	9.55	392.94	5.01	10.10	199.35	1.97	1.80	0.47	32.16	2.72	24.30
	18/03/19	IV	80	5	1.800	0.990	1.045	9.57	393.16	5.01	10.00	197.44	1.99	1.82	0.46	31.48	2.75	23.72
	18/03/19	V	80	5	1.800	0.994	1.039	9.62	393.50	5.01	10.06	198.19	1.99	1.81	0.46	31.71	2.74	23.92
	19/03/19	IV	90	5	1.800	0.992	1.037	9.65	393.24	5.01	10.02	197.68	1.99	1.81	0.46	31.59	2.74	23.82
18-5-F-ML	19/03/19	I	80	5	1.800	0.995	1.028	9.73	393.17	5.01	10.04	198.12	1.98	1.81	0.47	31.81	2.73	24.00
	20/03/19	I	90	5	1.800	0.996	1.040	9.62	393.13	5.02	10.04	198.40	1.98	1.81	0.47	31.84	2.73	24.03
	23/03/19	I	70	5	1.800	0.991	1.044	9.58	393.34	5.02	9.97	197.53	1.99	1.82	0.46	31.48	2.75	23.72
	26/03/19	II	90	5	1.800	0.990	1.051	9.52	393.46	5.02	10.00	197.54	1.99	1.82	0.46	31.43	2.75	23.68
	28/03/19	II	80	5	1.800	1.000	0.984	10.17	393.58	5.03	9.98	198.55	1.98	1.80	0.47	32.16	2.72	24.30
	30/03/19	II	70	5	1.800	0.996	1.012	9.89	393.67	5.02	10.02	198.16	1.99	1.81	0.47	31.83	2.73	24.02
19-3-F	16/03/19	I	80	3	1.900	1.002	1.044	9.58	415.25	5.02	10.10	199.76	2.08	1.90	0.39	28.25	1.75	24.14
	25/03/19	II	80	3	1.900	1.008	1.048	9.55	414.75	5.03	10.10	200.87	2.06	1.88	0.40	28.72	1.74	24.58
	25/03/19	III	80	3	1.900	1.002	1.011	9.89	415.69	5.02	10.07	199.42	2.08	1.90	0.39	28.26	1.75	24.14

APPENDICES B

SHEAR MODULUS ASSESSEMNT FOR CYCLIC UNCONFINED COMPRESSION TESTS

	Repetition	Moulding Date	Testing Date	H (mm)	Volume (cm^3)	$h/C_{IV}^{0.28}$	Actual %	Number of Cycles	Numeber of Cycles Rupture	0 CY					1 CY			
										Initial E (MPa)	Initial Bender (ms)	t_0 Bender (ms)	Intial G_0 (MPa)	E fromG_0 (MPa)	E (MPa)	Bender (ms)	H (mm)	G (MPa)
18-5-O	I	25/02/19	04/03/19	100.40	197.46	24.58	93	3	3	414.67	111.40	17.37	1539.16	3878.67	346.53	132.00	100.40	1035.66
	II	07/03/19	14/03/19	100.70	196.97	24.30	93	25	25	415.00	127.20	28.46	1410.86	3555.37	1430.61	132.60	100.62	1265.85
	III	08/03/19	15/03/19	100.70	198.75	24.61	91	23	23	414.54	113.20	28.46	1896.29	4778.65	1467.15	130.40	100.41	1301.05
	I	12/02/19	19/02/19	100.10	198.48	24.49	84	78	77	414.38	105.30	17.37	1736.83	4376.80	1329.05	116.50	100.39	1376.46
	II	26/02/19	05/03/19	100.51	198.57	24.40	82	245	245	414.42	108.30	17.37	1640.04	4132.91	1163.63	115.20	100.46	1415.30
	III	11/03/19	18/03/19	100.16	195.80	25.02	80	79	79	414.10	114.40	28.46	1844.60	4648.39	653.15	124.20	100.62	1503.30
	I	23/02/19	02/03/19	100.55	197.93	24.30	72	2000	2000	415.36	111.60	17.37	1537.25	3873.86	1378.07	125.40	100.52	1168.83
	II	14/03/19	21/03/19	100.45	198.31	24.77	74	2000	2000	415.22	121.60	28.46	1566.16	3946.73	1212.88	129.30	100.40	1334.20
	III	12/03/19	19/03/19	100.76	198.59	24.76	72	1231	1231	415.60	116.00	28.46	1795.69	4525.13	2436.81	122.70	100.99	1549.45
18-5-F	I	01/03/19	08/03/19	101.64	201.46	25.29	88	17	12	420.20	169.70	17.37	600.53	1513.34	310.77	204.70	101.65	397.23
	II	04/03/19	11/03/19	100.87	198.74	24.09	87	50	29	419.74	159.60	17.37	684.43	1724.76	417.88	191.80	100.21	447.67
	III	19/03/19	26/03/19	100.22	197.68	23.82	89	55	49	418.58	174.30	13.50	528.35	1331.45	174.34	210.60	99.68	346.96
	I	07/03/19	14/03/19	100.61	197.98	24.12	79	105	70	417.64	145.40	13.50	789.78	1990.24	338.20	191.80	99.65	422.02
	II	18/03/19	25/03/19	100.03	197.44	23.72	79	154	102	420.14	162.80	13.50	612.91	1544.54	237.36	202.80	99.54	376.66
	III	18/03/19	25/03/19	100.62	198.19	23.92	79	68	58	428.80	165.30	13.50	611.82	1541.78	160.62	206.10	99.59	370.36
	I	09/03/19	16/03/19	100.82	198.35	23.96	68	346	157	418.32	164.00	13.50	609.65	1536.32	289.76	202.30	100.58	385.13
	II	16/03/19	23/03/19	100.83	199.28	24.39	69	253	100	420.12	162.00	13.50	626.09	1577.75	157.73	201.50	99.98	382.48
	III	17/03/19	24/03/19	101.00	199.35	24.30	68	270	203	420.14	154.30	13.50	699.16	1761.87	139.17	192.10	99.03	413.70
18-5-F-ML	I	20/03/19	27/03/19	100.35	198.40	24.03	93	2000	2000	417.76	152.40	13.50	706.43	1780.21	292.08	175.45	98.98	502.08
	II	26/03/19	02/04/19	99.96	197.54	23.68	92	2000	2000	417.12	145.80	13.50	773.24	1948.56	150.23	169.15	98.47	538.00
	I	19/03/19	26/03/19	100.43	198.12	24.00	81	2000	2000	416.44	155.90	13.50	672.17	1693.87	160.27	183.70	99.96	465.04
	II	28/03/19	04/04/19	99.80	198.55	24.30	83	2000	2000	416.40	169.10	13.50	553.05	1393.68	140.83	202.90	99.19	367.58
	I	23/03/19	30/03/19	99.69	197.53	23.72	72	2000	2000	416.32	158.90	13.50	634.65	1599.32	113.84	184.90	99.26	451.87
	II	30/03/19	06/04/19	100.23	198.16	24.02	72	2000	2000	416.67	171.10	13.50	546.33	1376.74	196.79	203.00	99.60	371.93
19-3-0F	I	06/03/19	13/03/19	101.03	199.37	25.03	86	3	3	429.36	125.70	28.46	1499.15	3777.86	757.57	149.20	100.87	968.58
	II	13/03/19	20/03/19	100.50	198.29	24.47	82	5	5	428.42	116.40	13.50	1325.57	3340.43	1332.01	142.20	100.49	847.13
	III	14/03/19	21/03/19	100.92	199.29	24.97	82	10	10	429.24	111.00	13.50	1487.24	3747.85	1513.76	132.20	100.89	1002.68
19-3-F	I	16/03/19	23/03/19	100.98	199.76	24.14	75	45	4	431.80	151.00	13.50	751.54	1893.88	135.19	226.60	100.74	311.05
	II	25/03/19	01/04/19	100.98	200.87	24.58	79	37	9	432.62	148.50	13.50	776.86	1957.70	127.01	208.70	98.67	350.73
	III	25/03/19	01/04/19	100.73	199.42	24.14	81	61	10	433.16	147.80	13.50	786.81	1982.76	141.66	199.90	98.19	383.22

CONTINUATION

	Repetition	2 CY				10 CY				30 CY				50 CY				100 CY			
		E (MPa)	Bender (ms)	H (mm)	G (MPa)	E (MPa)	Bender (ms)	H (mm)	G (MPa)	E (MPa)	Bender (ms)	H (mm)	Go (MPa)	E (MPa)	Bender (ms)	H (mm)	Go (MPa)	E (MPa)	Bender (ms)	H (mm)	Go (MPa)
18-5-O	I																				
	II	1845.91	139.25	100.55	1116.47	2099.95	145.90	100.53	993.13												
	III	1754.74	134.70	100.34	1195.76	1824.87	138.00	100.29	1123.43												
	I	1128.72	116.68	100.39	1371.39	1324.82	118.30	100.33	1325.67	1462.11	122.80	100.28	1213.40	1880.37	128.00	100.25	1101.29				
	II	1258.02	118.95	100.48	1313.47	1907.48	122.70	100.50	1222.20	1241.45	126.00	100.50	1149.04	1060.20	128.60	100.48	1095.29	818.55	133.90	100.43	996.82
	III	801.34	129.70	100.62	1344.62	1478.28	127.90	100.65	1394.68	1320.44	131.00	100.61	1310.29	1238.76	134.70	100.60	1220.43				
	I	1022.85	127.40	100.50	1126.19	1299.23	134.50	100.53	994.35	1315.11	138.00	100.55	937.93	1893.70	141.00	100.55	892.96	1012.26	146.00	100.55	824.92
	II	1678.29	132.20	100.39	1260.42	1933.87	133.70	100.41	1225.27	1675.26	138.40	100.39	1122.40	1559.20	141.90	100.39	1054.12	1296.15	142.00	100.39	1052.21
	III	1384.38	123.33	100.97	1528.11	1209.91	129.00	100.93	1359.41	1177.12	132.80	100.86	1259.91	1023.90	133.83	100.80	1233.64	1139.19	136.40	100.71	1172.90
18-5-F	I	381.74	214.70	101.57	357.25	205.39	234.70	100.92	289.85												
	II	350.22	201.40	99.89	399.01	1010.56	216.70	99.20	334.31												
	III	195.08	221.00	99.66	312.87	160.88	228.90	98.95	285.18	196.31	236.90	98.70	263.46								
	I	360.80	192.70	99.66	417.87	329.80	200.80	99.86	384.43	613.74	225.35	99.92	301.00	542.79	249.90	100.15	243.10				
	II	249.19	212.80	99.53	339.71	300.37	221.80	99.48	310.59	337.42	239.80	99.16	261.03	297.30	248.00	97.78	234.68	268.94	265.00	96.88	199.39
	III	170.56	216.00	99.41	333.57	192.12	218.40	98.97	322.16	237.47	219.50	98.73	316.85	179.23	224.20	98.55	301.48				
	I	303.02	222.30	100.06	310.84	226.17	233.40	100.30	281.95	293.68	234.20	99.91	277.15	381.74	225.50	99.62	298.23	369.66	229.40	99.38	285.83
	II	171.93	217.00	99.82	325.18	186.66	219.00	99.38	315.36	149.24	223.00	98.34	295.52	174.28	225.00	98.90	294.14	156.04	225.70	98.19	286.94
	III	185.81	201.50	98.69	370.15	193.53	206.50	99.46	358.11	161.76	227.90	99.51	290.57	291.32	228.80	99.43	287.60	368.81	234.20	99.40	273.44
18-5-F-ML	I	180.04	198.50	99.61	390.94	194.63	192.70	98.92	409.40	278.46	226.20	98.89	290.36	235.21	231.60	99.00	277.00	231.45	225.60	98.92	292.27
	II	142.50	192.50	98.51	407.21	191.91	202.40	98.22	362.94	205.66	208.10	98.39	343.52	166.56	221.40	98.49	301.73	240.37	210.10	98.30	335.77
	I	207.39	192.60	99.82	418.58	261.37	194.00	99.53	409.05	111.39	202.50	99.92	376.76	345.79	233.50	99.30	273.78	341.80	229.20	99.30	284.84
	II	145.73	204.90	99.12	359.30	132.23	210.50	98.59	334.60	221.97	212.10	99.64	338.10	214.84	217.70	98.83	313.35	227.57	212.90	98.66	327.22
	I	112.82	185.95	99.16	445.20	97.95	195.40	98.00	388.51	142.19	194.60	97.39	385.93	122.81	194.60	97.35	385.44	111.47	195.70	98.54	392.63
	II	238.78	208.70	99.55	350.10	184.39	209.50	98.17	335.27	192.22	203.10	98.03	357.09	190.09	204.30	98.01	352.42	185.05	203.90	97.98	353.59
19-3-0F	I	1679.52	154.80	100.86	884.43																
	II	1068.24	153.30	100.49	718.02																
	III	1122.76	140.10	100.89	881.42	906.18	167.10	100.83	597.85												
19-3-F	I	130.56	234.50	100.08	284.49																
	II	121.76	225.80	98.37	294.21																
	III	131.54	216.40	97.99	321.71	185.43	232.20	97.00	269.95												

CONTINUATION

	Repetition	200 CY				300 CY				400 CY				500 CY				1000 CY			
		E (MPa)	Bender (ms)	H (mm)	Go (MPa)	E (MPa)	Bender (ms)	H (mm)	Go (MPa)	E (MPa)	Bender (ms)	H (mm)	Go (MPa)	E (MPa)	Bender (ms)	H (mm)	Go (MPa)	E (MPa)	Bender (ms)	H (mm)	Go (MPa)
18-5-O	I																				
	II																				
	III																				
	I																				
	II	988.36	152.00	100.26	743.63																
	III																				
	I	1235.92	149.10	100.51	785.82	1021.17	149.10	100.50	785.54	1108.24	150.20	100.48	772.32	1036.91	150.10	100.49	773.69	1371.95	146.60	100.42	814.70
	II	1262.15	139.30	100.40	1104.42	1157.59	139.00	100.40	1110.52	1098.30	138.40	100.40	1122.63	995.86	137.80	100.45	1136.27	725.56	136.45	100.40	1163.50
	III	1617.78	137.20	100.55	1151.15	2677.14	138.20	100.41	1126.44	1179.80	139.00	100.23	1105.07	847.10	139.80	99.85	1079.08	227.05	141.30	99.78	1048.66
18-5-F	I																				
	II																				
	III																				
	I																				
	II																				
	III																				
	I	362.23	233.40	99.35	275.31	240.59	273.40	97.96	190.24												
	II	175.05	242.50	95.92	232.33																
	III	333.95	258.40	99.09	220.35																
18-5-F-ML	I	252.10	226.20	98.78	289.57	303.23	227.00	98.62	286.29	314.34	228.00	98.57	283.21	245.84	227.00	98.64	286.41	351.68	220.60	98.38	302.34
	II	235.76	213.00	98.33	326.35	254.67	208.50	98.32	341.48	237.04	214.60	98.48	322.36	214.56	215.80	98.49	318.65	231.21	227.50	98.60	285.54
	I	428.81	222.60	99.23	302.57	365.54	220.30	99.28	309.66	429.43	224.90	99.24	296.11	462.89	222.30	99.20	303.15	479.47	222.90	99.23	301.67
	II	207.37	213.80	98.64	324.11	283.94	211.80	98.35	328.25	257.78	212.20	98.49	328.07	241.77	210.60	98.50	333.55	306.23	214.70	98.37	318.98
	I	172.37	190.40	97.41	404.67	169.14	186.00	97.14	422.57	176.36	186.40	97.33	422.73	151.35	182.30	97.05	440.33	192.23	183.60	97.21	435.34
	II	257.88	203.50	97.81	353.53	234.50	195.80	97.81	384.07	224.78	205.90	97.82	344.83	231.69	198.60	97.80	372.47	260.83	189.30	97.72	412.05
19-3-0F	I																				
	II																				
	III																				
19-3-F	I																				
	II																				
	III																				

CONTINUATION

	Repetition	1500 CY				2000 CY			
		E (MPa)	Bender (ms)	H (mm)	Go (MPa)	E (MPa)	Bender (ms)	H (mm)	Go (MPa)
18-5-O	I								
	II								
	III								
	I								
	II								
	III								
	I	1204.09	143.90	100.44	850.24	1559.64	130.30	100.38	1065.81
	II	1689.73	135.10	100.41	1193.30	1661.00	129.80	100.41	1321.54
	III								
18-5-F	I								
	II								
	III								
	I								
	II								
	III								
	I								
	II								
	III								
18-5-F-ML	I	390.33	227.90	98.35	281.92	546.17	207.70	98.12	341.63
	II	204.95	210.10	98.74	339.60	223.90	223.00	98.59	297.89
	I	478.79	209.50	99.29	344.88	585.19	207.40	99.27	352.17
	II	324.66	199.00	98.31	374.71	448.74	205.10	98.18	350.09
	I	206.29	171.90	97.17	501.51	231.29	175.90	97.07	475.96
	II	339.30	204.70	97.65	347.71	521.88	192.20	97.55	397.04
19-3-0F	I								
	II								
	III								
19-3-F	I								
	II								
	III								

APPENDICES C

MOULDING DATA FOR FATIGUE TESTS

Mixture	Rep.	Date	Ideal Load (%)	C (%)	γ_d (g/cm^3)	γ_{di}/γ_{df}	ω_i/ω_f	ω_{av}(%)	W_{SP} (g)	$D_{AVERAGE}$ (cm)	$H_{AVERAGE}$ (cm)	Vspec (cm^3)	γ_n (gf/cm^3)	γ_d (gf/cm^3)	e	η (%)	Civ (%)	η/Civ$^{0.28}$
18 kN/m^3 - 3% cement	I	20/05/20	80	3	1.80	0.999293	1.02598	9.75	779.40	10.04	4.98	394.27	1.98	1.80	0.48	32.56	1.67	28.22
	II	27/05/20	80	3	1.80	1.015923	0.925018	10.81	780.80	10.06	5.01	397.69	1.96	1.77	0.50	33.38	1.64	29.07
	III	10/06/20	80	3	1.80	0.999921	1.009041	9.91	779.00	10.05	4.96	393.72	1.98	1.80	0.48	32.32	1.66	28.02
18 kN/m^3 - 5% cement	I	09/10/19	90	5	1.80	1.006303	0.974238	10.26	777.63	10.03	4.99	394.27	1.97	1.79	0.50	33.49	2.70	25.35
	II	18/10/19	90	5	1.80	1.010145	0.964674	10.37	779.01	10.03	5.01	396.11	1.97	1.78	0.51	33.75	2.69	25.57
	III	25/10/19	90	5	1.80	1.014438	1.011778	9.88	778.47	10.02	5.06	399.27	1.95	1.77	0.52	34.03	2.68	25.81
	I	29/10/19	80	5	1.80	1.01664	0.972322	10.28	778.61	10.04	5.04	398.75	1.95	1.77	0.52	34.17	2.68	25.94
	II	28/11/19	89	5	1.80	1.00065	1.019101	9.81	778.30	10.02	4.99	394.01	1.98	1.80	0.50	33.12	2.72	25.03
	III	03/12/19	80	5	1.80	1.008006	1.050162	9.52	778.30	10.03	5.04	397.96	1.96	1.79	0.51	33.61	2.70	25.45
	I	07/11/19	70	5	1.80	0.996302	0.955943	10.46	778.94	10.03	4.94	390.31	2.00	1.81	0.49	32.83	2.73	24.78
	II	03/12/19	70	5	1.80	1.004365	1.000306	10.00	777.76	10.02	5.00	394.53	1.97	1.79	0.50	33.36	2.71	25.24
	III	29/10/19	70	5	1.80	0.998879	1.02844	9.72	779.05	10.02	5.00	394.01	1.98	1.80	0.49	33.00	2.72	24.92
19 kN/m^3 - 5% cement	I	06/09/19	80	5	1.90	0.989988	1.036091	9.65	830.80	10.05	4.97	394.78	2.10	1.92	0.40	28.64	2.90	21.25
	II	10/09/19	80	5	1.90	1.000051	0.944172	10.59	830.60	10.05	4.98	395.31	2.10	1.90	0.42	29.36	2.87	21.85
	III	26/09/19	80	5	1.90	1.006793	1.028486	9.72	821.30	10.05	5.00	396.63	2.07	1.89	0.43	29.83	2.85	22.24
18 kN/m^3 - 3% cement - 0.5% fibre	I	06/10/20	80	3	1.80	1.020067	1.047009	9.55	779.56	10.10	5.04	403.26	1.93	1.76	0.51	33.56	1.62	29.30
	II	29/10/20	80	3	1.80	1.023119	1.0225	9.78	773.21	10.07	5.02	400.34	1.93	1.76	0.51	33.76	1.62	29.50
	III	29/10/20	80	3	1.80	1.020664	0.988676	10.11	772.78	10.08	4.99	397.94	1.94	1.76	0.51	33.60	1.62	29.34
18 kN/m^3 - 5% cement - 0.5% fibre	I	10/12/19	90	5	1.80	1.016223	1.008633	9.91	778.36	10.03	5.06	399.80	1.95	1.77	0.50	33.49	2.66	25.45
	I	21/09/20	90	5	1.80	1.026176	1.006667	9.93	776.60	10.08	5.05	402.73	1.93	1.75	0.52	34.13	2.64	26.01
	II	22/09/20	90	5	1.80	1.017799	1.015221	9.85	776.20	10.07	5.01	399.54	1.94	1.77	0.51	33.59	2.66	25.54
	I	21/09/20	80	5	1.80	1.023932	0.944502	10.59	775.19	10.06	5.01	398.75	1.94	1.76	0.51	33.99	2.64	25.88
	II	22/09/20	80	5	1.80	1.021099	0.963348	10.38	775.37	10.04	5.04	398.49	1.95	1.76	0.51	33.80	2.65	25.72
	III	23/09/20	80	5	1.80	1.025484	0.955209	10.47	776.27	10.06	5.04	400.34	1.94	1.76	0.52	34.09	2.64	25.97
	I	21/09/20	70	5	1.80	1.021526	0.973335	10.27	774.80	10.08	5.00	398.74	1.94	1.76	0.51	33.83	2.65	25.75
	II	22/09/20	70	5	1.80	1.024795	0.964078	10.37	775.60	10.06	5.04	400.07	1.94	1.76	0.52	34.04	2.64	25.93
	III	23/09/20	70	5	1.80	1.0273	0.960805	10.41	774.47	10.07	5.03	400.34	1.93	1.75	0.52	34.20	2.64	26.07
19 kN/m^3 - 5% cement - 0.5% fibre	I	20/09/20	80	5	1.80	1.00578	0.990093	10.10	816.10	10.08	5.19	414.18	1.97	1.79	0.49	32.79	2.69	24.85
	II	20/09/20	80	5	1.80	0.992991	0.956486	10.45	813.82	10.08	5.09	406.46	2.00	1.81	0.47	31.93	2.73	24.11
	III	20/09/20	80	5	1.80	0.983189	0.989349	10.11	815.60	10.10	5.05	404.60	2.02	1.83	0.45	31.25	2.75	23.53